ALKALOIDS AND FLAVONOIDS FROM FICUS, ARTOCARPUS AND MACARANGA SPECIES: STRUCTURE AND ANTI-CANCER ACTIVITY

VERONICA ALICIA YAP

THESIS SUBMITTED TO THE UNIVERSITY OF NOTTINGHAM FOR THE DEGREE OF DOCTOR OF PHILOSOPHY (PHD)

JUNE 2015

PREFACE

This thesis is submitted for the degree of Doctor of Philosophy at the University of Nottingham. The study described herein was conducted under the supervision of Dr Lim K. H., Prof. Dr Sandy Loh H. S. and Dr Ting K. N. of the Faculty of Science, University of Nottingham Malaysia.

This work is to the best of my knowledge original, except where acknowledgements and references are made to previous work. This thesis has not been submitted for any degree and is not concurrently submitted in candidature of any other degree.

Part of this work has been presented in the following publication:

Yap, V. A.; Loong, B.-J.; Ting, K.-N.; Loh, S. H.-S.; Yong, K.-T.; Low, Y.-Y.; Kam, T.-S.; Lim, K.-H. *Phytochemistry* **2015**, *109*, 96–102.

ACKNOWLEDGEMENTS

The completion of this research study could not have been made possible without the participation and assistance of many whose names may not all be mentioned. Their contributions are sincerely and gratefully acknowledged. However, I would like to express my appreciation and indebtedness particularly to the following:

Dr. Lim K. H., my research supervisor for his utmost patience, guidance and support throughout the duration of this research. My greatest appreciation also goes out to my co-supervisors, Prof. Sandy Loh H. S. and Dr Ting K. N. for their constant encouragement and valuable advice.

Prof. Kam T. S., Dr Low Y. Y. and their research team at Chemistry Department, University of Malaya for assistance in acquiring most of the spectroscopic data. My deepest appreciation goes to Dr. Sim K. S. from University Malaya and Dr Tracey Bradshaw from University of Nottingham, UK for providing assistance throughout the biological aspects of this work.

My colleagues, friends and family, as I owe them a lot for their unceasing support and encouragement.

I would also like to thank the Ministry of Higher Education (MOHE) Malaysia for financial support.

ABSTRACT

Plant natural products have played a pivotal role in the discovery and development of many new drugs for the treatment of various infectious diseases and cancers. The present study was therefore aimed at isolation and identification of novel bioactive compounds from selected plants collected in Malaysia with anti-cancer activity. Plant crude extracts were obtained using solvent extraction methods, while various chromatographic and spectroscopic methods were employed for compound isolation and structure elucidation. Evaluation of pure compounds and crude extracts for anti-cancer activity involved the use of Neutral Red assay (NR), acradine orange – ethidium bromide (AO/EB) staining and cell cycle analysis.

Phytochemical investigations of five Malaysian plants, namely, *Ficus hispida, F. fistulosa, F. schwarzii, Artocarpus heterophyllus x integer* and *Macaranga hypoleuca*, with the focus on alkaloids and flavonoids, have resulted in the isolation of a total of 24 compounds, of which six are new. The leaf and stem-bark extracts of *Ficus hispida* yielded two new alkaloids, hispidacine **(1)** and hispiloscine **(2)**, and a known alkaloid, 13a(*S*)-(+)-deoxypergularinine **(3)**. Hispidacine represents the first example of an 8,4'-oxyneolignan incorporated an unusual 2-hydroxyethylamine moiety, while hispiloscine represents the first naturally occurring phenanthroindolizidine alkaloid with acetoxy substitution. The leaf and bark extracts of *Ficus fistulosa* provided two new septicine alkaloids, fistulopsines A and B (**4** and **5**), together with four known phenanthroindolizidine alkaloids, 13a(*R*)-(–)-3,6-didemethylisotylocrebrine **(6)**, 13a(*S*)-(+)-tylocrebrine **(7)**, 13a(*S*)-(+)-tylophorine **(8)** and 13a(*S*)-(+)-septicine **(9)**, and one known non-alkaloid (vomifoliol, **10**). The leaves of *Ficus schwarzii* gave two novel tri-*nor*-sesquilignan alkaloids, schwarzinicines A and B (**11** and **12**). The bark of *Artocarpus heterophyllus x integer* yielded five known compounds, of which four are

prenylated flavonoids, namely, cudraflavone C **(13)**, artocarpetin A **(14)**, cycloheterophyllin **(15)** and artonin J **(16)**, and one natural xanthone, lichexanthone **(17)**. The leaves of *Macaranga hypoleuca* provided seven known compounds, of which three are flavonoid glycosides, namely, quercetin-3-*O*-α-L-arabinopyranoside **(18)**, quercetin-3-*O*-α-L-arabinofuranoside **(19)** and quercetin-3-*O*-β-D-galactoside **(20)**, three are flavonoid aglycones, namely, quercetin **(21)**, kaempherol **(22)**, and 5,7-dihydroxy-2-(4-methoxyphenyl)-8-(3-methylbut-2-en-1-yl)chroman-4-one **(23)**, and one sterol 3-*epi*-taraxerol **(24)**. Preliminary screening by NR assay found that the crude extracts (except for *Artocarpus heterophyllus x integer*) showed growth inhibitory activities against human breast (MDA-MB-231 and MCF-7), lung (A549), and colon (HCT-116) cancer cell lines. Of the 24 pure compounds obtained, hispiloscine **(2)**, fistulopsine A **(4)**, fistulopsine B **(5)** and cudraflavone C **(13)** were found to show growth inhibitory activity against colon (HCT-116) and breast (MCF-7) cancer cells. Furthermore, **4** and **5** were found to dominantly arrest cells in G1 phase of the cell cycle without the induction of apoptosis. Cell cycle perturbation of these compounds was found to be reversible for HCT-116 cells at the onset of 72 hours. These results suggest that **4** and **5** have the potential to be further exploited for the development of new anti-cancer agents.

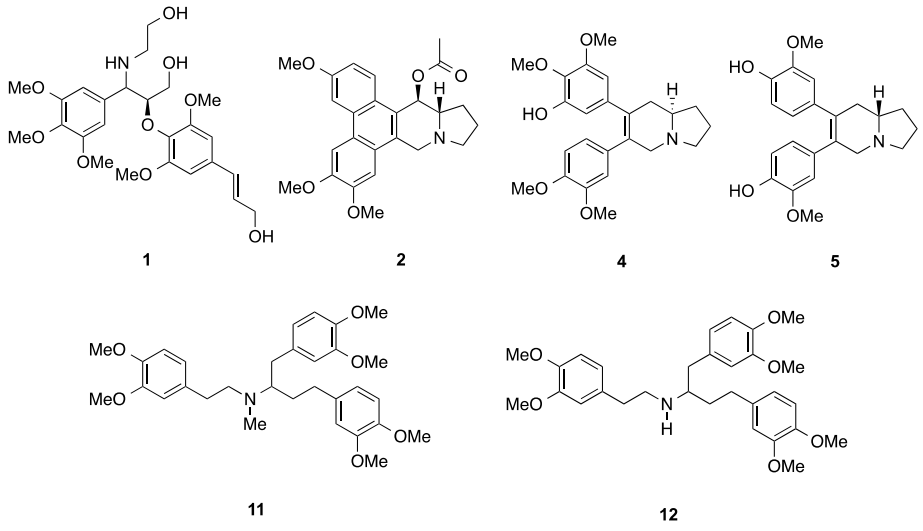

TABLE OF CONTENTS

LIST OF ABBREVIATIONS

$AlCl_3$	aluminium trichloride
µg	microgram
µM	micromolar
^{13}C	carbon-13
^{1}H	proton
br	broad
CD_3OD	deuterated methanol
$CDCL_3$	deuterated choloroform
CH_2Cl_2	dichloromethane
$CHCl_3$	chloroform
cm	centimetre
cm^{-1}	per centimetre
CO_2	carbon dioxide
COSY	Correlation Spectroscopy
d	doublet
dd	doublet of doublets
DMEM	Dubelcco's Modified Eagles Medium
DMSO	dimethyl sulphoxide
ESIMS	Electron Spray Ionisation Mass Spectroscopy
Et_2O	diethyl ether
EtOH	ethanol
HCl	hydrochloric acid
HMBC	Heteronuclear Multiple Bond Correlation
HRESIMS	High Resolution Electrospray Ionisation Mass Spectroscopy
HSQC	Heteronuclear Single Quantum Coherence
Hz	hertz
IC	Inhibition Correlation
IR	infrared
J	coupling constant
K_2HPO_4	potassium hydrogen phosphate
M	molar
m	multiplet
m.p	melting point
m/z	mass-to-charge ratio
Me	methyl
MeOH	methanol
mg	milligram
MHz	megahertz
mM	millimolar
MTT	3-(4,5-dimethylthiazol-2-yl)-2,5-diphenyltetrazolium bromide
nm	nanometre
nM	nanomolar
NMR	Nuclear Magnetic Resonance
NOESY	Nuclear Overhauser effect Spectroscopy

ppm	part per million
q	quartet
R_f	retention factor
s	singlet
t	triplet
td	triplet doublet
TLC	Thin Layer Chromatography
UV	ultraviolet
VLC	Vacuum Liquid Chromatography
α	alpha
β	beta
γ	gamma
δ	chemical shift
ε	epsilon
λ	lambda
EtOAc	ethyl acetate
Et_2O	diethyl ether
CTLC	Centrifugal Thin Layer Chromatography
Na_2CO_3	sodium carbonate
Na_2SO_4	sodium sulphate

LIST OF FIGURES

LIST OF TABLES

LIST OF APPENDICES

Chapter 1: Introduction

1.1 Bioactive compounds from natural sources

Plants have a long history of uses in the treatment of diseases throughout the world as they are the most exclusive therapy accessible to humans. Today, most of the populations in developing countries still rely on traditional medicines for basic healthcare.[1] This has brought the shift of focus towards ethnopharmacological intervention in addressing the current need to treat emerging health related issues such as drug resistance, relapses and incurable diseases. The diversity of compounds found in plants have provided a variety of lead structures that are suitable for further modification during drug development.[2] This holds true as a large proportion of drugs that are currently available are derived from the diverse structures and the intricate carbon skeletons of natural products.[2] For instance, the therapeutic areas of infectious diseases and oncology have benefitted from the numerous drugs that are derived from natural sources. These include paclitaxel (anti-cancer) from the plant *Taxus brevifolia*, artemisinin (anti-malaria) from the plant *Artemisia annua*, doxorubicin (anti-cancer) from the bacteria *Streptomyces peucetius* and lovastatin (cholesterol lowering) from the mold species *Aspergillus terreus* (Figure 1.1).[3,4] However, only a fraction (5-15%) of the approximately 250, 000 higher plants have been investigated for biological potential.[3] In light of this, the plant kingdom remains an essential source of new molecules with therapeutic potentials.[5]

Although the term natural product refers to any naturally occurring substance, it is generally taken to mean secondary metabolites.[6] In a natural environment, these compounds are produced by higher plants (and other organisms) as an evolution mechanism for protection, adaptation and overall survival but play little role in the growth

and development, or other primary functions of the producing organisms.[6,7] The palette of secondary metabolites can be divided into three broad groups which are the alkaloids, terpenoids and phenolics.[6] Since secondary metabolites from natural sources are found within living systems, arguably they are often perceived as showing more biological friendliness, with relatively non-toxic nature and defined mechanism of actions as compared to predominantly synthetic compounds.[2,3,8] The purpose of this study is therefore to identify novel secondary metabolites and their potential as medicinal agents from three plant genera, namely *Ficus, Artocarpus* and *Macaranga*, which are laden with alkaloids and flavonoids.

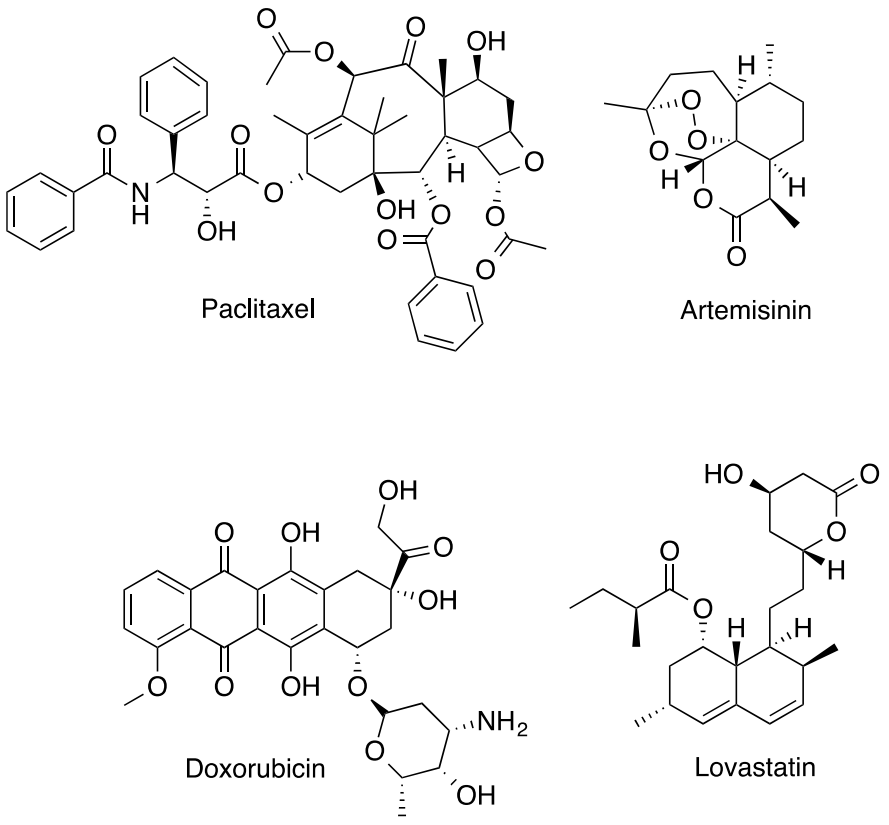

Figure 1.1: Examples of natural product derived drugs

1.2 Alkaloids

Alkaloids are nitrogen-containing organic substances of natural origin with greater or lesser degree of basic character where the nitrogen is derived from an amino acid.[9,10] Alkaloids and alkaloid-containing plant extracts are often biologically active and have prominent purpose as medicine, poisons and psychoactive drugs.[11] Well known plant families that are marked as alkaloid producers include Rubiaceae, Papaveraceae and Apocyanaceae.[12] The distribution of an alkaloid can differ greatly where some alkaloids are present only in selected genera while others are commonly found across more than one type of plant.[13] For example, cocaine is specific to the genus *Coca* (Erythroxylaceae) while caffeine which is common to the genus *Coffea* (Rubiaceae) can also be found in the genus *Camellia* (Theaceae) (Figure 1.2).[13] Although mainly found in higher plants, alkaloids have also been found in fungi, marine organisms, insects, micro-organisms and mammals.[14] Most alkaloids are chiral molecules which means the optical isomers may show different physiological activities.[15,16] Alkaloids are also naturally basic and the degree of basicity may vary depending on the number and position of nitrogen atoms, electron withdrawing (reduce basicity) or electron enhancing (enhance basicity) groups surrounding the nitrogen atom. It is believed that the basic character of alkaloids makes them unstable to heat, light and oxygen.[15]

Alkaloids constitute one of the most diverse structure classes of secondary metabolites showing a great variety in structural type. The main classification of alkaloids based on their structural types are shown in Figure 1.3.[17] Among these alkaloid classes, phenanthroindolizidine alkaloids are among those which have been identified for their significant therapeutic potential such as anti-microbial, anti-inflammatory and particularly

anti-cancer activity. This goes to show that there are much more to be discovered about the bioactivities of this class of compounds in the search of potential treatments for malignancy.[18–20]

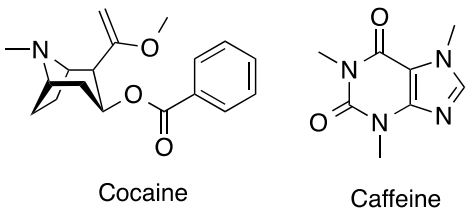

Figure 1.2: Alkaloids: cocaine and caffeine

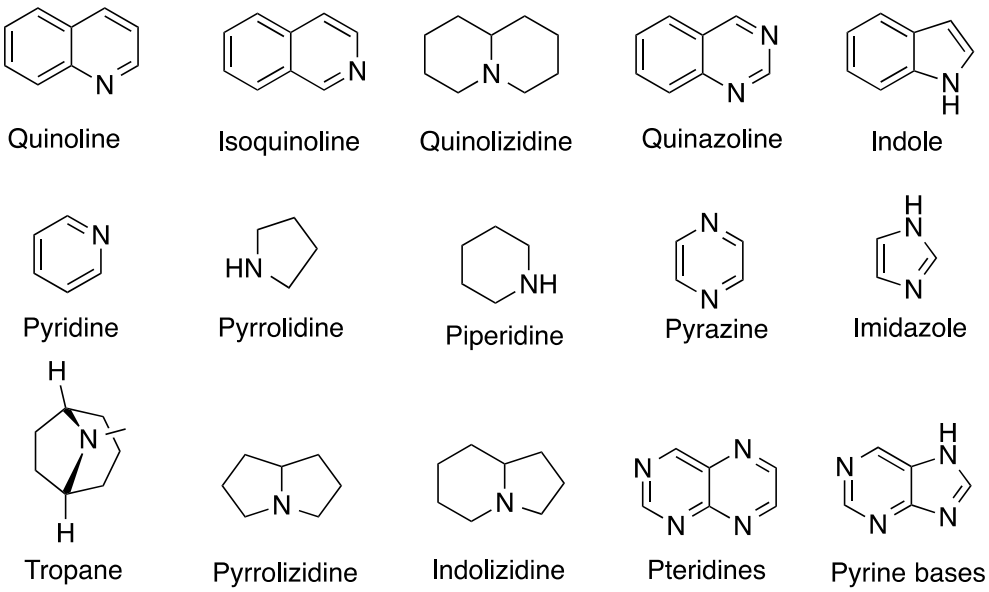

Figure 1.3: Classification of alkaloids based on structure

1.2.1 Phenanthroindolizidine alkaloids

Indolizidine alkaloids are classed as such when the alkaloid posses the indolizidine ring as a dominant heterocyclic system. With the addition of the phenanthrene ring system to the core indolizidine ring, they are classed as phenanthroindolizidine alkaloids (Figure 1.4). The phenanthrene portion is generally substituted with three to five methoxy or hydroxy groups.[19,21] Phenanthroindolizidines have been found in the plant families of Asclepiadaceae (genus *Cycnanchum*, *Pergularia*, *Vincetoxicum*) and Moraceae (genus *Ficus*).[22] Tylocrebrine **(7)**, tylophorine **(8)** and tylophorinine **(25)** were the first few phenanthroindolizidine alkaloids to be identified (Figure 1.5).

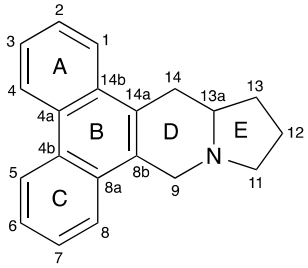

Figure 1.4: Basic skeleton of phenantroindolizidine alkaloid

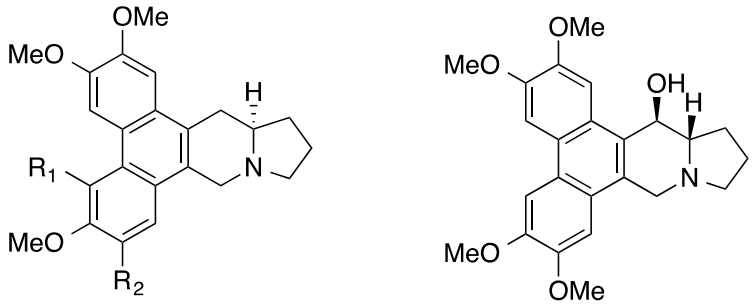

Tylocrebrine **(7)** R^1 = OMe, R^2 = H
Tylophorine **(8)** R^1 = H, R^2 = OMe

Tylophorinine **(25)**

Figure 1.5: Structures of first discovered phenantroindolizidines

1.3 Flavonoids

Flavonoids are a group of polyphenolic compounds with variable phenolic structures, occurring in virtually all plant parts particularly as a major colouring component of flowering plants.[23] They represent the largest and most diverse group comprising of more than 3000 varieties, many of which are responsible for a variety of biological activities.[24] Flavonoids and their polymers constitute a large class of food constituents and are thought to have health promoting properties due to their high antioxidant capacities both *in vitro* and *in vivo*.[25,26]

Chemically, flavonoids consist of two aromatic rings (rings A and B) that are connected through a three-carbon unit, which in most cases also forming part of the heterocyclic pyran ring C (Figure 1.6). They can be further divided into a variety of classes where each flavonoid class differed in the level of oxidation and pattern of substitution of the C-ring (Figure 1.7), while individual compounds within each class differ in the substitution pattern of the A and B rings.[27] Flavonoids are usually hydroxylated in positions-2, -3, -5, -7, -3', -4' and -5'.[23] Occasionally, aromatic and aliphatic acids, sulphates, and prenyl, or methelenedioxy groups are also attached to the flavonoid nucleus.[27] Flavonoids can occur as aglycones, glycosides and methylated derivatives. In most cases, flavonoids are present as glycosides in vacuoles of flowers, leaves, stems or roots, while flavonoid aglycones were reported as farinose exudates or wax on the leaves, bark and buds.[27] The basic flavonoid structure is an aglycone (Figure 1.6). However, when glycosides are formed, the glycosidic linkage is normally attached in position-3 or -7 and the carbohydrate can be L-rhamnose, D-glucose, glucorhamnose, D-galactose or L-arabinose.[23]

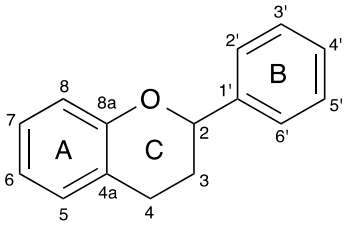

Figure 1.6: Basic structure of a flavonoid skeleton

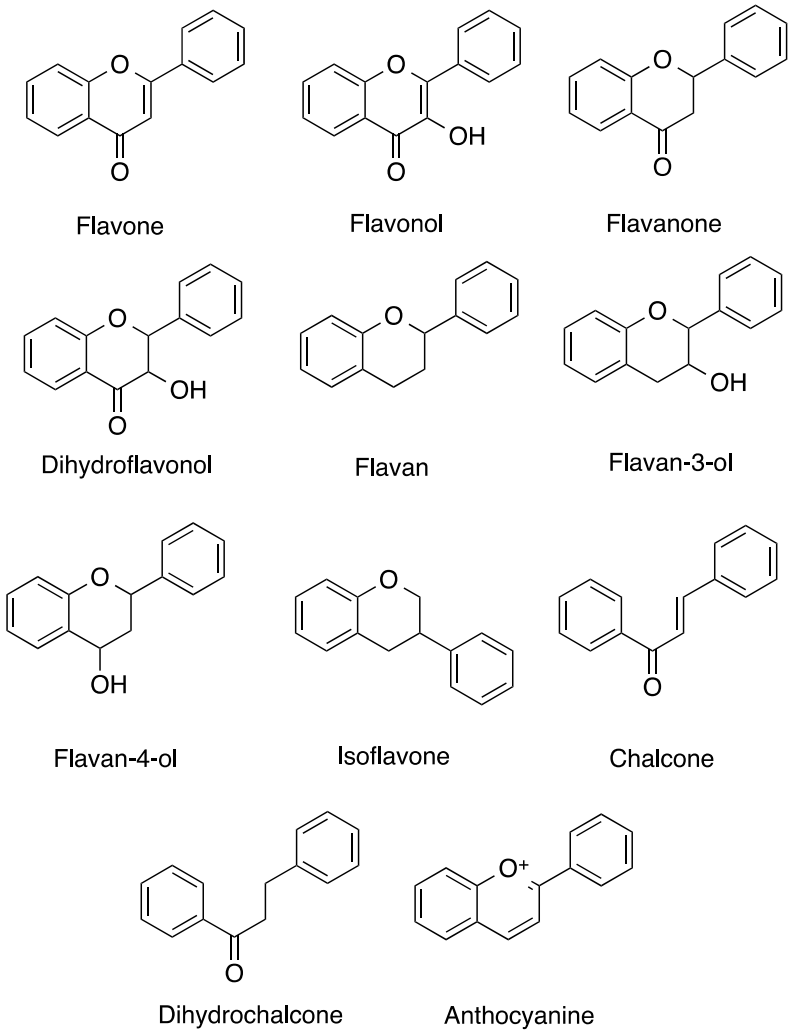

Figure 1.7: Structures of flavonoid classes

1.4 Genus *Ficus*

Globally, the genus *Ficus* consists of more than 800 species (more than 100 occurring in Peninsular Malaysia) of deciduous trees, shrubs, vines, epiphytes and semi-epiphytes in the family Moraceae.[28] Collectively known as "Fig trees", they are distributed primarily in sub-tropical and tropical regions.[29] Although, great majority of the species grow in lowlands, some can be found in altitudes that reach up to approximately 2000 meters above sea level.[30] *Ficus* are keystone species in the tropical rainforests that play an important role in the ecosystem as their fruits provide a source of nutrition to insects, birds and animals throughout the year.[31]

A number of *Ficus* species are used as food and for medicinal properties in ayurvedic and traditional Chinese medicine (TCM) where different plant parts ranging from roots, bark, leaves, latex and fruits are used for specific reasons. In ayurvedic medicine, figs are used as treatment for eczema, leprosy, rheumatism, sores, ulcers and pains.[32] In TCM, cooked figs are used for the treatment of diarrhea and as a gargle for sore throats, while the leaves are used as poultice for hemorrhoids.[33,34] In addition, the *Ficus* plants are also used to treat benign neoplasia such as warts and as an anti-inflammatory agent for boils and pains, which are suggestive of potential anti-cancer and anti-inflammatory actions of this plant genus.[34]

1.4.1 Phytochemicals and bioactivities of *Ficus* species

Some *Ficus* species have been evaluated for biological activities related to cancer, revealed promising anti-cancer activities. This include *in vitro* anti-proliferative activities against several cancer cell lines and *in vivo* inhibition of hepatic carcinoma xenographs in

mice.[34] In addition to that, a fraction from the extract of *F. citrifolia* have been found to induce accumulation and cytotoxicity of chemotherapeutic drugs such as vinblastine and daunomycin in cancer cells, thus, suggesting possible complementary role in cancer chemotherapy and addressing multidrug resistance of cancer cells.[35] Despite the significant pharmacological activities shown by the *Ficus* extracts, there are limited reports on the biologically active metabolites from the *Ficus* plants.

Previous phytochemical investigations involving eight *Ficus* species had led to the identification of over 100 compounds.[34] A substantial number of these compounds are phenanthroindolizidine alkaloids (from the leaves and stems of *F. septica* and *F. hispida*) and flavonoids,[36] along with several coumarins,[37] and triterpenoids.[38] The most promising cytotoxic class of compounds found in these *Ficus* species are the triterpenes and phenanthroindolizidine alkaloids.[34] The phenantroindolizidines are however found primarily in the genera, *Cynanchum*, *Pergularia*, and *Tylophora* of the Aspiadaceae family,[39] although they have also been previously isolated from *F. hispida, F. septica* and *F. fistulosa*.[19,34,40,41]

A significant number of novel and known alkaloids (Table 1.1, Figure 1.8) from five different alkaloid subclasses have been isolated from *F. septica* and *F. hispida* which include ficuseptine A **(26)**, ficuseptines E-N (**30**-**39**), (+)-tylophorine **(8)**, and a mixture of (+)-antofine **(50)** and (+)-isotylocrebrine **(49)**, and *O*-methyltylophorinidine **(62)** all of which exhibited potent cytotoxic activity against several cancer cell lines.[19,21,40] To date, phytochemical studies on *F. fistulosa* have resulted in the isolation of a new benzopyrroloisoquinoline alkaloid, fistulosine **(59)** which accounted for the anti-fungal activities observed in the crude alkaloidal extract.[41]

Table 1.1: Alkaloids from the genus *Ficus*.

Plant	Alkaloid class	Alkaloid name	Ref
F. septica	Phenanthroindolizidine	**Ficuseptine A (26)**	41
		Ficuseptine B (27)	18
		Ficuseptine C (28)	
		Ficuseptine D (29)	
		Ficuseptine E (30)	19
		Ficuseptine F (31)	
		Ficuseptine G (32)	
		Ficuseptine H (33)	
		Ficuseptine I (34)	
		Ficuseptine J (35)	
		Ficuseptine K (36)	
		Ficuseptine L (37)	
		Ficuseptine M (38)	
		Ficuseptine N (39)	
		10*R*,13a*R*-tylophorine-*N*-oxide (40)	18
		10*R*,13a*R*-tylocrebrine-*N*-oxide (41)	
		10*S*,13a*R*-tylocrebrine-*N*-oxide (42)	
		10*S*,13a*R*-isotylocrebrine-*N*-oxide (43)	
		10*S*,13a*S*-isotylocrebrine-*N*-oxide (44)	
		Dehydrotylophorine **(45)**	
		10*S*, 13a*R*-tylophorine-*N*-oxide **(46)**	
		10*S*, 13a*R*-antofine-*N*-oxide **(47)**	
		Tylophorine **(8)**	
		14-α-hydroxyisocrebine-*N*-oxide **(48)**	
		Isotylocrebrine **(49)**	
		Antofine **(50)**	
		14-Hydroxy-2,3,4,6,7-pentamethoxyphenanthroindolizidine **(51)**	
		14-Hydroxy-,3,4,6,7-tetramethoxyphenanthroindolizidine **(52)**	
	Seco-phenanthroindolizidine	Septicine **(9)**	42
		*Seco*antofine **(53)**	
	Aminocaprophenone	**Ficuseptamine A(54)**	
		Ficuseptamine B (55)	
	Pyrolidine	**Ficuseptamine C (56)**	
		Norruspoline **(57)**	
		Phyllosterone **(58)**	
F. fistulosa	Benzolopyrroloindolizidine	**Fistulosine (59)**	39
	Phenanthroindolizidine	Antofine **(50)**	
		*Seco*antofine **(53)**	
		14β-Hydroxyantofine **(60)**	
F. hispida	*Seco*-phenanthroindolizidine	**Hispidine (61)**	38
	Phenanthroindolizidine	*O*-Methyltylophorinidine **(62)**	

Bold highlights denote novel compounds isolated from respective plants.

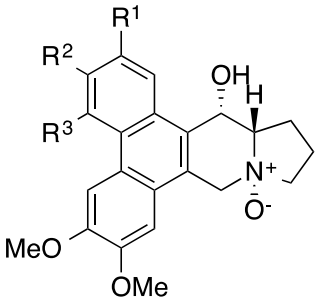

26 $R^1 = R^2 = R^3 = OMe$
38 $R^1 = H$, $R^2 = R^3 = OMe$

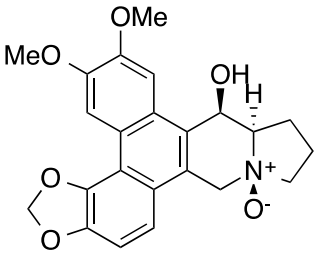

39

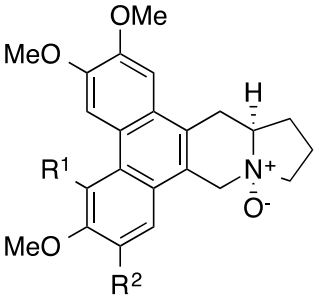

40 $R^1 = H$, $R^2 = OMe$
41 $R^1 = OMe$, $R^2 = H$

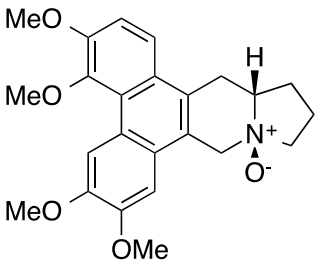

44

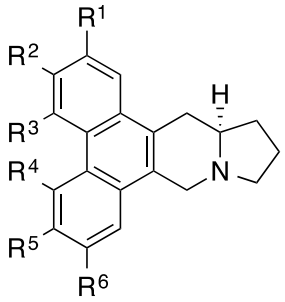

27 $R^1 = R^2 = R^4 = R^5 = OMe$, $R^3 = R^6 = H$
28 $R^1 = R^2 = R^5 = OMe$, $R^3 = R^4 = R^6 = H$
29 $R^1 = R^4 = H$, $R^2 = R^3 = R^5 = OMe$
30 $R^1 = R^3 = OH$, $R^2 = R^5 = OMe$, $R^4 = R^6 = H$
31 $R^1 = R^2 = R^3 = R^4 = R^5 = OMe$, $R^6 = H$
32 $R^1 = R^4 = H$, $R^2 = R^3 = R^6 = OMe$, $R^5 = OH$
33 $R^1 = R^4 = R^5 = OMe$, $R^2 = OH$, $R^3 = R^6 = H$
34 $R^1 = R^5 = R^6 = OMe$, $R^2 = OH$, $R^3 = R^4 = H$
35 $R^1 = R^2 = R^4 = OMe$, $R^3 = R^6 = H$, $R^5 = OH$

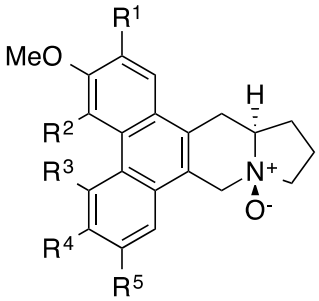

36 $R^1 = R^3 = OMe$, $R^2 = R^5 = H$, $R^4 = OH$
37 $R^1 = R^3 = R^5 = H$, $R^2 = R^4 = OMe$

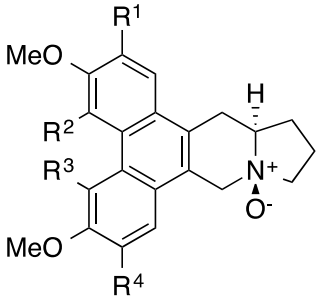

42 $R^1 = R^3 = OMe$, $R^2 = R^4 = H$
43 $R^1 = R^3 = H$, $R^2 = R^4 = OMe$

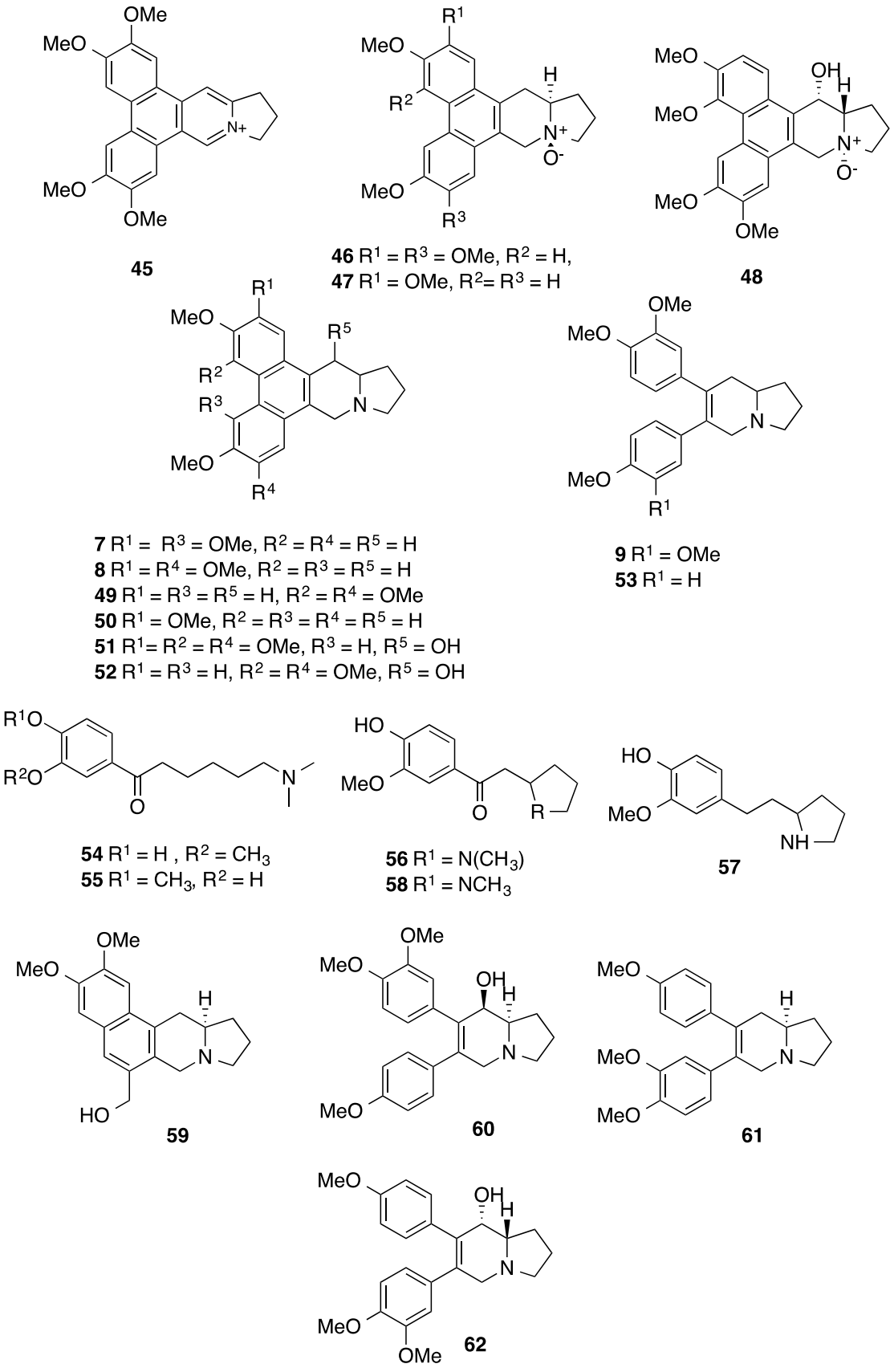

Figure 1.8: Alkaloids from *Ficus spp.*

1.5 Genus *Artocarpus*

The *Artocarpus* genus evergreen and deciduous trees from the of Moraceae family which covers approximately 60 genera of 1400 species.[43] They are distributed in the tropical and sub-tropical regions of Asia, and are native to South and Southeast Asia, New Guinea and the Southern Pacific.[43] The *Artocarpus* comprises mainly of jackfruit and breadfruit trees and are known as economic sources of food and widely used in traditional medicine, agriculture and industry. The use of the *Artocarpus* plants in traditional medicine included treatment of inflammation, malarial fever, diabetes, and other minor ailments such as diarrhea, ulcer and asthma.[43] This genus received great scientific interest as they contain important secondary metabolites possessing useful biological activities.

'Nangka' (*A. heterophyllus*), 'cempedak' (*A. integer*) and breadfruit or 'sukun' (*A. communis*) are among the local variety of *Artocarpus* fruits found in Malaysia and Indonesia which have been thoroughly investigated due to their significant bioactivities. Consequently, a hybrid between *A. heterophyllus* and *A. integer* has been developed to enhanced disease resistance, fruits that are larger in size with better texture and taste.[44] Owing to the vast medicinal potential of the parent plants, the phytochemical constituents within the hybrid plant are worth to be explored. A preliminary study on the hybrid plant was undertaken by Panthong *et al.*,[44] which uncovered a new prenylated flavone and was found to show significant antioxidant and antibacterial activities. Coincidentally, work on the hybrid plant extract was carried out by the author when Panthong *et al*. published their findings in 2013. [44]

1.5.1 Phytochemicals and bioactivity of *Artocarpus* flavonoids

The *Artocarpus* species are rich in phenolic compounds including flavonoids, stilbenoids and arylbenzofurans. The *Artocarpus* flavonoids constitute a relatively homogenous group of compounds, almost all derivatives are from the basic tricyclic structure of a flavone and differ only in the nature of substituents and substitution patterns of the A and B rings (Figure 1.6). Isoprenyl substituents at C-3 (3-prenylflavones) are mostly present in the form of a carbocyclic ring or an oxygen-bearing ring fused with rings B and C forming cyclic derivatives such as oxypinoflavones, pyranoflavones, dihydrobenzoxanthones, furanobenzoxanthones, and pyranodihydrobenzoxanthones (Figure 1.9).[45] The occurrence of an isoprenyl substituent at C-3 and a 2',4'-dioxygenated or 2',4',5'-trioxygenated B-ring in the flavone skeleton was deemed to be of chemotaxonomic significant and are broadly believed to be the requirements for cytotoxic activity.[46]

Known and novel flavonoids from selected *Artocarpus* plants are shown in Table 1.2 and Figure 1.10. Interesting biological activities have been described for many phenolic metabolites from the *Artocarpus*, which include anti-inflammatory, anti-viral, anti-bacterial and anti-platelet effects.[43] Certain members of these metabolites also displayed cytotoxic activity against various human cancer cell lines. Phytochemical investigations on *A. integer* yielded several new flavonoids, namely, artocarpones A **(63)** and B **(69)**,[47] cyclochempedol **(66)**,[48] artoindonesianins A **(71)** and B **(72)**,[49] and artoindonesianins U-T (**73-78**)[50,51] along with other known flavonoids. Artoindonesianins B **(72)**, U **(73)**, V **(74)** and T **(78)** together with two known flavonoids, heterophyllin **(65)** and cudraflavone C **(13)** showed strong cytotoxic activity against murine leukemia P-388 cells with IC_{50} values below 10 μM.[52] Similarly, a new oxepinoflavone artoindonesianin E1 **(126)**, isolated from the wood of *A. elasticus*, also showed cytotoxic activity against P388 cells.[53]

A. heterophyllus wood extract was found to exhibit strong tyrosine kinase inhibition activity, which is the key target involved in melanin biosynthesis.[54] Alterations in melanogenesis occur in many diseases including malignant melanoma. Bioassay guided fractionation of the extract yielded artocarpanone **(80)**, which proved to inhibit tyrosine kinase activity and melanin production in B16 melanoma cells with potent antioxidant activity.[54] Furthermore, a series of structurally related isoprenoid-substituted flavonoids was also isolated from the wood of *A. heterophyllus* and were tested on B16 melanoma cells.[55] Among the tested compounds, artocarpin **(83)**, cudraflavone C **(13)**, kuwanon C **(86)**, cudraflavone B **(84)** and brosimone I **(87)** were the most active, possibly due to the position and number of isoprenoid moieties per molecule, which is believed to influence flavonoid cytotoxicity.[55] In a separate study, artocarpanone **(80)**, artonin B **(88)** and cycloheterophyllin **(15)** were shown to exert anti-inflammatory activity by their inhibitory effects on chemical mediators released from inflammatory cells (mast cells, neutrophils and macrophages).[56]

Given the potency of *A. integer* and *A. heterophyllus*, a hybrid of these two plants naturally prompted the investigation of its constituents. A recent report identified a novel prenylated flavone **(96)** from the roots of a hybrid between *A. integer* and *A. heterophyllus* along with 24 other known compounds.[44] The known compounds isolated from the hybrid plant were among those that were novel to its parent plants such as artocarpanone **(80)** and norartocarpetin **(82)** from *A. heterophyllus* and artoindonesianin S **(77)** from *A. integer*. Bioactivity study of the novel flavone **(96)** demonstrated potent antioxidant activity and strong anti-bacterial activity against *Acenetobacter baumannii*.[44]

Three new geranyl chalcone derivatives from *A. communis*, namely, isolespeol **(117)**, 5'-geranyl-2',4',4-trihydroxychalcone **(118)** and 3,4,2',4'-tetradyhydroxy-3'-

geranyldihydrochalcone **(119)** were tested for *in vitro* anti-cancer activity against a panel of human cancer cell lines. The results indicated that **117** was the most potent against SW 872 human lipocarcinoma cells where treatment with the compound induced apoptosis in the cells through mitochondria-mediated pathways.[57] The novel prenylflavonoids, artoflavone A **(111)** and cyclogeracommunin **(112)** showed protective effect on DNA damage which serve as effective antioxidant agents that may provide chemopreventive measures against carcinogenesis.[58]

Phytochemical studies from the root bark of *A. rotunda* yielded new prenylated flavone artoindonesian L **(122)** along with known phenolic compounds identified as artonin M **(124)** and E **(123)**, cycloartobiloxanthone **(120)** and artonin O **(125)**. These compounds were found to show potent cytotoxicity against murine leukemia cells P-388 with IC_{50} values less than 10 μg/mL.[59] The prenylflavonoids **120**, **124** and **125** , which were also isolated from the stem-bark of *A. kemando* showed cytotoxicity against human oral epidermoid carcinoma KB cells, all of which showed IC_{50} values less than 4 μg/mL.[60] In a separate study, **120** showed cytotoxicity against breast cancer and human small cell lung cancer (NCI-H187) cell lines.[61]

Investigation of the twigs of *A. rigida* yielded four new prenylated flavonoids which were evaluated for their cytotoxicity against human colon cancer cell line HT-29. Among the novel prenylated flavonoids, artorigidin B **(132)** was found to be cytotoxic against HT-29 with IC_{50} value of 3.4 μM, while artorigidin A **(130)** exhibited NF-κB inhibitory activity.[62] Evidence suggested that activation of NF-κB contributes to the development of several types of human cancers; in as such NF-κB presents a good target for cancer therapy.

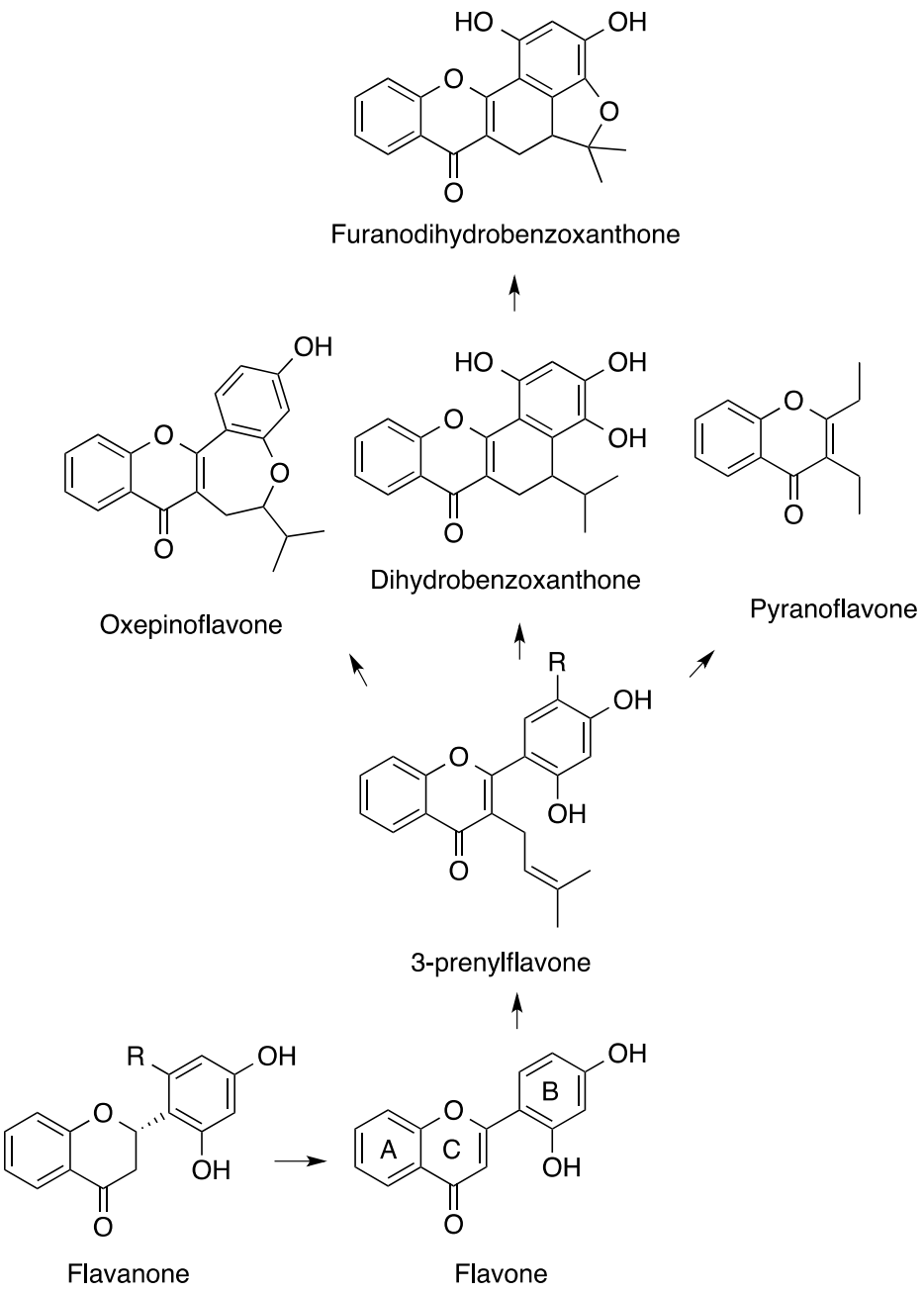

Figure 1.9: Distinct classes of flavonoids from *Artocarpus*[45]

Table 1.2: Flavonoids from *Artocarpus*

Plant	Class	Compound	Ref.
A. champedem (Synonym: *A. integer)*	Prenylflavone	**Artocarpones A** (**63**)	47
		Artoindonesianin R (**64**)	
		Heterophyllin (**65**)	
	Pyranoflavone	**Cyclochempedol** (**66**)	48
	Flavanone	Artoindonesianin E (**67**)	
		Heteroflavanone C (**68**)	
	Furanodyihydroxybenzoxanthone flavone	**Artocarpones B** (**69**)	
		Artonin A (**70**)	
	Pyranoflavones	Cycloheterophyllin (**15**)	
	Furanodyihydroxybenzoxanthone flavone	**Artoindonesianin A** (**71**)	49
	Oxepinoflavone	**Artoindonesianin B** (**72**)	
	Prenylflavone	**Artoindonesianin U** (**73**)	51
	Dihydrobenzoxanthone flavone	**Artoindonesianin V** (**74**)	
	Prenylflavones	**Artoindonesianin Q** (**75**)	50
		Artoindonesianin R (**76**)	
	Dihydrobenzoxanthone flavone	**Artoindonesianin S** (**77**)	
		Artoindonesianin T (**78**)	
A. heterophyllus	Flavanone	Artocarpanone A (**79**)	63
		Artocarpanone (**80**)	
	Flavone	**Artocarpetin A** (**14**)	
		Artocarpetin (**81**)	
		Norartocarpetin (**82**)	
	Prenylflavone	Artocarpin (**83**)	
		Cudraflavone B (**84**)	55
		Cudraflavone C (**13**)	
		6-prenylapigenin (**85**)	
		Kuwanon C (**86**)	
	Pyranoflavone	Brosimone I (**87**)	64
	Furanodyihydroxybenzoxanthone flavone	**Artonin A** (**70**)	65
	Dihydrobenzoxanthone flavone	**Artonin B** (**88**)	
	Furanodyihydroxybenzoxanthone flavone	**Artonin J** (**16**)	66
		Artonin K (**89**)	
		Artonin L (**90**)	
		Artonin Q (**91**)	67
		Artonin R (**92**)	
	Oxepinoflavone	**Artonin S** (**93**)	
	Furanodyihydroxybenzoxanthone flavone	**Artonin T** (**94**)	
	Flavone	**Artonin U** (**95**)	
A. heterophyllus x integer	Pyranoflavone	**2,8-Dihydroxy-3,10-dimethoxy-6-(2-methyl-1-propen-1-yl)-6*H*,7*H*-[1]benzopyrano[4,3-*b*]-[1]benzopyran-7-one** (**96**)	44

Table 1.2 continued

		Isocyclomulberin (**97**)	
		Cyclocommunol (**98**)	
		Cycloheterophyllin (**15**)	
	Chalcone	Flavokawain A (**99**)	
		Gemichalcone A (**100**)	
	Flavonone	Dihydromorin (**101**)	
		Sakuranetin (**102**)	
		Naringenin (**103**)	
		Artocarpanone (**80**)	
	Flavone	Isosinensetin (**104**)	
		Norartocarpetin (**82**)	
		Artonin Y (**105**)	
		Morusin (**106**)	
		Artocarpin (**83**)	
	Furanodihydroxybenxoxanthone	Artopeden A (**107**)	
		Artonin A (**88**)	
		Artonin F (**108**)	
	Dihydroxybenzoxanthone	Artoindonesianin S (**77**)	
	Isoflavone	5,3',4'-trimethoxy-6,7-methylene dioxyisoflavone (**109**)	
A. altilis Synonym: *A. communis)*	Prenylflavone	**Hydroxyartocarpin** (**110**)	[68]
		Morusin (**106**)	
		Artocarpin (**83**)	
		Artoflavone A (**111**)	[58]
	Pyranoflavone	**Cyclogeracommunin** (**112**)	
		Cycloartocarpin A (**113**)	[68]
	Flavanone	**Arcommunol C** (**114**)	[69]
		Arcommunol D (**115**)	
	Chalcone	**5'-geranyl-3,4,2',4'-tetradyhydroxydihydrochalcone** (**116**)	
		Isolespeol (**117**)	[57]
		5'-geranyl-2',4',4-trihydroxychalcone (**118**)	
		3,4,2',4'-tetradyhydroxy-3'-geranyldihydrochalcone (**119**)	
	Furanodihydrobenzoxanthone	Cycloartobiloxanthone (**120**)	[68]
		Artoindonesianin V (**74**)	
A. gomezianus	Prenylflavone	**Artogomezianone** (**121**)	[70]
A. rotunda	Prenylflavone	**Artoindonesianin L** (**122**)	[59]
		Artonin E (**123**)	
	Furanodihydrobenzoxanthone	Cycloartobiloxanthone (**120**)	
		Artonin M (**124**)	
	Quinonoxanthone	Artonin O (**125**)	
A. elasticus	Oxipinoflavone	**Artoindonesianin E1** (**126**)	[53]
	Prenylflavone	Artocarpin (**83**)	
		Cycloartocarpin (**127**)	

Table 1.2 continued

	Pyranoflavone	Cudraflavone A (**128**)	[53]
A. rigida	Pyranoflavone	**Cyclorigidol** (**129**)	[62]
	Quinonoxanthone	**Artorigidin A** (**130**)	
		Artorigidin C (**131**)	
		Artonin O (**125**)	
	Pyranoflavone	**Artorigidin B** (**132**)	

Bold highlights denote novel compounds isolated from respective plants.

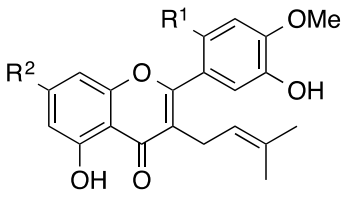

63 $R^1 = R^2 = OH$
64 $R^1 = OMe$, $R^2 = OH$
75 $R^1 = H$, $R^2 = OMe$
76 $R^1 = OMe$, $R^2 = OH$

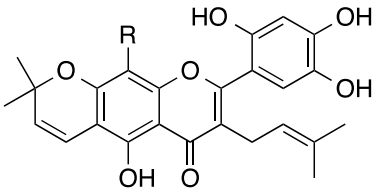

65 R = prenyl
73 R = geranyl

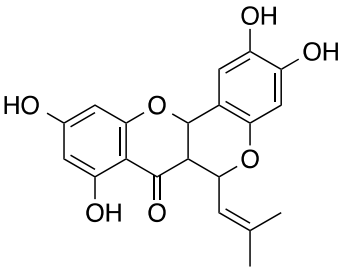

66

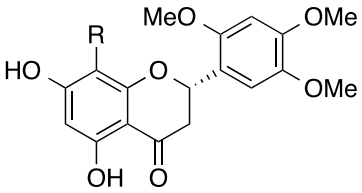

67 R = H
68 R = prenyl

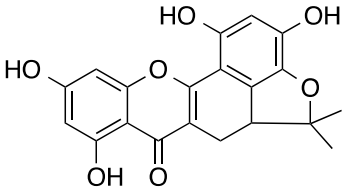

69

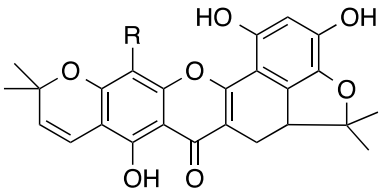

70 R = prenyl
71 R = geranyl

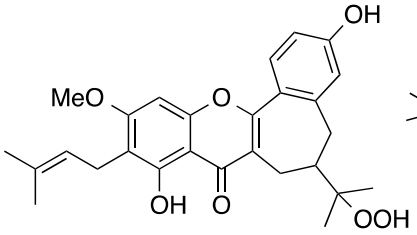

72

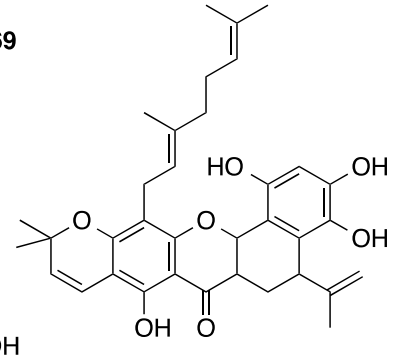

74

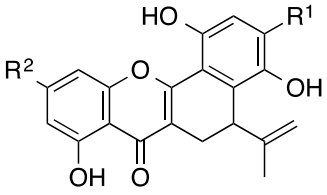

77 R^1 =OMe, R^2 = OMe
78 R^1 = OMe, R^2 = OH

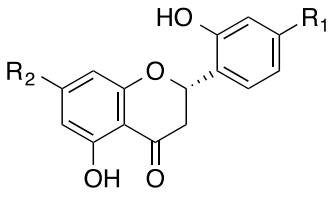

79 $R_1 = R_2$ = OMe
80 R_1 = OH, R_2 = OMe

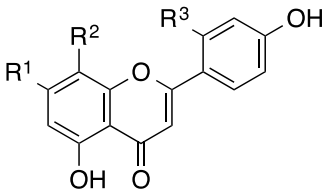

81 R^1 = OMe, R^2 = H, R^3 = OH
82 R^1 = OH, R^2 = H, R^3 = OH
95 R^1 = OMe, R^2 = prenyl, R^3 = H

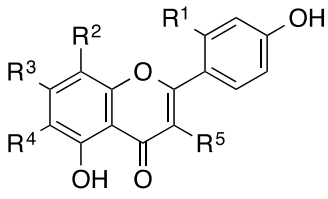

83 R^1 = OH, R^2 = H , R^3 = OMe, $R^4 = R^5$ = prenyl
85 $R^1 = R^2 = R^5$ = H, R^3 = OH, R^4 = prenyl
86 $R^1 = R^3$ = OH, $R^2 = R^5$ = prenyl, R^4 = H

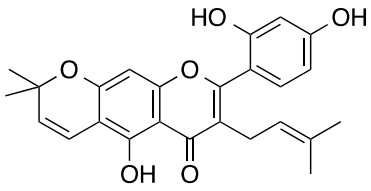

84

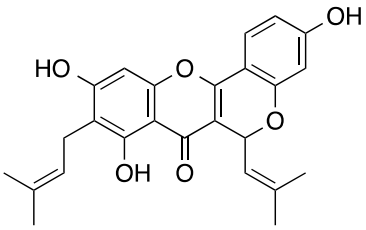

87

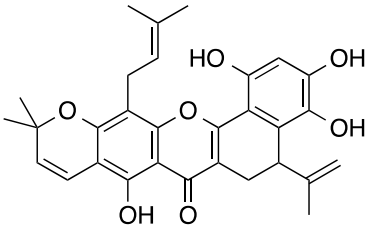

88

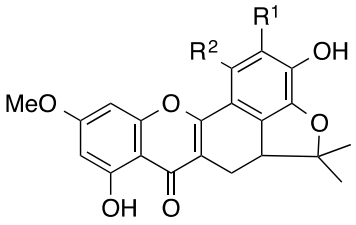

89 R^1 = H, R^2 = OH
90 R^1 = H, R^2 = OMe
94 R^1 = prenyl, R^2 = OH

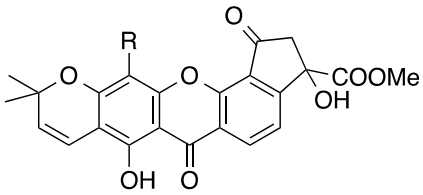

91 R =
92 R =

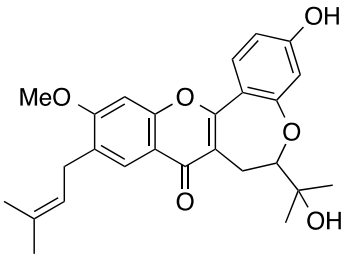

95

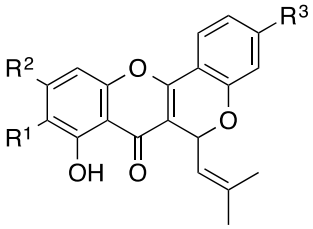

96 R^1 = H, R^2 = OMe, R^3 = OMe
97 R^1 = Prenyl, R^2 = OH, R^3 = OH
98 R^1 = H, R^2 = OH, R^3 = OH

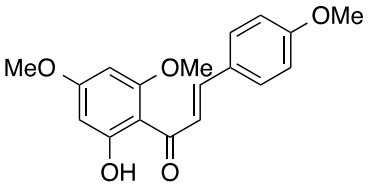

99

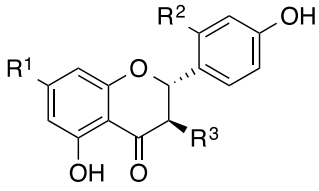

101 R^1= R^2 = R^3 = OH
102 R^1 = OMe, R^2 = R^3 = H
103 R^1 = OH, R^2= R^3 = H

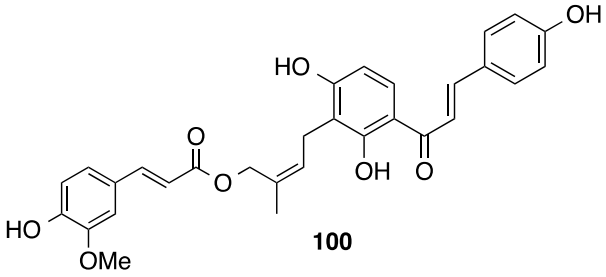

100

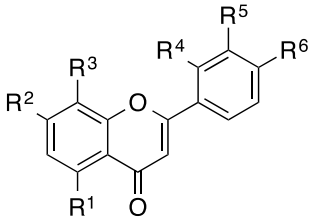

104 R^1= R^2 = R^3 = R^5 = R^6 = OMe, R^4 = H
105 R^1= R^2 = R^4 = R^6 = OH, R^3 = R^5 = H

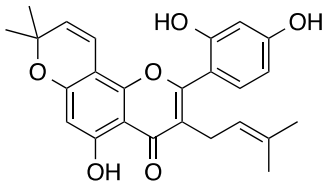

106

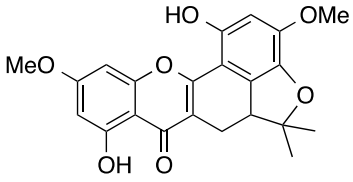

107

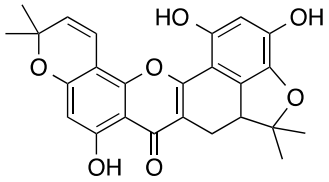

108

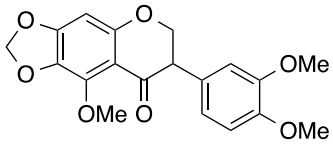

109

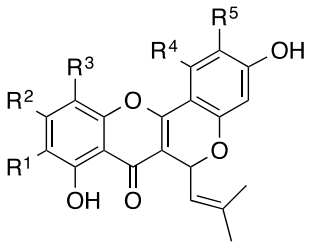

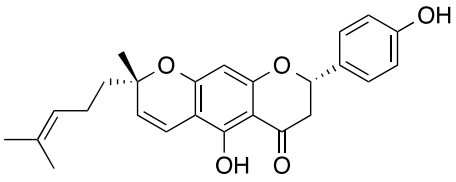

114

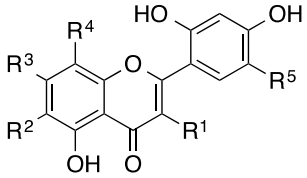

112 R^1= prenyl, R^2 = OMe, R^3 = R^5 = H, R^4 = OH
113 R^1= R^5 = H, R^2 = R^4= OH, R^3 = geranyl
127 R^1 = prenyl, R^2= OMe, R^3 = R^4 = R^5 = H
129 R^1 = R^3 = prenyl, R^2 = R^5= OH, R^4 = H

110 R^1= R^2 = prenyl, R^3 = OMe, R^4 = R^5 =H

111 R^1= prenyl, R^2 = R^5 = H, R^3 and R^4 =

121 R^2= prenyl, R^3= OMe, R^4 = R^5 = H, R^1=

122 R^1= geranyl, R^5= OH, R^2 and R^3 =

123 R^1= geranyl, R^2= H, R^5= OH, R^3 and R^4 =

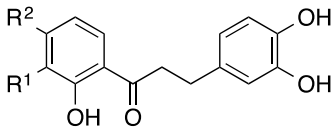

115 R^1 and R^2=

119 R^1= geranyl, R^2= OH

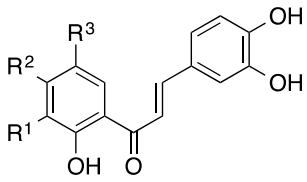

116 R^1= H, R^2= OH, R^3= geranyl
117 R^1= H, R^2 and R^3=
118 R^1= H, R^2= OH, R^3= geranyl

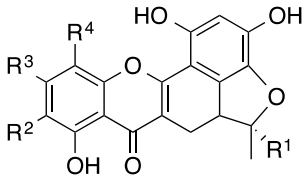

120 R^1= R^2= H, R^3 and R^4 =

124 R^1= prenyl, R^4= H, R^2 and R^3=

132 R^1= R^2 = prenyl, R^3= OH, R^4= H

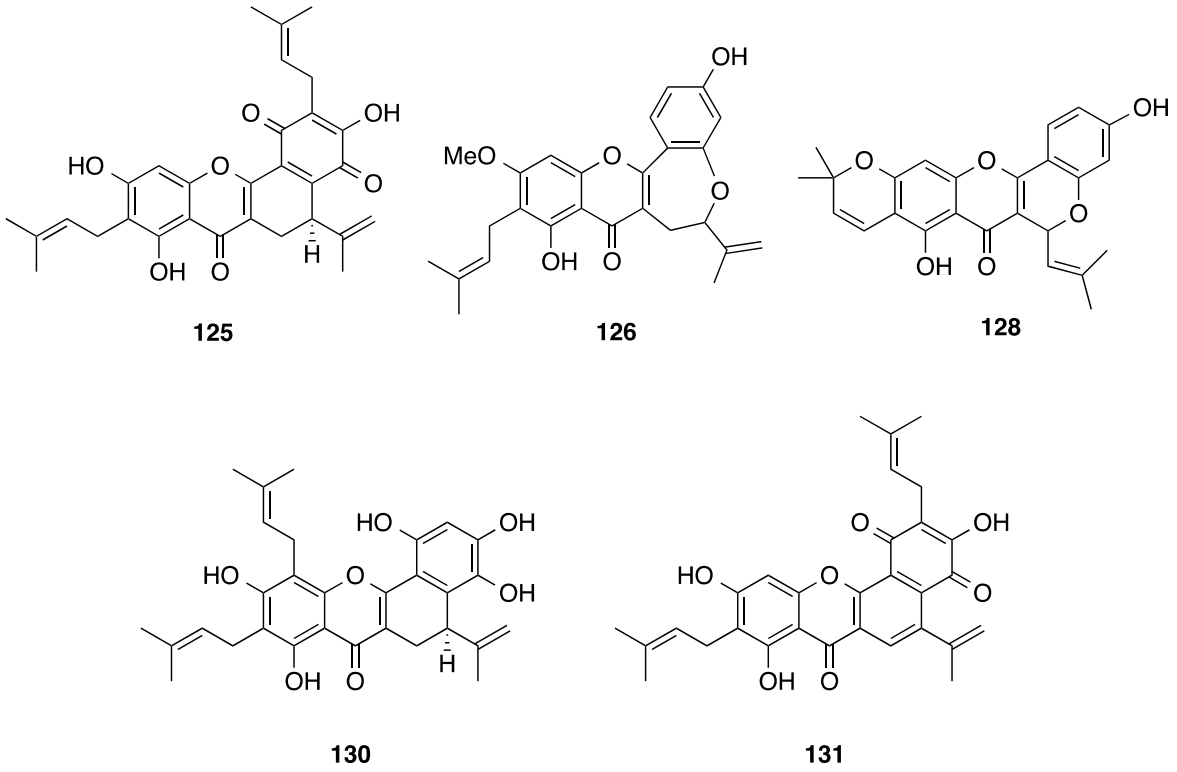

Figure 1.10: Flavonoids from *Artocarpus spp.*

1.6 Genus *Macaranga*

Macaranga is the largest genera of the Euphobiaceae family, comprising of approximately 300 species, 40 of which are found growing in the secondary forests of Malaysia.[71,72] Native to tropical Africa, Madagascar, South-East Asia, Australia and the Pacific region, they recolonize almost any undisturbed terrestrial habitat.[73] These plants are noted for their mutualistic association with ants due to the plant's hollow stems which serve as shelter and sometimes provide nectar for the ants, while the plant in return receives protection from herbivorous insects.[74] Traditionally, various species of *Macaranga* are used to treat swellings, cuts and boils.[75] The sap of the young shoots of *M. triloba* and *M. gigantea* are used to treat fungal infections while the leaf decoction is consumed for

stomachaches.[76] *M. hypoleuca* has been used as a febrifuge, expectorant and anti-spasmodic.[77]

1.6.1 Phytochemicals and bioactivity of *Macaranga* flavonoids

The *Macaranga* genus encompasses a wide variety of species, many of which still remain unexplored in regards to phytochemical and biological studies. To date approximately 26 *Macaranga* species (out of 300 plant species) have been studied, and resulted in the identification of close to 190 secondary metabolites.[74] Most of the isolated compounds have been reported from the leaves while approximately 10% of the isolated compounds were from other plant parts.[74] Phytochemical investigation revealed that flavonoids, particularly the isoprenylated and geranylated flavonoids and stilbenes, are the major phenolic constituents of *Macaranga* plants hence, are most likely responsible for most of the biological activities found in the plants of this genus.[78,79]

Known and novel flavonoids from the selected *Macaranga* plants are shown in Table 1.3 and Figure 1.11. A majority of the flavonoids isolated from the *Macaranga* plants were flavonoids of the flavanone variety. The occurrence of dihydroflavonol and flavones in the *Macaranga* genus are limited.[80] To date, dihydroflavonol derivatives have been isolated only from *M. alnifolia*[78], *M. conifera*[81], *M. pruinosa*[82] and *M. lowii*[80] while the presence of flavone was reported in *M. lowii*[80] and *M. gigantea*[83]. Therefore, the presence of these flavonoids may serve as a form of markers for a certain group of *Macaranga*.

Phytochemical and biological studies on the wide array of compounds from various *Macaranga* species have uncovered many bioactive constituents, particularly as potential anti-cancer agents. Phytochemical investigation of the leaves of *M. tanarius* yielded seven novel prenylflavones which were characterized as macaflavones A-G **(140-146)**. Biological

evaluation of the isolated compounds showed that macaflavone G **(146)** was the most active (IC_{50} ~ 10 μM) against oral and lung cancers, KB and A549 cell lines, respectively.[79] Cytotoxic evaluation of the flavonoids macagigantin **(167)**, glysperin A **(168)** and apigenin **(169)** from *M. gigantea* showed that **168** and **169** possessed moderate cytotoxicity, while **167** was only weakly active. This suggests that the presence of a farnesyl substituent at A-ring of the flavonoid structure (Figure 1.6) in **167** may be the cause of reduced cytotoxicity, while the presence of the isoprenyl substituent in the B-ring in **168** and **169** enhances cytotoxicity.[83] Cytotoxicity of the flavonoid macakurzin C **(175)** isolated from *M. kurzii* showed cytotoxicity against KB cells, while possessing moderate acetylcholisnestrace (AChE) inhibitory activity.[84] AChE inhibitors are therapeutic agents for the treatment of neurological disorders by preventing the hydrolysis of acetylcholine (neurotransmitter) thus making more acetylcholine avalaible at the cholinergic synapses.

In a study of bioactive compounds from *M. triloba*, three quercetin derivatives (**161**-**163**) were found to show specific cancer fighting potential, where **162** showed cytotoxicity towards murine hepatoma Hepa 1c1c7 cells, while compounds **161** and **162** showed promising activities in the Quinone Reductase (QR) assay indicating their potential as chemopreventive agents.[85] Lonchocarpol A **(150)**, a prenylated flavanone from the leaves of *M. conifera* showed strong inhibitory activities in both cyclooxygenase-1 (COX-1) and cyclooxygenase-2 (COX-2) and also exhibited significant inhibitory activities in the development of 7,12-dimethyl-benz(a)anthracene (DMBA)-induced pre-neoplastic lesions in mouse mammary organs, rendering this compound as a potential cancer chemopreventive agent.[81] The COX pathway is responsible for the regulation of prostaglandin under acute inflammation conditions hence, regulation of this pathway is a promising approach for cancer chemoprevention.[86,87] Flavan and stilbenoid derivatives have

been known to exhibit COX-1 and COX-2 inhibitory activites.[88,89] Since flavanones make up the major constituents of the *Macaranga* plants, they are potentials chemopreventive agents.

Many terpenoids are known to be biologically active.[74,90] Likewise, a wide range of bioactivities are described for flavonoids.[91–93] As a result, the combination of these two types of compounds could potentially lead to more active hybrid compounds, or compounds with new biological properties. Denticulaflavonol **(165)** isolated from *M. deticulata* is the first natural hybrid compound constituting a diterpene and a flavonol.[94] The synthesis of **165** along with macarangin **(166)** and several prenylflavonoids were attempted by Basabe *et al*.[53] whom later reported that the synthesized hybrid compounds showed moderate anti-tumorial activity towards the lung cancer (A549), colon cancer (HT-29), cervical cancer (HeLa) and human leukemia (HL-60) cell lines.

Table 1.3: Flavonoids from *Macaranga* plants

Plant	Class	Compound	Ref.
M. tanarius	Prenyl flavanone	**Tanariflavanone A (133)** **Tanariflavanone B (134)** **Tanariflavanone C (135)** **Tanariflavanone D (136)** Nymphaeol A **(137)** Nymphaeol B **(138)** Nymphaeol C **(139)** Tanariflavanone B **(134)**	95 96 79
		Macaflavanone A (140) **Macaflavanone B (141)** **Macaflavanone C (142)** **Macaflavanone D (143)** **Macaflavanone E (144)** **Macaflavanone F (145)** **Macaflavanone G (146)**	
M. conifera	Prenyl flavanone	**5-Hydroxy-4′-methoxy-2″,2″-dimethylpyrano-(7,8,6″,5″)flavanone (147)**	81

Table 1.3 continued

		5,4′-Dihydroxy-[2″-(1-hydroxy-1-methylethyl)dihydrofurano]-(7,8,5″,4″)flavanone (148) 5,7-Dihydroxy-4′-methoxy-8-(3-methylbut-2-enyl)flavanone **(149)** Lonchocarpol A **(150)** Sophoraflavanone B **(151)** 5,7-Dihydroxy-4′-methoxy-8-(2-hydroxy-3-methylbut-3-enyl)flavanone **(152)** Tomentosanol D **(153)**, Lupinifolinol **(154)**, **(2*S*)-5,7,3'-Trihydroxy-4'-methoxy-8-(3''-methylbut-2''-enyl)-flavonone (155)** (2*S*)-5,7,3',5'-Tetrahydroxy-6,8-(3",8"-dimethylobut-2",7"-dienyl)flavanone **(156)**	97
	Flavonol	Isolicoflavonol **(157)**	81
M. triloba	Flavanone	**Malaysianone A (158)**	98
	Prenylated flavanonne	6-Prenyl-3'-methoxy-eriodictyol **(159)** 6-Farnesyl-3',4',5,7-tetrahydroxyflavanone **(160)** Nymphaeol B **(138)** Nymphaeol C **(139)**	99
	Flavone	3,7,3',4'-Tetramethylquercetin **(161)** 3,7,3'-Trimethylquercetin **(162)** 3,7-Dimethylquercetin **(163)**	85
M. denticulata	Prenylated flavone	**3-*O*-Methyl-macarangin (164)** **Denticulaflavonol (165)** Macarangin **(166)**	94
	Flavonone	Sophoraflavanone B **(151)**	
M. gigantea	Farnesyl flavonol	**Macagigantin (167)** Glyasperin **(168)** Apigenin **(169)**	83
M. lowii	Isoprenylated dihydroflavonol	**Macalowiinin (170)**	80
	Flavonone	4'-*O*-Methyl-8-isoprenylnaringenin **(171)**	
	Flavone	4'-*O*-Methyl-5,7,4'-trihydroxyflavone **(172)**	
M. kurzii	Flavonol	**Macakurzin A (173)** **Macakurzin B (174)**	84

Table 1.3 continued

M. kurzii	Flavonol	**Macakurzin C (175)**	84
M. pruinosa	Flavonol	**Macapruinosin D (176)** **Macapruinosine E (177)** **Macapruinosine F (178)**	100
M. sampsonii	Prenylflavanol	Papyriflavonol A **(179)** **Macaranones A (180)** **Macaranones B (181)** **Macaranones C (182)** **Macaranones D (183)**	101
M. anifolia	Geranylated diydroflovonol	**Anifoliol (184)**	78
	Geranylated flavanones	Bonnaniol A **(185)** Diplacol **(186)** Bonnanione A **(187)**	

Bold highlights denote novel compounds isolated from respective plants.

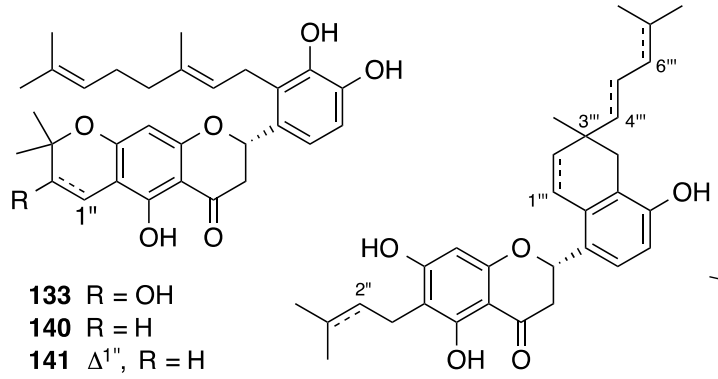

133 R = OH
140 R = H
141 $\Delta^{1''}$, R = H

134 $\Delta^{1'''}$ $\Delta^{2'''}$ $\Delta^{6'''}$ 3''' *R*
142 $\Delta^{1'''}$ $\Delta^{2'''}$ $\Delta^{6'''}$ 3''' *S*
143 $\Delta^{2'''}$ $\Delta^{4'''}$ $\Delta^{6'''}$ 3''' *R*
144 $\Delta^{2''}$ $\Delta^{4'''}$ $\Delta^{6'''}$ 3''' *S*
145 $\Delta^{2''}$ $\Delta^{6'''}$ 3''' *S*
146 $\Delta^{2''}$ $\Delta^{6'''}$ 3''' *R*

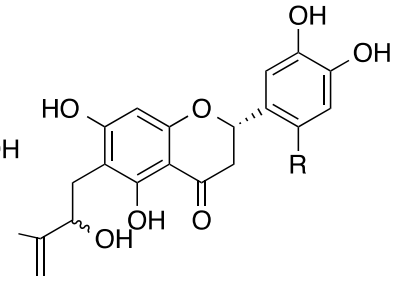

135 R = geranyl

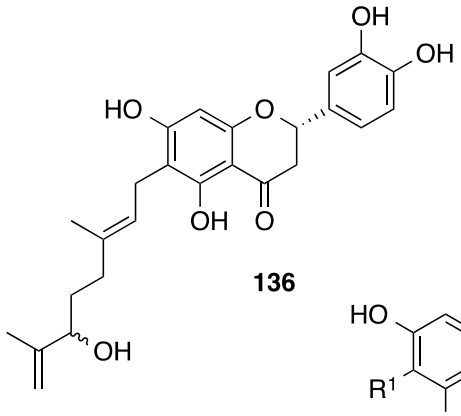

136

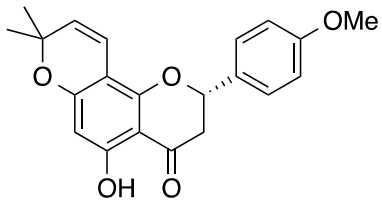

147

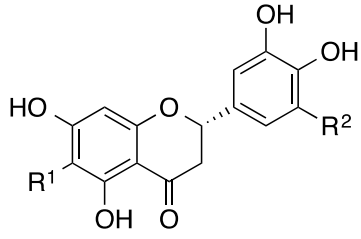

137 R^1 = geranyl, R^2 = H
138 R^1 = H, R^2 = geranyl
139 R^1 = prenyl , R^2 = geranyl

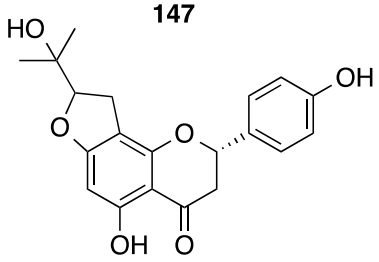

148

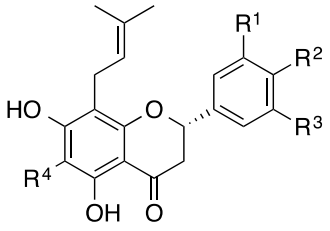

149 $R^1 = R^3 = R^4 = H$, $R^2 = OMe$
150 $R^1 = R^3 = H$, $R^2 =$ OH, $R^4 =$ prenyl
151 $R^1 = R^3 = R^4 = H$, $R^2 = OH$
155 $R^1 = R^4 = H$, $R^2 = OMe$, $R^3 = OH$
156 $R^1 = R^3 = OH$, $R^2 = H$, $R^4 =$ prenyl

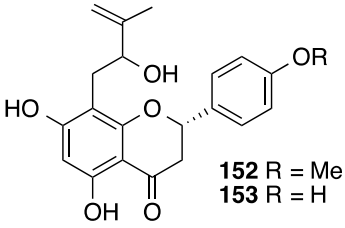

152 R = Me
153 R = H

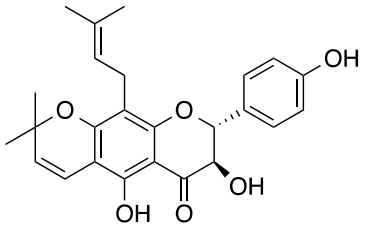

154

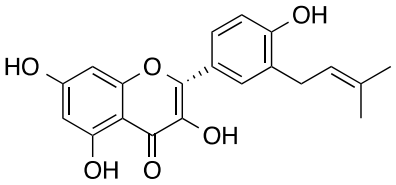

157

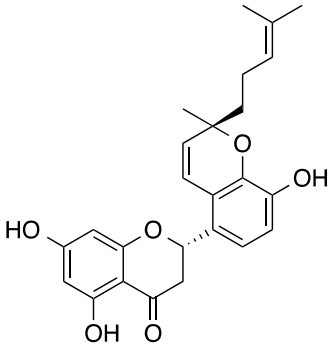

158

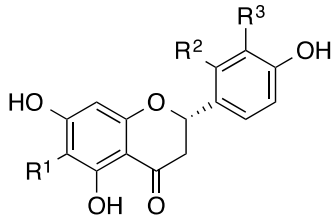

159 R^1 = prenyl, $R^2 = H$, $R^3 = OMe$
160 R^1 = farnesyl, $R^2 = H$, $R^3 = OH$

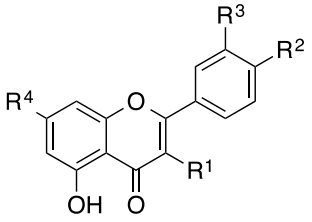

161 $R^1 = R^2 = R^3 = R^4 = OMe$
162 $R^1 = R^2 = R^4 = OMe$, $R^4 = OH$
163 $R^1 = R^4 = OMe$, $R^2 = R^3 = H$

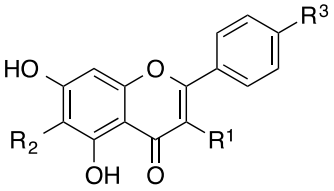

164 $R^1 = OMe$, R^2 = geranyl, $R^3 = OH$
166 $R^1 = OH$, R^2 = geranyl, $R^3 = OH$
172 $R^1 = H$, $R^2 = H$, $R^3 = OMe$

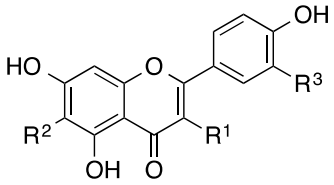

167 $R^1 = OH$, R^2 = farnesyl, $R^3 = H$
168 $R^1 = OH$, R^2 = prenyl, R^3 = prenyl
169 $R^1 = R^2 = R^3 = H$

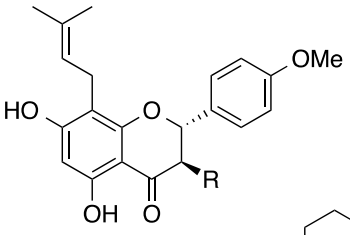

170 R = OH
171 R = H

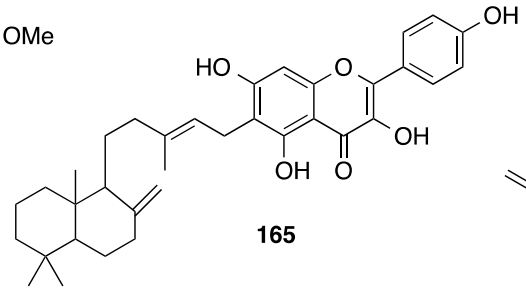

165

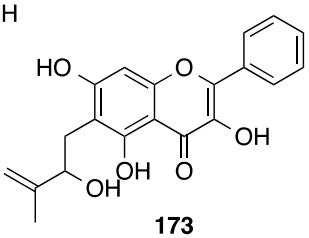

173

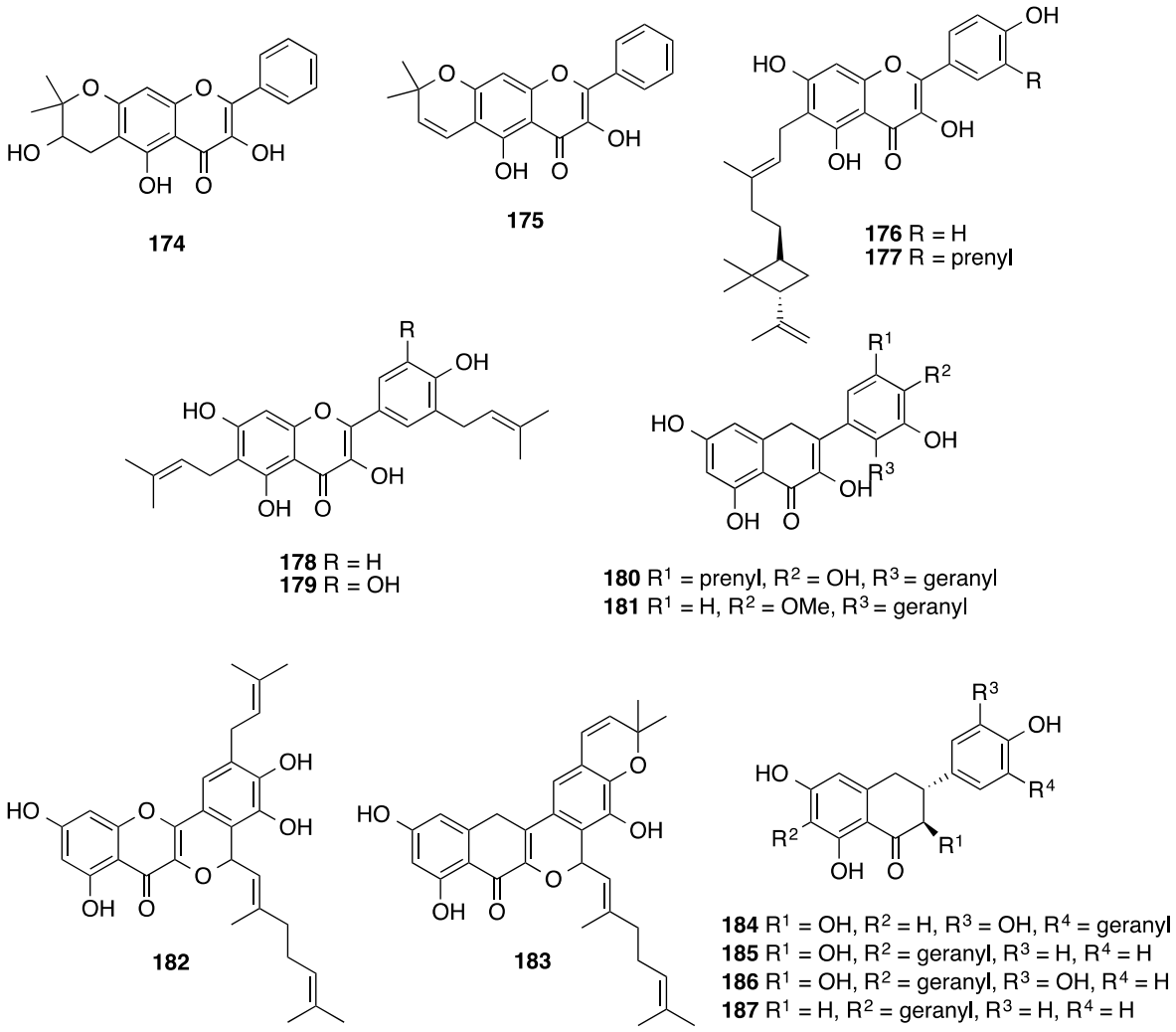

Figure 1.11: Flavonoids from *Macaranga spp.*

1.7 Anti-cancer activity of phenanthroindolizidine alkaloids and flavonoids

Phenanthroindolizidine alkaloids and flavonoids have been touted as promising anti-cancer agents because of their potent cytotoxicity with a broad range of cellular targets. The phenanthroindolizidine alkaloid, tylocrebrine **(7)**, was one of the first members of its class to advance into clinical trial soon after its discovery in the early 1960's but was later aborted due to central nervous system (CNS) toxicity which manifested as disorientation and ataxia.[102] However, medicinal interest in the phenanthroindolizidines was revived in

1990's when a number of these compounds were found to be highly potent with GI_{50} values in the low nanomolar to picomolar range. The National Cancer Institute (NCI) screening data from a panel of 60 tumor cell lines indicated that most of the alkaloids showed little discrimination between malignant and normal cells. However, the NCI collective data also found that these alkaloids retained their potency on drug sensitive and multidrug resistant (MDR) cell lines.[18]

Contrary to alkaloids, flavonoids have little toxicity and are common components in the human diet particularly in fruits, vegetables and seeds, therefore presenting a good oppurtunity as chemopreventive agents. They have been shown to dislay a remarkable spectrum of biochemical and pharmacological activities such as anti-inflammatory, antioxidant, anti-viral and anti-cancer.[102] Epidemiology studies showed lower risk of colon, prostate and breast cancers in Asians who generally consume more vegetables, fruits and tea than populations in the West hence, implicating that the flavonoid components in Asian diets may play a role as natural chemopreventive and chemotherapeutic agents.[104] The encouraging results of anti-cancer effects in preclinical studies have encouraged the clinical trials of flavonoids in humans. Most recent is the emergence of flavopiridol, a novel semisynthetic flavone analogue (flavonoid alkaloid) of rohitukine, a leading anti-cancer compound from an indigenous tree from India.[105] Flavopiridol was reported to inhibit cyclin-dependent kinases (CDKs) with cell cycle arrest at G1/S and G2M, induce apoptosis, promote differentiation, inhibit angiogenesis and modulate transcriptional events.[105] Flavopiridol, marketed under the name Alvocidib, is currently under clinical trial by Sanofi–Aventis for refractory/relapsed chronic lymphocytic leukaemia. If licensed, Alvocidib will be the first CDK inhibitor and may serve as an additional option for patients who generally have poor prognosis.

1.8 Structure-activity relationships

Structure activity studies have demonstrated common features of compounds that are highly important to their different activities. Due to their diverse and potent pharmacological actions, flavonoids and alkaloids continue to be targets for synthesis, modification, and structure-activity relationship (SAR) studies. The most recent SAR of phenanthroindolizidine alkaloids were conducted by Wang *et al.*[106] and Chemler.[20] Notable key features highlighted by Chemler[20] were the effect of the phenanthrene substitution pattern, the presence or lack of indolizidine ring fusion, the presence or lack of C-14-hydroxy groups on the indolizine ring and the oxidation state of the amine (e.g., *N*-oxides *vs.* free amine counterpart). These features were later supported by Wang *et al.*[106] who synthesized a series of phenanthroindolizidine alkaloids and their 14-amino derivatives for further evaluation of their anti-tumor activities against A549 and HL60 cell lines. Figure 1.12 shows the comparison of SAR between antofine and the effect on the cytotoxic activity of the different structural features of its analogues. Collectively, their findings indicated that: (1) hydroxy or alkoxy substituents in the phenanthrene system are mandatory for biological activity (e.g, **133** and **50**) but introducing hydroxy group at C-14 reduces its effectiveness (e.g., **60**), (2) *Seco*-analogues are substantially less active *in vitro* hence suggesting the importance of phenanthrene ring fusion (e.g., **50** *vs* **53**), (3) the oxidation state of phenanthroindolizidine amines (*N*-oxides) (e.g., **50** *vs* **46**) affects *in vitro* growth negatively, (4) introducing amino groups at C-14 was found to reduce cytotoxic activity (e.g., **50** *vs* **134**) which may be due to steric effects of the phenanthrene unit, however, this increased polarity may be beneficial to offset CNS side effects despite slight reduction in activity.[106]

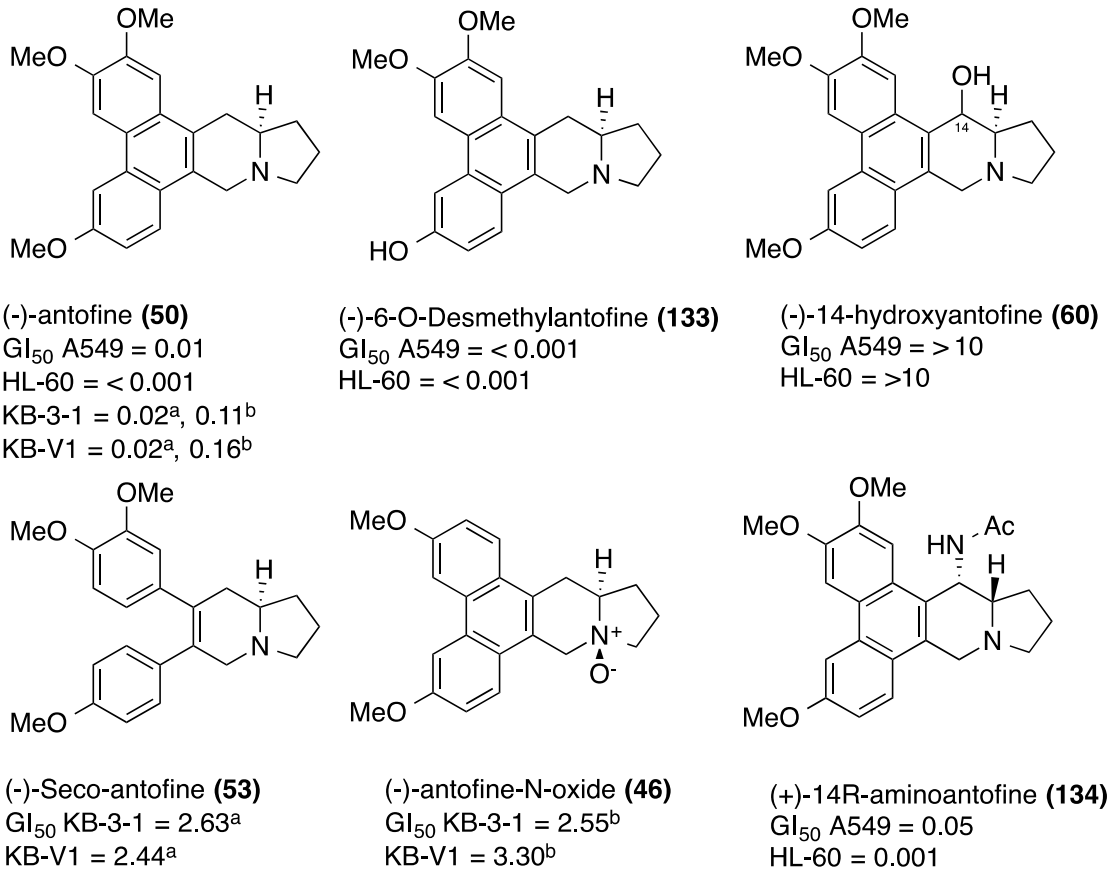

GI_{50} (μM) compiled from Wang *et al.*[106]: A549 = human lung adenocarcinoma, HL-60 = human promyelocytic leukemia cell line. [a] GI_{50} (μM) values measured from Stærk *et al.*[39], [b]GI_{50} (μM) from Stærk *et al*[18]: KB-3-1 = cervix carcinoma (HeLa deravative), KB-V1 = multidrug resistant cervical carcinoma.

Figure 1.12: Structure activity relationship of antofine analogues

Extensive research has been conducted on the potential anti-cancer effect of flavonoids. The underlying mechanisms of the different activities exhibited by flavonoids were alleged to be highly associated with specific structural features of the molecules.[107] Among the features identified include the presence of isoprenoid substituents in the flavonoid structure where an increasing number of such substituents showed enhanced cytotoxicity.[55] The enhanced biological activity with the presence of isopenoid moieties is believed to be due to the increase hydrophobicity of the molecule which enhances the

overall affinity for biological membranes and protein interaction.[55,107] Contrarily, flavonoids with sugar substituents (flavonoid glycosides) are generally rendered ineffective irrespective of the nature and position of the sugar moiety due to its reduced hydrophobicity which hinders them from entering the cytoplasm, hence decreasing its efficacy.[55] The presence of the C-2–C-3 double bond in the C-ring are considered as a general feature that contributes to the anti-cancer activity of flavonoids.[91,107] Accordingly, flavones and flavonols generally have better anti-cancer effects as compared to other sub-classes. Furthermore, Depint *et al.* inferred that role of the heterocyclic C-ring in the flavonoid structure is so crucial that any variation to its structure may lead to loss of the planarity of the flavonoid structure and thus reducing potency, such as in the case of flavanones and chalcones. The comparisons of activity observed by the structurally related flavonoids are shown in Figure 1.13.

Although there seem to be consistent relationships between flavonoids and phenanthroindolizidine structures and their cellular activities in accordance with literature, the innate differences in cell lines, anti-cancer mechanisms, test systems and the lack of internal standards used in most SAR studies makes generalization of SAR properties virtually impossible. As such, this information may serve only as a suggestive indicator of possible bioactivity.

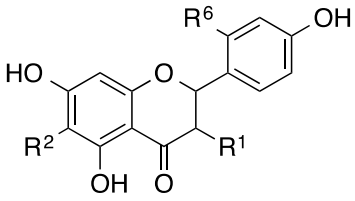

Flavonoids	R^1	R^2	R^3	IC_{50}[a]
Curdraflavone C (**13**)			OH	9.2
3-prenylapigenin (**135**)	H		H	32.5
Morin (**136**)	OH	H	OH	170.0

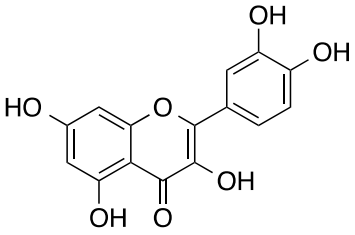

Flavonol: Quercetin (**21**)
Cell viability (%) = 20[b]

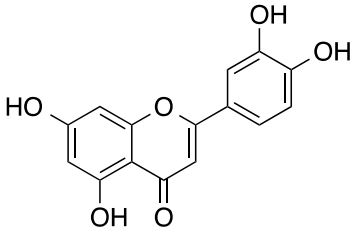

Flavone: Luteolin (**137**)
Cell viability (%) = 28[b]

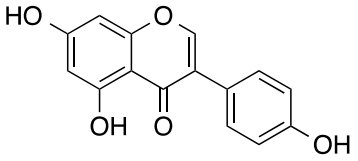

Isoflavone: Genistein (**138**)
Cell viability (%) = 65[b]

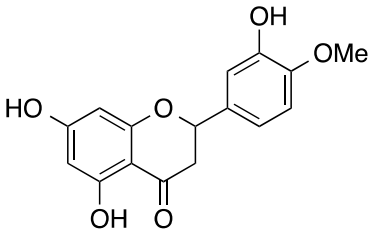

Flavonone: Hesperetin (**139**)
Cell viability (%) = 99[b]

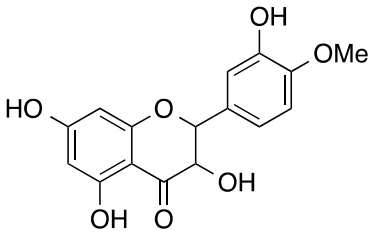

Flavanonol: Taxifolin (**140**)
Cell viability (%) = 92[b]

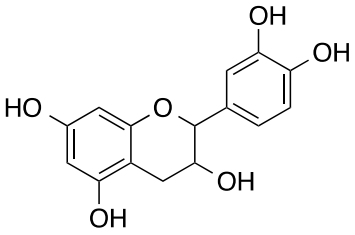

Flavanonol: Catechin (**141**)
Cell viability (%) = 97[b]

[a]IC_{50} (μM) compiled from Arung *et al.*[55] on B-16 bmelanoma cell line; [b]Percentage of cell viability (vs control) of HT-29 colon adenocarcinoma cell line following treatment with 60 μM of the selected compounds as reported by Agullo *et al.*[108].

Figure 1.13: Comparison of cytotoxic activity between structurally related flavanoids

1.9 Anti-cancer mechanisms of action

The anti-cancer properties of phenanthroindolizidine alkaloids and flavonoids have been explored up to the biochemical level and several targets have been proposed. Given the complexity of cancer as a disease, the multi-targeted approach of these compound classes may be beneficial in controlling the onslaught of tumorigenesis. Among major targets evoked by phenanthroindolizidine alkaloids and flavonoids are as follows:

1.9.1 Anti-proliferation/cytotoxicity

The inhibition of protein biosynthesis is the most extensively studied mechanism for phenanthroindolizidine's anti-cancer activity aside from its inhibitory action on RNA and DNA synthesis. Since protein synthesis is more potently inhibited than nucleic acid synthesis, this is probably the primary mode of growth inhibition for the phenanthroindolizidines. This was supported by Donaldson *et al.*[109] who first reported that tylocrebrine **(7)** and tylophorine **(8)** inhibited protein synthesis in Ehlich ascites-tumor cells by inhibiting the incorporation of leucine into protein. RNA synthesis was however not markedly affected.[109] In a separate study, tylocrebrine **(7)** was on the contrary found to inhibit both RNA and DNA synthesis by the lack of thymidine and uridine incorporation, respectively.[110] More recently, the phenanthroindolizidine derivative, YPC-100157, showed significant correlation between protein synthesis and its growth inhibition in A549 and HT-29 cancer cell lines.[111] It was postulated that YPC-100157 inhibited protein synthesis by blocking chain elongation, similar to tylophorine analogues.[110] Aberrantly, protein synthesis highly contributes to tumerogenesis where there is a higher threshold for protein synthesis in transformed cells which positively correlates to higher rate of translation thus, higher rate of cell proliferation. As such, it can be assumed that phenanthroindolizidines

exert their cytotoxic effect primarily, but not necessarily exclusive, through protein synthesis inhibition.

In flavonoids, the molecular mechanism of anti-proliferation may involve the inhibition of pro-oxidant process. This is because growth promoting oxidants (reactive oxygen species, ROS) are generally believed to be major catalysts of tumor promotion and progression.[112] The production of ROS is triggered in the events of inflammation where it is responsible for causing DNA damage, increased rate of mutations and over-secretion of growth factors. In light of this, inhibitors that target the production of ROS or mediators of inflammation are important therapeutic strategies for malignancy. Flavonoids are good candidates in this sense as they are effective in inhibiting xanthine oxidase (an enzyme that generates ROS),[113] COX-2 or LOX (inflammation mediators),[114] and therefore inhibit tumor cell proliferation.

1.9.2 Cell cycle arrest

The cell cycle is composed of G1 (cells that are committed to the cell cycle), S (synthesis of DNA), G2 (DNA damage checkpoints), and M (separation of daughter cells) phases where entry into each phase is controlled by a series of checkpoint pathways. Progression throughout the cell cycle is driven by cyclin-dependent kinases (CDK). Tumor-assosicated cell cycle perturbations are often linked to defective CDKs. Therefore, modulators of these components could potentially correct the faulty regulation that leads to uncontrolled cell proliferation in cancer. Checkpoints at G1/S and G2/M in the cell cycle have been found to be perturbed by both phenanthroindolizidine alkaloids such as antofine **(53)**[115] and tylophorine **(11)**,[116] and flavonoids such as quercetin **(24)**[117], kaempherol **(22)**[118]

and silymarin,[119] while flavopiridol, a flavonoid-derived chemotherapy drug is known as the first CDK inhibitor currently in clinical trial.[105]

1.9.3 Induction of apoptosis

Apoptosis is an induced cell death which is essential in the elimination of damaged or unwanted cells hence, keeping the damaged cells from proliferating and passing the damage to succeeding generation of cells. Deregulation of apoptosis plays a critical role in tumor oncogenesis. Literature suggests that the anti-cancer activities induced by flavonoids may be due to the induction of apoptosis selectively towards certain cancer cells but sparringly in normal cells.[112] Although the molecular mechanisms in which flavonoids induce apoptosis have not been established, several mechanisms which are thought to be involved include the release of cytochrome C, activation of caspases-3 and 9, alteration in Bax/Bcl2 (proapoptotic protein/oncogene-derived protein) ratio, and the down regulation of nuclear transcription factor kappaB (NF-kappaB) expression.[112,120] Apigenin **(104)**, quercetin **(21)**, and kaempherol **(22)** were among several other flavonoids which are able to induce apoptosis.[120–122] However, no evidence of apoptosis was observed for antofine **(53)** (in A549 and Col2), tylophorine **(8)** and its analogues (in HepG2 and KB) although the compounds showed potent inhibition of growth.[115,123] From these data, it is suggestive that the induction of apoptosis is not a significant target for the phenanthroindolizidines.

1.9.4 Cellular promotion and differentiation

Differentiation is the process which immature cells become mature cells that are capable of carrying out specific functions. In cancer, deregulation of growth control ultimately leads to a selection of cells that replicate and yet fail to respond to differentiation

and maturation signals.[112] As such, the induction of differentiation is a useful target for cancer therapy and prevention as this may lead to the eventual elimination of tumorigenic cells. Both phenanthroindolizidines and flavonoids were found to induce differentiation in a panel of cell lines. Tylophorine **(11)** [123] and its analogues have been reported to induce cell differentiation in HepG2 cells while the flavones genistein, apigenin **(104)**, luteolin, quercetin **(24)**, and phloretin were found to induce cell differentiation in human acute mylelogenous leukemia HL-60 cell into granulocytes and monocytes.[117]

1.9.5 Inhibition of angiogenesis

Angiogenesis is a process of growth of new blood vessels and is regulated by a variety of angiogenic and angiostatic factors. It is prominent in embryos but rather infrequent in adults, except in the case of tumor growth. When deprived of proper vascularization, tumor cells can no longer maintain its high proliferation rate due to lack of nutrients and oxygen. Targeting angiogenesis is therefore a highly effective way to suppress tumor growth. Tylophorine **(8)** (phenanthroindolizidine alkaloid) and flavonoids have been reported to potently inhibit angiogenesis by distruption of blood vessels, proliferation and migration of endothelial cells or inhibiting the binding of vascular endothelial growth factor (VEGF) to its receptors.[124,125] VEGF is an inducer of angiogenesis that results in the proliferation, migration and the formation of new blood vessels hence, the modulation of VEGF expression creates new therapeutic avenues to address malignancy.[126]

1.11 Research objectives

Ficus, Artocarpus and *Macaranga* have been regarded as plant genera that are associated either with phenanthroindolizidine alkaloids or flavonoids. Phenanthroindolizidine alkaloids and flavonoids have been regarded as potent anti-cancer metabolites hence, these plant genera represent potential sources of useful anti-cancer agents. As such, the aims of this research are to:

1) Extract and isolate alkaloids from *F. hispida, F. fistulosa and F. schwarzii,* and flavonoids from *A. heterophyllus x interger* and *M. hypoleuca*.

2) Elucidate the structures of the isolated compounds via various spectroscopic methods.

3) Screen the isolated compounds for biological activity, with the focus on cytotoxic activity against breast (MDA-MB-231 and MCF-7), lung (A549), colon (HT-116) cancer cell lines as well as a non-cancer cell line (MRC-5).

4) Propose on the anti-cancer mechanism of the active compounds.

Chapter 2: Isolation of alkaloids from *Ficus hispida, Ficus fistulosa* and *Ficus schwarzii*

Preliminary screening by thin layer chromatography (TLC) of the basic crude extracts of the leaves and/or stem-bark/bark of *F. hispida*, *F. fistulosa* and *F. schwarzii* following acid-base treatment of the crude ethanolic extracts showed a series of orange spots when sprayed with Dragendorff's reagent, indicating the presence of alkaloids. Acid-base extractions of the crude ethanolic extracts of the leaves and/or stem-bark/bark of the three *Ficus* species gave different percentage yields of the crude alkaloid mixtures, as summarized in Table 2.1. The crude alkaloid mixtures were subjected to repeated chromatography using column chromatography and preparative centrifugal thin layer chromatography (CTLC) techniques on silica gel until pure compounds were obtained.

Table 2.1: Percentage yield of crude alkaloid mixture.

Plant	Part	Dry weight (kg)	Yield (g) (%)
F. hispida	Leaves	3	1.67 (0.06)
	Stem-bark	3	0.67 (0.02)
F. fistulosa	Leaves	8	8.38 (0.28)
	Bark	8	1.87 (0.06)
F. schwarzii	Leaves	4	0.88 (0.02)

2.1 Alkaloids from *F. hispida*

Three alkaloids were isolated from the leaves and stem-bark of *F. hispida*, two of which are new. The new compounds were identified as hispidacine **(1)** isolated from the

bark and hispilosine **(2)** from the leaves.[127] The known alkaloid, which was isolated from the leaves was determined to be 13a(*S*)-(+)-deoxypergularinine **(3)**.

2.1.1 Hispidacine

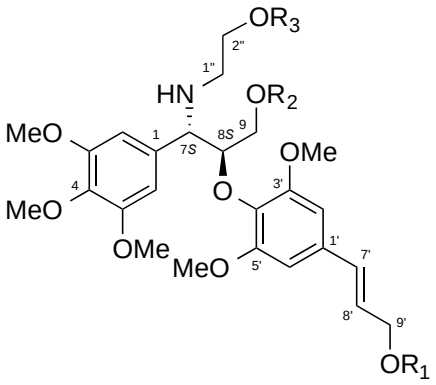

1 $R^1 = R^2 = R^3 = H$
1a $R^1 = R^2 = R^3 = COOH$

Hispidacine **(1)** was obtained in minute amounts from the stem-bark of *Ficus hispida* as a colourless oil, $[\alpha]_D^{25}$ +20 (*c* 0.28, $CHCl_3$). The IR spectrum (Appendix 8) showed absorption bands due to OH/NH functions (3385 cm^{-1}) and aromatic rings (1585 and 1505 cm^{-1}). The UV spectrum (Appendix 7) showed absorption maxima at 228 and 271 nm, confirming the existence of aromatic rings. The ESIMS showed a pseudo-molecular ion at *m/z* 494 $[M + H]^+$, and HRESIMS measurements established the molecular formula as $C_{25}H_{35}NO_9$, requiring nine degrees of unsaturation.

The ^{13}C NMR data (Table 2.2, Figure 2.4) showed the presence of 19 discrete carbon signals, six of which are due to six pairs of equivalent carbons. The total number of carbon resonances was therefore 25, comprising of five methoxy, four methylene, eight methine, and eight quaternary carbon atoms, in agreement with the molecular formula. The six pairs of chemically equivalent resonances were due to two pairs of oxygenated aromatic

carbons (C-3/C-5 and C-3'/C-5'), two pairs of aromatic methine carbons (C-2/C-6 and C-2'/C-6') and two pairs of aromatic methoxy groups (3-OMe/5-OMe and 3'-OMe/5'-OMe). This, coupled with the presence of four other substituted aromatic carbons, strongly suggested the presence of elements of symmetry in two tetrasubstituted aromatic rings, with each possessing a pair of equivalent aromatic methine and methoxy-substituted aromatic carbons. This was further supported by the presence of two 2H aromatic singlets (δ_H 6.57 and 6.61) and two 6H methoxy singlets (δ_H 3.81 and 3.82) in the ^{1}H NMR data (Table 2.2, Figure 2.3). The above observations established the presence of two 1,3,4,5-tetrasubstituted aromatic rings with a mirror plane of symmetry passing through C-1 and C-4 as well as C-1' and C-4', and requiring the pair of equivalent methoxy groups to be placed either at positions -3 and -5 or -2 and -6. The HMBC three-bond correlations from H-2/H-6 to C-7 and H-2'/H-6' to C-7' confirmed the placement of the two methoxy pairs at C-3/C-5 and C-3'/C-5', respectively (Figure 2.1).

The ^{1}H NMR data also showed the presence of a rather deshielded methylene signal at δ_H 4.30 (dd, *J* = 5.5, 1.6 Hz) and two olefinic signals at δ_H 6.28 (dt, *J* = 16, 5.5 Hz) and δ_H 6.52 (dd, *J* = 16, 1.6 Hz), which readily established the occurrence of a 3-hydroxypropenyl moiety that corresponds to the Ar-C-7'–C-8'–C-9'–OH partial structure in **1**. The large coupling constant observed between H-7' and H-8' (16 Hz) indicated the *E* geometry of the C-7'/C-8' double bond. This was also supported by the NOESY data that showed a correlation between H-7' and H-9' (Figure 2.1). On the other hand, the ^{1}H NMR signals at δ_H 4.07 (d, *J* = 5 Hz), 4.11 (td, *J* = 5, 3 Hz), 3.64 (dd, *J* = 12, 3 Hz) and 3.91 (dd, *J* = 12, 5 Hz), aided by the COSY data, established the occurrence of a CHCH(O)CH_2OH fragment, corresponding to the Ar-C-7–C-8–C-9–OH partial structure in **1** (Figue 2.1). Additionally, the presence of a 2-hydroxyethylamine fragment corresponding to the -NH-

C-1"–C-2"–OH partial structure in **1** was also shown by the COSY data (Figure 2.1, Apendix 3). From the observations disclosed thus far, it was evident that **1** consisted of two C_6-C_3 units and a 2-hydroxyethylamine moiety. Three-bond correlations from H-8' to C-1', H-7' to C-2'/C-6' and H-2'/H-6' to C-7' in the HMBC spectrum (Appendix 5) confirmed the attachment of the 3-hydroxypropenyl side chain at C-1', while correlations from H-2'/H-6' and H-8 to C-4' suggested attachment of C-8 to C-4' via an ether linkage. The C-7–C-8–C-9–OH fragment was deduced to be linked to the aromatic C-1 at C-7, from two- and three-bond correlations from H-7 to C-1, C-2/C-6 and H-2/H-6 to C-7. The three-bond correlations from H-1" to C-7 and H-7 to C-1" indicated the attachment of the 2-hydroxyethylamine side chain to C-7. This left the remaining methoxy group which must be linked to C-4, which was confirmed by the observed three-bond correlations from 4-OMe to C-4 and H-2/H-6 to C-4. The proposed structure of hispidacine (**1**) is entirely consistent with the HMBC and NOESY data (Figure 2.1, Appendix 5 and 6).

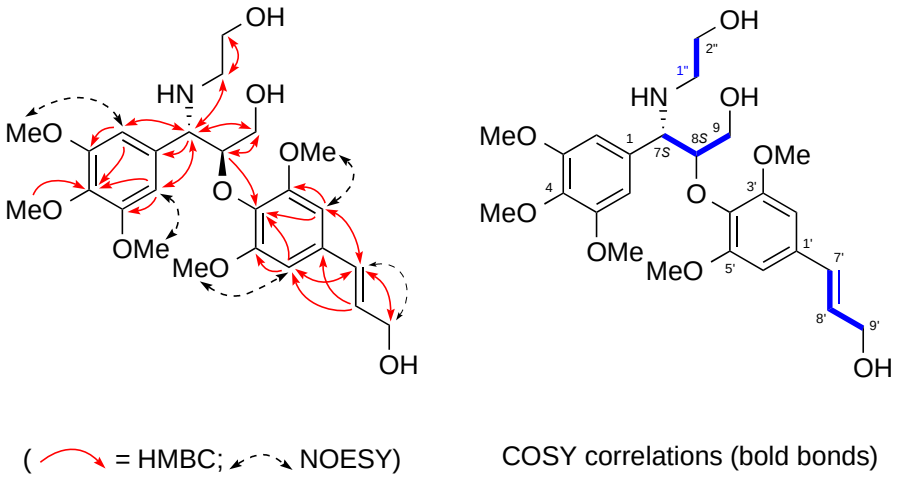

Figure 2.1: Selected HMBC, NOESY and COSY correlations of **1**

The presence of the three primary hydroxy groups in **1** was shown by acetylation, which yielded the triacetate derivative **1a**. The ^{1}H NMR spectrum of **1a** (Figure 2.5) showed the characteristic presence of 3 x CO$\underline{CH_3}$ signals at δ_H 1.94, 2.08 and 2.11, while in the IR spectrum (Appendix 12) a strong absorption band was observed at 1738 cm^{-1}. HRESIMS established the molecular formula of the triacetate derivative **1a** as $C_{31}H_{41}NO_{12}$. Additionally, the absence of the hydroxy groups in **1a** was clearly indicated by the disappearance of the broad IR band at 3385 cm^{-1} observed for **1**, which was replaced instead by a weaker but sharper band at 3325 cm^{-1} due to the secondary amine NH. Although acetylation could occur to hydroxy and amine groups, in the case of hispidacine, the amine group was not acetylated likely due to steric congestion. The positions of the three hydroxy groups at C-9, C-9' and C-2" were further confirmed by the three-bond correlations from H-9, H-9' and H-2" to the respective acetyl carbons observed in the HMBC data of **1a** (Appendix 10). The two germinal hydrogens of C-1", as well as C-2" in **1**, unexpectedly gave rise to two pairs of non-equivalent signals (H-1": δ_H 2.57 and 2.66; H-2": δ_H 3.64 and 3.71), suggesting restricted C-1"–N bond rotation. This could be due to the occurrence of intramolecular hydrogen bonding between the hydroxy (H donor) and secondary amine (H acceptor) groups within the 2-hydroxyethylamine side chain. Alternatively, the hydroxy group could form a hydrogen bond with the proximate aromatic methoxy group at C-3'/5'. This supposition is somewhat supported by the observation of two sets of equivalent geminal hydrogens due to H_2C-1" and H_2C-2" at δ_H 2.65 and 4.16, respectively, in the ^{1}H NMR data of the triacetate derivative **1a** (Table 2.2, Figure 2.5). This suggested free rotation about the C-1"–N bond due to the absence of intramolecular hydrogen bonding following replacement of the hydroxy group at C-2" with an *O*-acetyl group.

The structure of hispidacine **(1)** constitutes an 8,4'-oxyneolignan skeleton[128] featuring an unprecedented incorporation of a 2-hydroxyethylamine moiety at C-7. Due to the presence of two adjacent stereocentres (C-7 and C-8) in the molecule, there are two possible 8,4'-oxyneolignan diastereomers (*erythro* or *threo*). The relative configurations at the two stereocentres can be determined by analogy to the typical 8,4'-oxyneolignan system via examination of the magnitude of the coupling constant between H-7 and H-8. Accordingly, based on the energetically favourable staggered conformer with intermolecular hydrogen bonding between the benzylic hydroxy (at C-7) and aryloxy groups present in a typical 8,4'-oxyneolignan, large $J_{7,8}$ values (associated with dihedral angles of approx. 180°) correspond to *threo* configuration, while small $J_{7,8}$ values (associated with dihedral angles of approx. 60°) correspond to *erythro* configuration.[129–133] The main difference between **1** and the typical 8,4'-oxyneolignans is that the C-7 hydroxy group has now been replaced with a 2-hydroxyethylamine side chain. Examination of models suggested that the benzylic NH group in **1** is also able to form a similar intramolecular hydrogen bond with the adjacent aryloxy group (Figure 2.2). Since a small coupling constant $^{3}J_{7,8}$ = 5 Hz was observed in **1**, an *erythro* relative configuration was suggested for C-7 and C-8. Finally, the configuration of C-8 can be deduced by comparing the CD spectra of **1** and **1a** with those of 8,4'-oxyneolignans or related compounds with known absolute configurations.[129,131,132,134] In as such, the configuration of C-8 was proposed to be 8*S* by the negative Cotton effects observed at 237 and 235 nm in the CD spectra of **1** and **1a**, respectively. Consequently, an *S* configuration must be assigned to C-7 since the relative configuration between C-7 and C-8 was determined as *erythro*. Therefore, the structure of **1** was elucidated as (+)-(7*S*,8*S*,7'*E*)-3,3',4,5,5'-pentamethoxy-7-(2-hydroxyethylamino)-8,4'-oxyneolign-7'-ene-9,9'-diol.

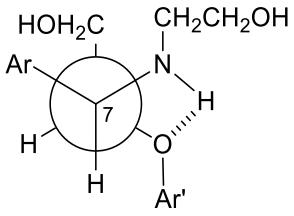

Figure 2.2: Staggered conformer of **1** with the lowest energy (viewed along the axis of the C-7–C-8 bond). Dotted bond shows intermolecular hydrogen bond between benzylic NH and adjecent aryloxy groups.

Table 2.2: ^{1}H and ^{13}C NMR data of hispidacine **(1)** and the triacetate derivative **(1a)**[a]

Position	**1**		**1a**	
	^{1}H (*J* in Hz)	^{13}C	^{1}H (*J* in Hz)	^{13}C
1	-	135.19	-	135.3
2	6.57 s	104.8	6.60 s	104.9
3	-	153.35	-	153.3
4	-	137.2	-	137.1
5	-	153.4	-	153.3
6	6.57 s	104.8	6.60 s	104.9
7	4.07 d (5)	64.6	3.88 m	63.9
8	4.11 td (5, 3)	86.6	4.56 dt (7, 3)	82.9
9	3.64 dd (12, 3) 3.91 dd (12, 5)	61.5	4.29 m 4.51 dd (12, 7)	63.2
1'	-	133.1	-	132.2
2'	6.61 s	103.6	6.65 s	103.8
3'	-	153.41	-	153.5
4'	-	135.18	-	134.7
5'	-	153.41	-	153.5
6'	6.61 s	103.6	6.65 s	103.8
7'	6.52 dt (16, 1.6)	130.6	6.60 d (16)	134.1
8'	6.28 dt (16, 5.5)	128.8	6.24 dt (16, 6.5)	123.0
9'	4.30 dd (5.5, 1.6)	63.4	4.73 dd (6.5, 1.3)	64.9
1"	2.57 ddd (12, 6, 3.8) 2.66 ddd (12, 6.9, 4)	49.8	2.65 m	42.3
2"	3.64 ddd (10.5, 6, 4) 3.71 m	62.0	4.16 m	64.7
3-OMe	3.81 s	56.18	3.84 s	56.1
4-OMe	3.80 s	60.9	3.83 s	60.8
5-OMe	3.81 s	56.18	3.84 s	56.10
3'-OMe	3.82 s	56.24	3.87 s	56.11
5'-OMe	3.82 s	56.24	3.87 s	56.11
3 x OH / 1 x	2.76 br s	-	Not observed	-
9-OCO$\underline{CH_3}$	-	-	1.94 s[d]	20.8[b]
9-O$\underline{CO}CH_3$				170.7
9'-OCO$\underline{CH_3}$	-	-	2.08 s[d]	20.9[b]
9'-O$\underline{CO}CH_3$				170.8
2"-OCO$\underline{CH_3}$	-	-	2.11 s[d]	21.0[b]
2"-O$\underline{CO}CH_3$				171.0[c]

[a] $CDCl_3$, 600 MHz; [b–d] Assignments are interchangeable

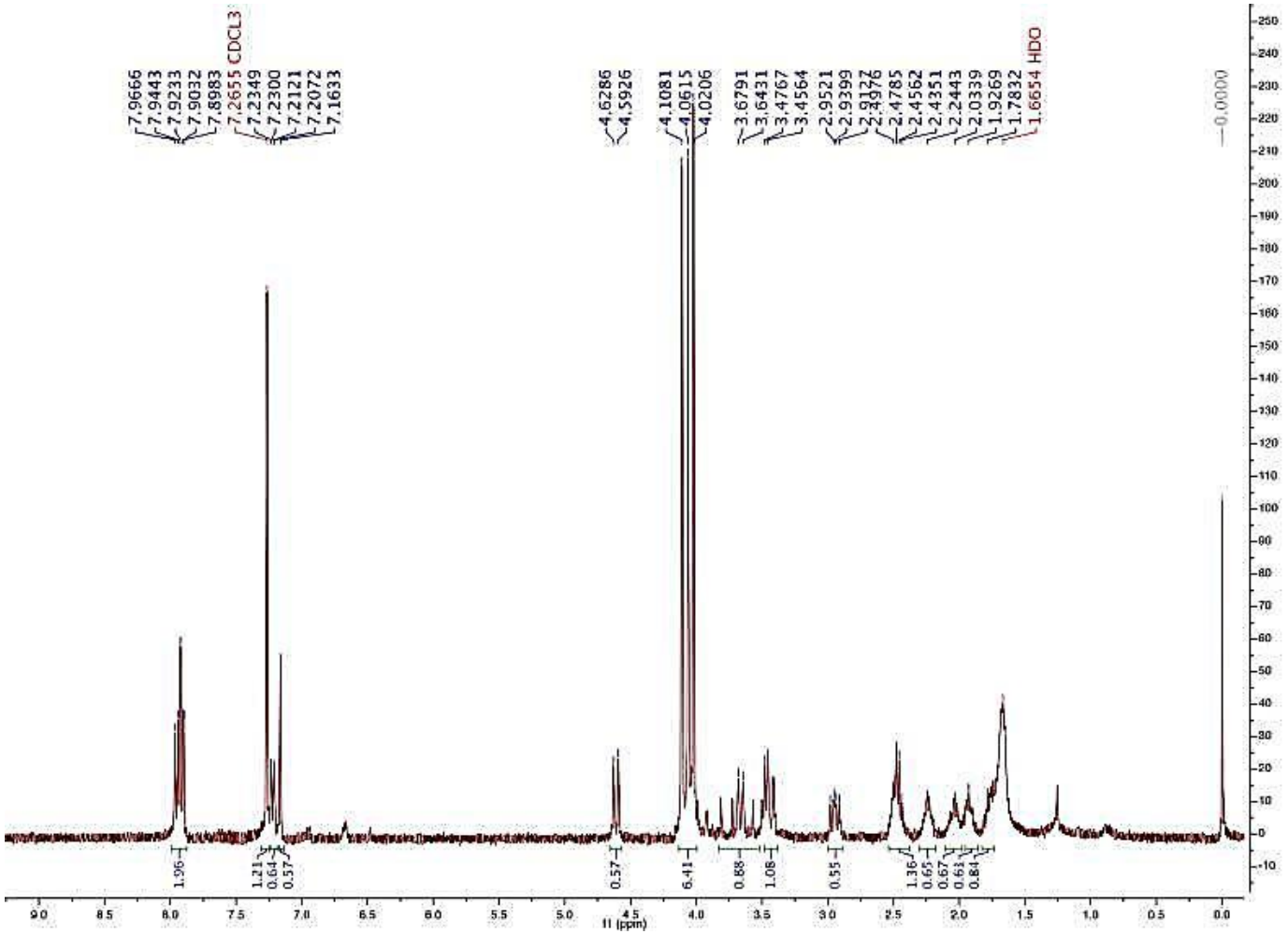

Figure 2.3: ^{1}H NMR spectrum ($CDCl_3$, 600 MHz) of hispidacine **(1)**

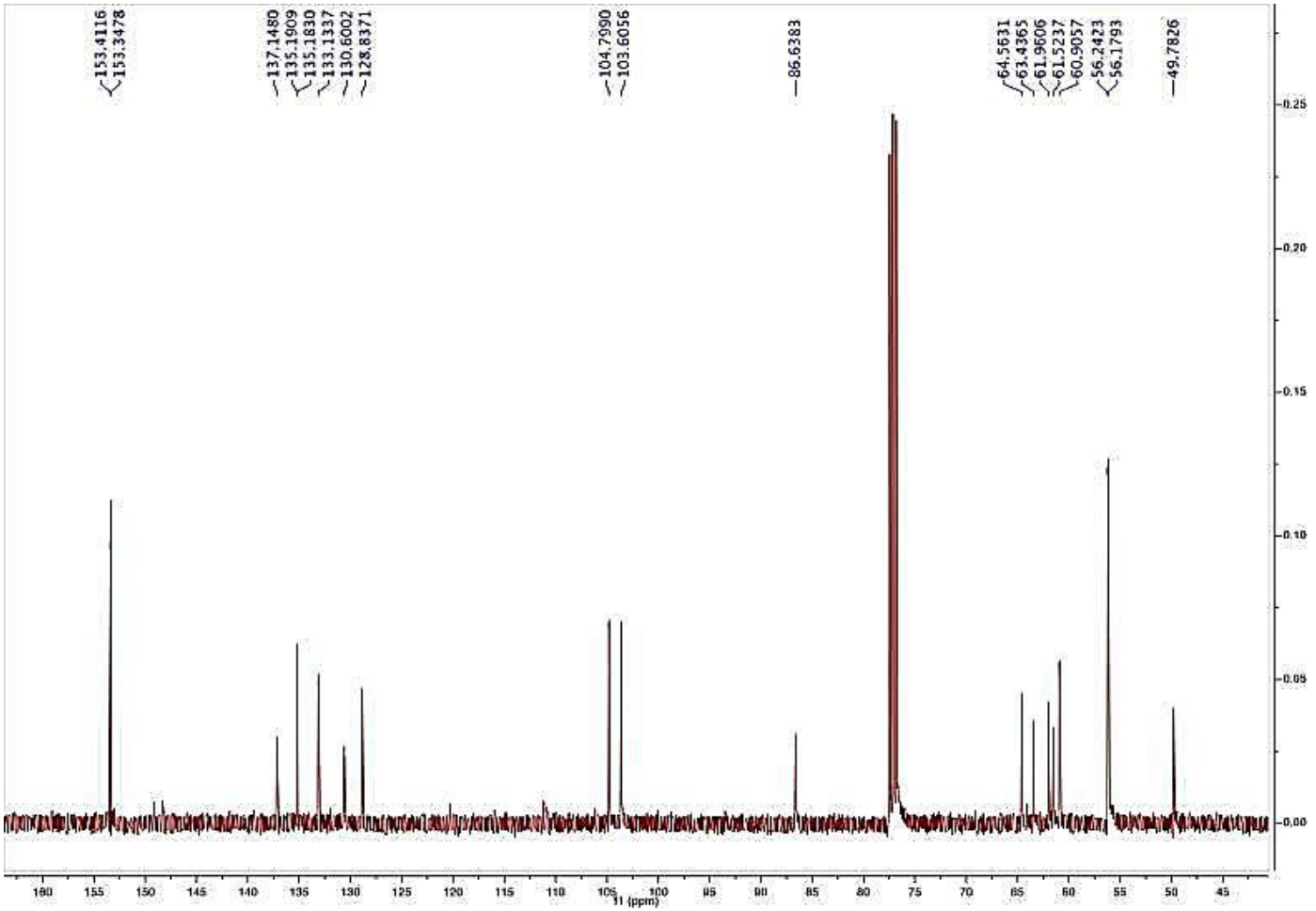

Figure 2.4: ^{13}C NMR spectrum ($CDCl_3$, 150 MHz) of hispidacine **(1)**

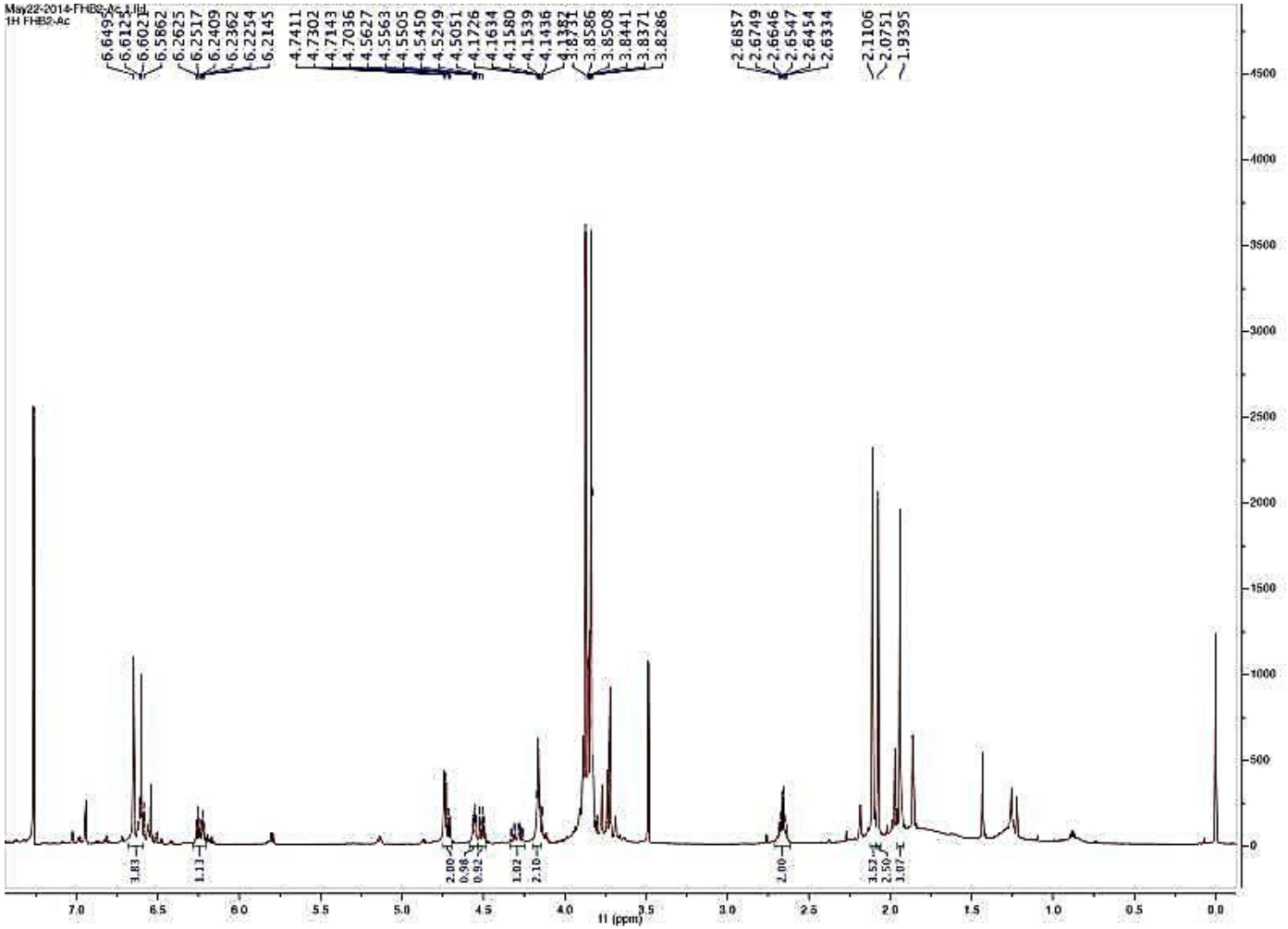

Figure 2.5: ^{1}H NMR spectrum ($CDCl_3$, 600 MHz) of hispidacine acetate **(1a)**

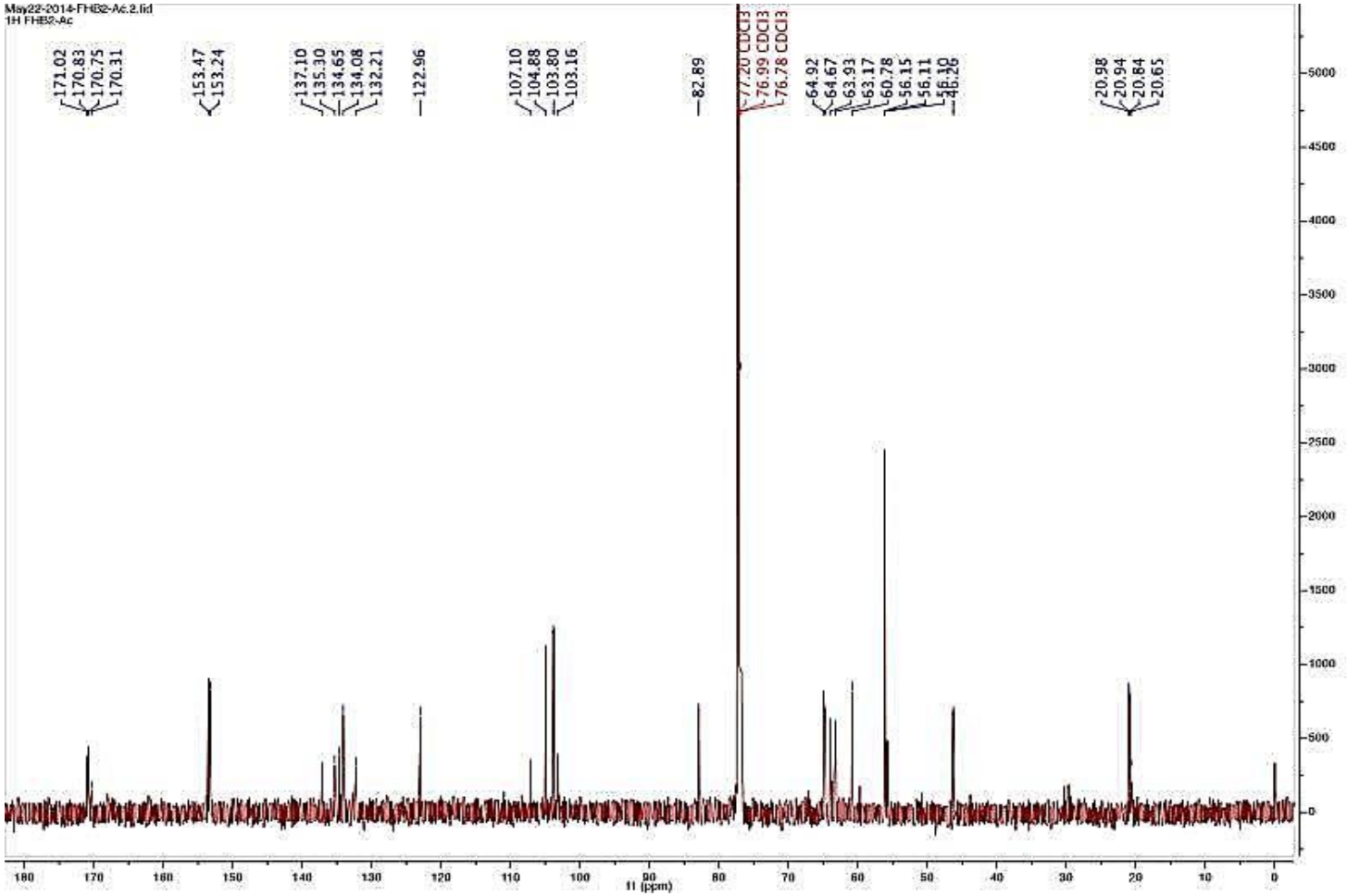

Figure 2.6: ^{13}C NMR spectrum ($CDCl_3$, 150 MHz) of hispidacine acetate **(1a)**

2.1.2 Hispiloscine

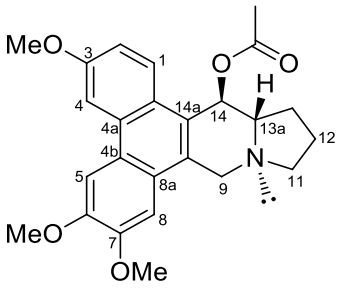

2

Hispiloscine **(2)** was a minor alkaloid obtained from the leaves of *F. hispida* as a light yellowish oil, $[\alpha]_D^{25}$ +1 (*c* 0.40, $CHCl_3$). The UV spectrum showed absorption maxima at 260, 286, 313 and 338 nm indicating the presence of a substituted phenanthrene chromophore,[135] while the IR spectrum (Appendix 16) showed a strong absorption band at 1736 cm^{-1} suggesting the presence of an ester carbonyl function. The ESIMS of **2** showed a pseudo-molecular ion at *m/z* 422 $[M + H]^+$, and HRESIMS measurements established the molecular formula as $C_{25}H_{27}NO_5$, requiring 13 degrees of unsaturation.

The ^{13}C NMR data of **2** (Table 2.3, Figure 2.11) indicated the presence of 25 carbon signals consisting of four methyl, four methylene, seven methine and 10 quaternary carbons, in agreement with the molecular formula. The most downfield carbon resonance at δ_C 171.0 supported the presence of an ester function as indicated by the IR spectrum. In addition, the carbon resonances at δ_C 149.1, 149.6 and 157.5 suggested the presence of three oxygenated aromatic carbons. The ^1H NMR data of **2** (Table 2.3, Figure 2.10) indicated the presence of a 1,2,4-trisubstituted aromatic ring from the ^1H signals observed at δ_H 7.15 (dd, *J* = 9, 2 Hz), 7.62 (d, *J* = 9 Hz), and 7.86 (d, *J* = 2 Hz), while the two aromatic singlets at δ_H 7.14 and 7.88 indicated the presence of a 1,2,4,5-tetrasubstituted

aromatic moiety. The four methyl singlets at δ_H 2.03, 3.99, 4.04, and 4.09, were readily assigned to an acetyl and three aromatic methoxy groups, respectively. In addition to a pair of AB doublets (J = 14.7 Hz) observed at δ_H 3.73 and 4.48, readily attributable to the isolated benzylic aminomethylene group (H-9), the ^{1}H NMR data also revealed the presence of a profoundly deshielded aliphatic signal at δ_H 6.62 (d, J = 7.4 Hz), which is characteristic of the benzylic methine H-14 when an acetoxy substituent is present at C-14.[136,137]

In addition to the isolated methylene (H-9) and aromatic CH=CH fragment noted previously, the COSY and HSQC data (Appendix 9 and 10) also revealed a $CH_2CH_2CH_2CHCH(O)$ fragment corresponding to the N-C-11–C-12–C-13–C-13a–C-14–Ar partial structure in **3**, indicating the presence of an indolizidine moiety with oxygenation at C-14. The substitution pattern of the phenanthrene moiety was established by detailed analysis of the NOE data (Figure 2.7). Reciprocal NOEs between H-14 and the aromatic doublet at δ 7.62 confirmed the latter signal to be due to H-1. This in turn allowed the aromatic signals at δ_H 7.15 (dd, J = 9, 2 Hz) and 7.86 (d, J = 2 Hz) to be assigned to H-2 and H-4, respectively. Similarly, reciprocal NOEs between H-9 and the aromatic singlet at δ_H 7.14 confirmed the assignment of the latter signal to H-8, and the other aromatic singlet at δ_H 7.88 to H-5. Thus, C-3, C-6 and C-7 were deduced to be the sites of methoxylation, which were confirmed from the NOEs observed between H-2, H-4/3-OMe, H-5/6-OMe, and H-8/7-OMe. Finally, attachment of the indolizidine moiety to the trimethoxylated-phenanthrene moiety was established by the HMBC data (Figure 2.7, Appendix 15). Two- and three-bond correlations from H-9 to C-8a, C-8b and C-14a, and H-14 to C-14a and C-8b, allowed the linking of C-9 to C-8b and C-14 to C-14a, respectively, while three-bond

correlation from H-14 to the ester carbonyl carbon confirmed the attachment of the acetoxy group at C-14.

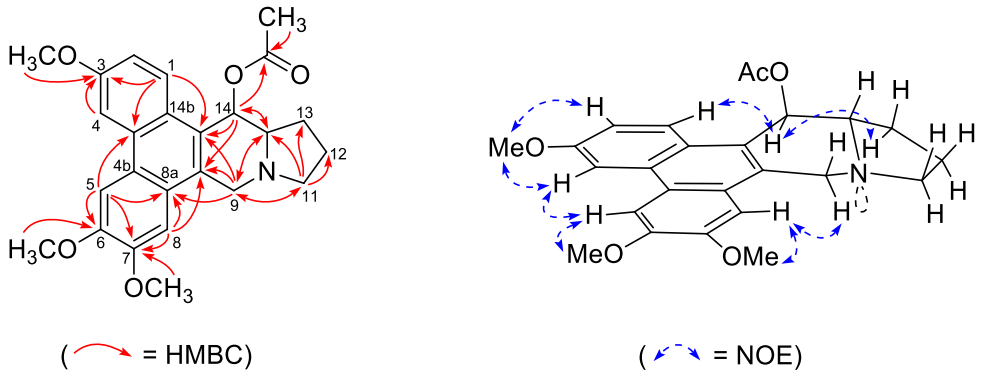

Figure 2.7: Selected HMBCs and NOEs of hispilocine **(2)**

The proposed structure of hispiloscine **(2)**, which was entirely consistent with the HMBC data, is identical to those of *O*-methyltylophorinidine acetate **(62a)** and tylophorinine acetate **(187a)**, both of which are semi-synthetic alkaloids derived from *O*-methyltylophorinidine **(62)** and tylophorinine **(187)**.[135,137,138] The ^{1}H NMR data of **2** presented a general similarity to those of **62a** and **187** (Table 2.3), except that the chemical shifts of H-1 (δ_H 7.62), H-9 (δ_H 4.48), H-11 (δ_H 3.35), H-13 (δ_H 2.05 and 2.21), and H-13a (δ_H 2.56) in **2** differed substantially from those of **62a** and **187a**, suggesting possible stereochemical variations at C-13a, C-14 and N (orientation of lone pair electrons) in **2**. Further confirmation of this view was the observation that the coupling constant observed for the aliphatic doublet of H-14 in **2** was 7.4 Hz, compared to 2 Hz in **62a** and **187a**.[135] Hispiloscine **(2)** was therefore deduced to be a diastereomer of **62a** and **187a**.

Indolizidine heterocycles that contain three stereocentres at C-13a, C-14 and N can essentially yield four possibilities of the relative stereochemistry between the two methine

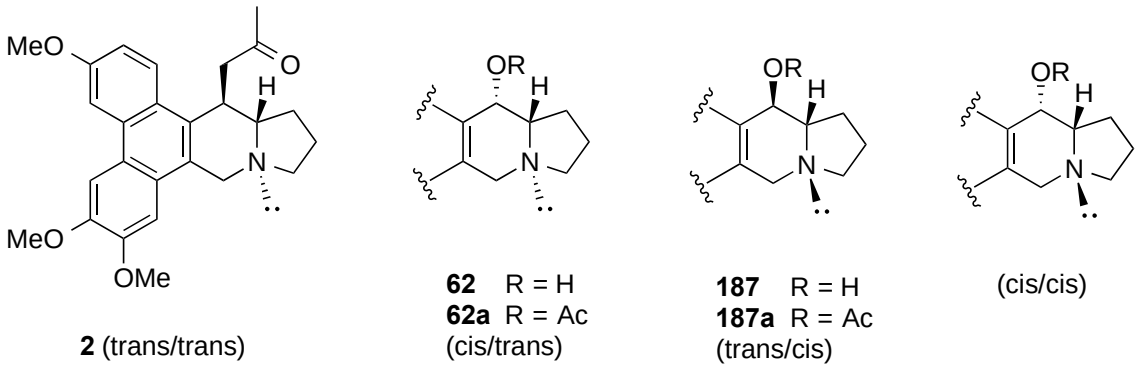

2 (trans/trans)

62 R = H
62a R = Ac
(cis/trans)

187 R = H
187a R = Ac
(trans/cis)

(cis/cis)

Figure 2.8: Structures of **2**, **62**, **62a**, **187** and **187a**

hydrogens and the N lone pair electrons, i.e., H-14,H-13a / H-13a,N-Lp: *trans*/*trans*, *cis*/*trans*, *trans*/*cis* or *cis*/*cis* (Figure 2.8).In addition to **62a** and **62**, other naturally occurring phenanthroindolizidine alkaloids bearing oxygenation at C-14 such as 3-demethyl-14α-hydroxyisotylocrebrine[139]and 14α-hydoxy-3,6-didemethylisotylocrebrine,[140] were previously shown to possess the *cis*/*trans* relative stereochemistry. On the other hand, **187a** and **187** as well as the naturally occurring tylophoricidine E[141] were shown to possess the *trans*/*cis* relative stereochemistry. The $^{3}J_{13a,14}$ coupling constants reported for phenanthroindolizidine alkaloids with oxygenation at C-14 and possessing either the *cis*/*trans* or *trans*/*cis* stereochemistry were shown to be 0-2 Hz. This is entirely consistent with the coupling constants calculated by a vicinal coupling constant calculator that uses the equation of Haasnoot and co-worker[142] and based on the dihedral angles obtained from energy-minimized models generated by MM2 calculations (ChemBioDraw 3D software): **62a**, θ = 57°, calcd. $^{3}J_{13a,14}$ = 1.5 Hz; **187a**, θ = 84°, calcd. $^{3}J_{13a,14}$ = 1.2 Hz (Figure 2.9). By invoking the same argument that the calculated $^{3}J_{13a,14}$ values corresponded well with the

actual coupling constants, the relative stereochemistry of **2** can possibly be deduced accordingly. Since **2** is a diastereomer of **62a** and **187a**, it can either assume the *trans*/*trans* or *cis*/*cis* relative stereochemistry. Consequently, the energy-minimized models for the *trans*/*trans* and *cis*/*cis* systems were constructed revealing dihedral angles (*trans*/*trans*, θ = 152°; *cis*/*cis*, θ = 41°) that corresponded to the calculated $^{3}J_{13a,14}$ values of 7.0 and 3.2 Hz, respectively (Figure 2.9). This strongly suggested that the indolizidine heterocycle in **2** assumed the *trans*/*trans* relative stereochemistry, since the doublet of H-14 showed a coupling constant of 7.4 Hz.

With regards to the configuration at C-13a, it appeared that phenanthroindolizidine alkaloids with the *S* configuration exhibited a positive optical rotation (the opposite was observed for alkaloids with the *R* configuration).[19,143] Furthermore, variation in the substituents and substitution pattern in both the phenanthrene and indolizidine moieties did not seem to significantly alter the optical rotational properties of the alkaloids.[39,144–148] On this basis, since a positive optical rotation was observed for **2**, the C-13a configuration of **2** can be assigned as *S*. Taken together, the *trans*/*trans* relative stereochemistry and the *S*-configured C-13a, revealed the configuration at C-14 as *R* and N as *S* (α-oriented lone pair electrons). Thus, hispiloscine **(2)** represents the first naturally occurring acetoxy-substituted phenanthroindolizidine, which is diastereomeric with both the semi-synthetic acetates of *O*-methyltylophorinidine and tylophorinine.

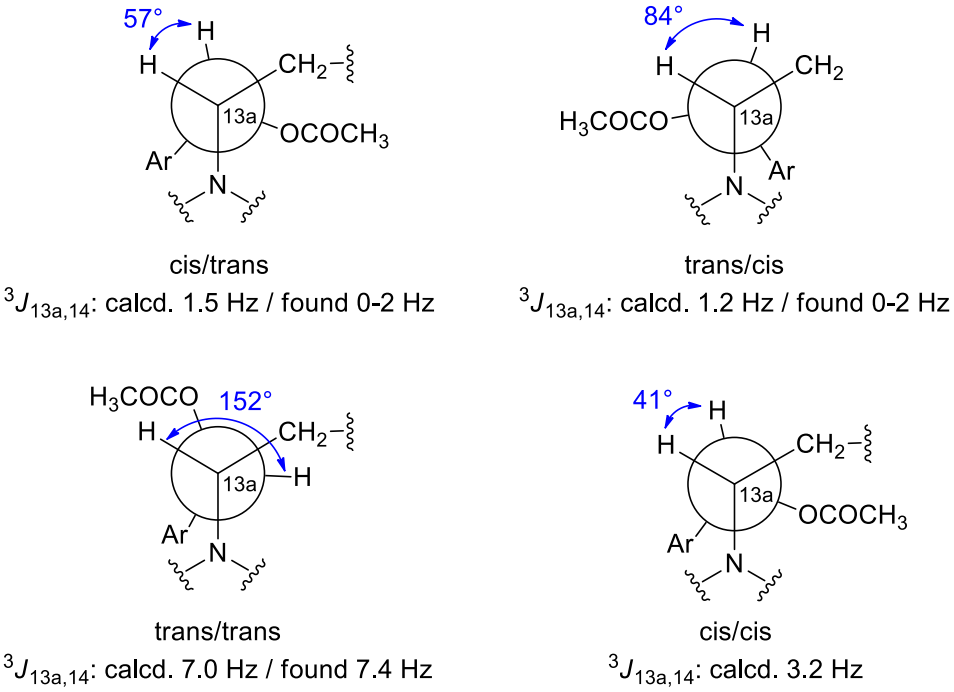

Figure 2.9: Energy-minimized structures of the four possible relative stereochemistry of a C-14-oxygenated phenanthroindolizidine alkaloid, viewed along the axis of the C-13a–C-14 bond and showing the dihedral angles between H-13a and H-14.

Table 2.3: ^{1}H and ^{13}C NMR data of hispiloscine **(2)**[a] and selected ^{1}H NMR data of *O*-methyltylophorinidine acetate **(62a)**[136] and tylophorinine acetate **(187a)**.[137]

Position	**2**		**62a**	**187a**
	^{13}C	^{1}H (*J* in Hz)	^{1}H (*J* in Hz)	^{1}H (*J* in Hz)
1	125.7	7.62 d (9)	7.84 d (9)	7.86 d (9)
2	103.6	7.15 dd (9, 2)	7.20 dd (9, 2)	7.22 dd (9, 2)
3	157.5	-	-	-
4	104.7	7.86 d (2)	7.85 d (2)	7.90 d (2)
4a	131.0	-	-	-
4b	124.0	-	-	-
5	103.8	7.88 s	7.88 s	7.91 s
6	149.6[b]	-	-	-
7	149.1[b]	-	-	-
8	115.0	7.14 s	7.16 s	7.19 s
8a	124.5[c]	-	-	-
8b	129.4	-	-	-
9	53.5	3.73 d (14.7)	3.57 d (16)	3.62 d (16)
		4.48 d (14.7)	4.75 d (16)	4.78 d (16)
11	54.5	2.54 q (8)	[f]	2.45 m
		3.35 t (8)	[f]	3.53 m
12	21.7	1.88 m	[f]	1.94 m
		1.99 m	[f]	2.02 m
13	30.1	2.05 m	[f]	1.69 m
		2.21 m	[f]	2.08 m
13a	66.0	2.56 m	[f]	2.71 m
14	73.5	6.62 d (7.4)	6.66 d (2)	6.71 br d
14a	125.9	-	-	-
14b	124.7[c]	-	-	-
3-OMe	55.4	3.99 s	3.97 s	4.01 s
6-OMe	55.9[d]	4.09 s[e]	4.09 s	4.11 s
7-OMe	56.0[d]	4.04 s[e]	4.04 s	4.06 s
14-OCO$\underline{CH_3}$	21.2	2.03 s	2.13 s	[f]
14-O$\underline{CO}CH_3$	171.0	-	-	-

[a] $CDCl_3$, 600 MHz; [b-e] Assignments are interchangeable; [f] Data not reported

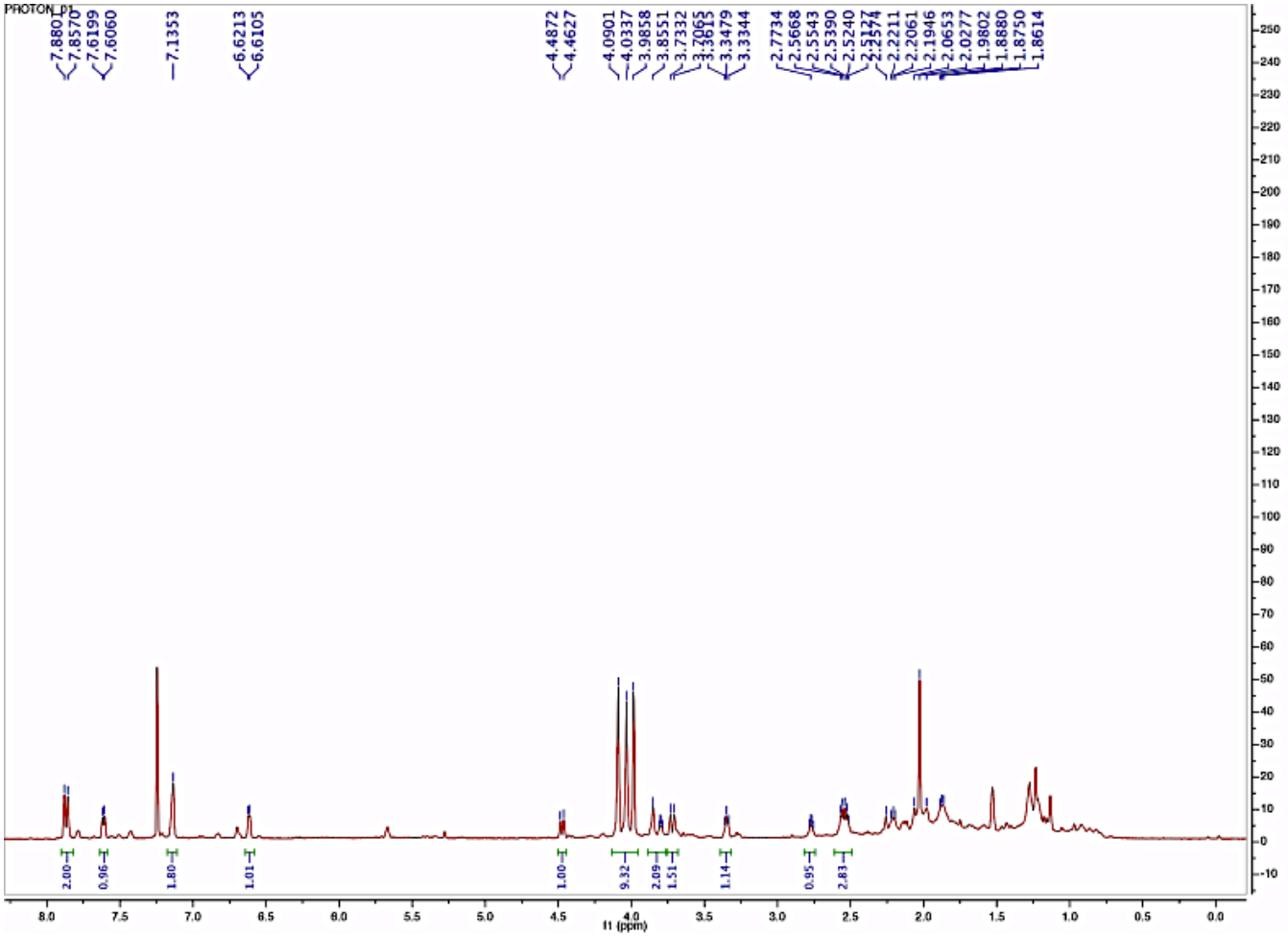

Figure 2.10: ^{1}H NMR spectrum ($CDCl_3$, 600 MHz) of hispiloscine **(2)**

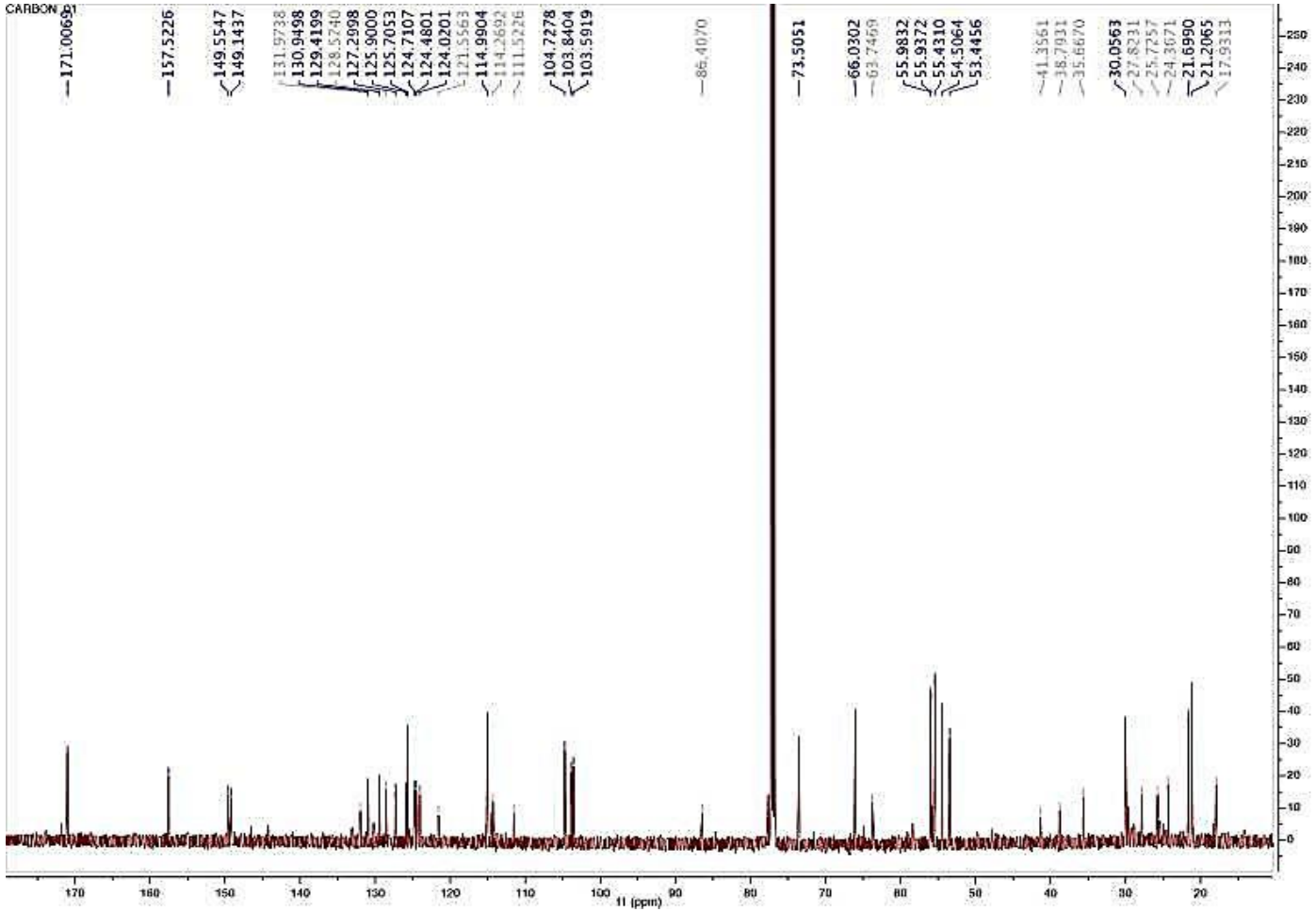

Figure 2.11: ^{13}C NMR spectrum ($CDCl_3$, 150 MHz) of hispiloscine **(2)**

2.1.3 13a(*S*)-(+)-Deoxypergularinine

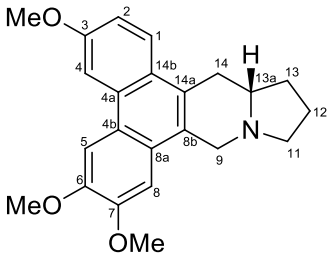

3

13a(*S*)-(+)-Deoxypergularinine **(3)** was isolated in minute amounts from the leaves of *F. hispida* as a colourless oil, with $[\alpha]_D^{25}$ +3 (*c* 0.11, $CHCl_3$). The ESIMS of **3** showed a pseudo-molecular ion at *m/z* 364 $[M+H]^+$ and HRESIMS measurements established the molecular formula as $C_{23}H_{25}NO_3$, requiring 12 degrees of unsaturation. The UV spectrum showed absorption maxima at 228, 261 and 287nm, while the IR spectrum showed absorption bands at 1609 and 1512 cm^{-1} due to aromatic moieties. The ^1H NMR spectrum (Table 2.4, Figure 2.13) showed characteristic patterns of a phenathroindolizidine alkaloid substituted with three methoxy groups from the presence of three 3H singlets at δ_H 4.02, 4.06 and 4.11, and five aromatic hydrogens. The aromatic hydrogens consist of a pair of *ortho*-coupled hydrogens (δ_H 7.96, d, *J* = 8 Hz and 7.22, dd, *J* = 8, 2 Hz), one *meta*-coupled hydrogen (δ_H 7.90, d, *J* = 2 Hz), and two isolated hydrogens (δ_H 7.92 and 7.16), clearly indicating the existence of a trisubstituted phenanthroindolizidine moiety in **3**. The distinct pair of AB doublets observed at δ_H 3.66 and 4.61 with *J* = 14.4 Hz can be readily assigned to the isolated aminomethylene group (NCH_2) at C-9. Additionally, the COSY data (Figure 2.12) disclosed the presence of a $NCH_2CH_2CH_2CHCH_2$ fragment, which together with the aminomethylene group at C-9, confirmed the presence of an indolizidine moiety in **3**.

The structural information obtained thus far allows the identity of **3** to be narrowed down to either deoxypergularinine or antofine, which are the 3,6,7-trimethoxy and 2,3,6-trimethoxy regioisomers, respectively. Due to scarcity of compound, NOE experiments were not carried out for **3**. However, the ^{1}H NMR data of **3** showed a close resemblance to those of deoxypergularinine, previously reported in the literature[149] providing support that **3** was indeed deoxypergularinine. Using the same argument invoked for hispiloscine (**2**) (*vide supra*), the positive optical rotation observed for **3** revealed that the configuration at C-13a is *S*.[18,143] Therefore, **3** is determined as 13a(*S*)-(+)-deoxypergularinine.

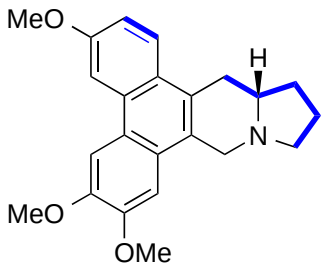

Figure 2.12: COSY correlations (bold bonds) of 13a(*S*)-(+)-deoxypergularinine **(3)**

Table 2.4: ^{1}H NMR data of 13a(*S*)-(+)-deoxypergularinine **(3)**[a] obtained from literature and those from the present study.

Position	Deoxypergularinine[149]	**3**
	^{1}H (*J* in Hz)	^{1}H (*J* in Hz)
1	7.91 d (9.2)	7.96 d (8)
2	7.21 dd (9.2, 2.5)	7.22 dd (8, 2)
4	7.86 d (2.5)	7.90 d (2)
5	7.88 s	7.92 s
8	7.09 s	7.16 s
9	4.62 d (14.5)	4.61 d (14.4)
	3.72 d (14.5)	3.66 d (14.4)
11	3.47 td (8.1, 2)	3.48 t (9)
	2.58 q (8.1)	2.47 q (9)
12	2.06 m	2.03 m
	1.96 m	1.92 m
13	2.22 m	2.24 m
	1.82 m	1.78 m
13a	2.59 m	2.5 m
14	3.40 dd (16.5, 3)	3.45 dd (16, 2.5)
	3.00 dd (16.5, 10.5)	2.95 dd (16, 10.9)
3-OMe	4.01 s	4.02 s
6-OMe	4.03 s	4.06 s
7-OMe	4.09 s	4.11 s

[a] $CDCl_3$, 600 MHz

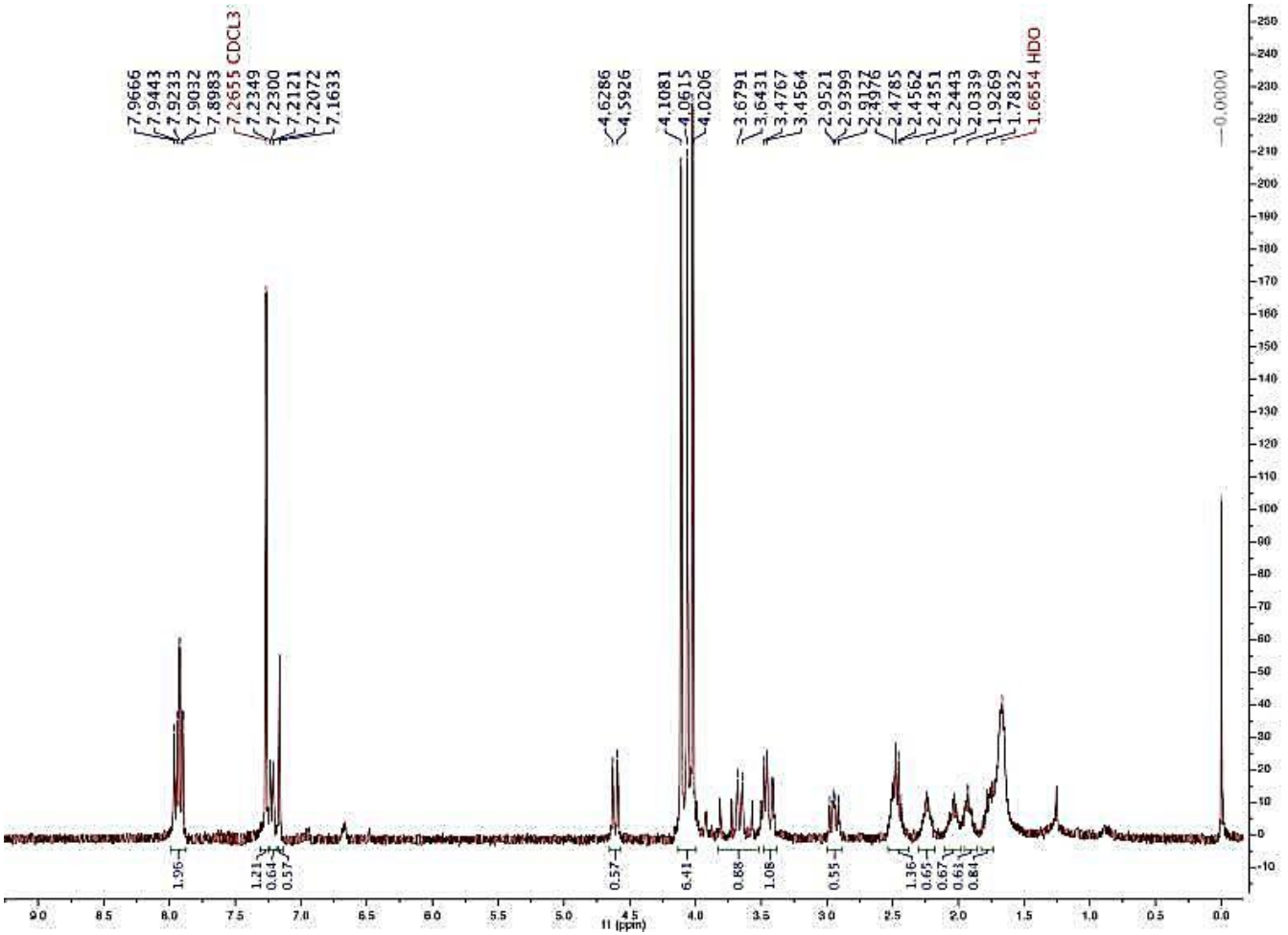

Figure 2.13: ^{1}H NMR spectrum ($CDCl_3$, 600 MHz) of 13a(*S*)-(+)-deoxypergularinine **(3)**

2.2 Alkaloids from *F. fistulosa*

Two new septicine alkaloids, fistulopsines A **(4)** and B **(5)**, together with four known alkaloids, 13a(*R*)-(-)-3,6-didemethylisotylocrebrine **(6)**, 13a(*S*)-(+)-tylocrebrine **(7)**, 13a(*S*)-(+)-tylophorine **(8)**, 13a(*S*)-(+)-septicine **(9)**, and a non-alkaloid, vomifoliol **(10)** were isolated from the leaves and bark of *F. fistulosa*. The structures of the isolated compounds were determined by spectroscopic methods as well as comparison with literature data.

2.2.1 Fistulopsine A

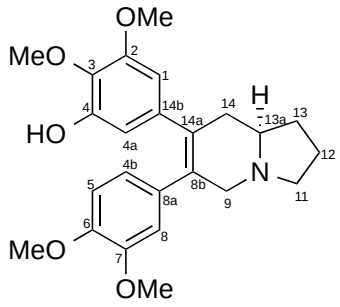

4

Fistulopsine A **(4)** was obtained in minute amounts from the bark of *F. fistulosa* as a colourless oil, with $[\alpha]_D^{25}$ –47 (*c* 0.30, $CHCl_3$). The IR spectrum (Appendix 22) showed absorption bands corresponding to the presence of hydroxy (3375 cm^{-1}) and aromatic moieties (1583 and 1515 cm^{-1}). The UV spectrum (Appendix 21) showed absorption maxima at 225, 265, and 282 (sh) nm, while on addition of aqueous sodium hydroxide the UV spectrum displayed a bathochromic shift, suggesting the presence of unsubstituted phenolic hydroxy group. The ESIMS of **4** showed a pseudo-molecular ion at *m/z* 412 and HRESIMS measurements established the molecular formula as $C_{24}H_{29}NO_5$, requiring 11 degrees of unsaturation.

The ^{13}C NMR data of fistulopsine A (Table 2.5, Figure 2.17) indicated the presence of 24 carbon signals consisting of four methoxy, five methylene, six methine, and nine quaternary carbons, in agreement with the molecular formula. The ^{1}H NMR spectrum (Table 2.5, Figure 2.16) showed the presence of a 1,3,4,5-tetrasubstituted aromatic ring from the two aromatic doublets observed at δ_H 6.05 and 6.41 with J = 1.5 Hz, which implied that the two aromatic hydrogens were *meta*-coupled. The remaining three aromatic hydrogen signals present in the ^{1}H NMR spectrum indicated the presence of a trisubstituted aromatic ring. On the other hand, the pair of distinct AB doublets in the upfield region at δ 3.88 and 3.08 with J = 15.5 Hz can be readily assigned to the isolated aminomethylene group at C-9. In addition to this, the COSY and HSQC data (Appendix 17 and 18) revealed the presence of an $NCH_2CH_2CH_2CHCH_2$ fragment (Figure 2.14) corresponding to the N-C-11–C-12–C-13–C-13a–C-14–Ar partial structure in **4**. The partial structures disclosed thus far indicated that **4** constituted of an indolizidine moiety substituted only by two aryl groups at C-8b and C-14a. As a result, the four methyl singlets observed between δ_H 3.51-3.81 in the ^{1}H NMR spectrum can be attributed to four aromatic methoxy groups. Since there are five oxygen atoms in the molecular formula of fistulopsine A **(4)**, the fifth oxygen atom must therefore be associated to a phenolic hydroxy group. The substitution pattern of the two aryl rings was determined from the HMBC data (Figure 2.14, Appendix 19). Three-bond correlations from H-1 to C-3 and C-4a; H-4a to C-1 and C-3; 2-OMe to C-2; and 3-OMe to C-3 allowed the 1,3,4,5-tetrasubstituted aromatic ring to be identified as a 3-hydroxy-4,5-dimethoxyphenyl moiety, which was subsequently linked to C-14a of the indolizidine portion by the H-4a to C-14a HMBC correlation. On the other hand, the trisubstituted aromatic ring was determined to be a 3,4-dimethoxyphenyl moiety from the HMBC three-bond correlations from H-4b to C-8; H-5 to C-7 and C-8a; H-8 to C-4b and

C-6; 6-OMe to C-6; and 7-OMe to C-7. This aromatic moiety was linked to the indolizidine portion at C-8b by the three-bond correlations from H-4b and H-8 to C-8b. In addition, the ^{13}C NMR data of the 3-hydroxy-4,5-dimethoxyphenyl and 3,4-dimethoxyphenyl moieties, which corresponded well with reported data,[150–152] provided further support for the substitution patterns proposed. The NOESY spectrum which showed correlations between H-1/2-OMe, H-5/6-OMe and H-8/7-OMe (Figure 2.15, Appendix 20), also supported the methoxylation pattern of the two aromatic moieties, while NOESY correlations between H-14/H-1, H-4a and H-9/H-4b, H-8 further confirmed the attachment of the two aromatic moieties at C-8b and C-14a. With regards to the configuration at C-13a, it appeared that *seco*-phenanthroindolizidine alkaloids with *R* configuration exhibited negative optical rotations (the opposite was observed for alkaloids with *S* configuration).[18,146] Accordingly, the negative optical rotation observed for fistulopsine A **(4)** suggested that the configuration at C-13a in **4** is *R*.[18,19] Therefore, fistulopsine A **(4)** was elucidated as 13a(*R*)-(-)-4-hydroxysepticine.

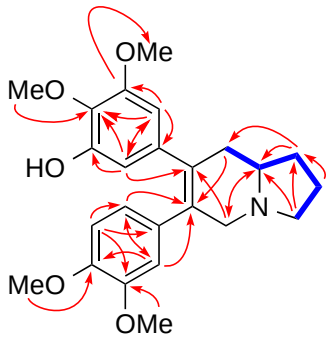

Figure 2.14: Selected HMBCs and COSY correlations (bold bond) of fistulopsine A **(4)**

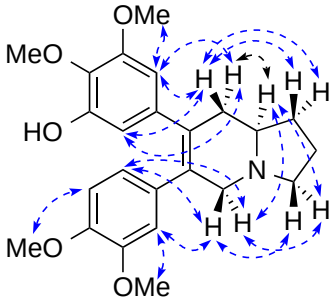

Figure 2.15: NOESY correlations of fistulopsine A **(4)**

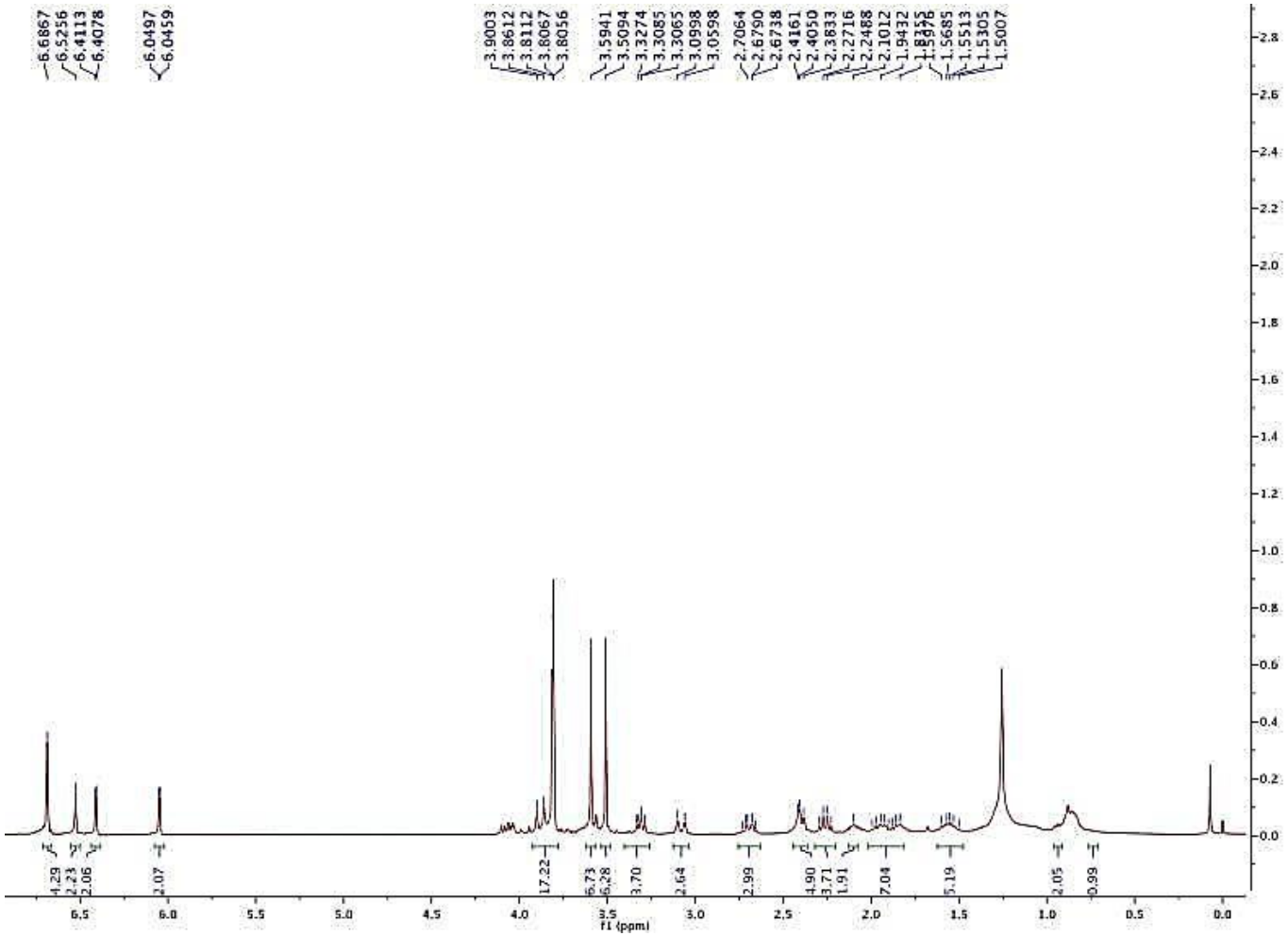

Figure 2.16: ^{1}H NMR spectrum ($CDCl_3$ CD_3OD, 600 MHz) of fistulopsine A **(4)**

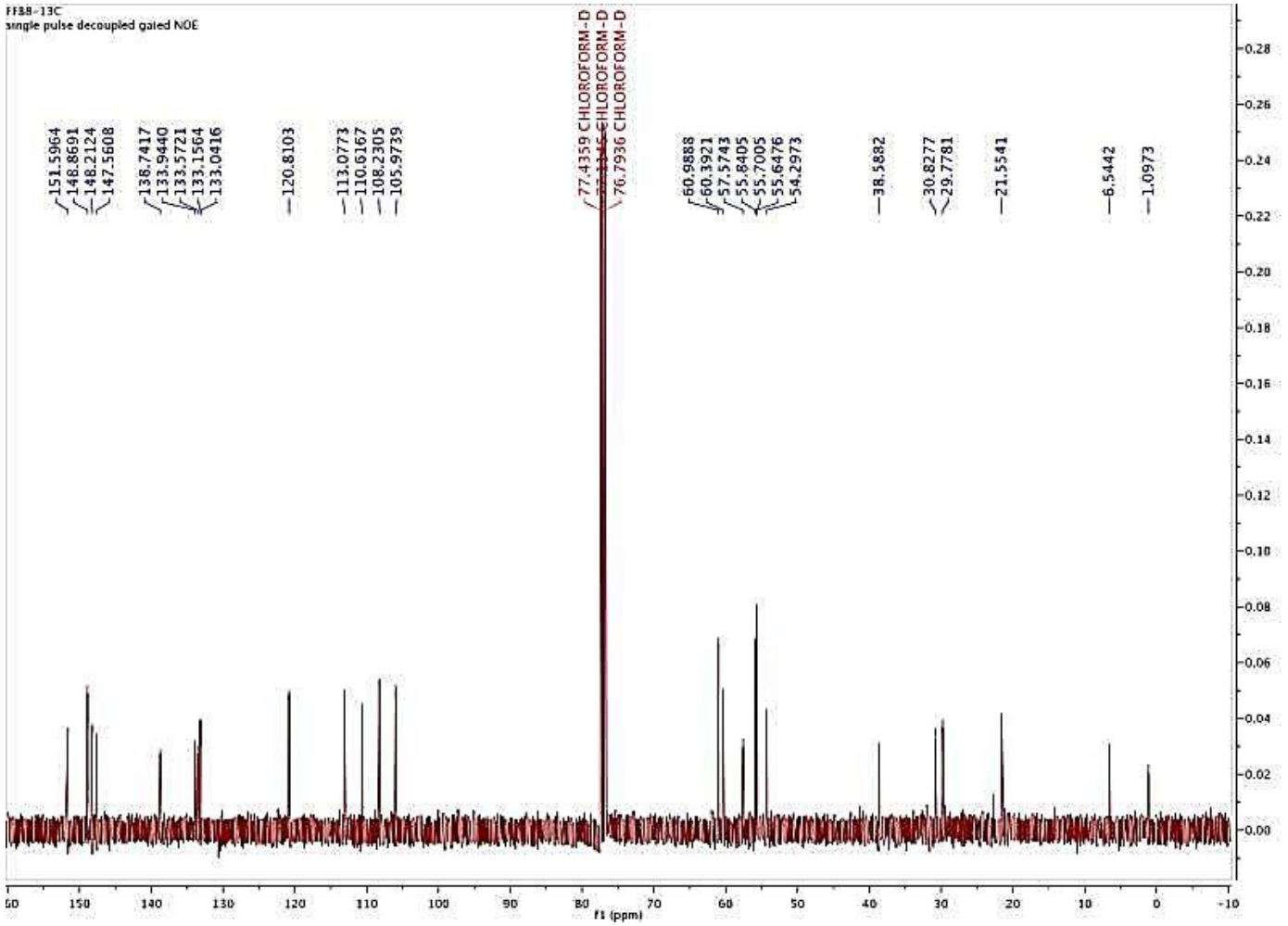

Figure 2.17: ^{13}C NMR spectrum ($CDCl_3$, 150 MHz) of fistulopsine A **(4)**

2.2.2 Fistulopsine B

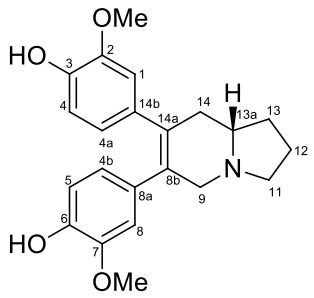

5

Fistulopsine B **(5)** was obtained as a light yellowish oil and subsequently as colourless needles (mp 209-210 °C) from $CHCl_3$/MeOH, with $[\alpha]_D^{25}$ +18 (*c* 0.32, MeOH). The IR spectrum (Appendix 28) showed absorption bands due to hydroxy (3350 cm^{-1}) and aromatic moieties (1594 and 1508 cm^{-1}). The UV spectrum showed absorption maxima at 225, 239, 263 and 286 nm, while as in the case of **4**, a bathochromic shift was also observed in the UV spectrum of **5** (Appendix 27), upon addition of aqueous sodium hydroxide indicating the presence of unsubstituted phenolic hydroxy. The ESIMS showed a pseudo-molecular ion at *m*/*z* 368, and HRESIMS measurements established the molecular formula as $C_{22}H_{25}NO_4$, requiring 11 degrees of unsaturation.

Similar to fistulopsine A **(4)**, the ^1H and ^{13}C NMR data of **5** (Table 2.5, Figures 2.21 and 2.22) showed the presence of an identical indolizidine moiety. This was confirmed by the COSY and HSQC spectra (Appendix 23 and 24) which also disclosed the presence of the two partial structures, i.e., isolated NCH_2 and $NCH_2CH_2CH_2CHCH_2$, that constituted the indolizidine moiety present in fistulopsine A **(4)**. On the other hand, the molecular formula of fistulopsine B **(5)** was 44 mass units lower than that of fistulopsine A **(4)**, suggested the replacement of a methoxy and methyl group in **4** with two hydrogen atoms in

5, which must have taken place within the two aromatic rings. Inspection of the downfield region of the ^{13}C NMR spectrum of **5** revealed the presence of four oxygenated aromatic carbon resonances at δ_C 144.3, 144.5, 146.4 and 146.6, which are consistent with the presence of four oxygen atoms in the molecular formula of **5**. The observation of only two aromatic methoxy singlets in the ^1H NMR spectrum therefore suggested the presence of two phenolic OH groups in the aromatic rings. The presence of two 1,3,4-substituted aryl moieties was deduced from the observation of two ABX systems in the ^1H NMR spectrum: δ_H 6.44 (1H, d, *J* = 1.6 Hz), 6.45 (1H, d, *J* = 1.6 Hz), 6.62 (2H, dd, *J* = 8.0, 1.6 Hz), 6.70 (1H, d, *J* = 8.0 Hz), 6.71 (1H, d, *J* = 8.0 Hz). Finally, the substitution pattern of the two aryl rings, i.e., 3-hydroxy-2-methoxyphenyl, was revealed by the HMBC data (Figure 2.18, Appendix 25), which showed three-bond correlation from H-1 to C-3 and C-4a; 2-OMe to C-2; H-4 to C-2 and C-14b; H-4a to C-1 and C-3; H-4b to C-6 and C-8; H-5 to C-7 and C-8a; 7-OMe to C-7; H-8 to C-4b and C-6. Subsequently, the two 3-hydroxy-2-methoxyphenyl moieties were shown to be connected to C-8b and C-14a by the HMBC three-bond correlations from H-9 to C-8a and H-14 to C-14b, respectively. This conclusion was further supported by the NOESY spectrum that showed correlations (Figure 2.19, Appendix 26) between H-1/H-14α, H-14β; H-4a/H-14α, H-14β; H-8/H-9α, H-9β; and H-4b/H-9α, H-9β. Finally, the positive optical rotation of **5** suggested that the configuration at C-13a is *S*.[18,143] Since suitable crystals of **5** were available, X-ray diffraction analysis was carried out (Figure 2.20), which confirmed the structure deduced from the NMR data. Therefore, the structure of **5** was elucidated as 13a(*S*)-(+)-3,6-didemethylsepticine.

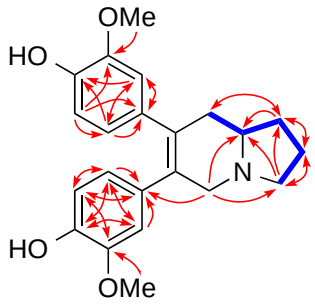

Figure 2.18: Selected HMBCs and COSY correlations (bold bonds) of fistulopsine B **(5)**

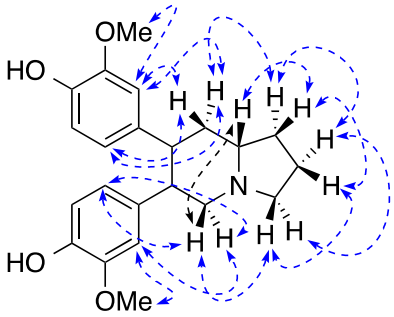

Figure 2.19: NOESY correlations of fistulopsine B **(5)**

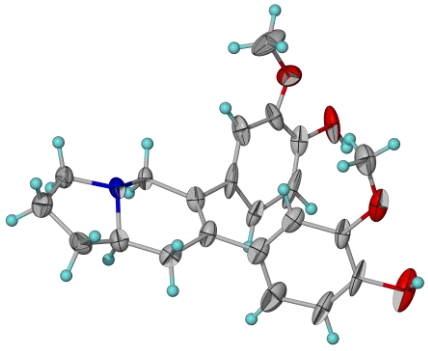

Figure 2.20: X-ray crystal structure of fistulopsine B **(5)**

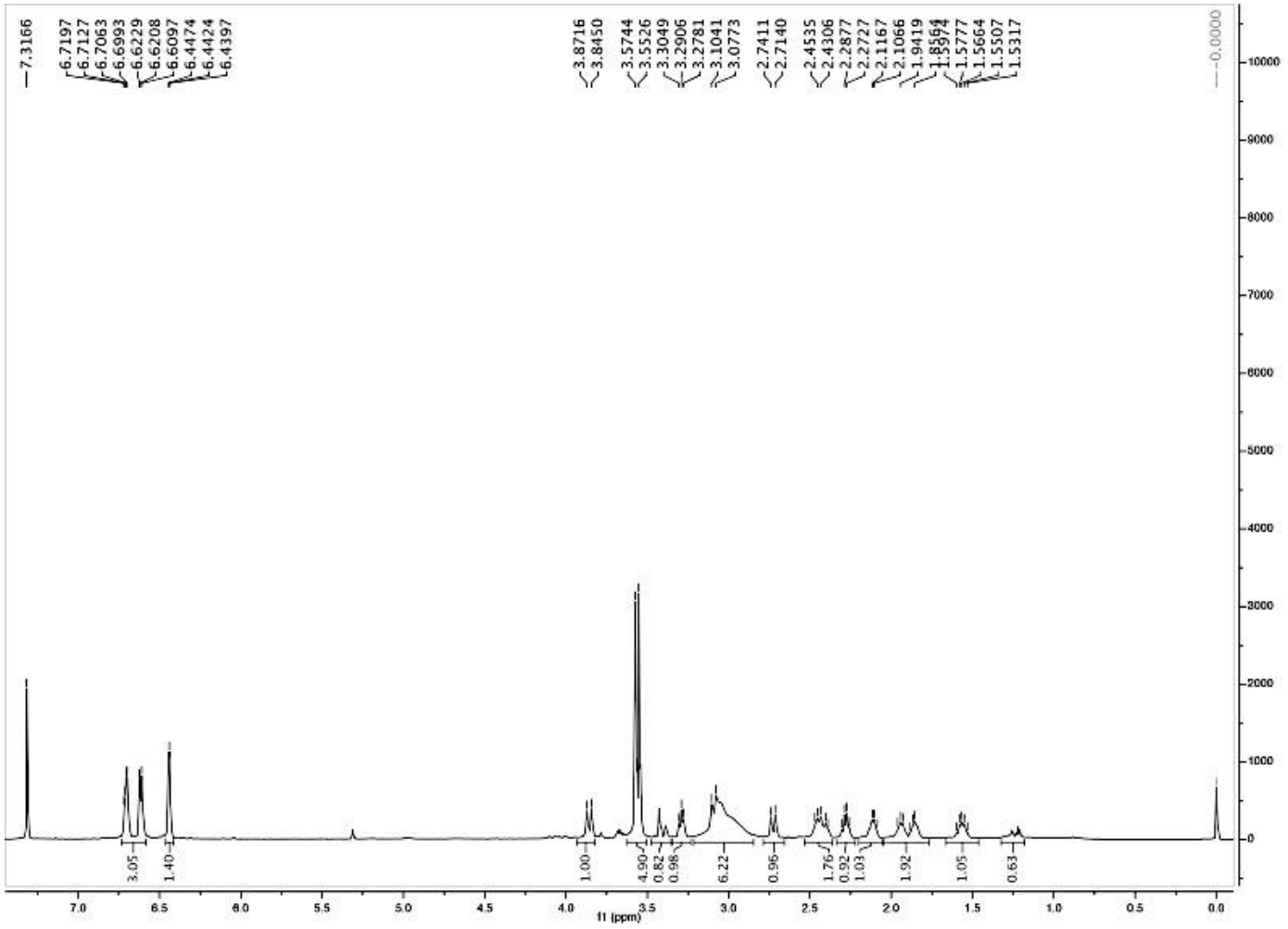

Figure 2.21: ^{1}H NMR spectrum ($CDCl_3/CD_3OD$, 600 MHz) of fistulopsine B **(5)**

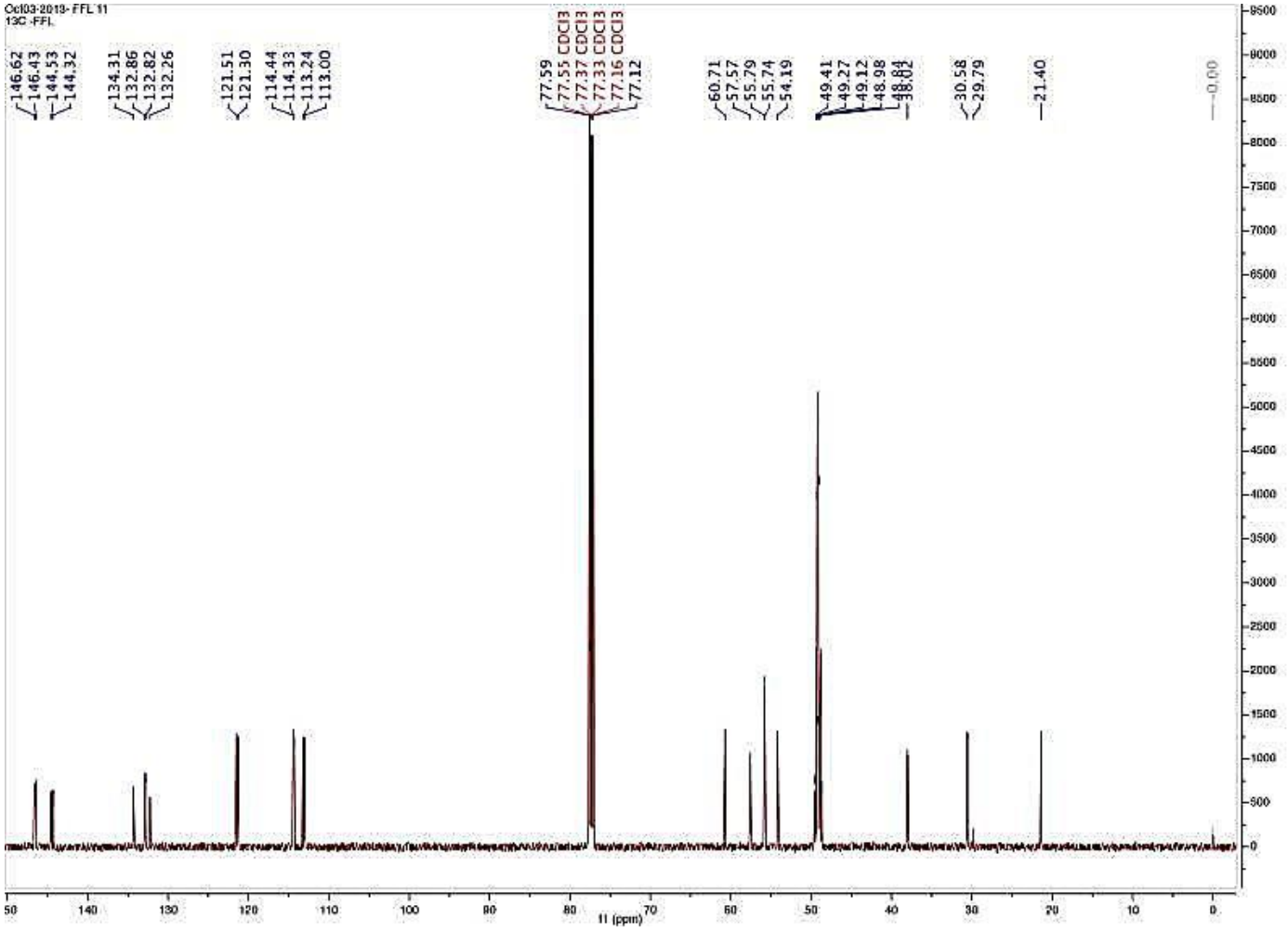

Figure 2.22: ^{13}C NMR spectrum ($CDCl_3/CD_3OD$, 150 MHz) of fistulopsine B **(5)**

Table 2.5: ^{1}H and ^{13}C NMR data of fistulopsines A **(4)** and B **(5)**[a]

Position	**4**		**5**	
	^{1}H (*J* in Hz)	^{13}C	^{1}H (*J* in Hz)	^{13}C
1	6.05 d (1.5)	106.0	6.44 d (1.6)[i]	113.0[b]
2	-	151.6	-	146.4[c]
3	-	133.9	-	144.3[d]
4	-	148.9	6.70 d (8.0)[j]	114.3[e]
4a	6.41 d (1.5)	108.2	6.62 dd (8.0, 1.6)[k]	121.3[f]
4b	6.69 br s	120.8	6.62 dd (8.0, 1.6)[k]	121.5[f]
5	6.69 br s	110.6	6.71 d (8.0)[j]	114.4[e]
6	-	147.6	-	144.5[d]
7	-	148.2	-	146.6[c]
8	6.53 br s	113.1	6.45 d (1.6)[i]	113.2[b]
8a	-	133.6	-	132.8[g]
8b	-	133.0	-	132.3
9α	3.08 d (15.5)	57.6	3.09 d (16.0)	57.6
9β	3.88 d (15.5)		3.86 d (16.0)	
11α	2.26 q (9)	54.3	2.28 q (9)	54.2
11β	3.31 t (9)		3.29 t (9)	
12α	1.83 m	21.6	1.86 m	21.4
12β	1.94 m		1.94 m	
13β	1.56 m	30.8	1.57 m	30.6
13α	2.10 m		2.11 m	
13a	2.40 m	60.4	2.45 m	60.7
14β	2.39 m	38.6	2.42 m	38.0
14α	2.69 d (13)		2.73 d (16)	
14a	-	133.2	-	134.3
14b	-	138.7	-	132.9[g]
2-OMe	3.51 s	55.65	3.55[l]	55.7[h]
3-OMe	3.81 s	61.0	-	-
6-OMe	3.81 s	55.8	-	-
7-OMe	3.59 s	55.70	3.57 s[l]	55.8[h]

[a] $CDCl_3/CD_3OD$, 600 MHz; [b-l] Assignments are interchangeable

2.2.3 13a(*R*)-(-)-3,6-Didemethylisotylocrebrine

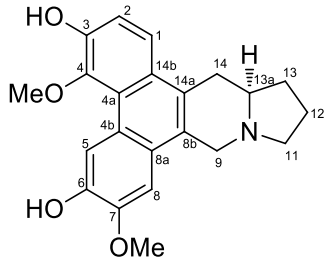

6

13a(*R*)-(-)-3,6-Didemethylisotylocrebrine **(6)** was obtained from the leaves of *F. fistulosa* as a light yellowish oil, with $[\alpha]_D^{25}$ -113 (*c* 0.13, $CHCl_3$/MeOH). The IR spectrum showed absorption bands corresponding to the presence of hydroxy (3385 cm^{-1}) and aromatic moieties (1601 and 1514 cm^{-1}). The UV spectrum showed absorption maxima at 262, 279, 304, and 317 nm. The ESIMS of **6** showed a pseudo-molecular ion at *m/z* 366 $[M + H]^+$ and HRESIMS measurements established the molecular formula as $C_{22}H_{23}NO_4$, requiring 12 degrees of unsaturation. The ^{13}C NMR data of **6** (Table 2.6, Figure 2.25) indicated the presence of 22 carbon signals (consisting of two methoxy, five methylene, five methine, and ten quaternary carbons), which are in agreement with the molecular formula. The ^1H NMR spectrum (Table 2.6, Figure 2.24) showed the distinct presence of a pair of *ortho*-coupled hydrogen signals (δ_H 7.22 and 7.69, J = 9 Hz), two aromatic singlets due to two *para*-positioned hydrogens of a tetrasubstituted benzene ring (δ_H 7.14 and 9.01), and two methoxy signals at δ_H 3.85 and 4.06. Due to the presence of four oxygen atoms in the molecular formula of **6**, the phenanthrene moiety must therefore be substituted with two hydroxy groups in addition to the two methoxy groups mentioned earlier. The profoundly deshielded aromatic singlet observed at δ_H 9.01 was characteristic of paramagnetic

deshielding of an aromatic hydrogen that is spatially proximate to an oxygen lone pair electrons, a case which is only possible if hydroxy substitution occurs at C-4 while C-5 remains unsubstituted or *vice versa*. The characteristic AB doublets observed at δ_H 3.66 and 4.58 (J = 14 Hz) were readily assigned to the isolated aminomethylene group (NCH_2) at C-9. The presence of an unsubstituted indolizidine moiety was confirmed by COSY and HSQC data which revealed the presence of an $NCH_2CH_2CH_2CHCH_2$ fragment corresponding to the N-C-11-C-12-C-13-C-13a-C-14-Ar partial structure (Figure 2.23, Appendix 29 and 30). The substitution pattern of the phenanthrene moiety was determined to be 3,6-dihydroxy-4,7-dimethoxy, deduced from the HMBC data (Figure 2.23, Appendix 31), which showed correlations from H-1 to C-3 and C-4a; H-2 to C-3, C-4 and C-14b; H-5 to C-4b, C-6 and C-7; H-8 to C-6 and C-7; 4-OMe to C-4; 7-OMe to C-7. This tetraoxygeated-phenanthrene moiety is linked to the indolizidine fragment at C-8b and C-14a by three bond correlations from H-1 to C-14a and H-8 to C-8b. The negative optical rotation observed for **6** suggested that the configuration at the C-13a stereocentre is *R*.[18,21] Therefore, the structure of **6** was elucidated as 13a(*R*)-(-)-3,6-didemethylisotylocrebrine. The structure of **6** is consistent with COSY, HSQC and HMBC data as well as with published data.[140]

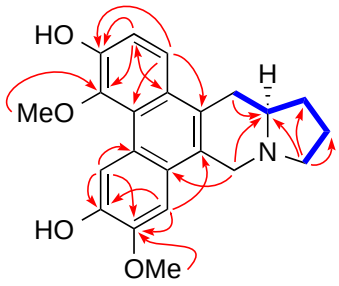

Figure 2.23: Selected HMBC and COSY correlations (bold bonds) of 13a(*R*)-(-)-3,6-didemethylisotylocrebrine **(6)**

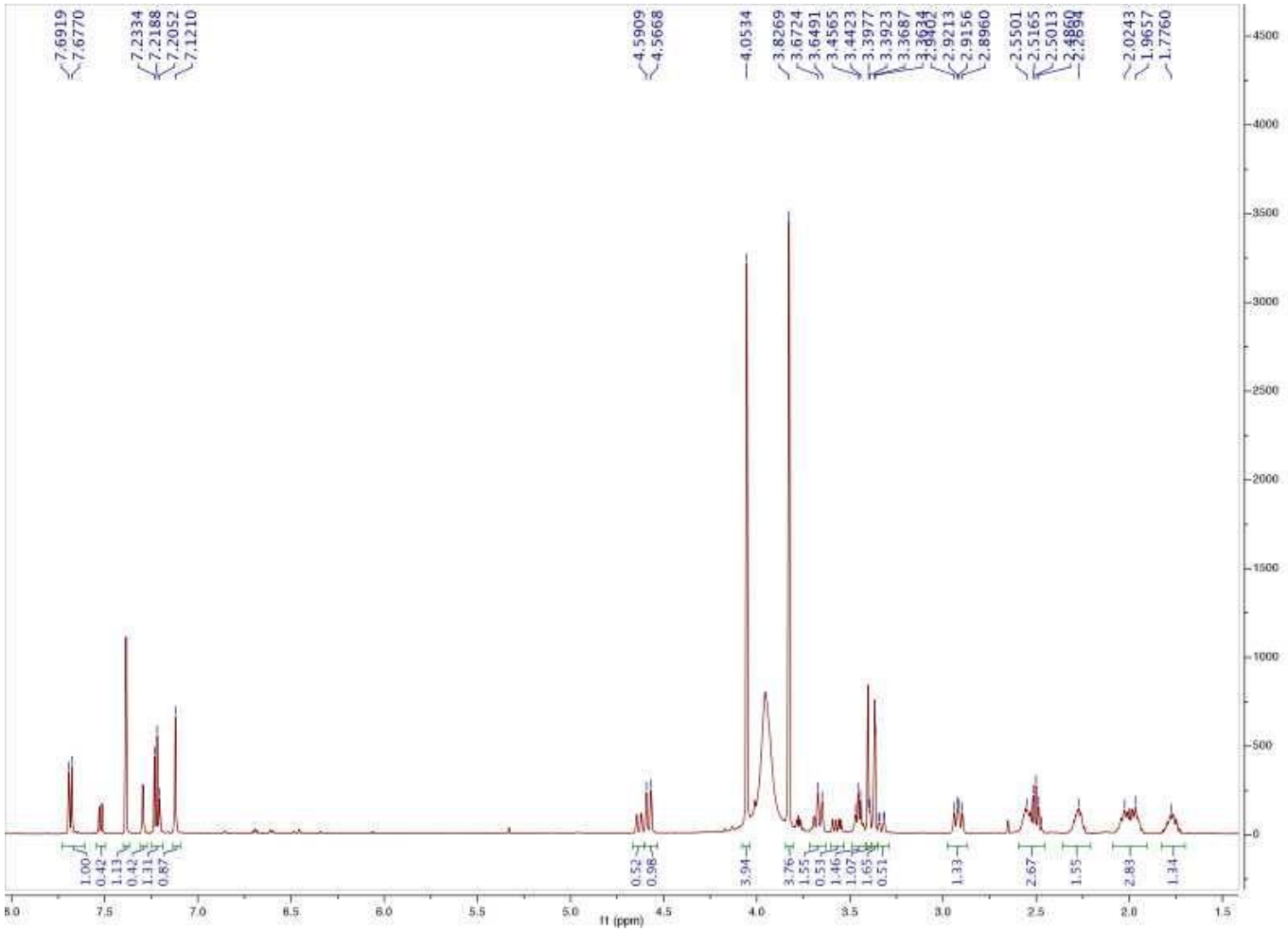

Figure 2.24: ^{1}H NMR spectrum ($CDCl_3/CD_3OD$, 400 MHz) of 13a(*R*)-(-)-3,6-didemethylisotylocrebrine **(6)**

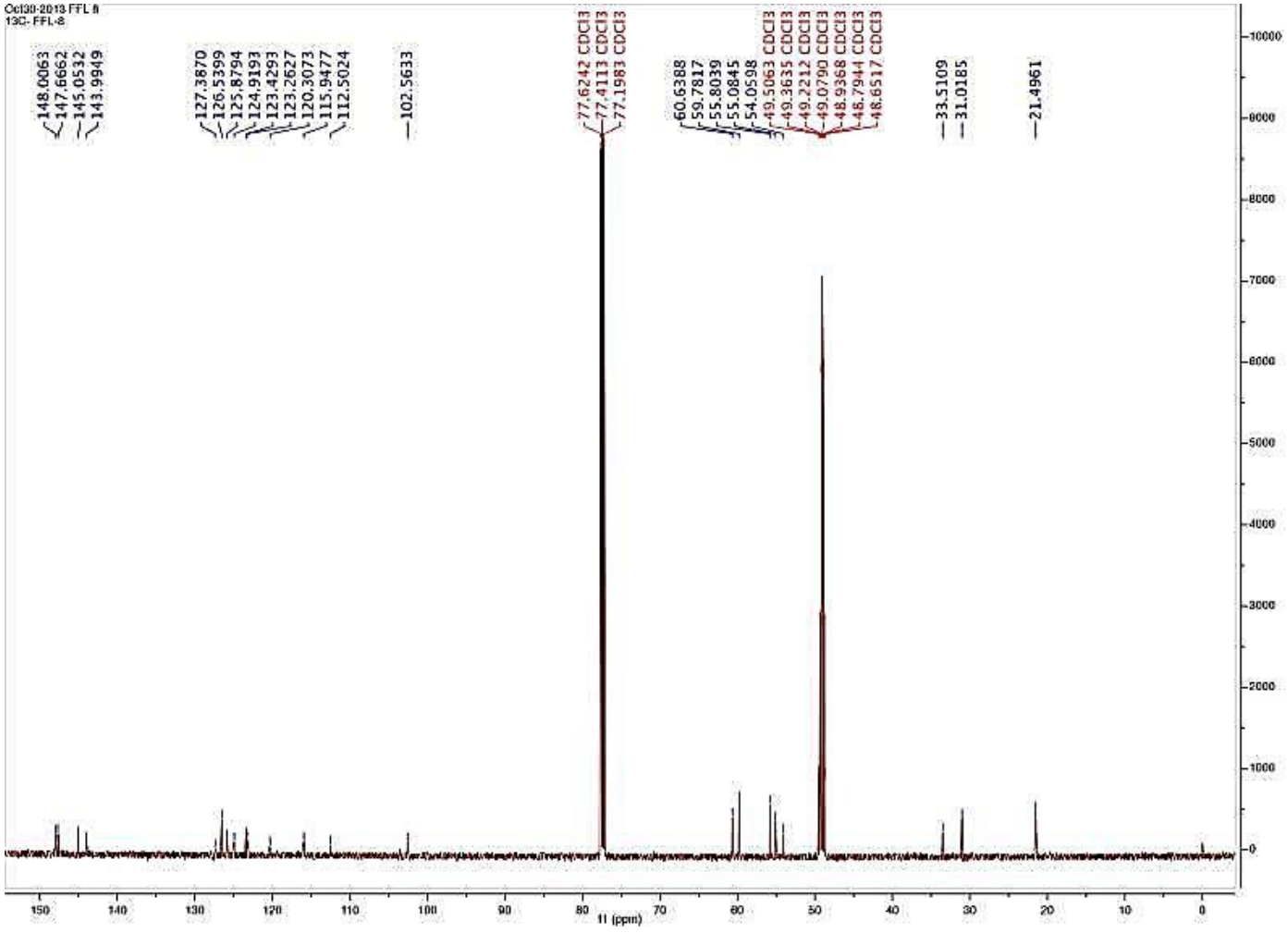

Figure 2.25: ^{13}C NMR spectrum ($CDCl_3/CD_3OD$, 100 MHz) of 13a(*R*)-(-)-3,6-didemethylisotylocrebrine **(6)**

2.2.4 13a(*S*)-(+)-Tylocrebrine

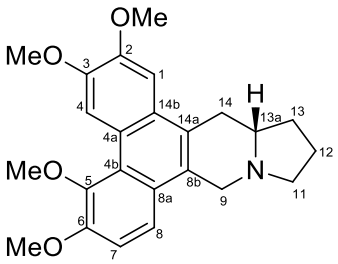

7

13a(*S*)-(+)-Tylocrebrine **(7)** was obtained from the bark of *F. fistulosa* as a light yellowish oil, with $[\alpha]_D^{25}$ +19 (*c* 0.15, $CHCl_3$). The IR spectrum showed absorption bands corresponding to the presence of aromatic moieties (1600 and 1515 cm^{-1}). The UV spectrum showed absorption maxima at 244, 264, 276, 309 and 321 nm. The ESIMS of **7** showed a pseudo-molecular ion at *m/z* 394 $[M + H]^+$ and HRESIMS measurements established the molecular formula as $C_{24}H_{27}NO_4$, requiring 12 degrees of unsaturation. The ^{13}C NMR data (Table 2.6, Figure 2.28) indicated the presence of 24 carbon resonances (consisting of four methoxy, five methylene, five methine, and ten quaternary carbons), which was in agreement with the molecular formula. The ^1H NMR spectrum (Table 2.6, Figure 2.27) showed signals due to four aromatic hydrogens and four methoxy groups (δ_H 3.48, 3.48, 3.44, 3.51). The two aromatic doublets observed at δ_H 7.30 and 7.79 with J = 9 Hz, was attributed to a pair of *ortho*-coupled aromatic hydrogens, while the remaining two aromatic singlets at δ_H 7.15 and 9.34 were due to a pair of *para*-positioned hydrogens of a tetrasubstituted benzene ring. Additionally, the aromatic singlet that was profoundly deshielded at δ_H 9.34 was characteristic of paramagnetic deshielding of an aromatic hydrogen that is spatially proximate to an oxygen lone pair electron. This is only possible if oxygenation occurs at C-4 while C-5 remains unsubstituted or *vice versa*. A distinct pair of

AB doublets observed at δ_H 3.71 and 4.63 with J = 16 Hz can be readily assigned to the isolated aminomethylene group (NCH_2) at C-9. Furthermore, the COSY data (Figure 2.26, Appendix 32) confirmed the presence of an $NCH_2CH_2CH_2CHCH_2$ fragment which corresponds to the N-C-11-C-12-C-13-C-13a-C-14-Ar partial structure of an unsubstituted indolizidine moiety. The ^1H, ^{13}C NMR and COSY data obtained suggested two possible gross structures for **7**, which corresponds to the known phenanthroindolizidine alkaloids, tylocrebrine and isotylocrebrine **(49)**. However, further comparison with literature data[153] confirmed the identity of **7** as tylocrebrine. The positive optical rotation observed for **7** suggested that the configuration at the C-13a stereocentre is *S*.[18,143] Therefore, the structure of **7** was elucidated as 13a(*S*)-(+)-tylocrebrine.

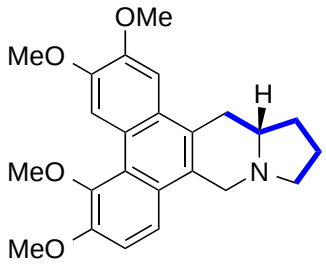

Figure 2.26: COSY correlations of 13a(*S*)-(+)-tylocrebrine **(7)**

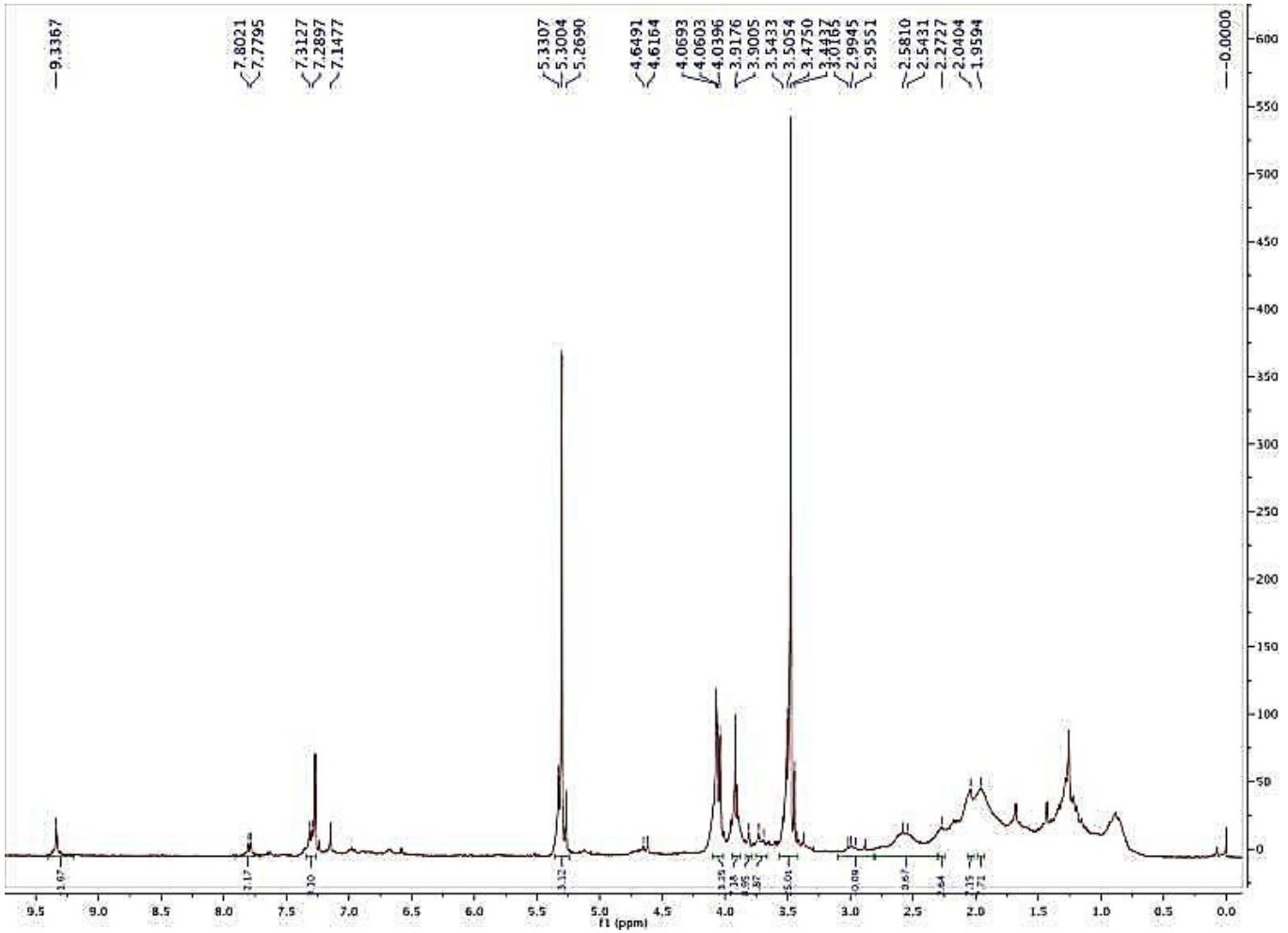

Figure 2.27: ^{1}H NMR spectrum ($CDCl_3$, 400MHz) of 13a(*S*)-(+)-tylocrebrine **(7)**

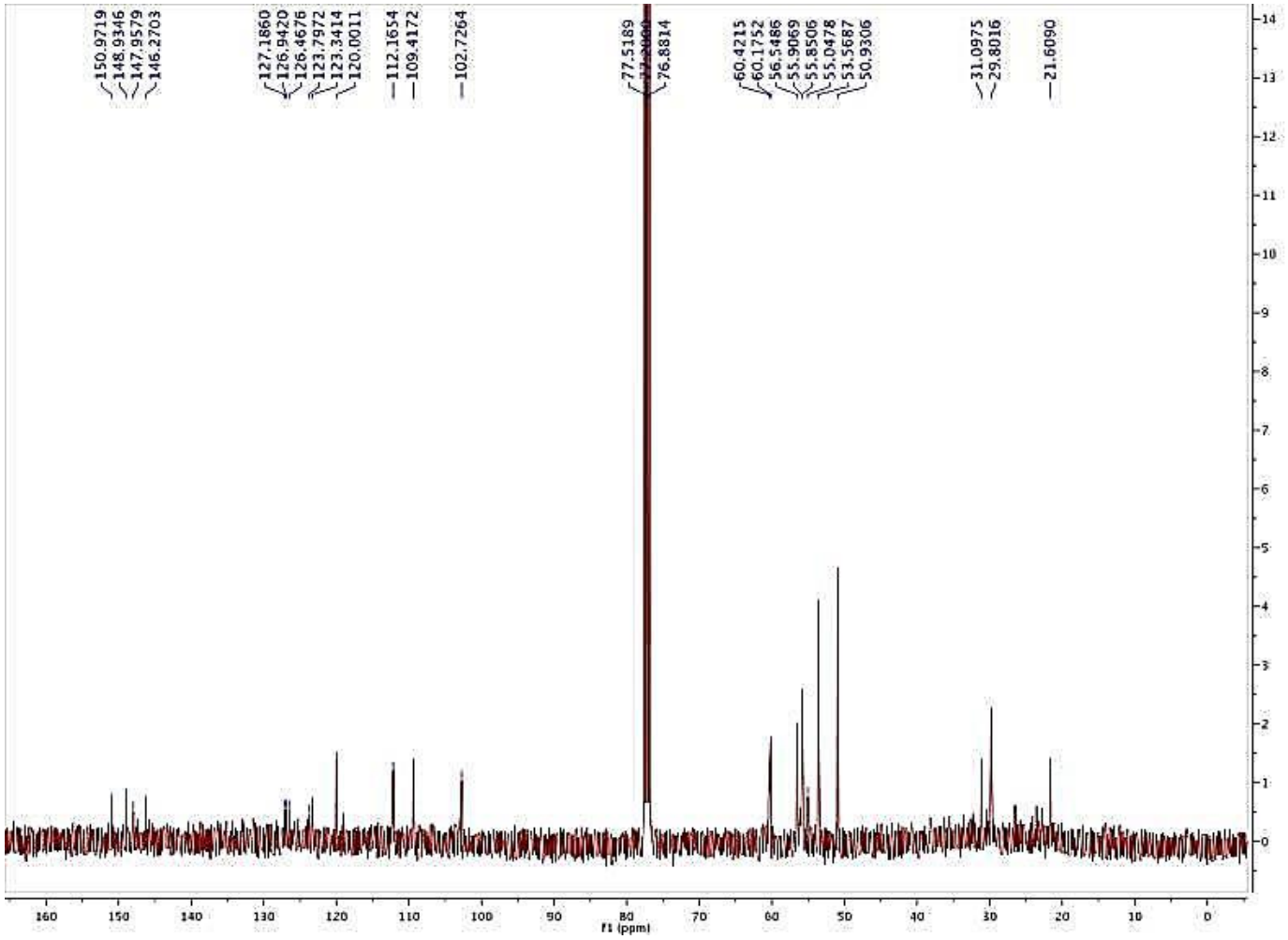

Figure 2.28: ^{13}C NMR spectrum ($CDCl_3$, 100MHz) of 13a(*S*)-(+)-tylocrebrine **(7)**

Table 2.6: ^{1}H and ^{13}C NMR data of 13a(*R*)-(-)-3,6-didemethylisotylocrebrine **(6)**[c] and 13a(*S*)-(+)-tylocrebrine **(7)**[a]

Position	**6**		**7**	
	^{1}H (*J* in Hz)	^{13}C	^{1}H (*J* in Hz)	^{13}C
1	7.69 d (9)	120.3	7.15 s	102.7
2	7.22 d (9)	115.9	-	151.0
3	-	147.7	-	148.9
4	-	144.0	9.34 s	109.4
4a	-	127.4	-	127.2
4b	-	126.5	-	126.9
5	9.01 s	112.5	-	146.3
6	-	145.1	-	148.0
7	-	148.0	7.30 d (9)	112.2
8	7.14 s	102.6	7.79 d (9)	120.0
8a	-	125.9	-	126.5
8b	-	123.3	-	123.8
9α	4.58 d (14)	54.1	4.63 d (16)	53.6
9β	3.66 d (14)		3.71 d (16)	
11α	3.67 t (8)	55.1	3.54 m	55.0
11β	2.49 q (8)		2.54 m	
12α	1.99 m	21.5	2.04 m	21.6
12β	2.02 m		1.68 m	
13α	1.77 m	31.0	2.27 m	29.8
13β	2.29 m		1.96 m	
13a	2.54 m	60.6	2.58 m	60.4
14α	3.38 dd (16, 1)	33.5	3.40 dd (16, 4)	31.1
14β	2.91 dd (16, 8)		2.97 dd (16, 10)	
14a	-	123.4	-	123.3[b]
14b	-	124.9	-	123.3[b]
2-OMe	-		3.48 s	55.85
3-OMe	-		3.48 s	56.5
4-OMe	3.85 s	59.8	-	
5-OMe	-		3.44 s	60.2
6-OMe	-		3.51 s	55.91
7-OMe	4.06 s	55.8	-	

[a] $CDCl_3$, 400 MHz;[c] $CDCl_3/CD_3OD$, 400MHz; [b]Overlapping signals.

2.2.5 13a(*S*)-(+)-Tylophorine

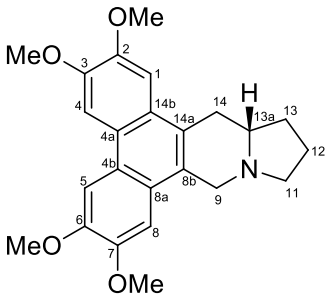

8

13a(*S*)-(+)-Tylophorine **(8)** was isolated from the leaves of *F. fistulosa* as white amorphous, with $[\alpha]_D^{25}$ +44 (c 0.12, $CHCl_3$). The UV spectrum showed absorption maxima at 240, 257, 288, 304 and 399 nm. The IR spectrum showed absorption bands corresponding to the presence of aromatic moieties (1619 and 1515 cm^{-1}). The ESIMS of **8** showed a pseudo-molecular ion at *m/z* 394 $[M + H]^+$ and HRESIMS measurements established the molecular formula as $C_{24}H_{27}NO_4$, requiring 12 degrees of unsaturation.

The ^{13}C NMR data of **8** (Table 2.7, Figure 2.31) indicated the presence of 24 carbon signals consisting of four methoxy, five methylene, five methine, and ten quaternary carbons, in agreement with the molecular formula. The ^1H NMR spectrum (Table 2.7, Figure 2.30) showed the presence of four sharp aromatic singlets at δ_H 7.12, 7.28, 7.80, 7.80, indicating the presence of a 2,3,6,7-tetrasubstituted phenanthrene moiety. In addition to this, the characteristic AB doublets observed at δ_H 4.57 and 3.65 with J=14.4 Hz can be readily assigned to the isolated aminomethylene group (NCH_2) at C-9. The COSY and HSQC data on the other hand confirmed the presence of the isolated NCH_2 group and the $NCH_2CH_2CH_2CHCH_2$ fragment that constituted the indolizidine moiety (Figure 2.29, Appendix 33 and 34). The four methyl singlets occurred between δ_H 4.05 - 4.11 were

attributed to four aromatic methoxy groups. HMBC correlations (Figure 2.29, Appendix 35) deduced that these methoxy groups are attached to the phenanthrene moiety at C-2, C-3, C-6 and C-7, thus revealing the presence of a 2,3,6,7-tetramethoxylated phenanthrene moiety. This phenanthrene moiety was linked to the indolizidine portion at C-8b and C-14a by the observed three bond correlations from H-1 to C-14a and H-8 to C-8b in the HMBC spectrum. The positive optical rotation observed for **11** suggested that the configuration at C-13a is *S*.[18,143] Therefore, the structure of **8** was elucidated to be 13a(*S*)-(+)-tylophorine. The structure of **8** is consistent with COSY, HSQC and HMBC data as well as with published data.[139,154]

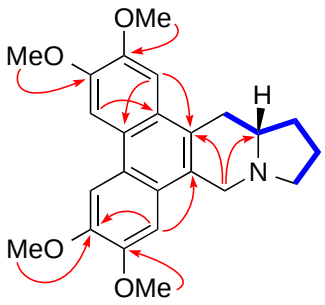

Figure 2.29: Selected HMBCs and COSY correlations (bold bonds) of 13a(*S*)-(+)-tylophorine **(8)**

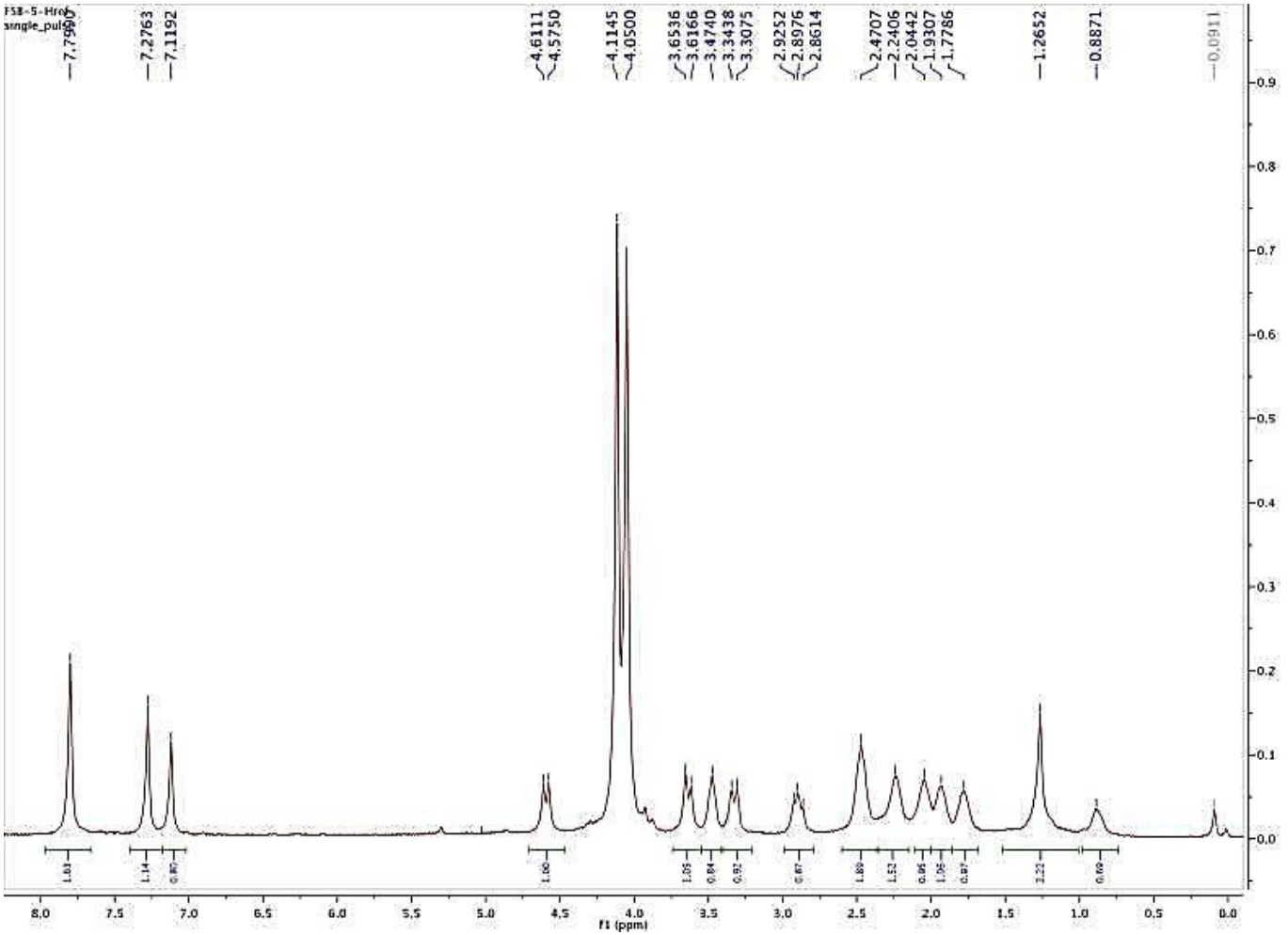

Figure 2.30: ^{1}H NMR spectrum ($CDCl_3$, 400MHz) of 13a(*S*)-(+)-tylophorine **(8)**

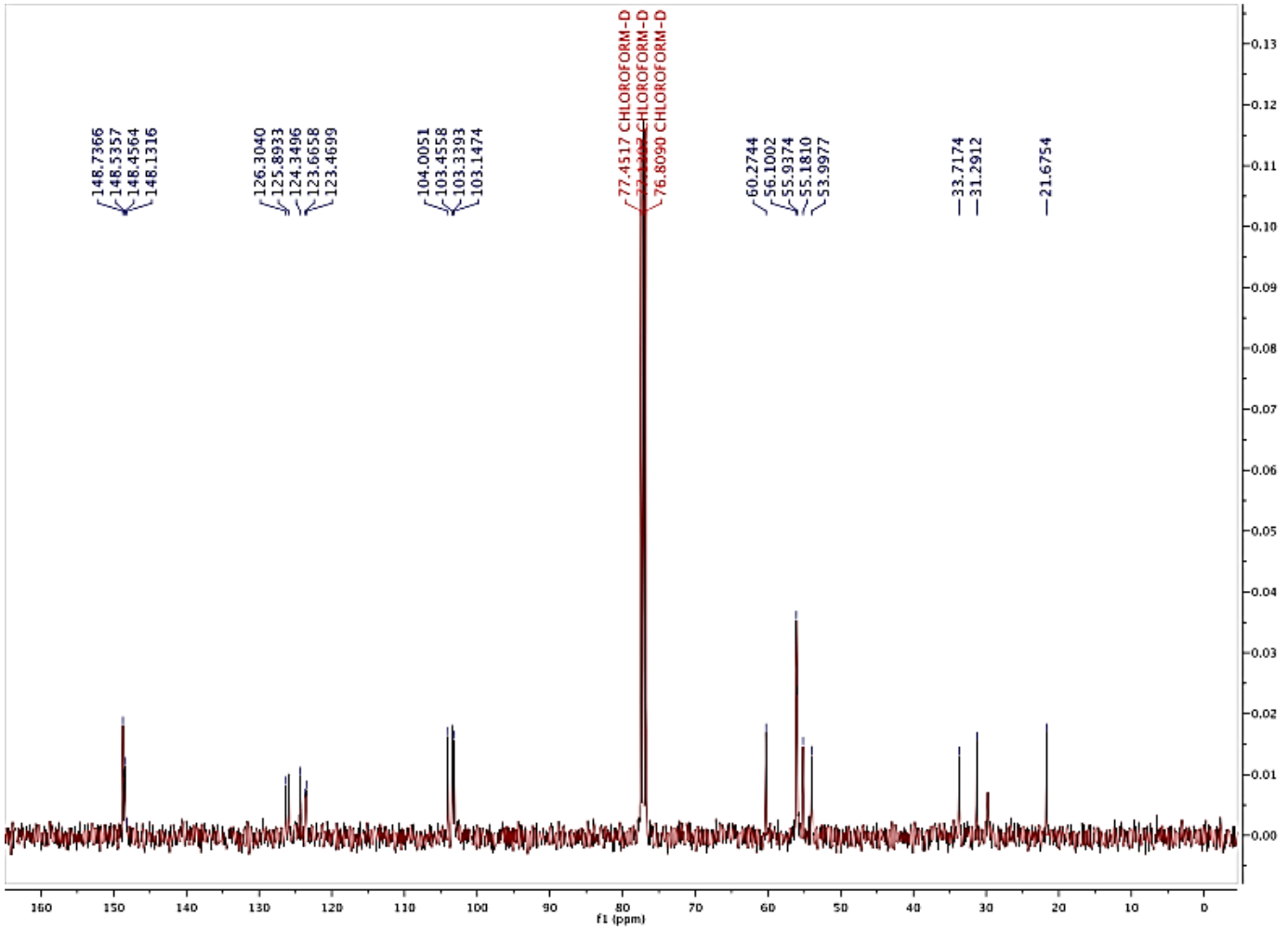

Figure 2.31: ^{13}C NMR spectrum ($CDCl_3$, 100MHz) of 13a(*S*)-(+)-tylophorine **(8)**

2.2.6 13a(*S*)-(+)-Septicine

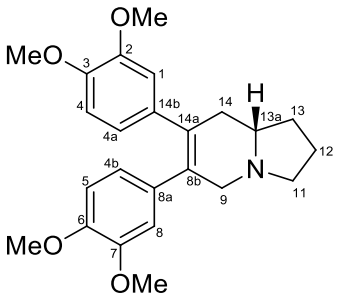

9

13a(*S*)-(+)-Septicine **(9)** was isolated as a light yellowish oil from the bark of *F. fistulosa*, with $[\alpha]_D^{25}$ +7 (*c* 0.28, $CHCl_3$). The UV spectrum showed absorption maxima at 204, 235, 263, 280 and 353 nm indicative of a *seco*-phenanthroindolizidine chromophore.[18,155] The ESIMS of **9** showed a pseudo-molecular ion at *m/z* 396 $[M + H]^+$ and HRESIMS measurements established the molecular formula as $C_{24}H_{29}NO_4$, requiring 11 degrees of unsaturation.

The ^{13}C NMR data of **9** (Table 2.7, Figure 2.34) indicated the presence of 24 carbon signals consisting of four methoxy, five methylene, seven methine, and eight quaternary carbons, in agreement with the molecular formula. The six carbon resonances at δ_C 113.0, 110.6, 120.7, 121.0, 110.7 and 112.9 were readily assigned to the aromatic methines in **9**, while the quaternary aromatic carbon signals observed between δ_C 132.7–135.2 are characteristic of C-8a, C-8b, C-14a, and C-14b of *seco*-phenanthroindolizidine alkaloids.

The ^1H NMR spectrum (Table 2.7, Figure 2.33) showed signals due to six distinct aromatic hydrogens and four methoxy groups (δ_H 3.55, 3.57, 3.78, 3.78), which indicated the presence of two dimethoxylated benzene rings. Characteristic AB doublets in the upfield region at δ_H 3.07 and 3.87 with *J*=16 Hz was assigned to the isolated

aminomethylene group (NCH_2) at C-9. Furthermore, the COSY and HSQC data revealed the presence of the $NCH_2CH_2CH_2CHCH_2$ partial structure of the indolizidine moiety, i.e., N-C-11-C-12-C-13-C13a-C-14 (Figure 2.32, Appendix 36 and 37). The substitution pattern of the two aryl rings was determined by HMBC data (Figure 2.32, Appendix 38). Three-bond correlations from H-1 to C-3 and C-4a; H-4a to C-1 and C-3; 2-OMe to C-2; 3-OMe to C-3; H-4b and H-8 to C-6; H-5 to C-7 and C-8a; 6-OMe to C-6; 7-OMe to C-7, established the substitution pattern of the two aryl rings to be 2,3-dimethoxyphenyl. HMBC correlations from H-9 and H-4a to C-14a, and H-8 and H-9 to C-8b established the attachment sites of the two dimethoxylated aryl rings as C-8b and C-14a. The positive optical rotation observed for **9** suggested an *S* configuration at the C-13a stereocentre.[18,143] Therefore, the structure of **9** was elucidated to be 13a(*S*)-(+)-septicine. The structure of **9** is entirely consistent with the COSY, HSQC and HMBC data and the ^{1}H and ^{13}C NMR data are identical to published data.[156]

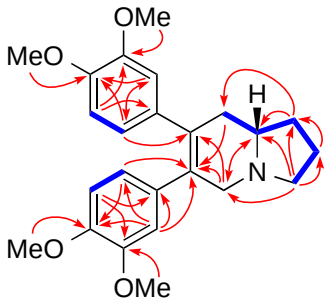

Figure 2.32: Selected HMBCs and COSY correlations (bold bonds) of 13a(*S*)-(+)-septicine **(9)**

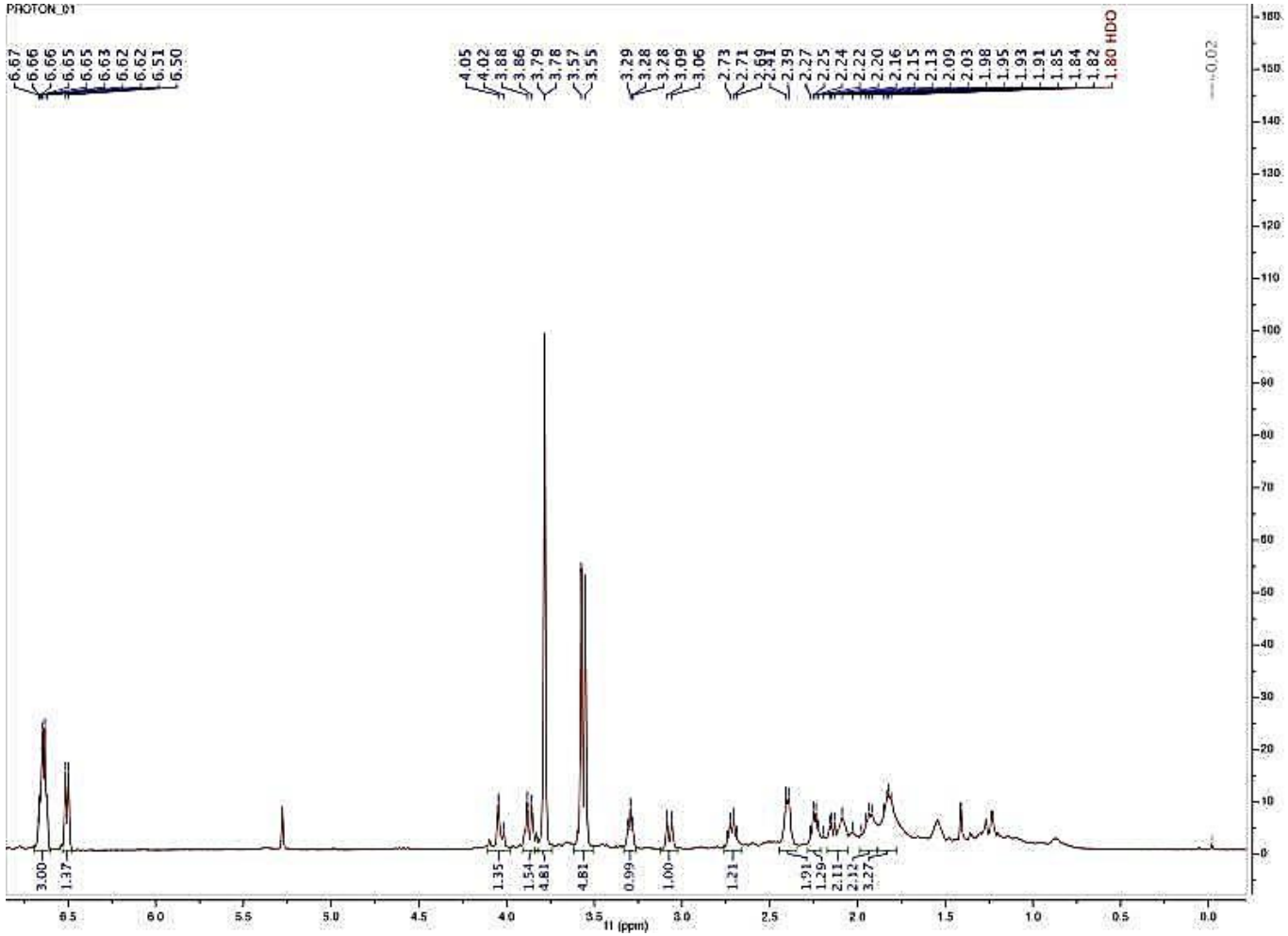

Figure 2.33: ^{1}H NMR spectrum ($CDCl_3$, 400 MHz) of 13a(*S*)-(+)-septicine **(9)**

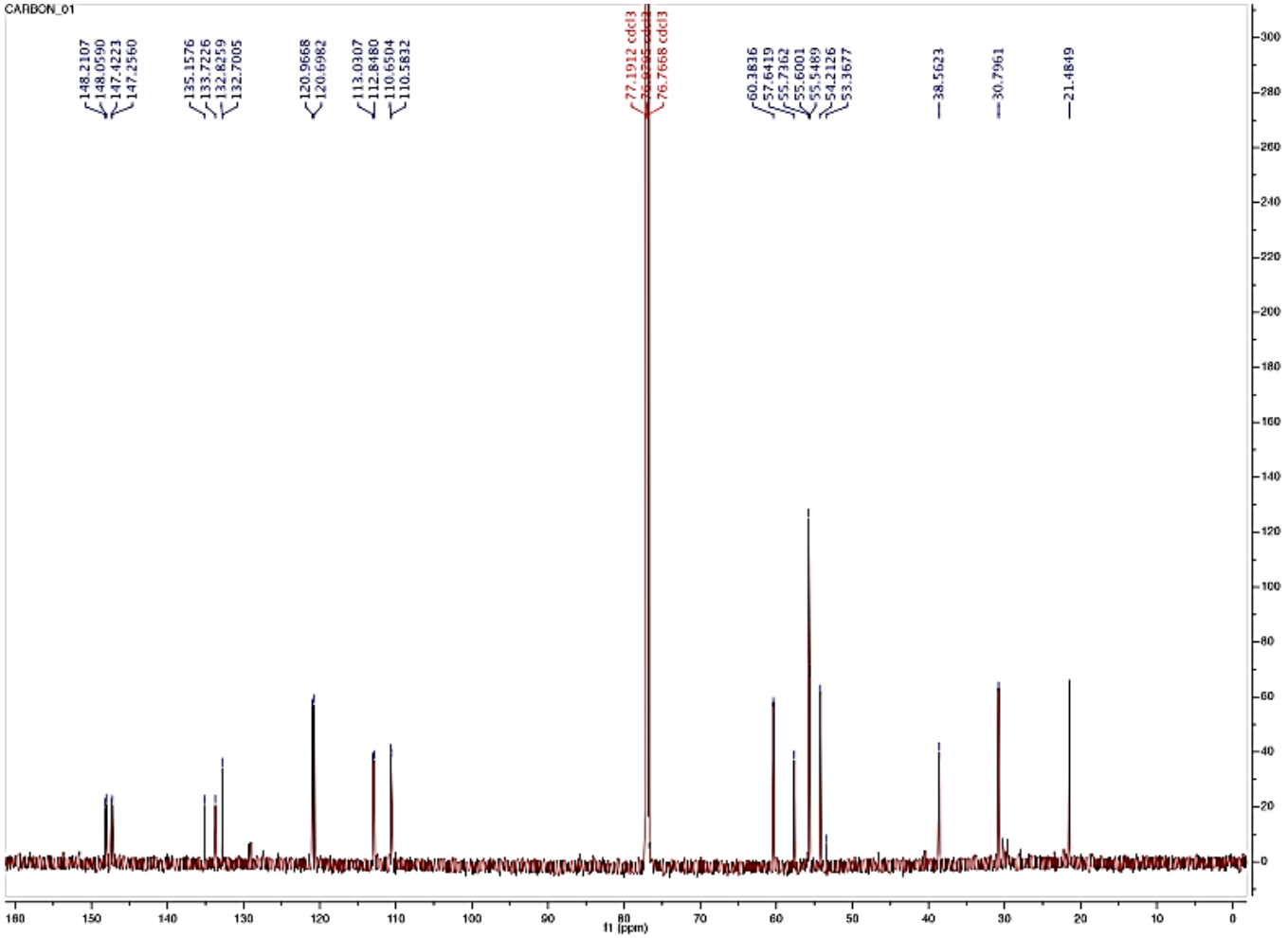

Figure 2.34: ^{13}C NMR spectrum ($CDCl_3$, 100 MHz) of 13a(*S*)-(+)-septicine **(9)**

Table 2.7: ^{1}H ($CDCl_3$, 400 MHz) and ^{13}C ($CDCl_3$, 100 MHz) NMR data of 13a(S)-(+)-tylophorine **(8)** and 13a(*S*)-(+)-septicine **(9)**[a]

Position	**8**		**9**	
	^{1}H (*J* in Hz)	^{13}C	^{1}H (*J* in Hz)	^{13}C
1	7.28 s	104.0	6.25 d (2)[b]	113.0[b]
2	-	148.54[b]	-	148.1[c]
3	-	148.46[b]	-	147.3[d]
4	7.80 s	103.4	6.66 m[c]	110.6[e]
4a	-	123.7	6.65 m[d]	120.7[f]
4b	-	123.4	6.65 m[d]	121.0[f]
5	7.80 s	103.3	6.63 m[c]	110.7[e]
6	-	148.1	-	147.4[d]
7	-	148.7	-	148.2[c]
8	7.12 s	103.1	6.50 d (2)[b]	112.9[b]
8a	-	125.9[j]	-	135.2
8b	-	124.3	-	132.7[g]
9α	4.57 d (14)	55.2	3.07 d (16)	57.6
9β	3.65 d (14)		3.87 d (16)	
11α	3.47 td (7, 6)	54.0	2.24 m	53.4
11β	2.49m		3.29 t (8.5)	
12α	2.04 m	21.6	1.82 m	21.5
12β	1.93 m		1.93 m	
13α	2.24 m	31.2	1.54	30.8
13β	1.78 m		2.07 m	
13a	2.47 m	60.3	2.40 m	60.4
14α	3.31 dd (15, 3)	33.7	2.40 m	38.6
14β	2.89 dd (15, 10)		2.73 dd	
14a	-	125.9[j]	-	132.8[g]
14b	-	126.3	-	133.7
2-OMe	4.05 s	56.1[k]	3.55 s[e]	57.6[h]
3-OMe	4.11 s	55.9[l]	3.78 s	55.60[i]
6-OMe	4.11 s	55.9[l]	3.78 s	55.55[i]
7-OMe	4.05 s	56.1[k]	3.57 s[e]	54.2[h]

[a] $CDCl_3$, 400 MHz; [b-h]Assignments are interchangeable; [k-l]Overlapping signals

2.2.7 Vomifoliol

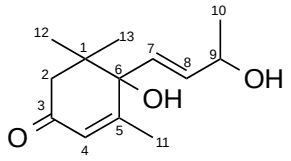

10

Vomifoliol **(10)** was isolated from the bark of *F. fistulosa* as colourless needles, mp 105-109 °C (lit., 107-109 °C)[157] with $[\alpha]_D^{25}$ +117 (*c* 0.41, $CHCl_3$). ESIMS of **10** showed a pseudo-molecular ion at *m/z* 225 $[M + H]^+$ and HRESIMS measurements established the molecular formula as $C_{13}H_{20}O_3$, requiring four degrees of unsaturation. The UV spectrum showed absorption maxima at 237 nm, while the IR spectrum showed absorption bands due to OH (3369 cm^{-1}) and conjugated ketone function (1663 cm^{-1}).

The ^1H NMR spectrum (Table 2.8, Figure 2.35) showed the distinct presence of three 3H singlets and one 3H doublet. The two 3H singlets at δ_H 1.02 and 1.08 were attributable to the gem dimethyl group at C-1, while the 3H singlet at δ_H 1.91 can be assigned to the methyl group attached to the olefinic C-5 and the 3H doublet at δ_H 1.30 (*J* = 5.8) to the oxymethine C-9. The large coupling constant observed between δ_H 5.78 and δ_H 5.85 (16 Hz) implied a *trans* geometry of the C-7/C-8 double bond. Comparison between the NMR spectral data of **10** with those in the literature revealed **10** to be either (+)-(6*S*,9*S*)-vomifoliol or (-)-(6*R*,9*R*)-vomifoliol. Since a positive optical rotation value was obtained for **10**, it is therefore (+)-(6*S*,9*S*)-vomifoliol.[157]

Table 2.8: ^{1}H NMR data ($CDCl_3$, 400 MHz) of vomifoliol **(10)**

Position	**10**	Vomifoliol[157]
	^{1}H (*J* in Hz)	^{1}H (*J* in Hz)
1-Me	1.02 s	1.00 s
	1.08 s	1.07 s
2	2.24 d (17.1)	2.23 d (17)
	2.45 d (17.1)	2.45 d (17)
4	5.91 br s	5.90 br s
5-Me	1.91 s	1.90 s
7	5.78 d (15.6)	5.77 d (15.5)
8	5.85 dd (15.7, 5)	5.87 dd (15.5, 5)
9	4.40 quintet-like	4.41 quintet-like
9-Me	1.30 d (5.8)	1.30 d (6.5)

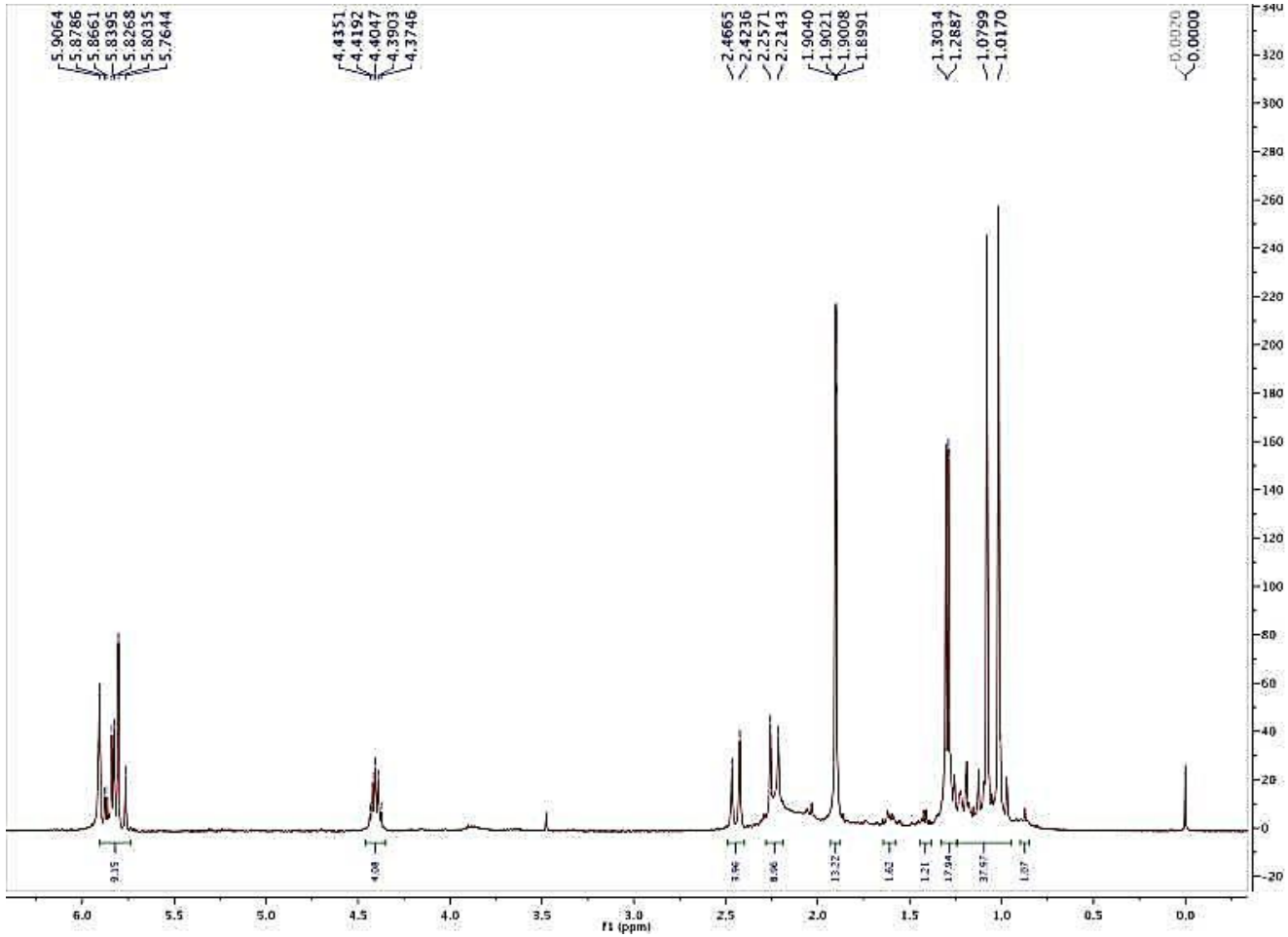

Figure 2.35: ^{1}H NMR spectrum ($CDCl_3$, 400 MHz) of vomifoliol **(10)**

2.3 Alkaloids from *F. schwarzii*

A preliminary study on the leaves of *F. schwarzii* has resulted in the isolation of two major alkaloids, namely, schwarzinicines A **(11)** and B **(12)**, which represent the first members of a novel class of plant alkaloids, i.e., tri-*nor*-sesquilignan alkaloids. The structures of the isolated compounds were determined by spectroscopic methods.

2.3.1 Schwarzinicine A

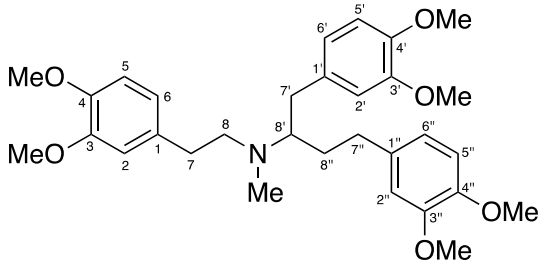

11

Schwarzinicine A **(11)** was obtained from the leaves of *F. schwarzii* as a light yellowish oil with $[\alpha]_D^{25}$ +24 (*c* 0.50, $CHCl_3$). The UV spectrum (Appendix 42), which showed absorption maxima at 228 and 280 nm, is characteristic of a 3,4-dimethoxylated benzene chromophore. The ESIMS showed a pseudo-molecular ion at *m/z* 524 $[M + H]^+$, and HRESIMS measurements established the molecular formula as $C_{31}H_{41}NO_6$, requiring 12 degrees of unsaturation.

The ^{13}C NMR data (Table 2.9, Figure 2.38) showed the presence of 31 carbon signals, comprising of three dioxygenated aromatic rings (6C x 3), five methylene, one methine, one N-methyl and six methoxy carbons, in agreement with the molecular formula. Additionally, the 18 carbon resonances found within the region of δ_C 110-150 were seen to

cluster in four distinct chemical shift ranges, i.e., δ_C 146-149 (six signals), δ_C 132-136 (three signals), δ_C 120-122 (three signals) and δ_C 111-113 (six signals), which were indicative of the presence of three units of trisubstituted 3,4-dioxygenated aryl ring. Comparison of the aromatic carbon shifts with those of natural products containing 3,4-dioxygenated aryl moieties,[158,159] readily allowed the assignment of the four distinct clusters of carbon resonances to the corresponding aromatic carbon types. The three quaternary carbons resonated between δ_C 132-136 were assigned to C-1, -1' and -1". The three methine carbons resonated between δ_C 120-122 were readily assigned to C-6, -6', -6", while the remaining six methine carbons that resonated between δ_C 111-113 are characteristic of aromatic carbons adjacent to an oxygenated aromatic carbon, and thus were attributable to C-2, -2', -2", C-5, -5' and -5". Finally, the six highly deshielded quaternary carbon resonances at δ_C 146.9, 147.1, 147.3, 148.6, 148.7 and 148.8 suggested that these carbons are sites of oxygenation, which coupled with the presence of six methoxy groups (δ_C 55-56), indicated the presence of three 3,4-dimethoxylated aryl moieties.

The ^{1}H NMR spectrum (Table 2.9, Figure 2.37) showed the presence of nine aromatic protons, six aromatic methoxy groups, an N-methyl, and eleven aliphatic protons. The presence of the 1,3,4-trisubstituted aromatic rings were further supported by the splitting patterns observed for the aromatic proton signals for H-2/2'/2" [δ_H 6.73 m, 6.62 (d, *J* = 8 Hz), 6.56 (d, *J* = 2 Hz)], H-5/5'/5" [δ 6.79 (d, *J* = 8 Hz), 6.76 (d, *J* = 8 Hz), 6.73m] and H-6/6'/6" [δ 6.74 m, 6.65 (dd, *J* = 8, 2 Hz), 6.57 (dd, *J* = 8, 2 Hz)]. The six methoxy singlets were detected between δ_H 3.80 – 3.87 while the NMe singlet at 2.38 ppm.

The HSQC and COSY data revealed the presence of CH_2CH_2 and $CH_2CHCH_2CH_2$ fragments which correspond to the C(7)-C(8) and C(7')-C(8')-C(8")-C(7") partial structures, respectively (Figure 2.36, Appendix 39 and 40). The most important information provided

by the HMBC data (Figure 2.36, Appendix 41) are those that linked the three aryl rings deduced above to C-7/7'/7" of the aliphatic backbone. The attachment of one of the aryl rings to C-7 was supported by the long range correlations observed from H-8 to C-1; H-7 to C-2 and C-6; H-2 and H-6 to C-7. The attachment of the second aryl ring to C-7' was supported by the correlations observed from H-7' to C-2' and C-6'; H-2' to C-7'. Finally, the last aryl ring was deduced to be attached to C-7" from the correlations observed from H-8" to C-1"; H-7" to C-1", C-2" and C-6"; H-2" to C-7". The HMBC data have therefore successfully connected the three 3,4-dimethoxybenzene rings to the aliphatic carbon skeleton. Therefore the structure of schwarzinicine A **(11)** was elucidated to be *N*-(3,4-dimethoxyphenethyl)-1,4-bis(3,4-dimethoxyphenyl)-*N*-methylbutan-2-amine. However, because of severe overlapping of signals in the ^{1}H and ^{13}C NMR spectra, the unambiguous assignments of some aromatic signals were not possible, and these are indicated in Table 2.9.

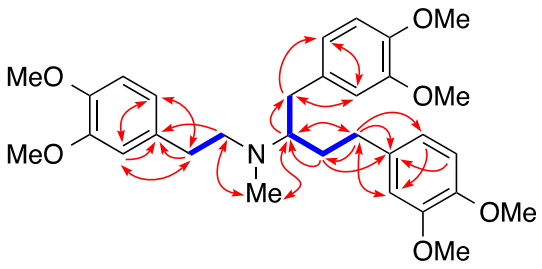

Figure 2.36: Selected HMBCs and COSY correlations (bold bonds) of **(11)**

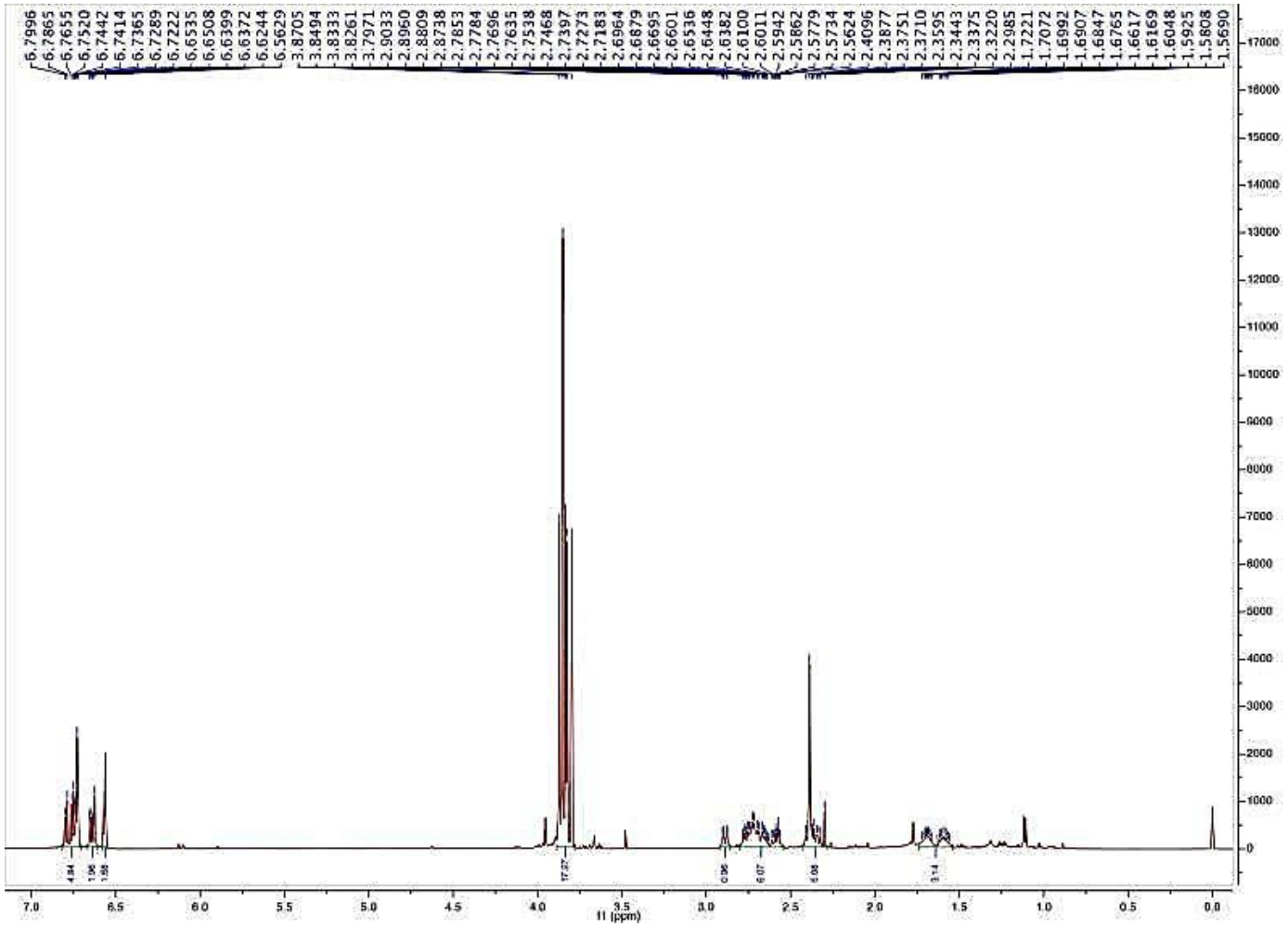

Figure 2.37: ^{1}H NMR spectrum ($CDCl_3$, 600 MHz) of schwarzinicine A **(11)**

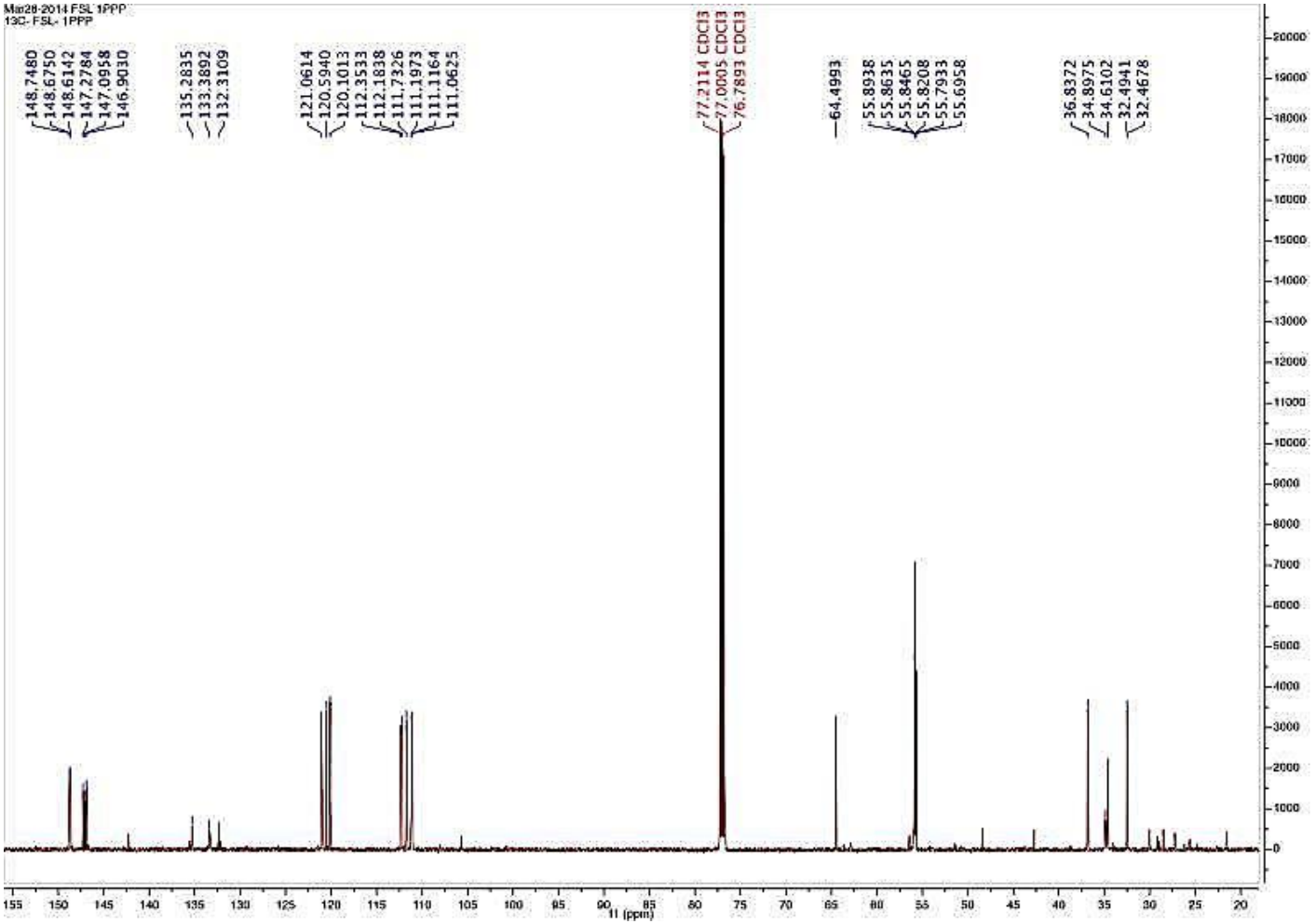

Figure 2.38: ^{13}C NMR spectrum ($CDCl_3$, 150 MHz) of schwarzinicine A **(11)**

2.3.2 Schwarzinicine B

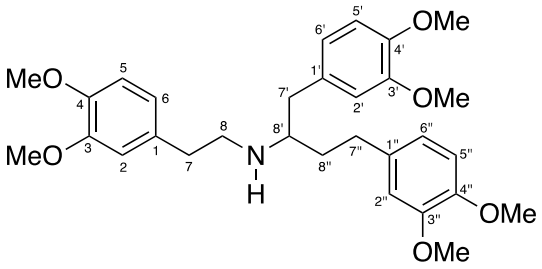

12

Schwarzinicine B **(12)** was obtained as a major alkaloid from the leaves of *F. schwarzii* as a light yellowish oil $[\alpha]_D^{25}$ +2 (*c* 0.45, $CHCl_3$). The IR spectrum (Appendix 48) showed absorption band at 3587 cm^{-1} indicating the presence of a secondary amine. The UV spectrum (λ_{max} 230 and 281 nm) of **12** (Appendix 47) was essentially identical to that of **11**. The ESIMS showed a pseudo-molecular ion at *m/z* 510 $[M + H]^+$, and HRESIMS measurements established the molecular formula as $C_{30}H_{39}NO_6$, differing from **12** by 14 mass units and suggesting that **12** differed from **11** in having a methyl group replaced with a hydrogen atom.

Comparison of the ^1H and ^{13}C NMR spectra (Table 2.9) indicated a general similarity of **11** and **12**, except for some notable differences in the aliphatic region. The ^1H NMR spectrum of **12** (Figure 2.40) showed a distinct absence of the NMe signal (δ_H 2.38) present in that of **11**, replaced instead by a broad singlet at δ_H 1.98 in **12**, attributable to an NH group. Similarly the ^{13}C NMR spectrum of **12** (Figure 2.41) showed the absence of the NMe signal present in that of **11**. Analysis of HSQC, COSY and HMBC data (Figure 2.39, Appendix 44 - 46) revealed the presence of identical partial structures in both **11** and **12**. Therefore, schwarzinicine B **(12)** was determined to be the N-demethyl derivative of

schwarzinicine A **(11)** or *N*-(3,4-dimethoxyphenethyl)-1,4-bis(3,4-dimethoxyphenyl)-*N*-methylbutan-2-amine.

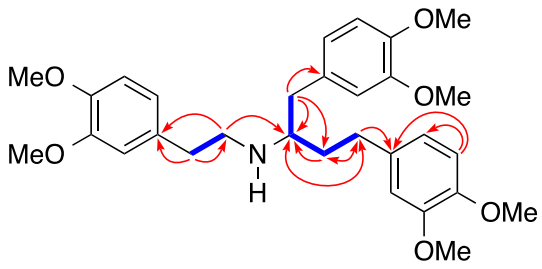

Figure 2.39: Selected HMBCs and COSY correlations (bold bonds) of schwarzinicine B **(12)**

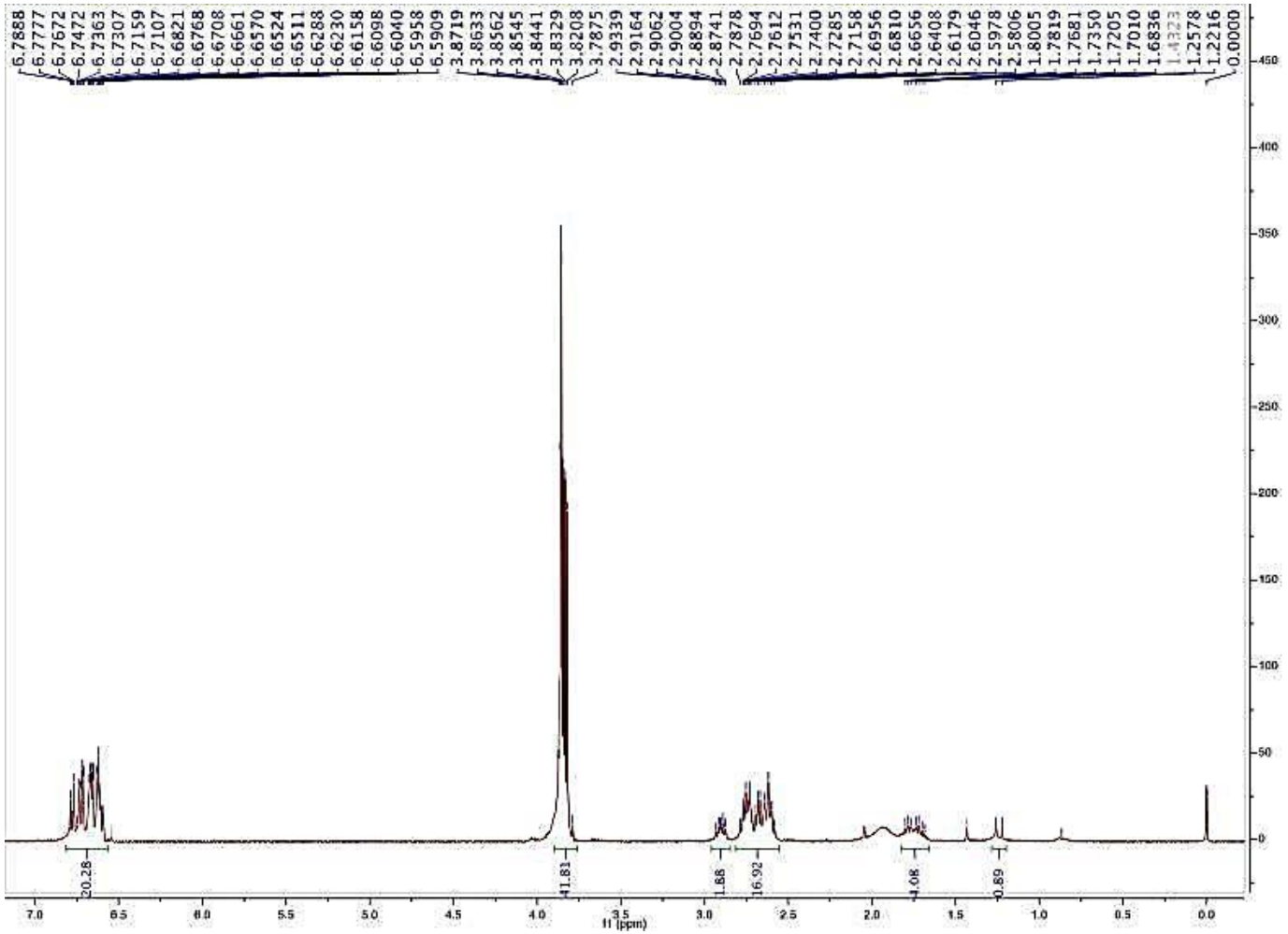

Figure 2.40: ^{1}H NMR spectrum ($CDCl_3$, 600 MHz) of schwarzinicine B **(12)**

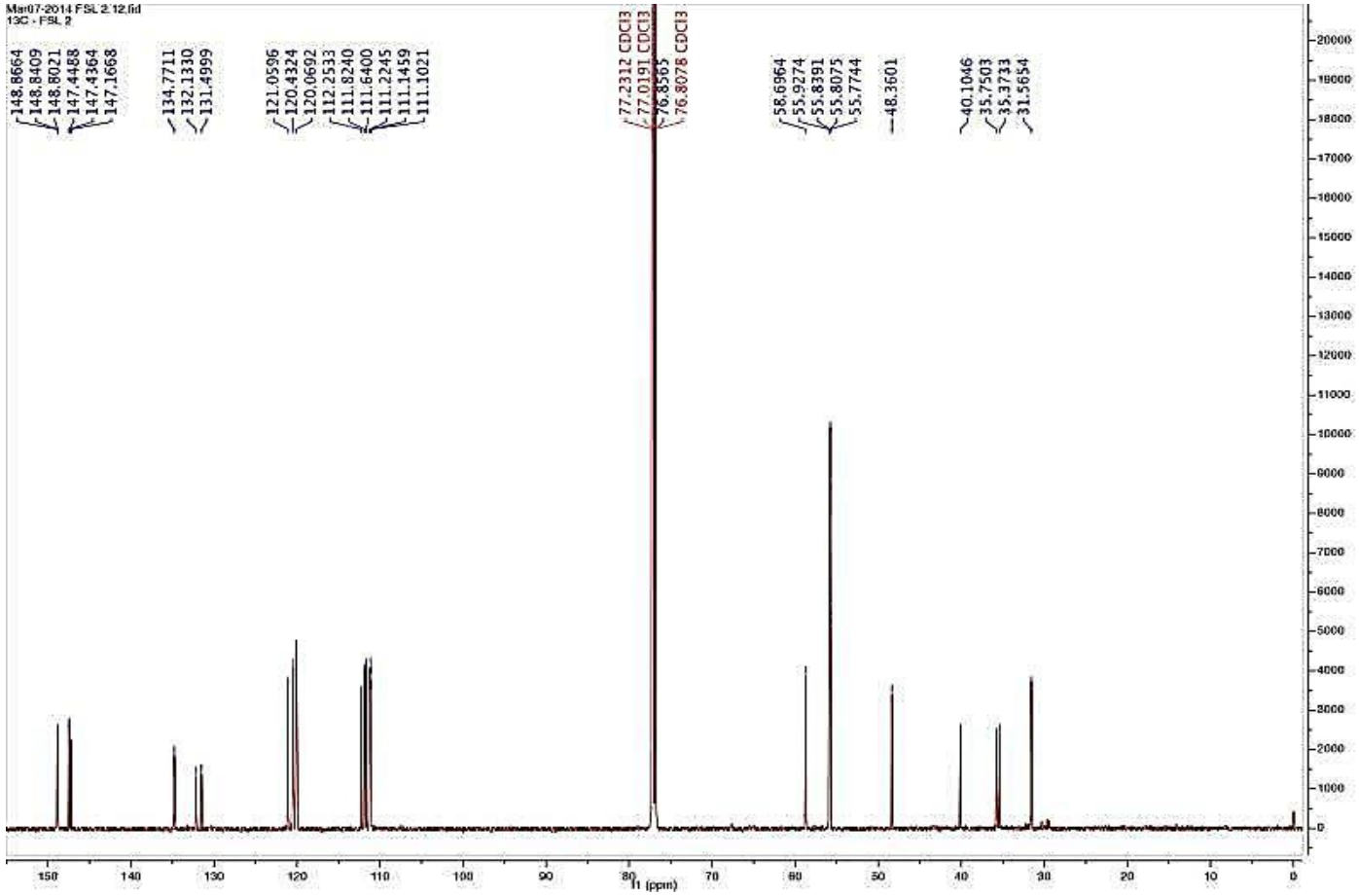

Figure 2.41: ^{13}C NMR spectrum ($CDCl_3$, 150 MHz) of schwarzinicine B **(12)**

Table 2.9: ^{1}H and ^{13}C NMR data of schwarzinicines A **(11)** and B **(12)**[a]

Position	**11**		**12**	
	^{1}H (*J* in Hz)	^{13}C	^{1}H (*J* in Hz)	^{13}C
1	-	132.3[c]	-	132.13
2	6.73 m	112.2	6.67 d (2)[b]	111.64[f]
3	-	147.3[d]	-	147.17[g]
4	-	148.6[d]	-	147.44[g]
5	6.79 d (8)	111.12[e]	6.72 d (8)[c]	111.10[h]
6	6.74 m	120.6	6.66 dd (8, 2)[d]	120.43[i]
7	2.71 m	34.9	2.67 dt (11, 7)	35.75
8	2.65 m	55.7	2.75 m	48.36
	2.77 m		2.90 dt (11, 7)	
1'	-	133.4[c]	-	131.50
2'	6.62 d (2)	112.4	6.66 d (2)[b]	111.82[f]
3'	-	146.9[d]	-	147.45[g]
4'	-	147.1[d]	-	148.80[g]
5'	6.76 d (8)	111.06[e]	6.72 d (8)[c]	111.15[g]
6'	6.65 dd (8, 2)	121.1	6.61 dd (8, 2)[d]	121.06[i]
7'	2.32 m	34.6	2.62 m	40.10
	2.89 m		2.73m	
8'	2.73 m	64.5	2.73 m	58.70
1"	-	135.3	-	134.77
2"	6.56 d (2)	111.7	6.62 d (2)[b]	112.25[f]
3"	-	148.68[d]	-	148.84[g]
4"	-	148.75[d]	-	148.87[g]
5"	6.73 m	111.2	6.77 d (8)[c]	111.22[h]
6"	6.57 dd (8, 2)	120.1	6.60 dd (8)[d]	120.07
7"	2.39 m	32.47	2.62 m	31.57
	2.59 m			
8"	1.59 m	32.49	1.79 m	35.37
	1.69 m		1.72 m	
3-OMe	3.80 s[b]	55.79[f]	3.82 s[e]	55.77[j]
3'-OMe	3.83 s[b]	55.79[f]	3.83 s[e]	55.77[j]
3"-OMe	3.83 s[b]	55.82[f]	3.84 s[e]	55.81[j]
4-OMe	3.85 s[b]	55.85[f]	3.85 s[e]	55.81[j]
4'-OMe	3.85 s[b]	55.86[f]	3.85 s[e]	55.84[j]
4"-OMe	3.87 s[b]	55.89[f]	3.86 s[e]	55.93[j]
N-Me	2.38 s	36.8	-	-
N-H	-	-	1.98 br s	-

[a]$CDCl_3$, 600 MHz; [b-j] Assignments are interchangeable.

Chapter 3: Isolation of flavonoids from *Artocarpus heterophyllus x integer* and *Macaranga hypoleuca*

Sequential extraction of the dried macerated bark of *Artocarpus heterophyllus x integer* and the leaves of *Macaranga hypoleuca* using solvents of varying polarity, namely hexane, ethyl acetate and ethanol, have afforded crude extracts as summarized inTable 3.1.

Table 3.1: Percentage yield of plant crude extracts.

Plant	Part	Dry weight	Extract	Weight of extract (% Yield)
A. heterophyllus x integer	Bark	4 kg	Hexane	77 g (1.93)
			Ethyl acetate	60 g (1.50)
			Ethanol	51 g (1.28)
M. hypoleuca	Leaves	2.2 kg	Hexane	93g (4.23)
			Ethyl acetate	54 g (2.45)
			Ethanol	226 g (10.27)

Preliminary screening by TLC of the crude extracts of *A. heterophyllus x integer* and *M. hypoleuca* revealed a series of dark spots when visualized under UV_{254}, indicating the presence of chromophoric compounds. Some of these compound appeared as bright yellow spots under UV_{365} when reacted with ethanolic aluminium chloride solution, thus indicating the presence of flavonoids. In general, only the ethyl acetate extracts showed strong presence of flavonoids. Determination of total phenolic and flavonoid contents of the crude ethyl acetate extracts of *A. heterophyllus x integer* and *M. hypoleuca* (Appendix 1) reinforced the presence of flavonoids in these extracts. The crude ethyl acetate extracts of *A. heterophyllus x integer* and *M. hypoleuca* were then subjected to repeated chromatographic separation, i.e., column chromatography (VLC, silica gel or Sephadex LH-20) and centrifugal thin layer chromatography (CTLC, silica gel).

3.1 Isolation of flavonoids from *A. heterophyllus x integer*

Four prenylated flavonoids and a xanthone compound were isolated from the bark ethyl acetate extract of *A. heterophyllus x integer.* Analysis of spectroscopic data as well as comparison with literature identified these compounds as cudraflavone C **(13)**, artocarpentin A **(14)**, cycloheterophyllin **(15)**, artonin J **(16)** and lichexanthone **(17)**.

3.1.1 Cudraflavone C

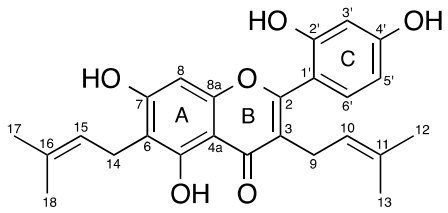

13

Cudraflavone C **(13)** was obtained as a light orange oil. TLC of this compound gave a bright yellow colour with ethanolic aluminium chloride solution. ESIMS showed a pseudo-molecular ion peak at *m/*z 423 $[M + H]^+$, and HRESIMS measurements gave the molecular formula $C_{25}H_{26}O_6$. The UV spectrum showed absorption maxima at 201, 232, 261, and 314 nm, similar to those of 3-prenylflavones,[160] while the IR spectrum showed absorption bands at 3364 and 1649 cm^{-1} due to hydroxy and conjugated carbonyl functions, respectively.

The ^1H NMR spectrum (Table 3.2, Figure 3.2) of cudraflavone C **(13)** showed the distinct presence of four allylic methyl singlets (δ_H 1.42, 1.55, 1.63 and 1.77), two allylic methylene doublets (δ_H 3.09 and 3.34), and two vinylic methine triplets (δ_H 5.11 and 5.25), indicating the presence of two prenyl side chains. In addition to the isolated aromatic

hydrogen at δ_H 6.38 (due to a pentasubstituted aromatic ring), the ^{1}H NMR spectrum showed three aromatic hydrogens at δ_H 6.54 (d, *J* = 2.3 Hz), 6.50 (dd, *J* = 8.3, 2.3 Hz), and 7.17 (d, *J* = 8.3 Hz), clearly indicated the existence of a 1,2,4-trisubstituted benzene ring. Furthermore, the absence of alkoxy signal such as OMe suggested that all phenolic OH groups are free, while the signal observed at δ 13.50 is characteristic of the presence of the hydrogen bonded 5-OH at ring A.

The ^{13}C NMR spectrum (Table 3.1, Figure 3.3) showed a total of 25 carbon signals (four methyl, two methylene, six methine, and thirteen quaternary carbons). As far as the number of carbon atoms is concerned, the structure of **13** constituted of only a flavone nucleus (9xC), a 1,2,4-trisubstituted benzene ring (6xC) and two prenyl moieties (10xC). The quaternary carbon signal observed at δ_C 182.3 (C-4) was readily attributed to the conjugated ketone carbonyl, while the signals at δ_C 155.1, 156.0, 158.97, 159.01, 159.57, and 161.3 suggested that these aromatic/olefinic carbons are sites of oxygenation.

The presence of two prenyl side chains as well as a 1,2,4-trisubstituted benzene ring were further supported by the COSY and HSQC data (Figure 3.1, Appendix 49 and 50). Since there are a total of six oxygen atoms in **13**, and two are due to ring C of the flavone nucleus, the remaining four oxygen atoms must be due to four phenolic hydroxy groups attached to both rings A and B. Attachment of the 1,2,4-trisubstituted benzene ring to C-2 (δ_C 159.57) was deduced from the observed three-bond correlation from H-6' (δ_H 7.17) to C-2 in the HMBC spectrum (Figure 3.1, Appendix 51), while the *ortho* and *para* positions of this benzene ring (B) were hydroxy-substituted. The location of one of the two prenyl side chains at C-3 was deduced from three-bond correlations observed from H-9 (δ_H 3.12) to C-2 and C-4 (δ_C 182.3). The other prenyl side chain was deduced to be linked to C-7 from the observed HMBC correlations from H-14 to C-6, and C-7. HMBC correlations

observed from H-8 to C-4a, C-6, C-7, and C-8a provided firm support that C-8 is unsubstituted, hence the final hydroxy group must therefore be attached to C-5 in ring A. The structure of **13** is consistent with the HSQC, COSY, HMBC and NOESY data, as well as literature data.[161]

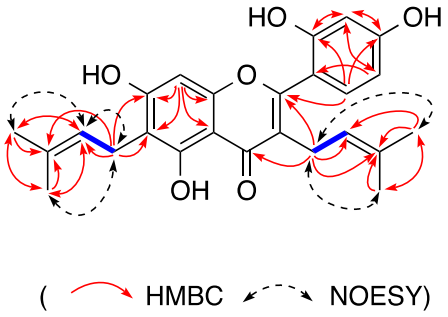

Figure 3.1: Selected HMBC, NOESY and COSY (bold bonds) correlations of cudraflavone C **(13)**

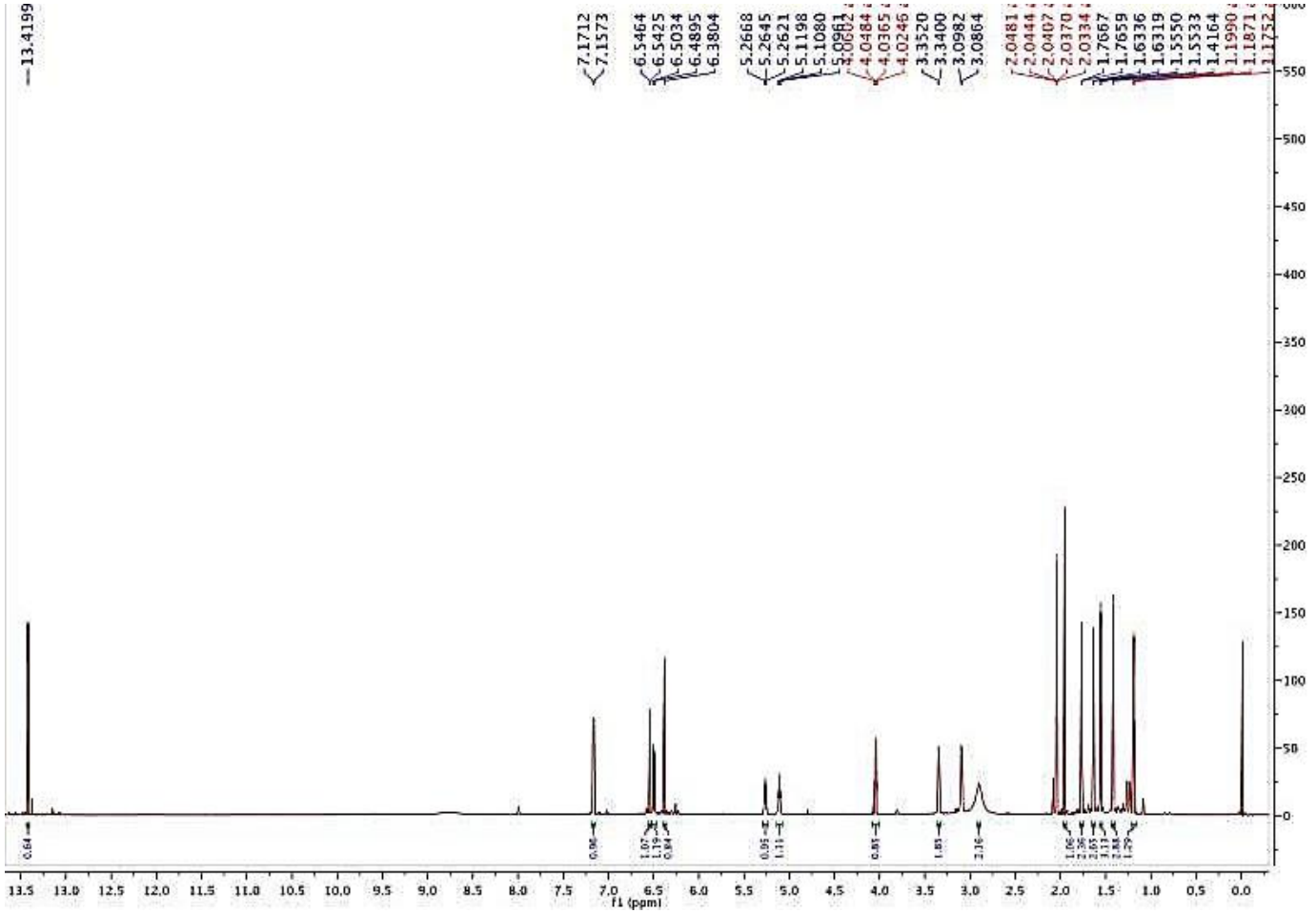

Figure 3.2: ^{1}H NMR spectrum ($CDCl_3/CD_3OD$, 400 MHz) of cudraflavone C **(13)**

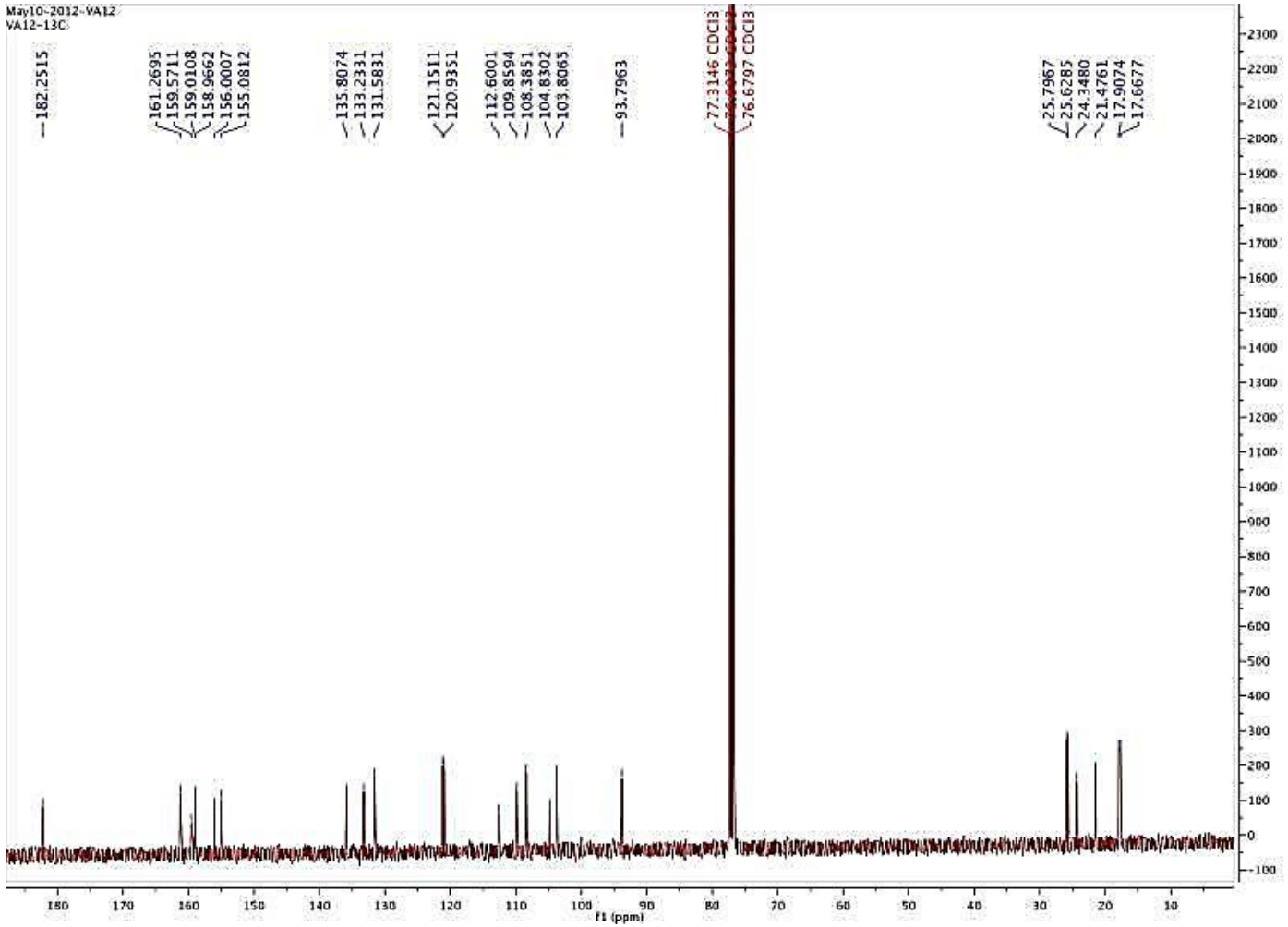

Figure 3.3: ^{13}C NMR spectrum ($CDCl_3/CD_3OD$, 100 MHz) of cudraflavone C **(13)**

3.1.2 Artocarpetin A

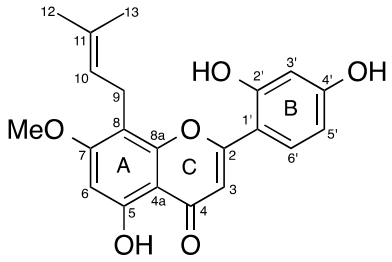

14

Artocarpetin **(14)** was obtained in minute amounts as a yellowish amorphous. The ESIMS showed a pseudo-molecular ion at *m/*z 369 $[M + H]^+$, and HRESIMS gave the molecular formula $C_{21}H_{20}O_6$. IR spectrum showed absorption bands for hydroxy groups at 3400 cm^{-1} and a conjugated carbonyl function at 1651 cm^{-1}. The UV spectrum showed absorption maxima at 208, 253, 269 nm.

The ^{13}C NMR spectrum (Table 3.2, Figure 3.6) showed a total of 21 carbon signals, which is in agreement with the molecular formula. The quaternary carbon resonance observed at δ_C 182.9 (C-4) was readily attributed to the conjugated ketone carbonyl, while the resonances at δ_C 155.6, 161.6, 162.1, 162.7, 163.2, and 164.0 are due to six oxygenated aromatic/olefinic carbons. The ^1H NMR spectrum (Table 3.2, Figure 3.5) of **14** showed the presence of a methoxy signal at δ_H 3.94, a set of signals due to a prenyl side chain at δ_H 1.64 and 1.78 (each 3H, s), 3.51 (2H, d, 7.0 Hz) and 5.21 (1H, t, 7.0 Hz), and a chelated phenolic hydroxy signal at δ_H 13.17 attributed to the hydroxy group at C-5. HMBC correlations (Figure 3.4, Appendix 54) suggested that the aromatic proton signals at δ_H 6.62 (d, 1.9 Hz), 6.55 (dd, 8.8, 1.9 Hz) and 7.84 (d, 8.8 Hz) corresponded to H-3', H-5' and H-6' of the 2',4'-dihydroxylated ring B, while the three bond correlation from H-3 to C-1' established the attachment of the B ring at C-2. The two remaining aromatic proton singlets at δ_H 7.19 and

6.43 are attributable to the isolated H-3 and H-6, respectively. Attachment of the prenyl side chain to C-8 was deduced from the HMBC correlations observed from H-9 to C-8 and C-7, while a three bond correlation from the methoxy group to C-7 established C-7 as the site of methoxylation. The structure of **14** is entirely consistent with the COSY, HSQC and HMBC data (Apendix 52-54) as well as by comparison with literature.[63]

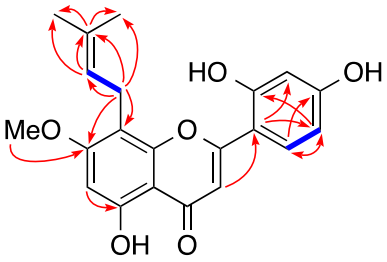

Figure 3.4: Selected HMBCs and COSY (bold bonds) correlations of artocarpetin A **(14)**

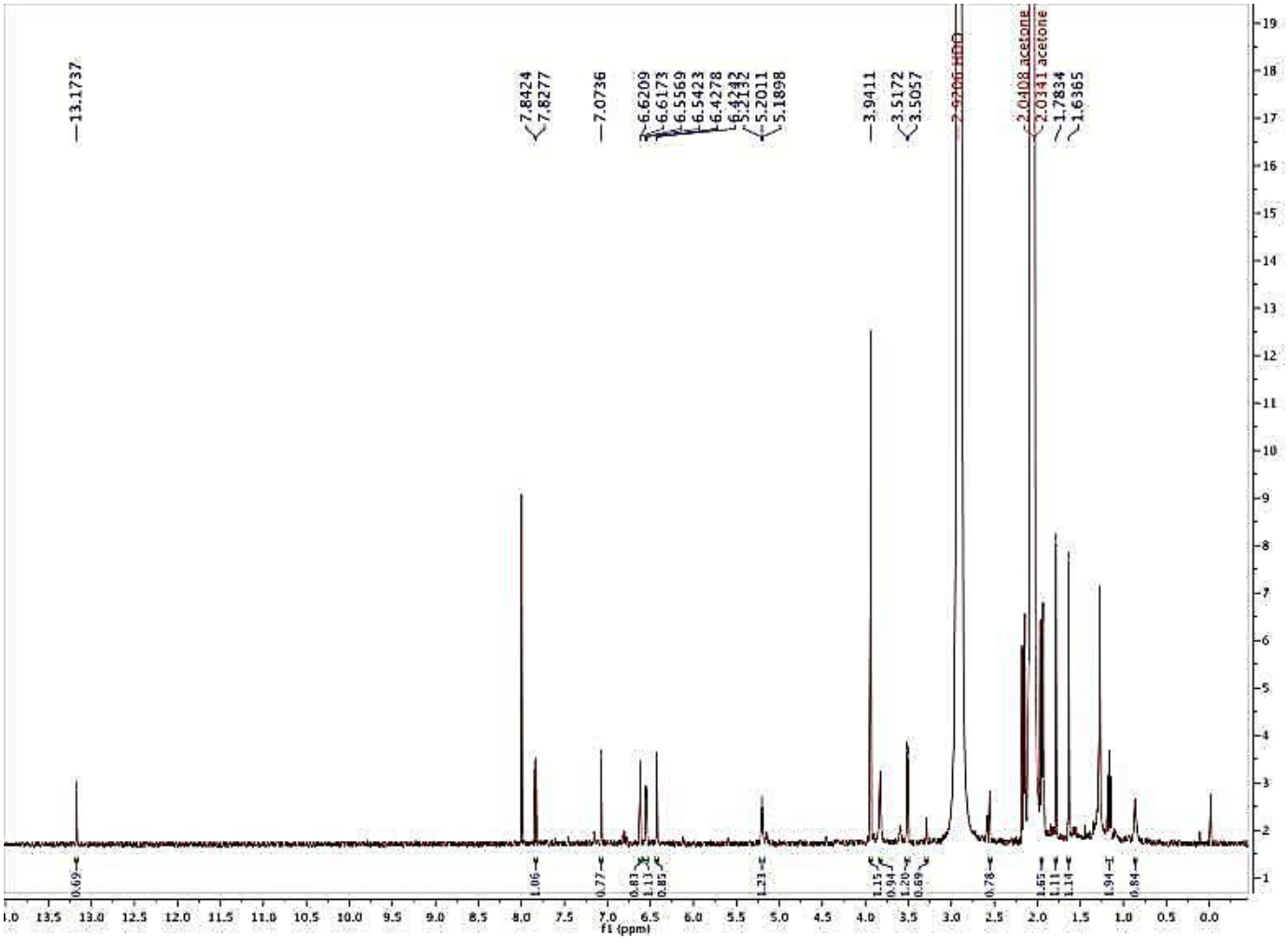

Figure 3.5: ^{1}H NMR spectrum ($CDCl_3/CD_3OD$, 400 MHz) of artocarpetin A **(14)**

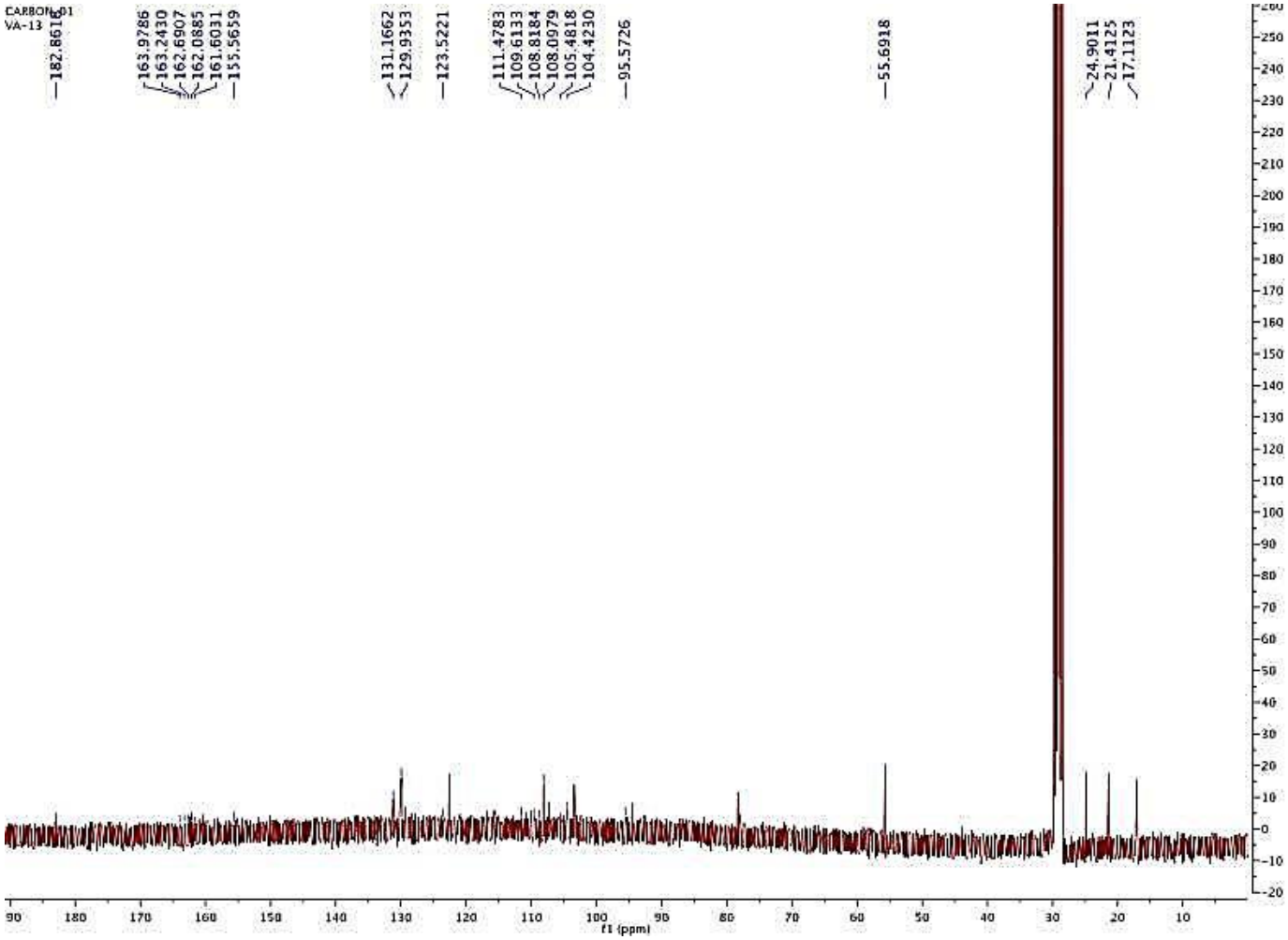

Figure 3.6: ^{13}C NMR spectrum ($CDCl_3/CD_3OD$, 100 MHz) of artocarpetin A **(14)**

Table 3.2: ^{1}H and ^{13}C NMR data of cudraflavone C **(13)** and artocarpetin A **(14)**[a]

Position	**13**		**14**	
	^{1}H (*J* in Hz)	^{13}C	^{1}H (*J* in Hz)	^{13}C
2	-	159.57	-	162.7[b]
3	-	121.2	7.19 s	109.6
4	-	182.3	-	182.9
4a	-	104.8	-	104.4
5	-	158.97[b]	-	162.1
6	-	109.9	6.43 s	95.6
7	-	161.3	-	164.0
8	6.38 s	93.8	-	108.1
8a	-	156.0	-	161.6
9	3.09 d (7.1)	24.4	3.51 d (7.0)	21.4
10	5.11 t (7.1)	120.9[c]	5.21 t (7.0)	123.5
11	-	133.2	-	131.2
12	1.42 s	17.7	1.64 s	17.1
13	1.55 s	25.6	1.78 s	24.9
14	3.34 d (7.2)	21.5	-	-
15	5.25 tt (7.2, 1.4)	121.2[c]	-	-
16	-	135.8	-	-
17	1.77 s	25.8	-	-
18	1.63 s	17.9	-	-
1'	-	112.6	-	111.5
2'	-	155.1	-	155.6
3'	6.54 d 2.3	103.8	6.62 d (1.9)	105.5
4'	-	159.01[b]	-	163.2[b]
5'	6.50 dd (8.3, 2.3)	108.4	6.55 dd (8.8, 1.9)	108.8
6'	7.17 d (8.3)	131.6	7.84 d (8.8)	129.9
5-OH	13.50 s	-	13.17 s	-
7-OH	Not observed	-	-	-
2'-OH	Not observed	-	Not observed	-
4'-OH	Not observed	-	Not observed	-
7-OMe	-	-	3.94 s	55.7

[a] $CDCl_3/CD_3OD$, 400 MHz; [b-c] Assignments are interchangable

3.1.3 Cycloheterophyllin

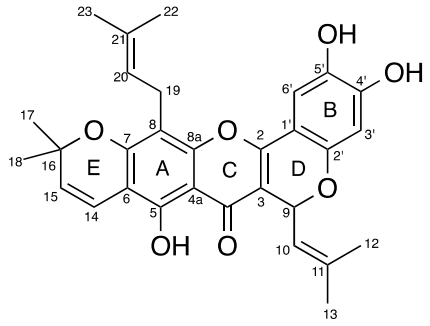

15

Cycloheterophyllin **(15)** was obtained as yellow powder. The ESIMS showed a pseudo-molecular ion peak at *m/z* 501 $[M - H]^-$, which corresponds to the molecular formula $C_{30}H_{30}O_7$, requiring 16 degrees of unsaturation. The IR spectrum showed absorption bands at 3346 cm^{-1} and 1652 cm^{-1} due to hydroxy and conjugated carbonyl groups, respectively. Additionally, the IR absorption bands at 1375 and 1346 cm^{-1} were attributable to the gem-dimethyl group attached to C-16. The UV spectrum showed absorption maxima at 273, 299, and 405 nm resembling those of cycloheterophyllin reported in the literature and other flavone derivatives such as artonin A and cyclochampedol.[48,65]

The ^{13}C NMR spectrum (Table 3.3, Figure 3.10) gave a total of 30 carbon resonances (six methyls, a conjugated ketone carbonyl, 12 aromatic carbons, eight olefinic carbons, a methylene carbon, a methine carbon and a quaternary carbon) consistent with the molecular formula. The ^1H NMR spectrum (Table 3.3, Figure 3.9) of cycloheterophyllin showed characteristic pattern of a dimethylchromene system with the presence of two singlets integrated for three protons each at δ_H 1.40 (H-17) and 1.43 (H-18) (Figure 3.7). The two AB doublets at δ_H 5.57 and 6.66 (1H each, J = 10 Hz) were assigned to the olefinic H-14

and H-15, respectively, while the two singlets at δ_H 7.21 and 6.45 were attributable to the isolated aromatic protons in ring B, i.e., H-2' and H-5', respectively.

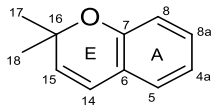

Figure 3.7: A dimethylchromene partial structure in **15**

The two vinylic methyls observed at δ_H 1.63 (H-13) and 1.89 (H-12), coupled to the two doublets (J = 9.2 Hz) at δ_H 6.14 (H-9) and 5.43 (H-10), revealed an oxygenated prenyl partial structure where C-9 is linked to C-2' of ring B via an oxygen atom, and as a result formed the D ring. This was supported by the HMBC data which showed correlations from H-9 to C-3 and C-11; H-10 to C-12; H-12 to C-13; H-13 to C-12 (Figure 3.8, Appendix 57). The ^{1}H NMR spectrum also showed a set of signals characteristic of an unaltered prenyl side chain, i.e., δ_H 1.63 (3H, s, H-23), 1.80 (3H, s, H-22), 3.41 (2H, m, H-19) and 5.19 (1H, t, J = 6.9 Hz, H-20). In addition to confirming the presence of the prenyl side chain, the COSY and HMBC data also confirmed that the prenyl unit is attached to the core structure at C-8. The relevant HMBC correlations include H-19 to C-7 and C-8a; H-19 to C-20; H-20 to C-23; H-22 to C-23; H-23 to C-20 and C-22. Full assignments of the ^{1}H and ^{13}C NMR data of cycloheterophyllin **(15)** were in complete agreement with the COSY, HSQC and HMBC data (Appendix 55-57) as well as comparison with literature. Cycloheterophyllin **(15)** is a known flavonoid previously isolated from the bark of *A. heterophyllus.*[65]

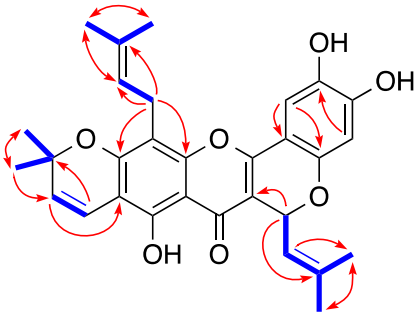

Figure 3.8: HMBC and COSY (bold bonds) correlations of cycloheterophyllin **(15)**

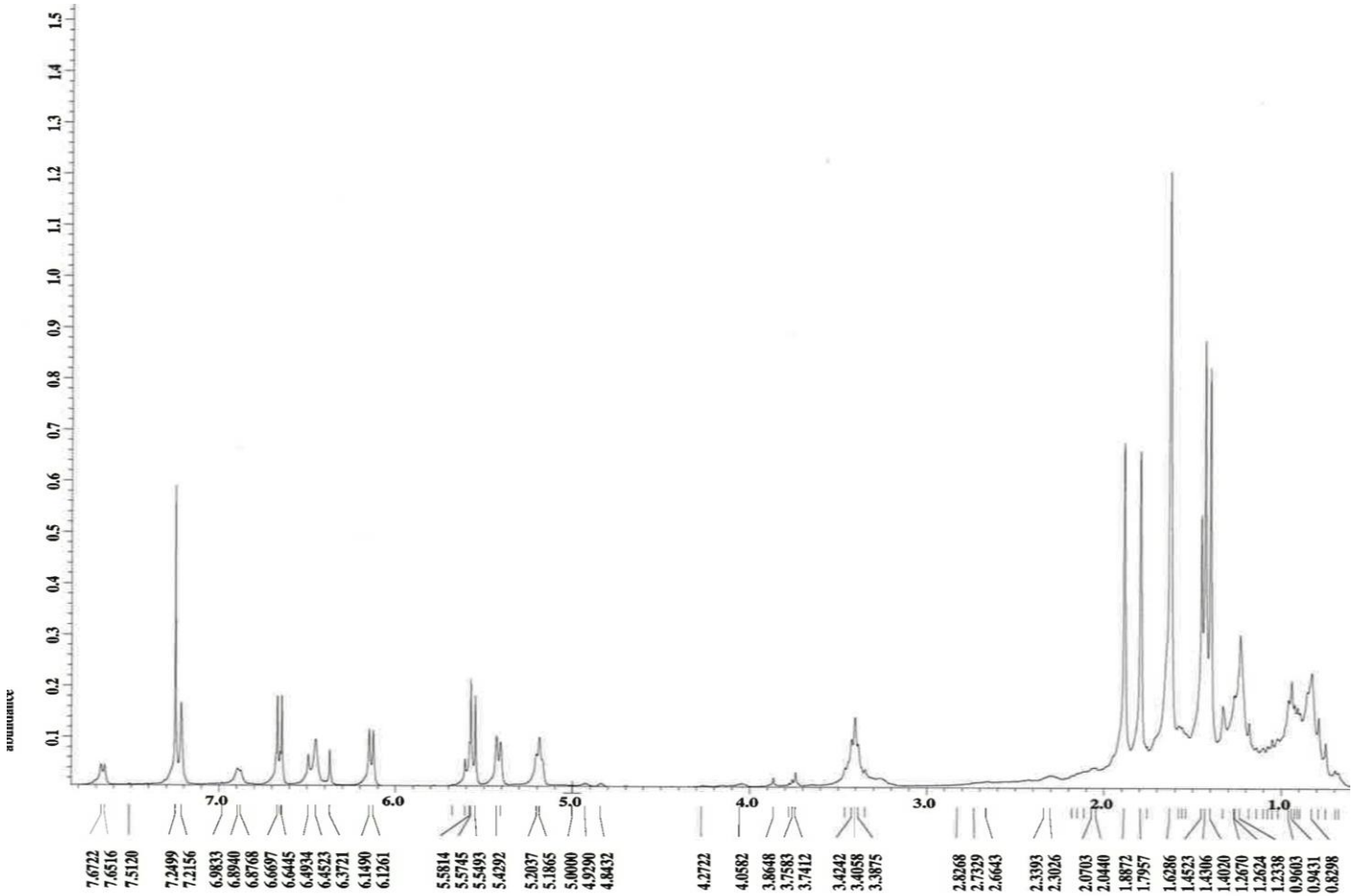

Figure 3.9: ^{1}H NMR spectrum ($CDCl_3/CD_3OD$, 400 MHz) of cycloheterophyllin **(15)**

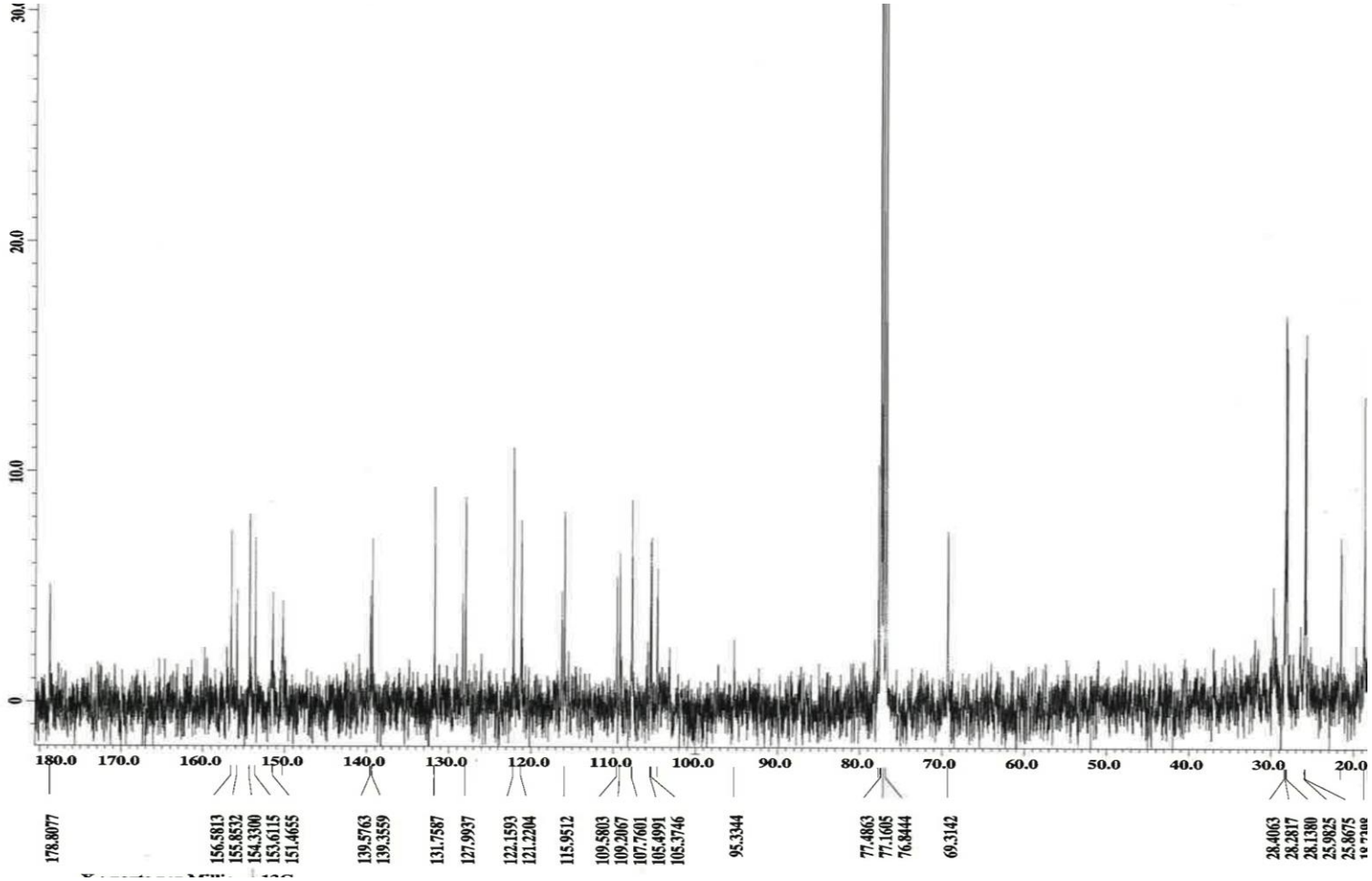

Figure 3.10: ^{13}C NMR spectrum ($CDCl_3/CD_3OD$, 100 MHz) of cycloheterophyllin **(15)**

3.1.4 Artonin J

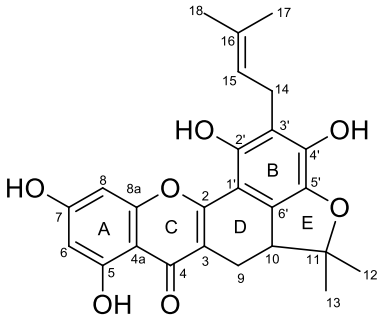

16

Artonin J **(16)** was obtained in minute amounts from the bark of *A. heterophyllus x integer* as yellowish crystals, mp: 280 – 285 °C (lit., 281 – 282 °C)[66]. ESIMS of **16** showed a pseudo-molecular ion peak at *m/z* 437 $[M + H]^+$ and HRESIMS which corresponds to the molecular formula $C_{25}H_{24}O_7$. The IR spectrum showed absorption bands at 3399 cm^{-1} and 1713 cm^{-1} attributable to hydroxy and conjugated carbonyl groups, respectively. The UV spectrum showed absorption maxima at 380, 264, 231 and 210 nm, resembling those from molecules with similar chromophore such as cycloartobiloxanthone.[46]

The ^{13}C NMR spectra (Table 3.3, Figure 3.14) showed peaks accountable for 25 carbons, comparable to data reported in the literature which are consistent with the molecular formula.[66] Analysis of the ^{13}C NMR data revealed the presence of four methyl carbons at δ_C 17.7 (C-18), 25.7 (C-17), 22.4 (C-13), and 28.0 (C-12); two methylene carbons at δ_C 22.6 (C-14) and 19.9 (C-9); a methine carbon at δ_C 46.1 (C-10); four olefinic carbons; 12 aromatic carbons; a conjugated ketone at δ 179.1 (C-4); and a quaternary carbon at δ_C 94.0 (C-11).

The ^{1}H NMR spectrum (Table 3.3, Figure 3.13) showed the presence of a set of signals characteristic of a prenyl substituent: two methyl singlets at δ_H 1.70 (H-17) and 1.81 (H-18), a 1-H olefinic signal at δ_H 5.26 (H-15), and a 2H doublet at δ_H 3.39 (H-14). The COSY spectrum (Figure 3.11, Appendix 58) of **16** revealed an ABX spin system at δ_H 2.39 (1H, t, *J* = 15 Hz, H-9), 3.18 (1H, dd, *J* = 15, 7 Hz, H-9) and 3.39 (1H, dd, *J* = 15, 7 Hz, H-10), which is a typical pattern for the furanoxanthone core structure that acquired its D ring from the linkage between C-3 of ring C and C-6' of ring B via a prenyl unit. Similar ABX spin systems were observed in compounds having the same furanoxanthone core structure such as artonin A and artoindosianin A.[65] The gem-dimethyl group attached at C-11 of the furan moiety was observed as two methyl singlets at δ_H 1.34 (H-12) and 1.66 (H-13). The two singlet signals at δ_H 6.28 (H-6) and 6.39 (H-8) were readily attributable to the two isolated aromatic protons.

Due to compound degradation and insufficient yield, HSQC and HMBC spectra could not be obtained. However, due to the presence of suitable crystals at hand, X-ray diffraction analysis was carried out, which revealed compound **16** as artonin J (Figure 3.12). The spectroscopic data available including MS, 1D NMR, IR and UV spectroscopy are in good agreement with those of literature.[66]

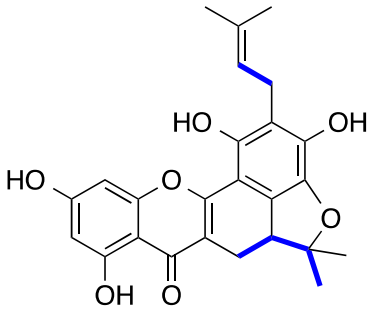

Figure 3.11: COSY correlations of artonin J **(16)**

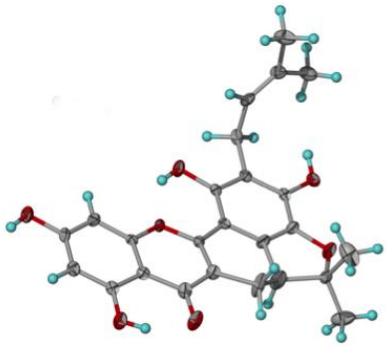

Figure 3.12: X-ray diffraction crystal structure of artonin J **(16)**

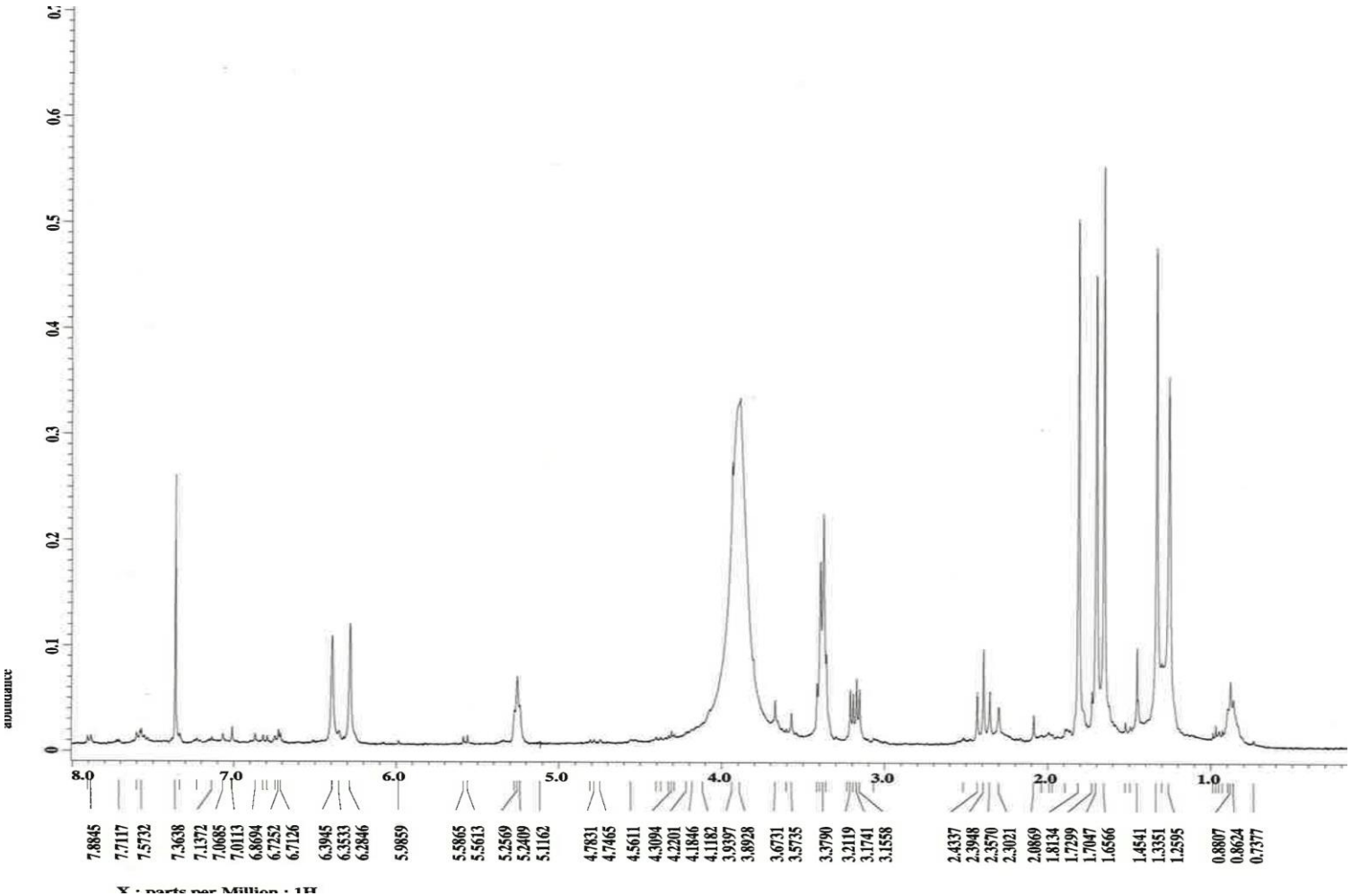

Figure 3.13: ^{1}H NMR spectrum ($CDCl_3/CD_3OD$, 400 MHz) of artonin J **(16)**

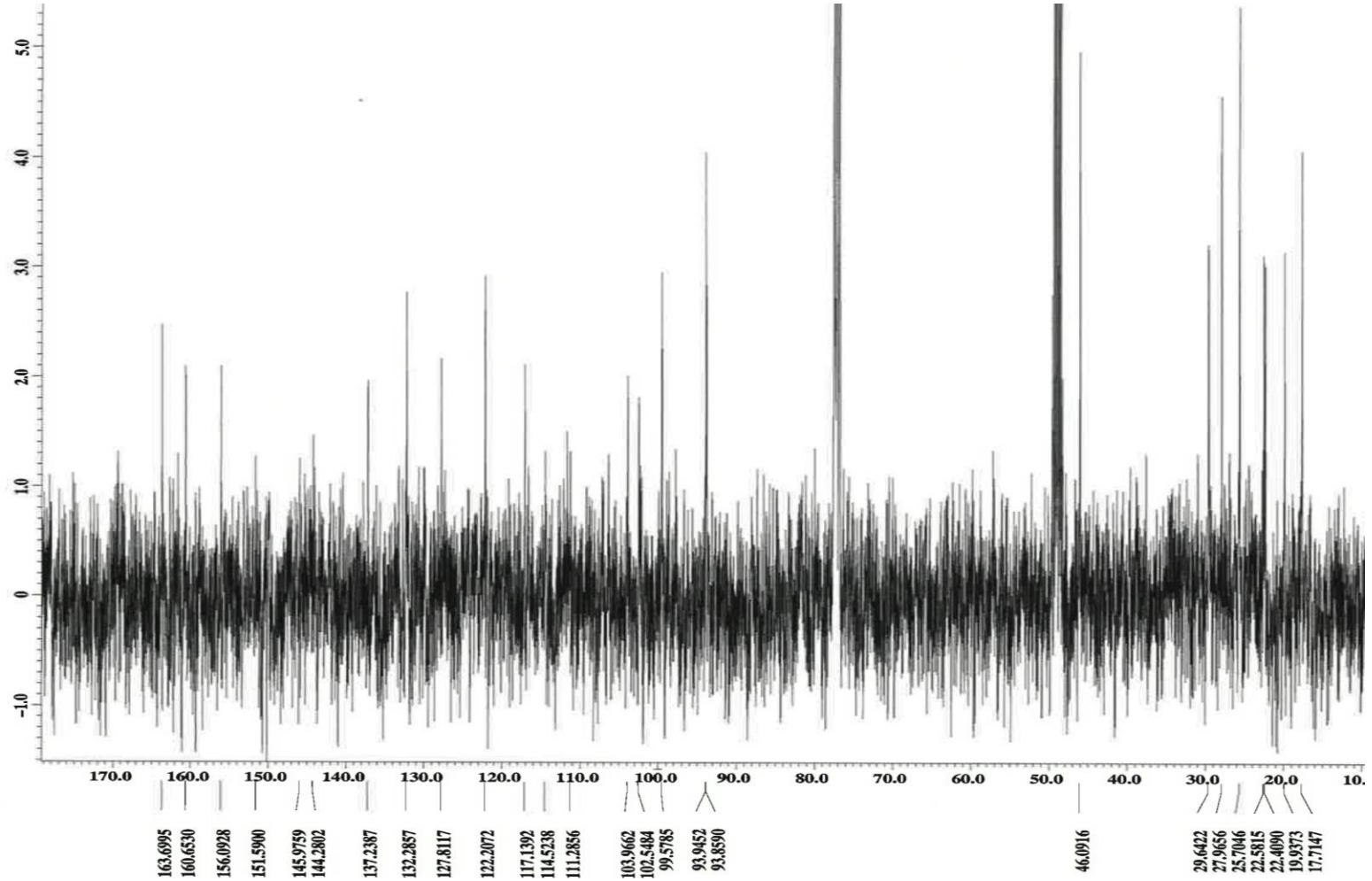

Figure 3.14: ^{13}C NMR spectrum ($CDCl_3/CD_3OD$, 100 MHz) of artonin J **(16)**

Table 3.3: ^{1}H and ^{13}C NMR data of cycloheterophyllin **(15)** and artonin J **(16)**[a]

Position	**15**		**16**	
	^{1}H (*J* in Hz)	^{13}C	^{1}H (*J* in Hz)	^{13}C
2	-	155.8	-	161.3
3	-	109.6	-	111.8
4	-	178.8	-	179.1
4a	-	105.4[b]	-	103.5
5	-	154.3	-	160.7
6	-	105.5[b]	6.28 s	99.6
7	-	153.6[c]	-	163.7
8	-	107.8	6.39 s	94.0
8a	-	156.6[c]	-	156.1
9	6.14 d (9.2)	69.3	2.39 t (15) 3.18 dd (15, 7)	19.9
10	5.43 d (9.2)	121.2	3.39 dd (15, 7)	46.1
11	-	139.4	-	93.9
12	1.89 s	18.7	1.34 s	28.0
13	1.63 s	26.0	1.66 s	22.4
14	6.66 d (10.1)	116.0	3.39 d (7)	22.6
15	5.57 d (10.1)	128.0	5.26 t (7)	122.2
16	-	77.8	-	132.3
17	1.40 s	28.1	1.70 s	25.7
18	1.43 s	28.3	1.81 s	17.7
19	3.41 m	21.6	-	-
20	5.19 t (6.9)	122.1	-	-
21	-	131.8	-	-
22	1.80 s	18.1	-	-
23	1.63 s	25.9	-	-
1'	-	107.7	-	104.0
2'	-	151.5	-	146.0
3'	6.45 s	104.7	-	117.1
4'	-	150.3	-	144.3
5'	-	139.6	-	137.2
6'	7.21 s	109.2	-	127.8

[a] $CDCl_3/CD_3OD$, 400 MHz; [b-c] Assignments are interchangeable

3.1.5 Lichexanthone

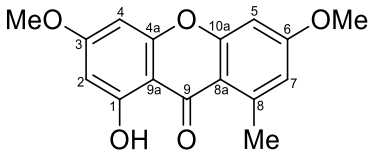

17

Lichexanthone **(17)** was obtained from the ethyl acetate bark extract of *A. heterophyllus x integer* as yellow needles, mp: 185-190 °C (lit., 188-190 °C)[162] and was identified by X-ray diffraction analysis (Figure 3.15). ^{1}H NMR spectrum of **17** (Figure 3.16) showed the presence of a methyl signal at δ_H 2.83 (3H, s, H-8), and two methoxy groups at δ_H 3.84 (3H, s) and 3.88 (3H, s). A pair of aromatic doublet signals due to H-2 and H-4 were seen at δ 6.28 (1H, d, *J* = 2.8 Hz) and 6.31 (1H, d, *J* = 2.8 Hz) respectively, while the signals for H-5 and H-7 appeared as singlet signals at δ_H 6.64 and 6.66, respectively. ^{1}H NMR assignments were made by comparison with literature (Table 3.4).[162,163]

It is believed that lichexanthone **(17)** is not produced first hand by *A. integer x heterophyllus*. Since lichexanthone is a major metabolite produced by epiphytic lichens, which commonly grow on leaves, branches and bark of trees in rainforests and woodlands, isolation of lichexanthone in the present study is suspected to be the due to the epiphytic lichens that were found on the bark of *A. integer x heterophyllus*.[164]

Table 3.4: Comparison of ^{1}H NMR data of lichexanthone **(17)**[a] obtained with published data.

Position	**Literature**[162]	**Literature**[163]	**17**
	^{1}H (*J* in Hz)	^{1}H	^{1}H (*J* in Hz)
1-OH	13.36 s	13.39	
2	6.26 d (2.6)	6.29	6.28 d (2.8)
4	6.28 d (2.6)	6.32	6.31 d (2.8)
5	6.63 d (2.6)	6.65	6.64 s
7	6.62 s	6.67	6.66 s
8 -Me	2.81 s	2.84	2.83 s
12 -OMe	3.85 s	3.86	3.84 s
13 -OMe	3.87 s	3.89	3.88 s

[a] $CDCl_3$, 400 MHz

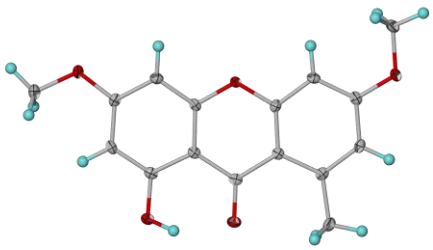

Figure 3.15: X-ray diffraction crystal structure of lichexanthone **(17)**

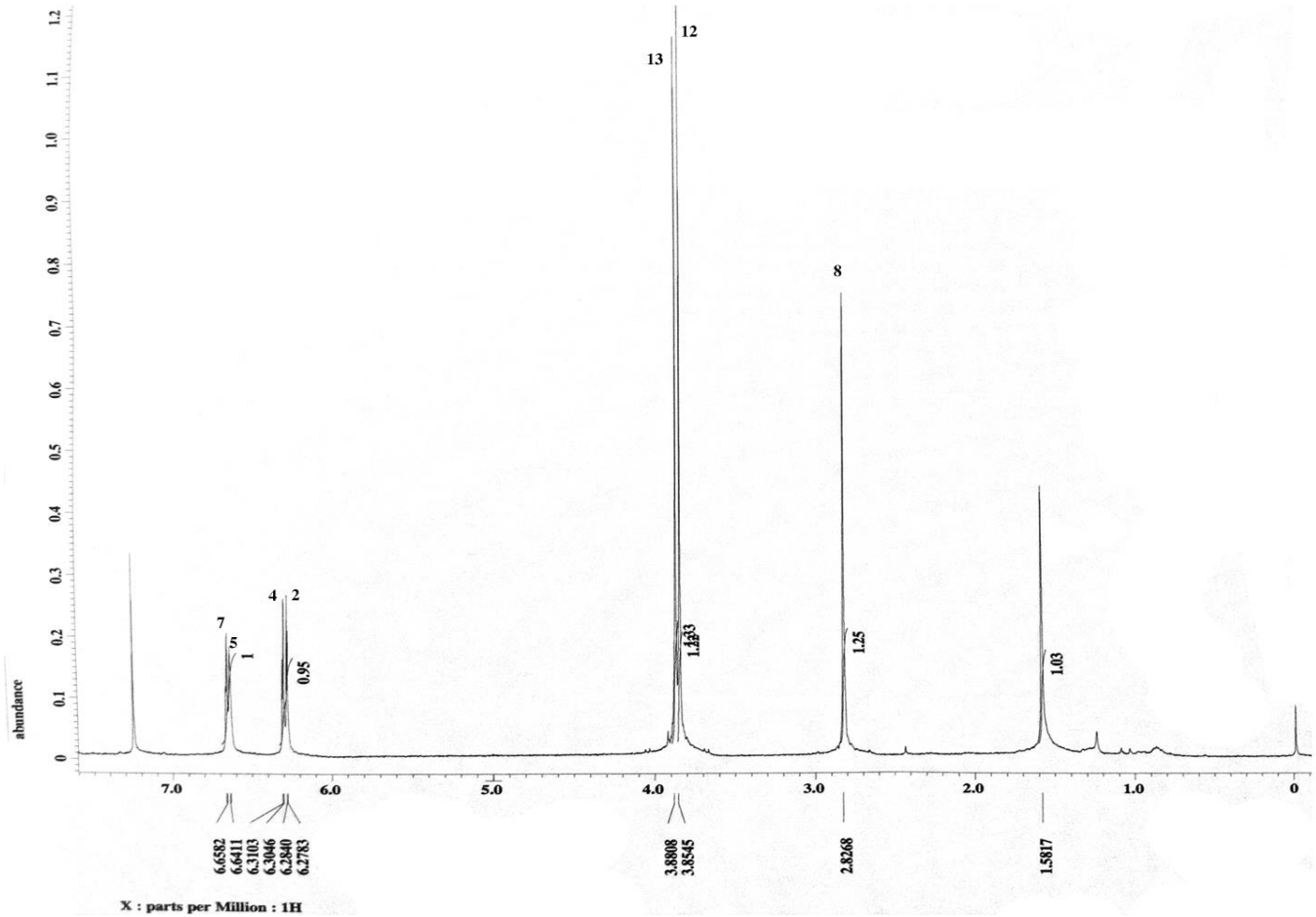

Figure 3.16: ^{1}H NMR spectrum ($CDCl_3$, 400 MHz) of lichexanthone **(17)**

3.2 Isolation of flavonoids from the leaves of *Macaranga hypoleuca*

Six known flavonoids and a triterpenoid were isolated from the leaf ethyl acetate extract of *M. hypoleuca*. These compounds were identified as quercetin-3-*O*-α-L-arabinopyranoside **(18)**, quercetin-3-*O*-α-L-arabinofuranoside **(19)**, quercetin-3-*O*-β-D-galactoside **(20),** quercetin **(21)**, kaempherol **(22)**, 5,7-dihydroxy-2-(4-methoxyphenyl)-8-(3-methylbut-2-en-1-yl)chroman-4-one **(23)** and 3-epi-taraxerol **(24)** based on spectroscopic data as well as comparison with literature.

3.2.1 Quercetin-3-*O*-α-L-arabinopyranoside

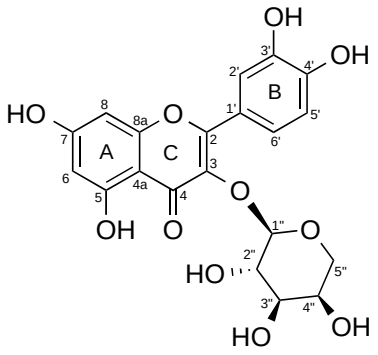

18

Quercetin-3-*O*-α-L-arabinopyranoside **(18)** was obtained as yellow crystals, mp: 242-244 **º**C (lit., 250-260 **º**C).[165] ESIMS of **18** showed a pseudo-molecular ion peak at *m/z* 435 $[M + H]^+$, while HRESIMS measurements gave the molecular formula $C_{20}H_{18}O_{11}$. The IR spectrum showed broad absorption bands at 3476 and 1654 cm^{-1} attributable to the presence of hydroxy and conjugated carbonyl groups, respectively. The UV spectrum showed absorption maxima at 256 and 357 nm, resembling the UV spectra reported in literature for this compound and other similar flavonol monoglycosides.[166,167]

The ^{13}C NMR spectrum (Table 3.5, Figure 3.20) showed a total of 20 carbon signals attributed to a flavonol nucleus (9xC), a 1',3',4'-trisubstituted aromatic ring (6xC) and an aldopentose moiety (5xC). The carbon signal observed at δ_C 179.1 was readily attributed to the conjugated ketone carbonyl, while the signals at δ_C 165.3, 163.0, 157.9, 149.4, and 145.5 are due to aromatic carbons that are sites of oxygenation. Pyranose and furanose forms of a sugar moiety can be distinguished readily by considering the chemical shift of C-4" as well as the hydrogen signals for H-5". The C-4" chemical shifts are distinctly different for both pyranose and furanose moieties, i.e., ca. δ_C 67 and 87, respectively.[168,169] On the other hand, the pyranose moiety normally possesses a pair of anisochronous C-5" methylene hydrogen signals, while the furanose moiety shows an isochronous C-5" methylene hydrogen signal.[169] The pyranose form of the arabinoside in **18** was thus indicated by the chemical shift of C-4" at δ_C 68.2 and the presence of a pair of anisochronous C-5" methylene hydrogens at δ_H 3.46 and 3.79.

The ^{1}H NMR spectrum (Table 3.5, Figure 3.19) showed three aromatic hydrogen signals at δ_H 6.92 (d, J = 8.5 Hz), 7.63 (dd, J = 8.5, 2.2 Hz), and 7.88 (d, J = 2.2 Hz) attributed to the 1',3',4'-trisubstituted ring B, and two aromatic doublets at δ_H 6.25 (d, J = 2.1 Hz) and 6.49 (d, J = 2.1 Hz) attributed to the two hydrogens in *meta* arrangements in ring A. These observations are consistent with the presence of the 5,7,3',4'-tetraoxygenated flavonoid core structure of **18**. The broad singlet at δ_H 12.49 is readily attributed to 5-OH, which is hydrogen bonded to the oxygen atom of the ketone function at C-4. Not all hydroxy signals are visible, only those exchanging at a slower rate will be visible as in the case of flavonoids where 5-OH hydrogen is bonded to C=O at C-4.

The ^{1}H NMR spectrum showed signals (δ_H 3.4-5.3 ppm) that are distinctive of the presence of a sugar moiety, with an anomeric hydrogen (H-1") signal normally appearing

within δ_H 4.3-5.9 ppm.[168] The coupling constant between the anomeric H-1" and H-2" of the sugar ring moiety is normally quite diagnostic of the stereochemistry at the anomeric carbon.[170] This is because carbohydrates form relatively rigid ring conformations where the attached hydrogens adopt either the axial or equatorial orientation. Thus, according to the Karplus correlation a H-1"-H-2" equatorial-axial relationship leads to a small coupling constant (J < 7 Hz, dihedral angle *ca* 60°), which is associated with α-L-arabinopyranosides, while the opposite is observed for a *trans*-diaxial relationship of H-1"/H-2" (J > 7 Hz, dihedral angle *ca* 180°), which is associated with β-L-arabinopyranosides.[168] For **18**, the anomeric H-1" signal appeared as a well resolved doublet at δ_H 5.26 (d, J = 6.2 Hz) implying an equatorial-axial configuration with H-2" and corresponding to an α-anomer. This determined the sugar moiety in **18** to be an α-L-arabinopyranoside linked to the flavonol nucleus via an α-glycosidic bond. On the other hand, the H-2"/H-3" coupling constant of J = 7.9 Hz also indicated a *trans*-diaxial configuration between H-2"and H-3", while the H-3"/H-4" coupling constant of J = 4.0 Hz implied an axial-equatorial orientation between H-3" and H-4". These observations are entirely consistent with the configuration of α-L-arabinopyranose.[169,170]

The presence the 5,7,3',4'-tetraoxygenated flavonoid core structure, which was further supported by 2D NMR data, was identified as quercetin. The COSY, HSQC and HMBC data (Figure 3.17, Appendix 59 - 61) further supported the assignment of the arabinopyranose substituent. HMBC correlation between H-1" to C-3 essentially confirmed the attachment of the α-L-arabinopyranosyl moiety to the quercetin structure at C-3. The NMR data of **18** are in good agreement with those reported in literature.[166,169,171] Since suitable crystals of **18** were obtained, X-ray diffraction analysis was carried out (Figure 3.18) and re-confirmed the structure of **18** as quercetin-3-*O*-α-L-arabinopyranoside.

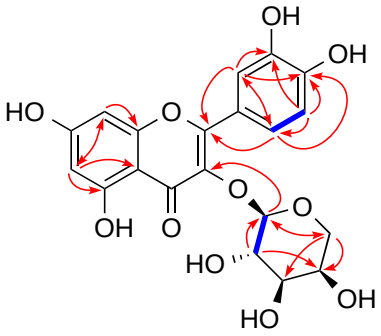

Figure 3.17: Selected HMBC and COSY (bold bonds) correlations of quercetin-3-*O*-α-L-arabinopyranoside **(18)**

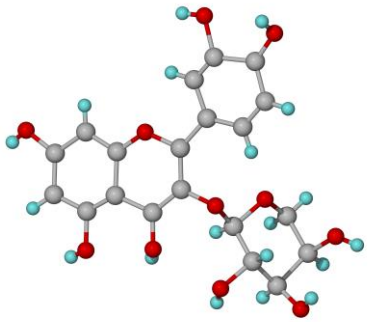

Figure 3.18: X-ray crystal structure of quercetin-3-*O*-α-L-arabinopyranoside **(18)**

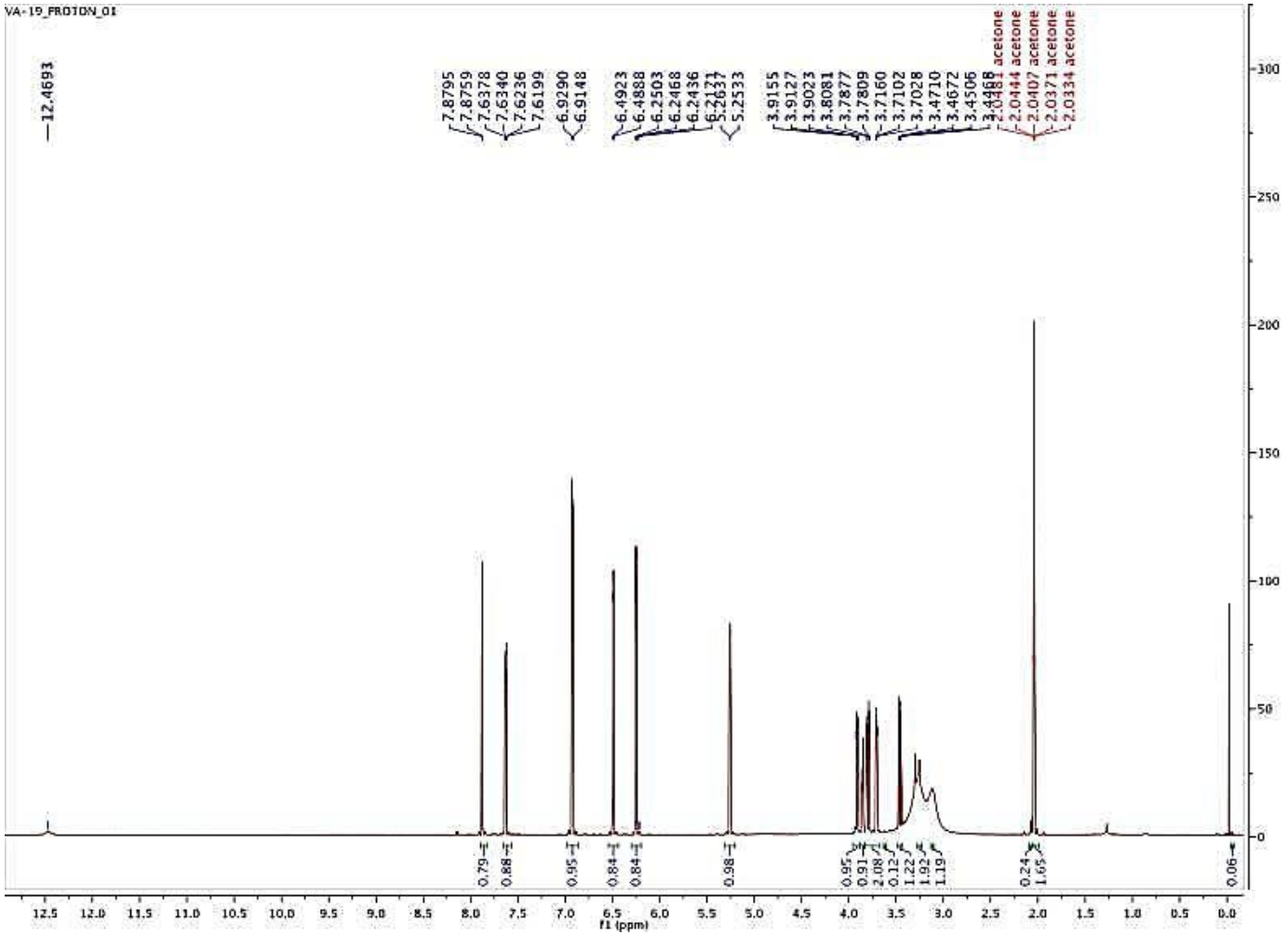

Figure 3.19: ^{1}H NMR spectrum (acetone-$d_{6,}$, 600 MHz) of quercetin-3-*O*-α-L-arabinopyranoside **(18)**

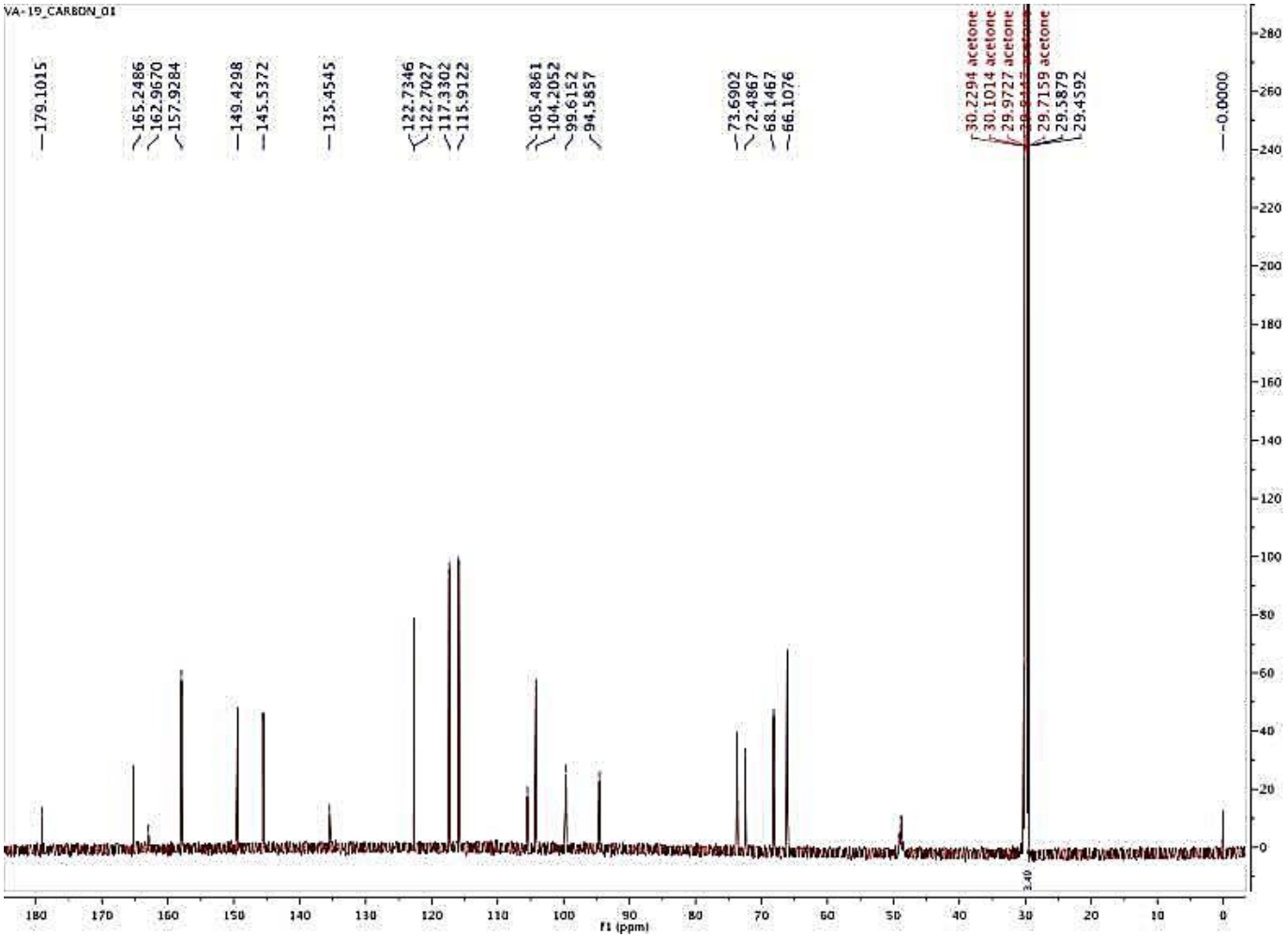

Figure 3.20: ^{13}C NMR spectrum (acetone-$d_{6,}$, 150 MHz) of quercetin-3-*O*-α-L-arabinopyranoside **(18)**

3.2.2 Quercetin-3-*O*-α-L-arabinofuranoside

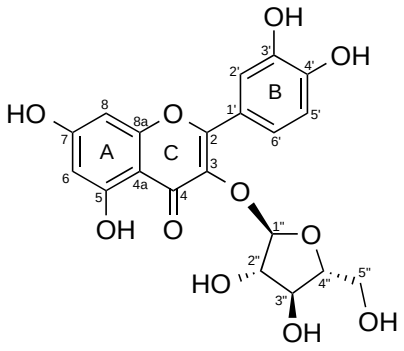

19

Quercetin-3-*O*-α-L-arabinofuranoside **(19)** was obtained as a yellow amorphous. ESIMS of **19** showed a pseudo-molecular ion peak at *m/z* 435 $[M + H]^+$ and HRESIMS gave the molecular formula $C_{20}H_{18}O_{11}$. The IR spectrum showed absorption bands due to the presence of hydroxy and carbonyl groups respectively at 3400 $cm^{-1}$and 1613 cm^{-1}. The UV spectrum showed absorption maxima at 258, 292 and 358 nm, resembling the UV spectra of similar flavonol monoglycosides.[166,167]

The ^{13}C NMR spectrum (Table 3.5, Figure 3.23) showed a total of 20 carbon signals attributed to a flavone nucleus (9xC), a 1',3',4'-trisubstituted aromatic ring (6xC) and an aldopentose moiety (5xC). The carbon signal observed at δ_C 178.9 was readily attributed to the conjugated ketone carbonyl, while the signals at δ_C 164.3, 161.8, 157.12, 157.06, 148.4 and 144.9 suggested that these quaternary carbons are sites of oxygenation. In contrast to **18**, the furanose form of **19** was indicated by the carbon chemical shift of C-4" at δ_C 88.4 and the isochronous C-5" methylene signal at δ_H 3.57 (2H, d, J = 3.9 Hz).[168,169]

The ^1H NMR spectrum (Table 3.5, Figure 3.22) showed three aromatic hydrogen signals at δ_H 6.97 (d, J = 8.4 Hz), 7.56 (dd, J = 8.4, 2.2 Hz), and 7.70 (d, J = 2.2 Hz)

attributed to the 1',3',4'-trisubstituted ring B, and two aromatic doublets at δ_H 6.26 (d, *J* = 2.1 Hz) and 6.49 (d, *J* = 2.1 Hz) attributed to two hydrogens in *meta* arrangements in ring A. These observations are consistent with the 5,7,3',4'-tetraoxigenated flavonoid core structure of **19**. The broad singlet at δ_H 12.48 is readily attributed to 5-OH, which is hydrogen bonded to the oxygen atom of the ketone function at C-4. The flavonol moiety was determined to be quercetin as in the case of **18**, and was confirmed by comparison with published data.[172] A comparison of the anomeric hydrogen chemical shifts and coupling constants for the sugar moiety in **19** with α- and β-arabinofuranosides suggested that the sugar moiety is an arabinose in the furanose form and α-linked to the flavonoid structure.[173–175] The attachment of the arabinofuranosyl moiety to C-3 was supported by HMBC correlation from H-1" to C-3 (Figure 3.21). The structure of quercetin-*O*-α-L-arabinofuranoside is consistent with COSY and HMBC (Figure 3.2, Appendix 62 - 63) data as well as by comparison with literature data.[169,171] Quercetin-3-*O*-arabinoside exists in *M. hypoleuca* in two sugar forms, i.e., as a pyranose **(18)** and furanose **(19)**.

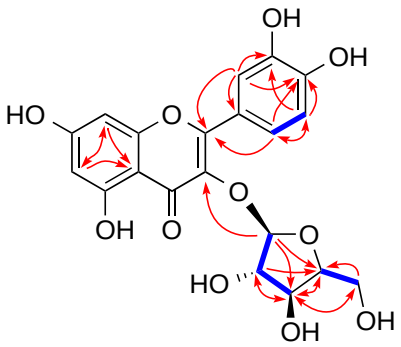

Figure 3.21: Selected HMBCs and COSY (bold bonds) correlations of quercetin-3-*O*-α-L-arabinofuranoside **(19)**

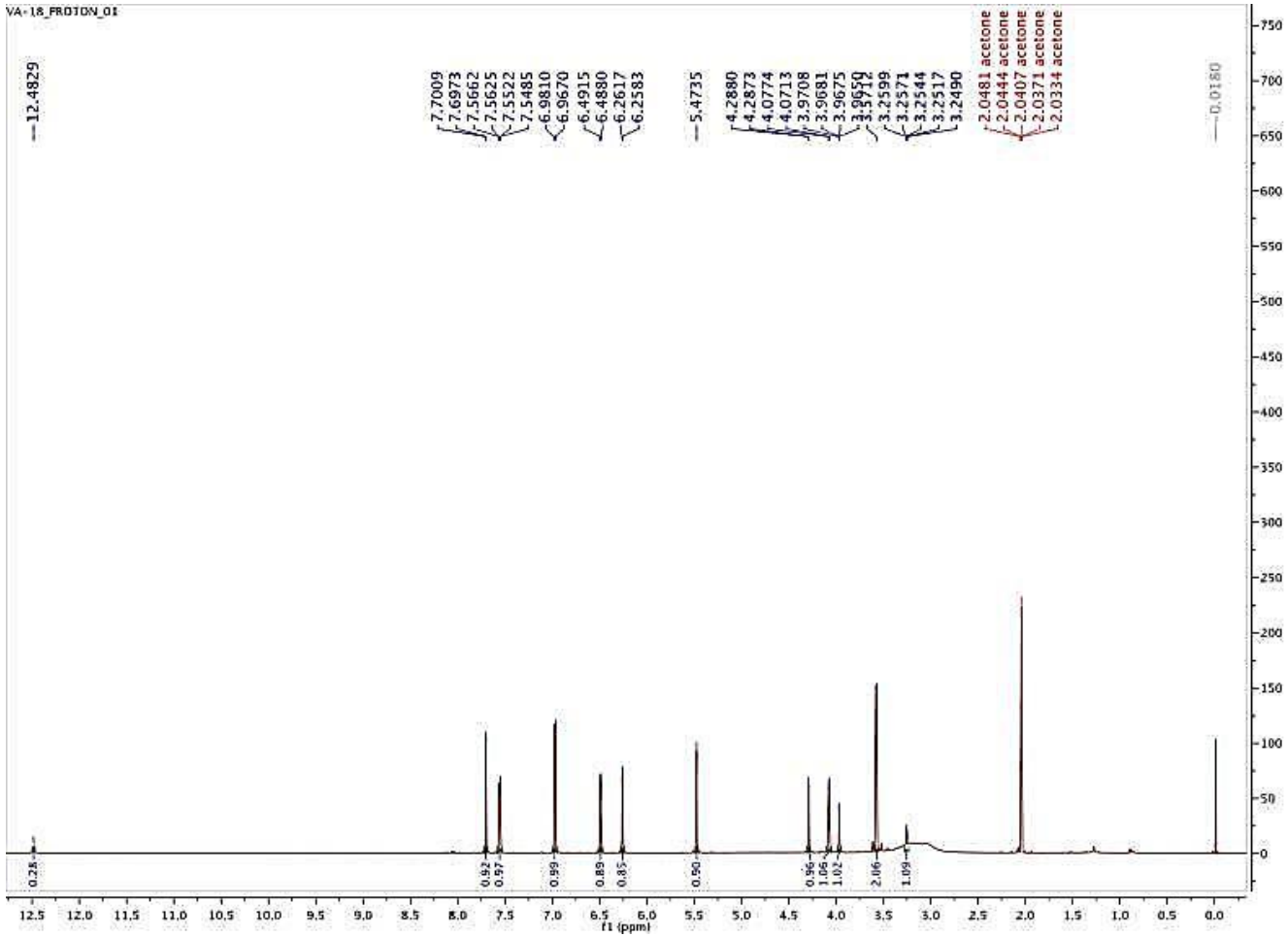

Figure 3.22: ^{1}H NMR spectrum (acetone-d_6, 600 MHz) of quercetin-3-*O*-α-L-arabinofuranoside **(19)**

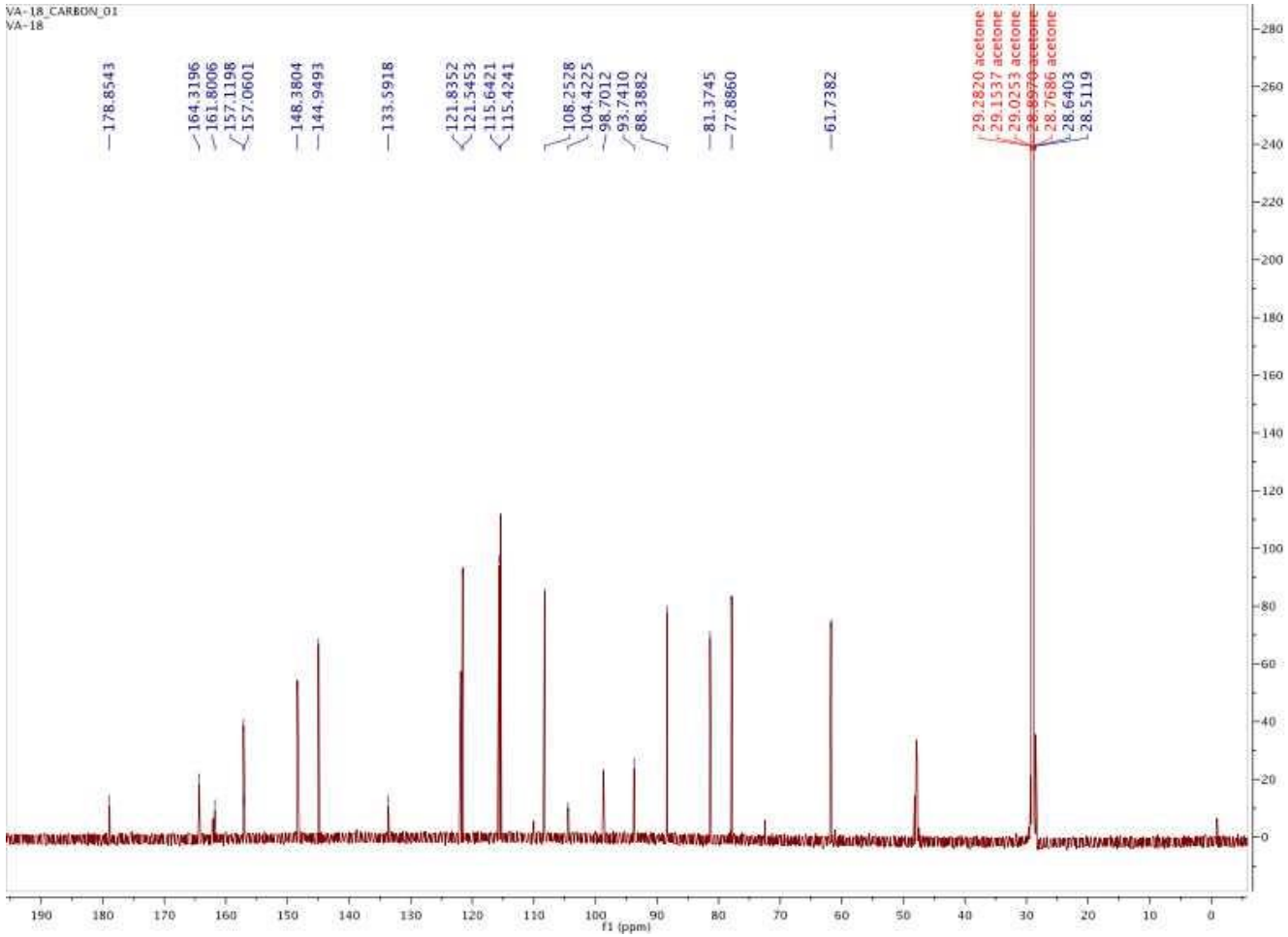

Figure 3.23: ^{13}C NMR spectrum (acetone-d_6, 150 MHz) of quercetin-3-*O*-α-L-arabinofuranoside **(19)**

3.2.3 Quercetin-3-*O*-β-D-galactoside

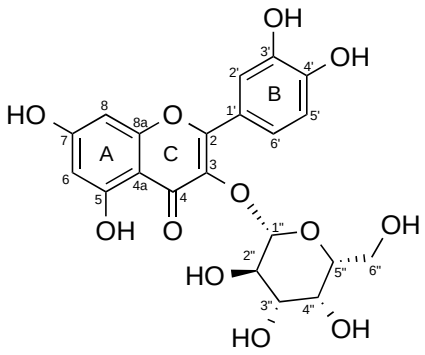

20

Quercetin-3-*O*-β-D-galactoside **(20)** was obtained as a yellow amorphous. ESIMS showed a pseudo-molecular ion peak at *m/z* 465 $[M + H]^+$ and HRESIMS gave the molecular formula $C_{21}H_{20}O_{11}$. The IR spectrum showed absorption bands due to the presence of hydroxy and conjugated ketone groups at 3400 and 1608 cm^{-1}, respectively. The UV spectrum showed absorption at 258, 306, 363 nm, resembling the UV spectra of similar flavonol monoglycosides.[166,167]

The ^{13}C NMR spectrum (Table 3.5, Figure 3.26) showed a total of 21 carbon signals attributed to a flavone nucleus (9xC), a 1',3',4'-trisubstituted aromatic ring (6xC) and an aldohexose moiety (6xC). The carbon signal observed at δ_C 178.3 was readily attributed to the conjugated ketone carbonyl, while the signals at δ_C 164.4, 161.7, 157.7, and 157.1 are due to aromatic carbons that are sites of oxygenation. The C-4" carbon shift at δ_C 68.7 and the anisochronous C-5" methylene hydrogen signals at δ_H 3.57 and 3.68, are consistent with those of β-flavonol gylcosides in the pyranose form.[168,169]

The ^1H NMR spectrum (Table 3.5, Figure 3.25) showed three aromatic hydrogen signals at δ_H 6.91 (d, J = 8.5 Hz), 7.80 (dd, J = 8.5, 2.2 Hz), and 8.03 (d, J = 2.2 Hz)

attributed to the 1',3',4'-trisubstituted ring B, and two aromatic doublets at δ_H 6.26 (d, *J* = 2.1 Hz) and 6.5 (d, *J* = 2.1 Hz) attributed to the two hydrogens in *meta* arrangement in ring A. These observations are consistent with the 5,7,3',4'-tetraoxygenated flavonol core structure of **20**. The broad singlet at δ_H 12.36 is readily attributed to 5-OH, which is hydrogen bonded to the oxygen atom of the ketone function at C-4. The flavonol moiety was determined to be quercetin by comparison with published data.[172] The observation of an anomeirc hydrogen signal at δ_H 5.16 (d, *J* = 7.8 Hz) along with six hydrogen signals in the region δ_H 3.61 – 3.91 indicated the presence of a sugar unit. The large coupling constant (7.8 Hz) observed between H-1" and H-2" suggested both hydrogens are *trans*-diaxially oriented requiring the sugar moiety to be a β-anomer. Comparison of the ^{1}H and ^{13}C NMR data of the sugar moiety with literature values revealed the presence of a β-galactopyranose.[176] The HMBC correlation (Figure 3.24) from H-1" to C-3 confirmed the attachment of the galactopyranosyl moiety to the quercetin structure at C-3. Overall, the structure of **20** is consistent with COSY, HSQC, HMBC (Appendix 65 - 67) and literature data of 3-*O*-β-D-galactopyranoside flavonoids.[167,169,176].

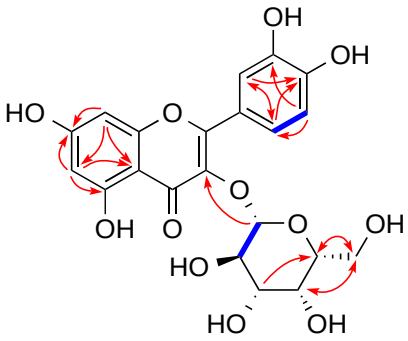

Figure 3.24: Selected HMBCs and COSY (bold bonds) correlations of quercetin-3-*O*-β-D-galactoside **(20)**

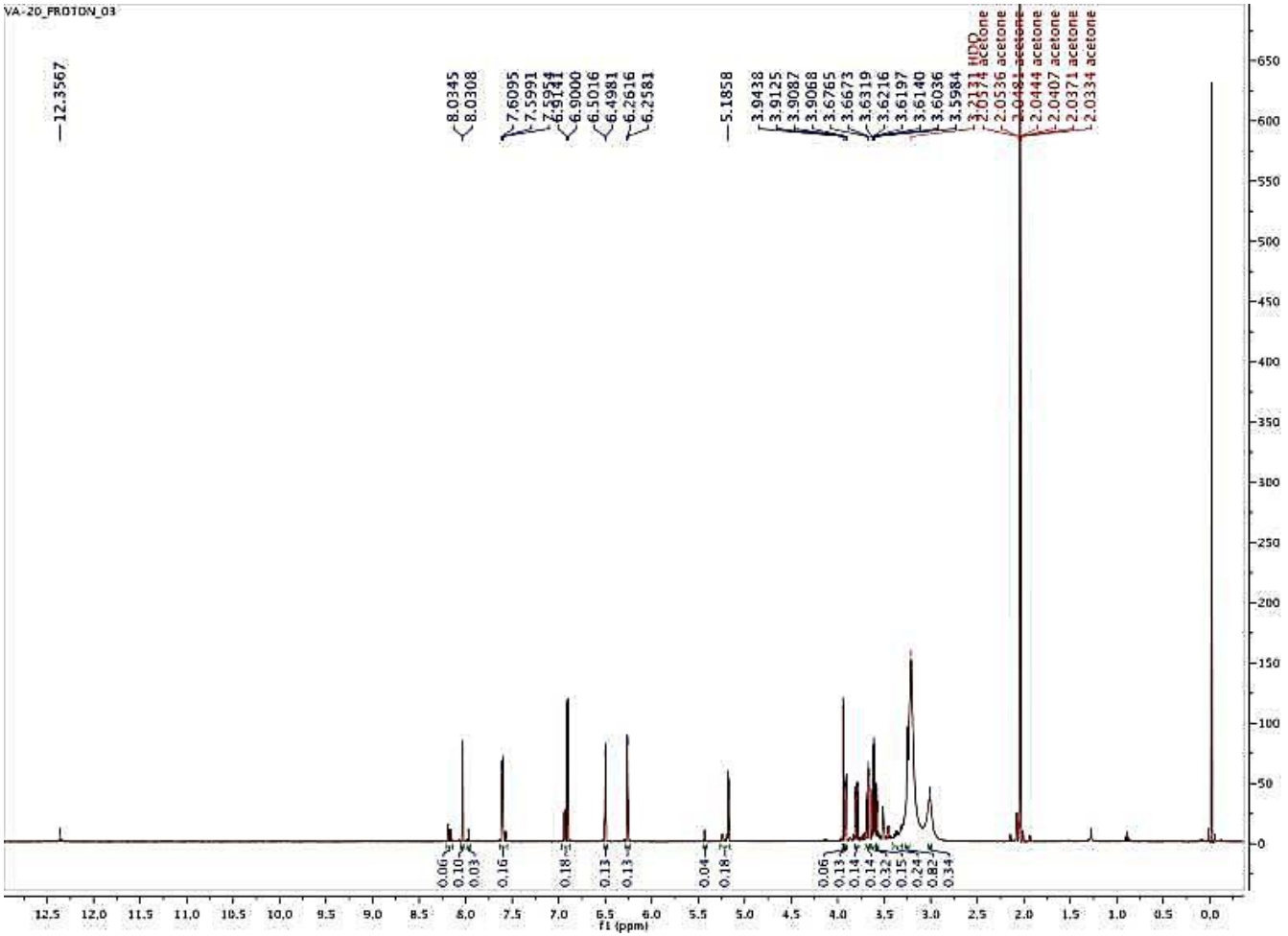

Figure 3.25: ^{1}H NMR spectrum (acetone-d_6, 600 MHz) of quercetin-3-*O*-β-D-galactoside **(20)**

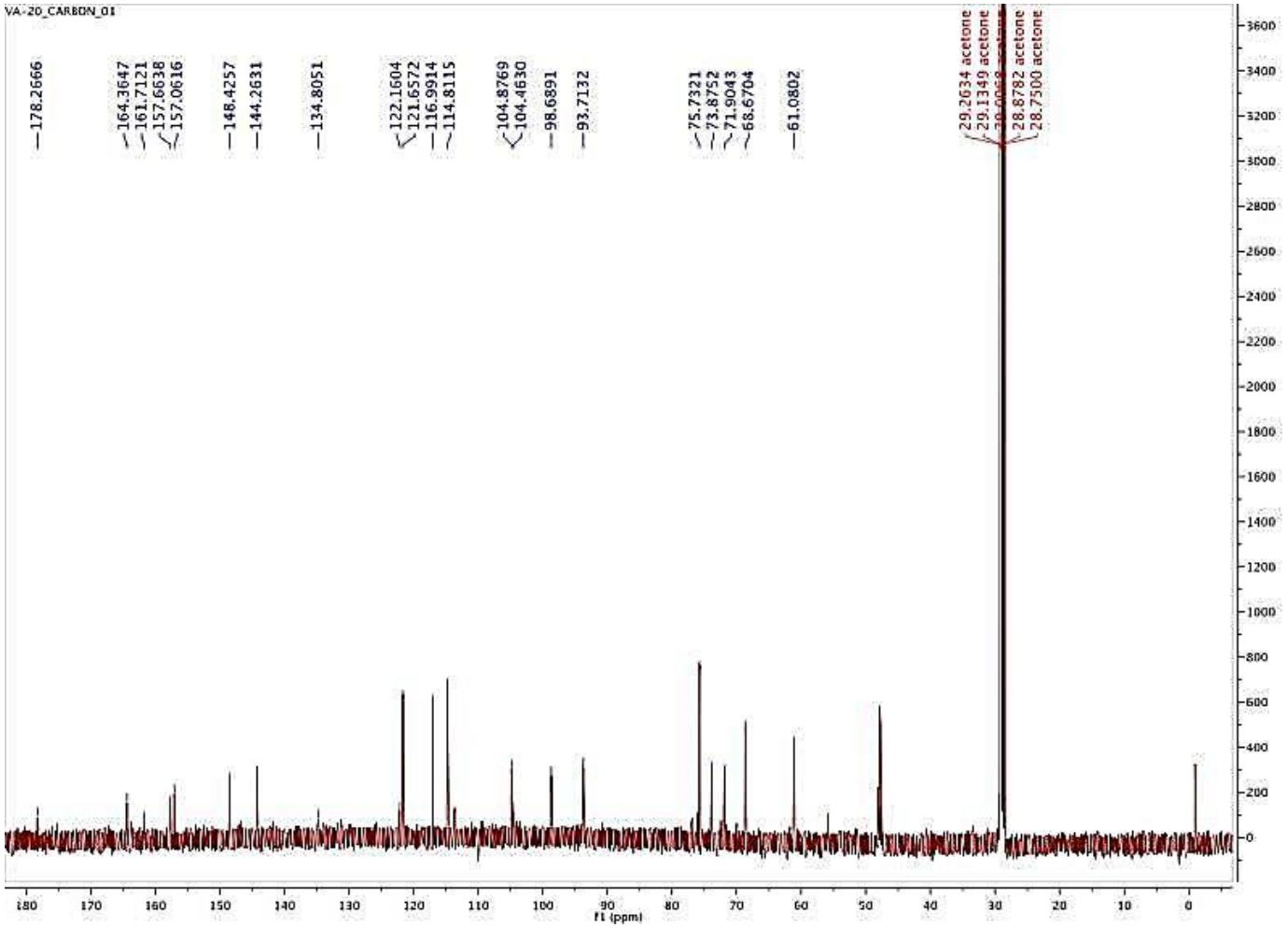

Figure 3.26: ^{13}C NMR spectrum (acetone-d_6, 150 MHz) of quercetin-3-*O*-β-D-galactoside **(20)**

Table 3.5: ^{1}H and ^{13}C NMR data of quercetin-*O*-α-L-arabinopyranoside **(18)**, quercetin-*O*-α-L-arabinofuranoside **(19)** and quercetin-*O*-β-D-galactoside **(20)**[a]

C	**18**		**19**		**20**	
	^{1}H (*J* in Hz)	^{13}C	^{1}H (*J* in Hz)	^{13}C	^{1}H (*J* in Hz)	^{13}C
2	-	157.9[b]	-	157.12[c]	-	157.7[c]
3	-	135.5	-	133.6	-	134.8
4	-	179.1	-	178.9	-	178.3
4a	-	105.5	-	104.4	-	104.5
5	-	163.0	-	161.8	-	161.7
6	6.25 d (2.1)	99.6	6.26 d (2.1)	98.7	6.26 d (2.1)	98.7
7	-	165.3	-	164.3	-	164.4
8	6.49 d (2.1)	94.6	6.49 d (2.1)	93.7	6.50 d (2.1)	93.7
8a	-	157.9[b]	-	157.06[c]	-	157.1[c]
			-			
1'	-	122.8	-	121.6	-	122.2
2'	7.88 d (2.2)	117.3	7.70 d (2.2)	115.4	8.03 d (2.2)	117.0
3'	-	145.5	-	144.9	-	144.3
4'	-	149.4	-	148.4	-	148.4
5'	6.92 d (8.5)	116.0	6.97 d (8.4)	115.6	6.91 d (8.5)	114.8
6'	7.63 dd (8.5, 2.2)	122.7	7.56 dd (8.4, 2.2)	121.8	7.80 dd (8.5, 2,2)	121.7
1"	5.26 d (6.2 Hz)	104.2	5.47 br s	108.3	5.18 d (7.8)	104.9
2"	3.91 dd (7.9, 6.2)	72.5	4.29 dd (2.0, 0.7)	81.4	3.80 dd (9.5, 7.8)	71.9
3"	3.71 dd (7.9, 4)	73.7	3.97 dd (3.7, 2.0)	77.9	3.61 dd (9.5, 3.3)	73.9
4"	3.85 td (4, 2.3)	68.2	4.07 q (3.7)	88.4	3.91 dd (3.4, 1.1)	68.7
5"	3.79 dd (12.2, 4)	66.1	3.57 d (3.7)	61.7	3.84 br t (8.7)	75.7
	3.46 dd (12.2, 2.3)					
6"	-	-	-	-	3.68 dd (11, 6)	61.1
	-	-	-	-	3.61 m	-
5-OH	12.49 s	-	12.48 s	-	12.36 br s	-

[a] Acetone-d_6, 600 MHz; [b] Overlapping signals; [c] Assignments are interchangable

3.2.4 Quercetin

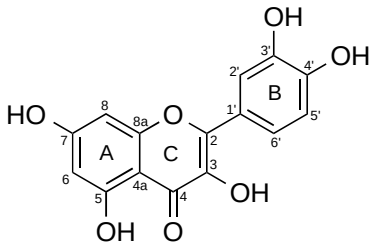

21

Quercetin **(21)** was obtained as a yellow powder. ESIMS of **21** showed a pseudo-molecular ion peak at *m/z* 303 $[M + H]^+$ which corresponds to the molecular formula $C_{15}H_{10}O_7$. The IR spectrum showed absorption bands attributable to the presence of hydroxy (at 3476 cm^{-1}) and conjugated carbonyl (1614 cm^{-1}). The UV spectrum showed absorption at 257, 303 and 374 nm.

The ^1H NMR spectrum (Table 3.6, Figure 3.27) showed three aromatic hydrogen signals at δ_H 6.86 (d, J = 8.5 Hz), 7.57 (dd, J = 8.5, 2.0 Hz), and 7.70 (d, J = 2.0 Hz) attributed to the trisubstituted aromatic ring B, and two aromatic doublets at δ_H 6.13 (d, J = 2.0 Hz) and 6.40 (d, J = 2.0 Hz), attributed to a pair of *meta*-coupled hydrogens in ring A.[177] The absence of a singlet signal at approximately δ_H 6.3 ppm due to H-3 indicated that C-3 is substituted. These results agreed with a 3,5,7,3',4'-pentaoxygenated flavonoid. In addition, the signal at δ_H 12.04 indicated the presence of a hydroxy group at C-5. Although ^{13}C NMR was not carried out, comparison of mass, IR, UV and ^1H NMR data with literature was sufficient for the identification of quercetin **(21)**.[166,169,172,178]

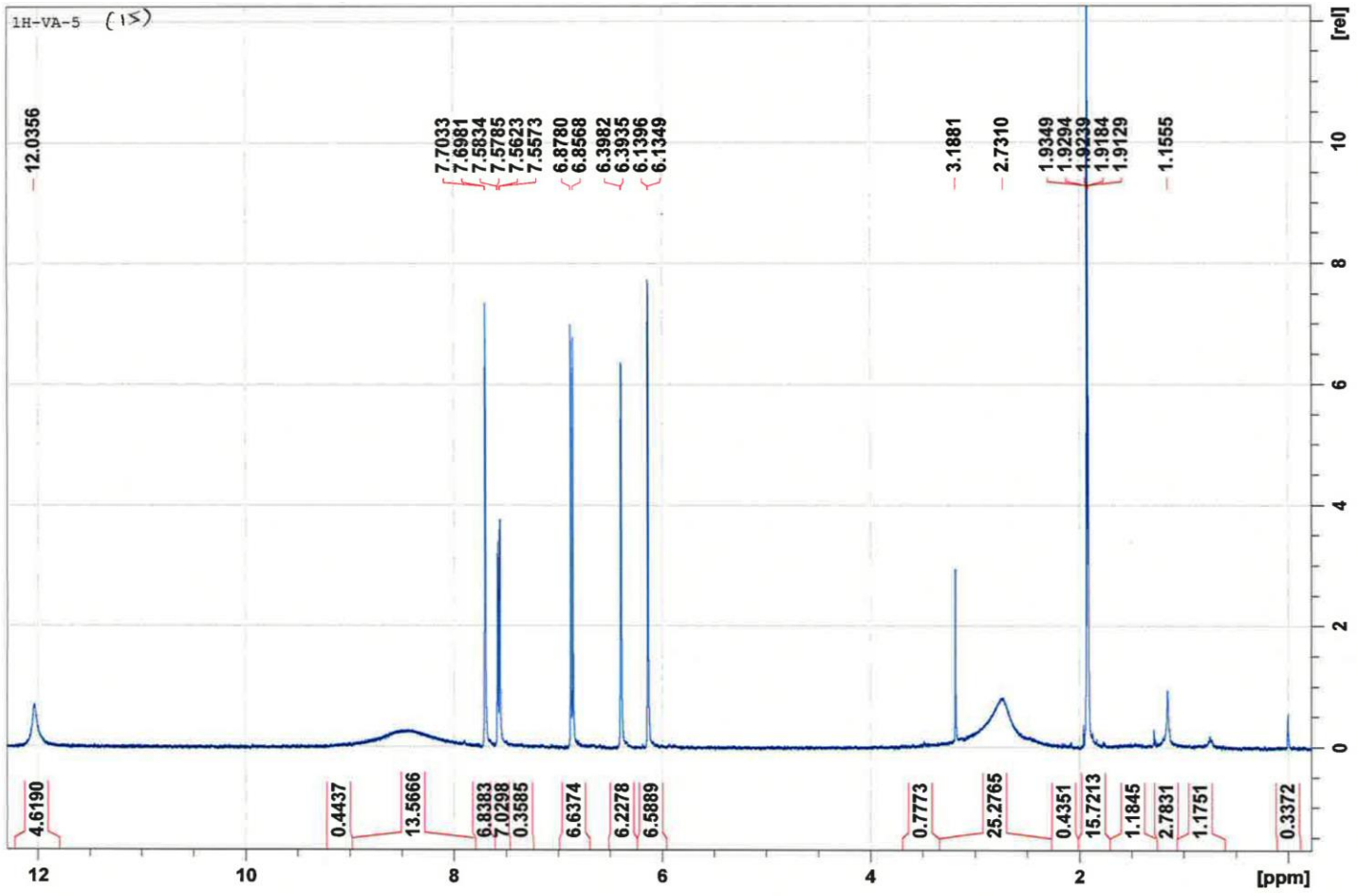

Figure 3.27: ^{1}H NMR spectrum (acetone-d_6, 400 MHz) of quercetin **(21)**

3.2.5 Kaempferol

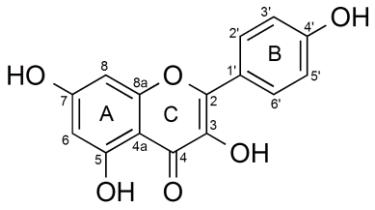

22

Kaempherol **(22)** was obtained as a yellow powder. ESIMS showed a pseudo-molecular ion peak at *m/z* 287 $[M + H]^+$ which corresponds to the molecular formula $C_{15}H_{10}O_6$. The IR spectrum showed absorption bands attributable to the presence of hydroxy and conjugated ketone groups at 3476 and 1614 cm^{-1}, respectively. The UV spectrum showed absorption at 265 and 367 nm.

The ^{13}C NMR spectrum (Table 3.6, Figure 3.29) showed a total of 15 carbon signals (six methines and nine quaternary carbons). The quaternary carbon signal observed at δ_C 176.6 was readily attributed to the conjugated ketone carbonyl, while the resonances at δ_C 160.2, 162.5 and 165.5 suggested that these aromatic carbons are sites of oxygenation while the resonance at δ_C 136.7 is attributed to the C-3.[167,179]

The ^1H NMR spectrum (Table 3.6, Figure 3.28) showed two singlets at δ_H 6.28 (H-6) and 6.54 (H-8), attributed to a pair of *meta*-coupled aromatic hydrogens in ring A, usually appear between δ_H 6.0-6.5.[177] On the other hand, two sets of 2H aromatic doublets observed at δ_H 7.03 (d, J = 8.8 Hz, 2H) and 8.17 (d, J = 8.8 Hz, 2H) confirmed the presence of the *para*-disubstituted ring B. The more upfield signal (δ_H 7.03) was attributed to H-3' and H-5' due to the shielding effect from the OH at C-4', while the more downfield signal (δ_H 8.17) was attributed H-2' and H-6'. The absence of a singlet signal at approximately δ_H

6.3 due to H-3 indicated a substitution at C-3, which is consistent with the structure of flavonol.[177] Additionally, a broad signal at δ_H 12.20 is attributed to the presence of hydroxy group at C-5. The NMR (^{1}H and ^{13}C, HSQC), MS, IR, and UV data of **22** are in complete agreement with those of kaempherol, as available in the literature.[170,179]

Table 3.6: ^{1}H and ^{13}C NMR data of quercetin **(21)** and kaempherol **(22)**[a]

Position	**21**	**22**	
	^{1}H (*J* in Hz)	^{1}H (*J* in Hz)	^{13}C
2	-	-	147.1
3	-	-	136.7
4	-	-	176.6
4a	-	-	104.1
5	-	-	162.5[b]
6	6.13 d (2.0)	6.28 s	99.2
7	-	-	165.5
8	6.40 d (2.0)	6.54 s	94.5
8a	-	-	157.8
1'	-	-	123.3
2'	7.70 d (2.0)	8.17 d (8.8)	130.5
3'	-	7.03 d (8.8)	116.3
4'	-	-	160.2[b]
5'	6.86 d (8.5)	7.03 d (8.8)	116.3
6'	7.57 dd (8.5, 2.0)	8.17 d (8.8)	130.5
5-OH	12.04 s	12.20 s	-

[a] Acetone-d_6, 400 MHz; [b] Assignments are interchangeable

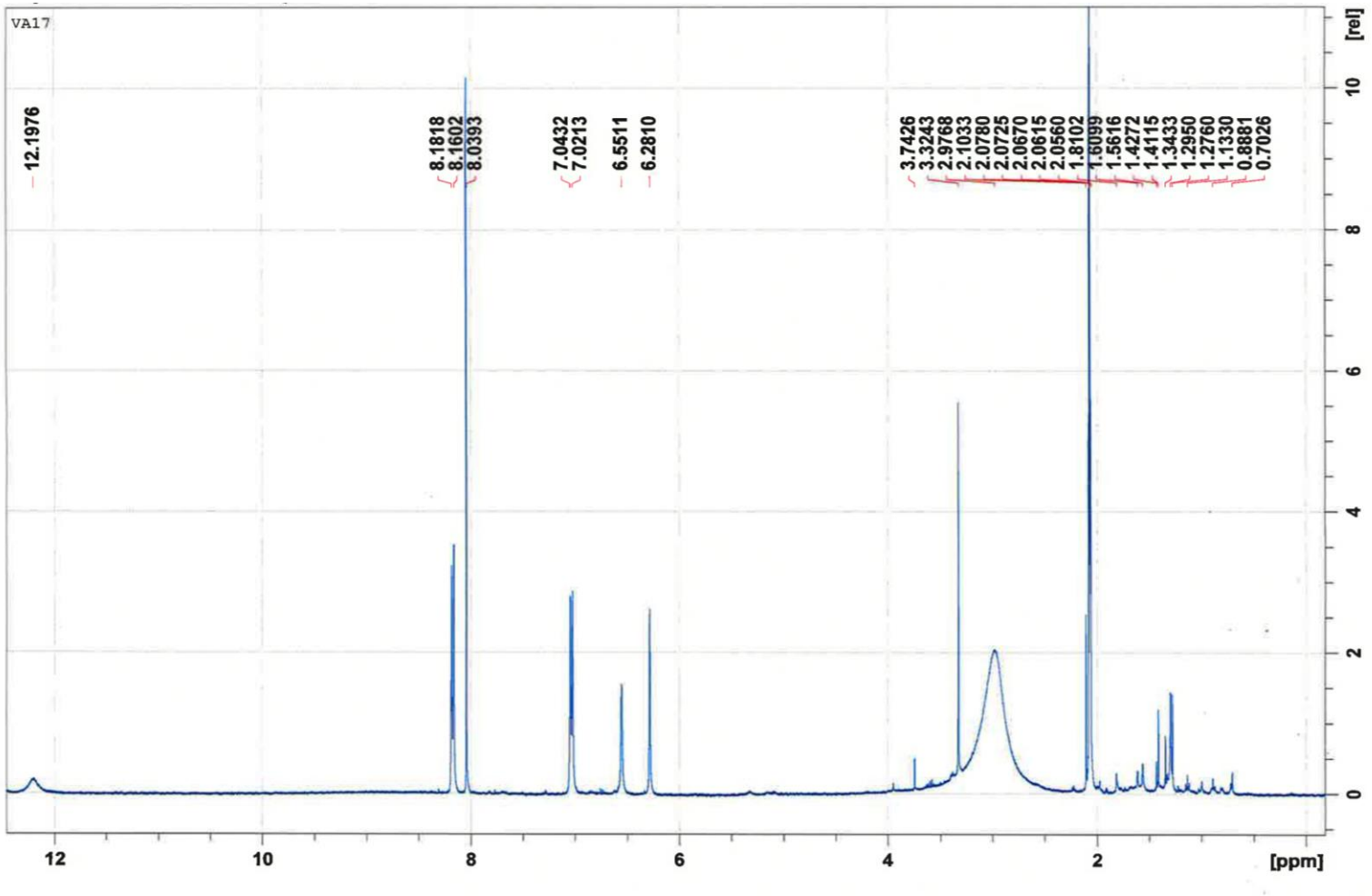

Figure 3.28: ^{1}H NMR spectrum (acetone-d_6, 400 MHz) of kaempherol **(22)**

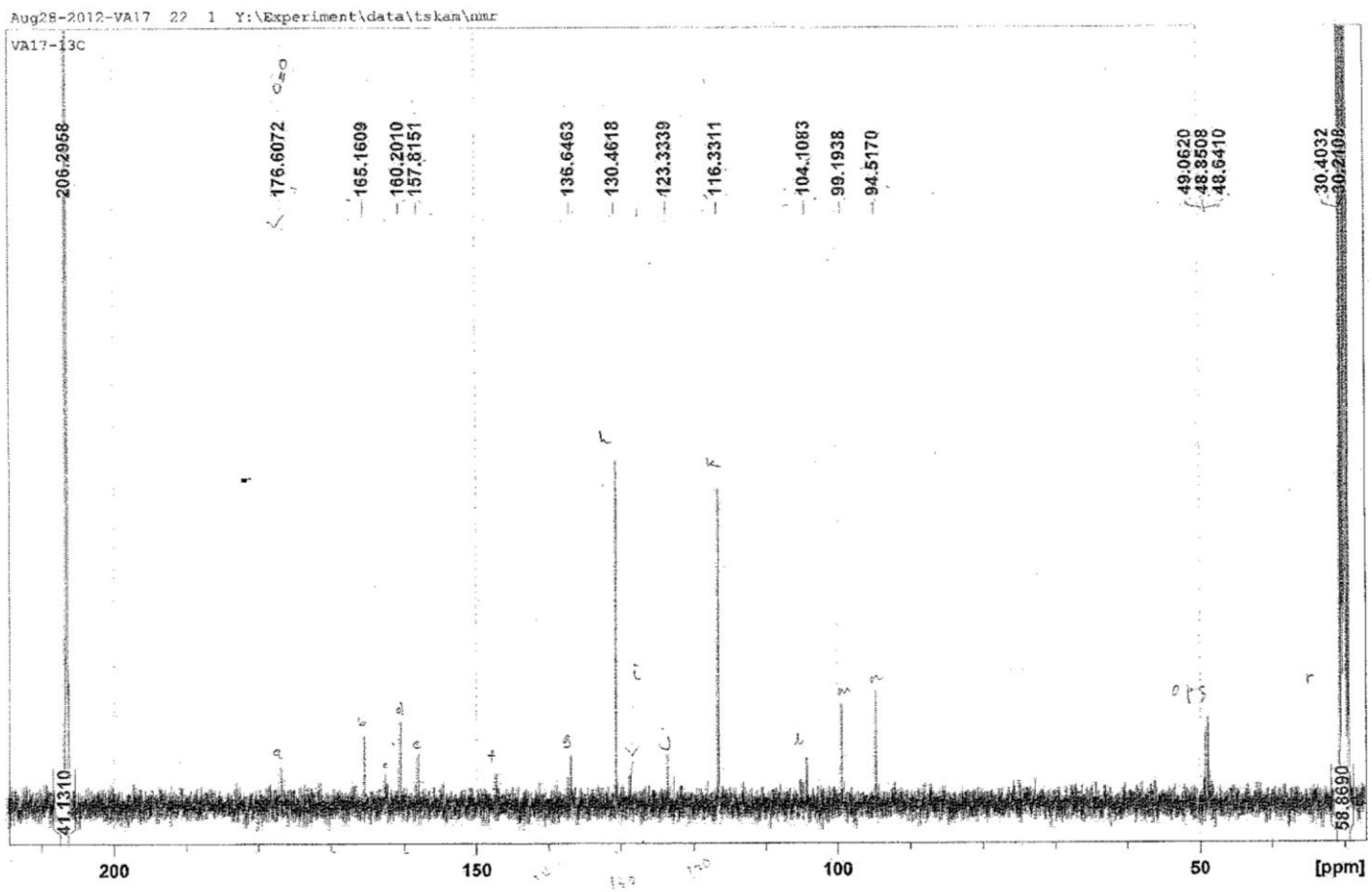

Figure 3.29: ^{13}C NMR spectrum (acetone-d_6, 100 MHz) of kaempherol **(22)**

3.2.6 5,7-Dihydroxy-2-(4-methoxyphenyl)-8-(3-methylbut-2-en-1-yl)chroman-4-one

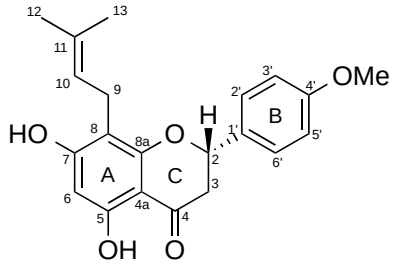

23

5,7-Dihydroxy-2-(4-methoxyphenyl)-8-(3-methylbut-2-en-1-yl)chroman-4-one **(23)** was obtained in minute amounts as yellow crystals, mp: 215-218 °C. ESIMS measurements showed a pseudo-molecular ion peak at *m/*z 355 $[M + H]^+$ and HRESIMS gave the molecular formula $C_{21}H_{22}O_5$. IR spectrum showed absorption bands due to hydroxy (3241 cm^{-1}) and conjugated ketone (1643 cm^{-1}) functions. The UV spectrum showed absorption maxima at 219, 296 and 336 nm.

The ^{13}C NMR spectrum (Table 3.7, Figure 3.32) showed a total of 21 carbon signals (three methyls, two methylenes, seven methines, and nine quaternary carbons). The quaternary carbon signal observed at δ_C 197.4 was readily attributed to the conjugated ketone carbonyl, while the signals at δ_C 160.9, 161.0, 163.0, and 165.0 suggested that these aromatic carbons are sites of oxygenation.

The ^1H NMR spectrum (Table 3.7, Figure 3.31) were indicative of a flavonone structure with three sets of doublet of doublets observed at δ_H 2.77 (dd, J = 17.0, 3.1 Hz), 3.13 (dd, J = 17.0, 12.0 Hz) and 5.48 (dd, J = 12.0, 3.1 Hz) attributed to the H-3_{eq}, H-3_{ax} and H-2, respectively.[45] Two typical 2H aromatic signals appearing as a pair of doublets at δ_H 6.98 (d, J = 9.0 Hz) and 7.49 (d, J = 9.0 Hz) suggested two pairs of equivalent aromatic

hydrogens, while the methoxy signal at δ_H 3.82, which is assignable to C-4' suggested a 1',4'-disubstituted aromatic B-ring with a mirror plane of symmetry passing through C-1' and C-4'. The equatorial position of the B-ring was assigned based on the the coupling constant $J_{2,3ax}$ = 12.0 Hz, which requires H-2 and H-3_{ax} to be trans-diaxial.[45] The presence of two allylic methyl singlets at (δ_H 1.59 and 1.60), an allylic methylene doublet (δ_H 3.21) and a vinylic methine triplet (δ_H 5.18) were indicative of a prenyl side chain. HMBC correlations (Figure 3.30, Appendix 69) from H-9 to C-8 and H-6 to C-8 established the connectivity of the prenyl unit to C-8. The remaining singlet at δ_H 6.03 were attributed to H-6 while the signal observed at δ_H 12.12 are attributed to the hydroxy group at C-5. The structure of **23** is entirely consistent with COSY and HMBC data (Figure 3.30, Appendix 67 and 68) as well as literature.[180,181]

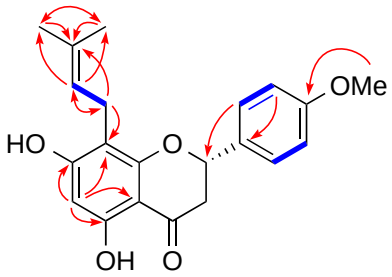

Figure 3.30: Selected HMBCs and COSY (bold bonds) correlations of 5,7-dihydroxy-2-(4-methoxyphenyl)-8-(3-methylbut-2-en-1-yl)chroman-4-one **(23)**

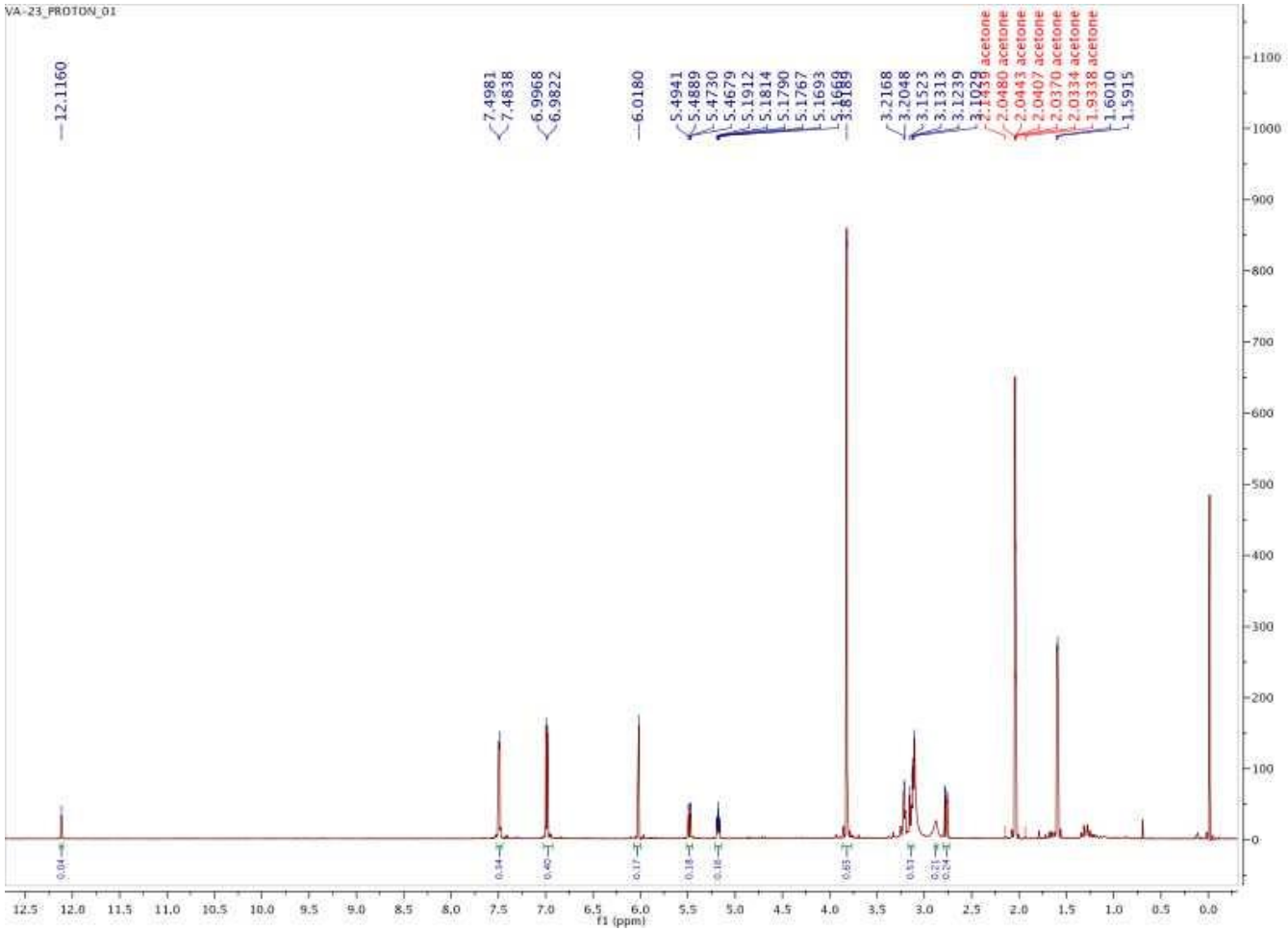

Figure 3.31: ^{1}H NMR spectrum (acetone-d_6, 600 MHz) of 5,7-dihydroxy-2-(4-methoxyphenyl)-8-(3-methylbut-2-en-1-yl)chroman-4-one **(23)**

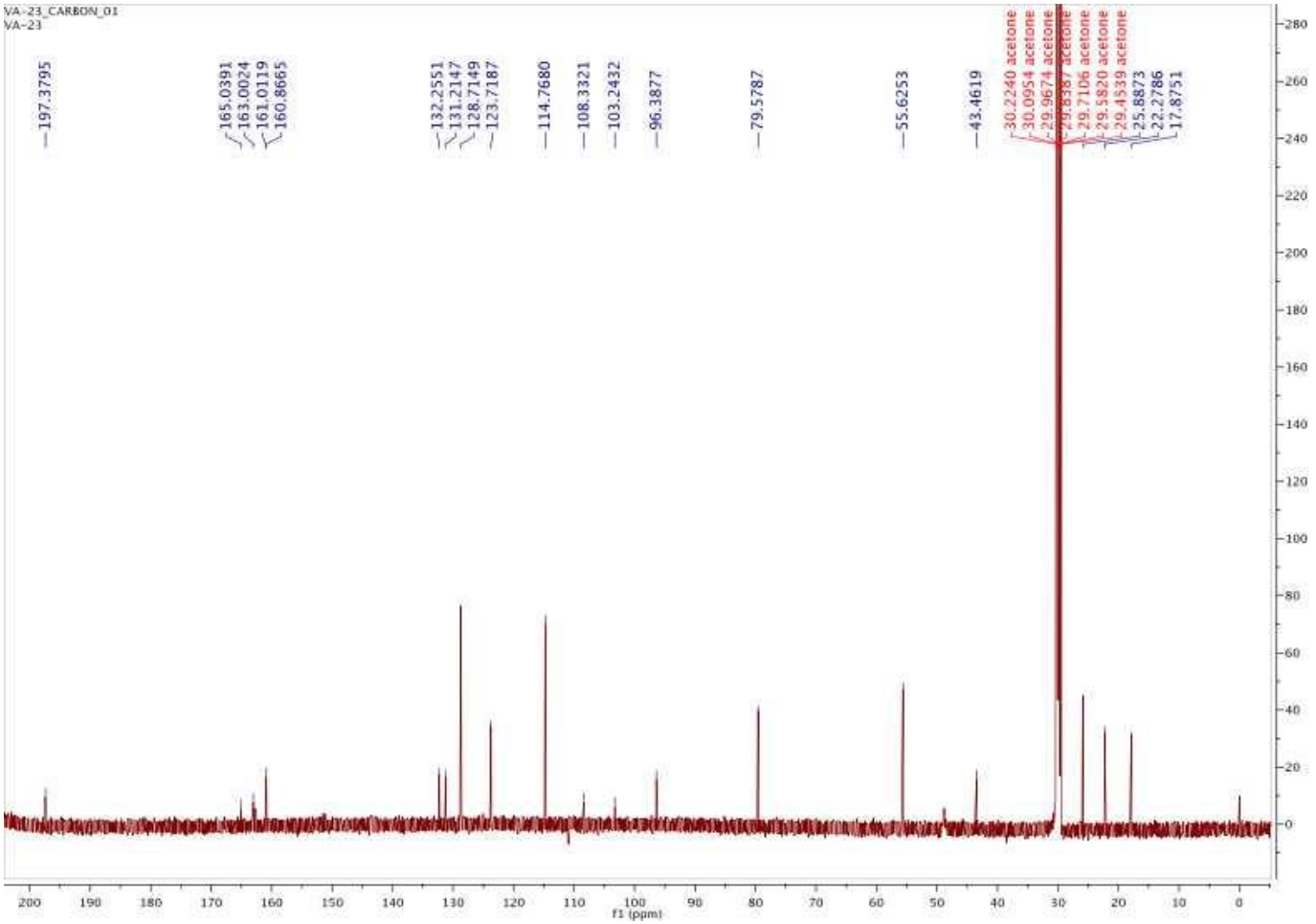

Figure 3.32: ^{13}C NMR spectrum (acetone-d_6, 150 MHz) of 5,7-dihydroxy-2-(4-methoxyphenyl)-8-(3-methylbut-2-en-1-yl)chroman-4-one **(23)**

Table 3.7: ^{1}H and ^{13}C NMR data of 5,7-dihydroxy-2-(4-methoxyphenyl)-8-(3-methylbut-2-en-1-yl) chroman-4-one **(23)** [a]

Position	**23**		Literature data[181]	
	^{1}H (*J* in Hz)	^{13}C	^{1}H (*J* in Hz)	^{13}C
2	5.48 dd (12, 3.1)	79.6	5.36 dd (12.9, 3)	78.7
3_{ax}	3.13 dd (17, 12)	43.5	3.06 dd (17.1, 12.9)	43.0
3_{eq}	2.77 dd (17, 3.1)		2.80 dd (17.1, 3)	-
4	-	197.4	-	196.5
4a	-	103.2	-	103.1
5	-	165.0	-	162.1
6	6.03 s	96.4	6.02 s	96.7
7	-	163.0	-	163.7
8	-	108.3	-	106.4
8a	-	161.0	-	159.8
9	3.21 d (7.2)	22.3	Not available	21.7
10	5.18 t (7.2)	123.7	Not available	121.6
11	-	131.2	-	134.6
12	1.59 s	17.9	Not available	17.8
13	1.60 s	25.9	Not available	25.6
1'	-	132.3	-	130.7
2'	7.49 d (9)	128.7	7.37 d (8.7)	127.5
3'	6.98 d (9)	114.8	6.95 d (8.7)	114.1
4'	-	160.9	-	159.8
5'	6.98 d (9)	114.8	6.95 d (8.7)	114.1
6'	7.49 d (9)	128.7	7.37 d (8.7)	127.5
4'-OMe	3.82 s	55.6	3.84 s	55.3
5-OH	12.12 s	-	12.01 s	-

[a] Acetone-d_6, 600 MHz

3.2.7 3-*Epi*-taraxerol

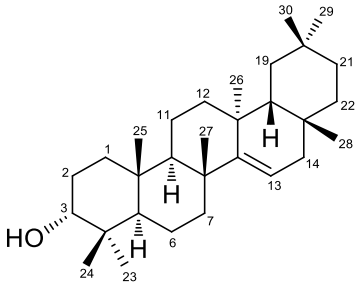

24

3-*Epi*-taraxerol (**24)** was obtained from the leaves of *M. hypoleuca* as colourless crystals, mp: 260-263 °C (lit., 261-263 °C)[182]. Since suitable crystals of **24** were at hand, X-ray diffraction analysis was carried out (Figure 3.33) and revealed **24** as 3-*epi*-taraxerol. The ^{1}H NMR spectrum (Figure 3.34) of **24** was also obtained which revealed seven singlets in the upfield region (δ_H 0.81 – 1.25), attributable to the seven methyl groups. Additionally, a carbinolic hydrogen was observed at δ_H 3.40 (t, 2.28 Hz) and an olefinic hydrogen at δ_H 5.5 (dd, 8.2, 3.1 Hz), assignable to H-3 and H-13, respectively. Due to severe overlapping of the ^{1}H NMR signals, detailed hydrogen assignment was not possible without 2D NMR analysis (not done due to insufficient compound). However, the ^{1}H NMR data of **24** are largely similar to those of taraxerol and tarexerone (structurally similar compounds).[182,183] *Epi*-taraxerol **(24)** is commonly found in the *Macaranga* genus as it is one of the principal component of the epicutilar wax crystals that coats the stems of many *Macaranga* plants.[184]

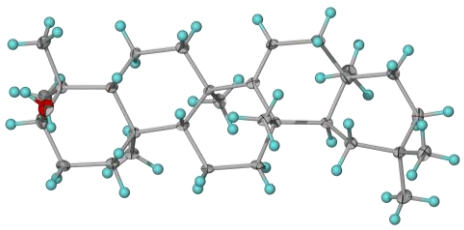

Figure 3.33: X-ray diffraction crystal structure of 3-*epi*-taraxerol **(24)**

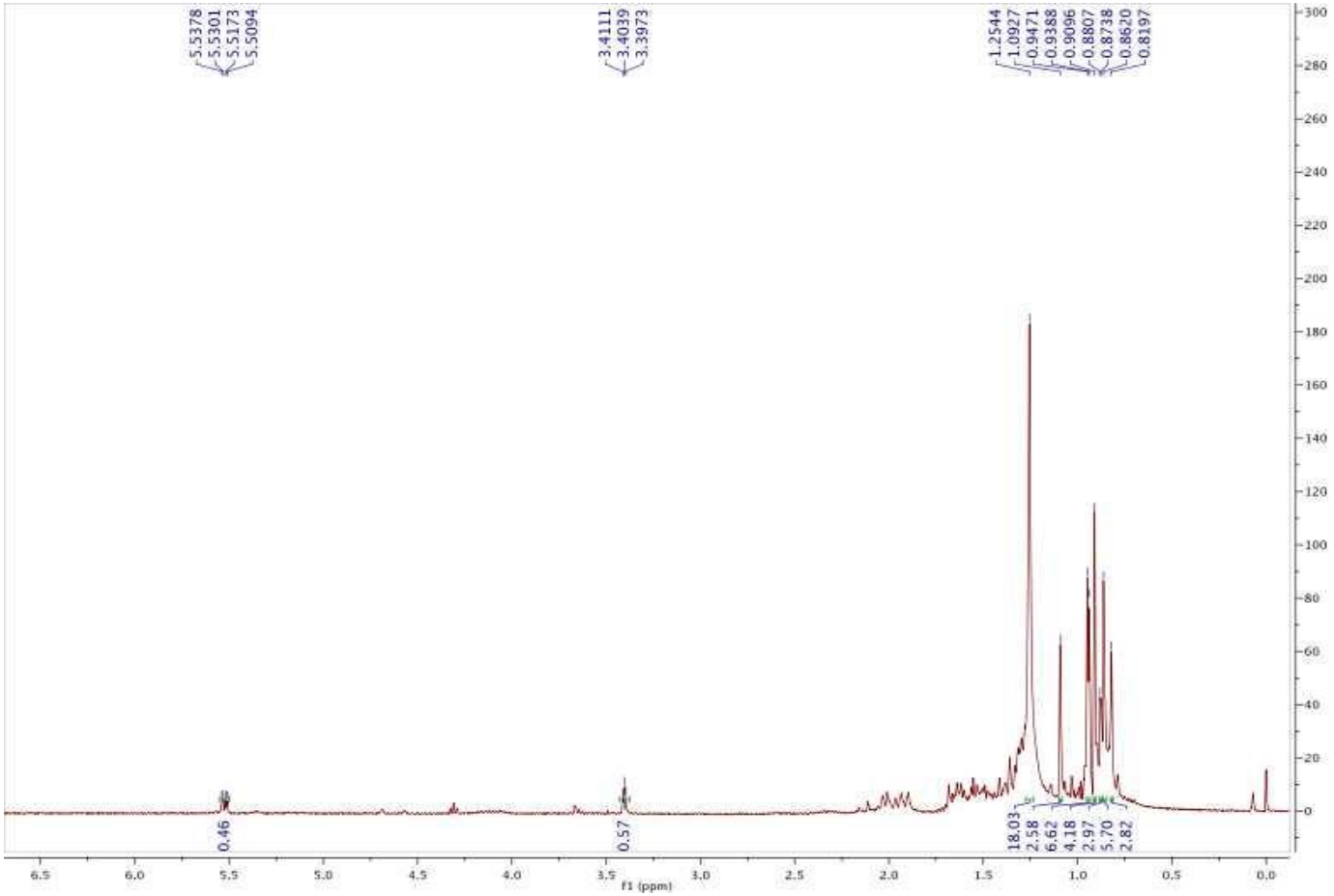

Figure 3.34: ^{1}H NMR spectrum ($CDCl_3$, 600 MHz) of 3-*epi*-taraxerol **(24)**

Chapter 4: Characterisation of anti-cancer properties of crude extracts and isolated compounds

4.1 Introduction

One of the distinct characteristics of cancer cells is their ability for uncontrolled cell proliferation by evading normal regulation in cell growth thus giving them the ability to resist apoptosis. As a result, cell proliferation assay which takes into account this trait is an effective preliminary screening tool that uncovers potential compounds which contribute to advances in cancer drug discovery. The present study yielded 24 pure compounds from three plant genera, namely *Ficus*, *Artocarpus* and *Macaranga*, among which include known compounds that are well established for their anti-cancer properties. These are alkaloids: 13a(*S*)-(+)-tylocrebrine, 13a(*S*)-(+)-tylophorine (**8**), 13a(*S*)-(+)-septicine **(9)**, and flavonoids: quercetin **(21)** and kaempherol **(22)**. The anti-cancer studies of the named alkaloids dated back to the 1960s where tylophorine **(8)** and tylocrebrine **(7)** became clinical candidates only to be aborted due to central nervous system (CNS) toxicity.[102] In comparison to tylophorine **(8)**, septicine **(9)** was reported to be profoundly weaker in activity despite its structural similarities.[146] Quercetin **(21)**[121,185] and kaempherol **(22)**[122,186] on the other hand are highly regarded for their therapeutic potential against several types of cancer by induction of apoptosis as well as the possibility to overcome resistance in tumor cell growth. Given the well established studies that have been carried out on these compounds, they were excluded from the preliminary anti-cancer screening in this study.

13a(*R*)-(-)-3,6-Deoxypergularinine **(3)**, artocarpetin A **(14)**, quercetin-3-*O*-α-L-arabinofuranoside **(19)**, lichexanthone **(17),** 5,7-Dihydroxy-2-(4-methoxyphenyl)-8-(3-methylbut-2-en-1-yl)chroman-4-one **(23)** and 3-*epi*-taraxerol **(24)** can not be included in

the screening effort due to scarcity of the compounds. Similar to other phenanthroindolizidines, literature survey of **3** showed potent cytotoxicity against various tumor cell lines including the drug resistant variants.[149] Contrary to other prenylated flavonoids, there were no reports of anti-cancer properties exhibited by artocarpetin A **(14)**. Furthermore, **14** was found to show no effect as an antioxidant agent rendering this compound as possibly biologically inactive.[187] No reports were found on the anti-cancer activities of lichexanthone **(17)** and 3-*epi*-taraxerol **(24)**. The remaining compounds (**1**-**2**, **4**-**6**, **10**-**13**, **15**-**16**, **18**, **20**) together with the crude extracts were screened for their anti-proliferative potential against four US National Cancer Institute (NCI) recognized human cancer cell lines, namely lung carcinoma (A549), breast carcinoma (estrogen receptor positive: MCF-7 and estrogen receptor negative: MDA-MB-231) and colon carcinoma (HCT-116) cell lines, in addition to one non-cancer variant, i.e., human lung fibroblast (MRC-5).

4.2 Anti-proliferative activity of crude extracts and the selected isolated compounds

The anti-proliferative potential of the selected compounds and crude extracts were evaluated using the Neutral Red uptake (NR) assay. The NR assay measures lysosomal uptake and accumulation of NR dyes in the viable and uninjured cells. Since the amount of retained dye is proportional to the number of viable cells, it is thus possible to quantitate cell viability and can be used to measure cytostatic effects and cell death.[188]

The anti-proliferative effects were measured in terms of IC_{50}, which denotes the concentration required to reduce cell viability by 50% as compared to the control. IC_{50} values are extracted from concentration-response curves by linear interpolation.[189] Based on the NCI guidelines, a crude extract is considered to have *in vitro* anti-proliferative activity if the IC_{50} value in cancer cells following treatment between 48-72

hours is ≤ 20 µg/mL, while for a pure compound, the IC_{50} value should be ≤ 4 µg/mL to be considered active.[190] Selectivity of a particular compound can be evaluated based on the calculated selectivity index (SI) which is defined as the ratio of cytotoxicity on non-cancer cells to cancer cells. Samples with SI values > 3 is considered to be highly selective towards cancer cells.[191] For ease of comparison of activity amongst the tested compounds within this study, IC_{50} values were categorized as active, moderately active and inactive according to Figure 4.1.

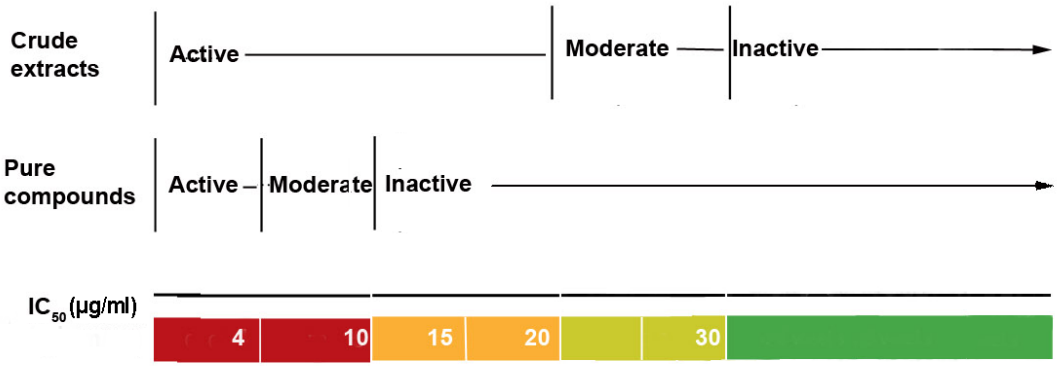

Figure 4.1: Classification of anti-proliferative activity based on IC_{50} (µg/mL) concentration. (Information adapted from Boik, J., 2001[190])

The anti-proliferative activities of the crude extracts and the selected compounds are summarized in Tables 4.1 and 4.2. The most promising anti-proliferative activity was found to be the crude alkaloidal mixture of the *Ficus* species with IC_{50} values < 1.5 µg/mL across all the tested cell lines (Table 4.1). Hispiloscine **(2)**, obtained as a new alkaloid from the leaves of *F. hispida*, showed profound anti-proliferative activities against all the tested cancer cell lines with IC_{50} values ranging from 0.13 to 1.21 µg/mL. Although hispiloscine **(2)** also seemed to affect the non-cancer cell line MRC-5, the SI values calculated were all above 3, with the exception towards MDA-MB-231, indicating that the anti-proliferative activity of **2** is selective towards certain cancer cell

lines. The bark of *F. hispida* on the other hand yielded a new lignan-alkaloid, hispidacine **(1)**, which essentially did not show any anti-proliferative activity against the cancer cell lines tested (IC_{50} > 10 μg/mL). Although found to be inactive for anti-proliferative activity, **1** have been reported to induce moderate vasorelaxant activity in rat isolated aorta.[127]

The leaves and bark of *Ficus fistulosa* yielded two new septicine-like alkaloids, fistulopsines A and B (**4** and **5**), a known alkaloid 13a(*R*)-(-)-3,6-didemethylisotylocrebrine **(6)**, and a non-alkaloid vomifoliol **(10)**. Fistulopsine A **(4)** showed potent anti-proliferative activity against MCF-7 and HCT-116 cell lines ($IC_{50} \leq$ 4 μg/mL) and moderate anti-proliferative activity against A549 and MDA-MB-231 cell lines. Among these compounds, SI indices showed that the anti-proliferative activity of 4 was selective towards cancer cells with SI values ranging from 3.5 to 7.4 (Table 4.1). Fistulopsine B **(5)** also exerted anti-proliferative activity and selectivity towards MCF-7 and HCT-116 cell lines. However, the potency of **5** can be considered only as moderately active as the IC_{50} values for all tested cell lines were ranged between 4.70 to 8.54 μg/mL. On the other hand, **6** was shown to be active as an anti-proliferative agent with IC_{50} values in the nanogram range where it is the most potent and selective towards MCF-7 and HCT-116 cell lines. In contrast to the alkaloids, vomifoliol **(10)** was shown to have poor cytotoxic activity with IC_{50} values above the treatment range of 50 μg/mL. The two new lignan alkaloids, schwarzinicines A and B (**11** and **12**), obtained from the leaves of *F. schwarzii* were also shown to be inactive towards all the cancer cell lines tested.

The potency of the *Ficus* plant extracts and the isolated compounds observed in the present study is in agreement with literature which states that *Ficus* plants are highly cytotoxic. The *Ficus* genus have been highly appraised for its efficacy in anti-cancer research where some of the most promising cytotoxic compounds in *Ficus* plants

include triterpenoids and phenanthroindolizidine alkaloids.[18,19,123] The bioactivity of phenanthroindolizidines has been linked to its substitution nature and pattern of on the phenanthrene ring.[106] The pronounced cytotoxic activity shown by hispiloscine (**2**) and (-)-3,6-didemethylisotylocrebrine **(6)** compared to fistulopsines A **(4)** and B **(5)** (septicine-like alkaloids), provided further support that a rigid phenanthrene structure favours higher cytotoxicity.[39] The rigid phenanthrene structure is essentially lost in the structures of **4** and **5** due to the disconnection between C-4a in ring A and C-4b in ring C. A similar case was encountered previously which showed that septicine **(9)** exhibited less profound anti-cancer activity compared to its phenanthrene analogue, tylophorine **(8)**, despite their overall structural similarities.[42,146]

Biological studies have suggested that some flavonoids possess anti-tumour properties which somewhat justifies the use of flavonoid-rich plants in traditional medicine. Many phenolic compounds including flavonoids have been isolated from various plants including the *Artocarpus* and *Macaranga* genus. In the present study, three flavonoid aglycones, namely, cudraflavone C **(13)**, cycloheterophyllin **(15)** and artonin J **(16)** obtained from the bark of *A. heterophyllus x integer* and two flavonoid glycosides, namely, quercetin-3-*O*-*α*-L-arabinopyranoside **(18)** and quercetin-3-*O*-*β*-D-galactoside **(20)**, which were isolated from the leaves of *M. hypoleuca* were evaluated for anti-proliferative activity. Both flavonoid glycosides were found to be inactive against all the cell lines tested.

It is noteworthy that the crude extract of the hybrid species, *A. heterophyllus x integer*, showed inactive for anti-proliferative activity against the tested cancer cell lines (Table 4.2) (IC_{50} > 100 μg/mL). This was rather unexpected considering the fact that not only that the two parent species, namely, *A. heterophyllus* and *A. integer*, were shown to individually possess anti-proliferative property in the present study (Appendix 2), but phytochemical screening also revealed a higher flavonoid content in the hybrid

species as compared to its parent plants (Appendix 1). It was presumed that flavonoids are the agents responsible for the observed anti-proliferative activity for the crude extracts of *Artocarpus* plants. Therefore having a crude extract of the hybrid plant that is more flavonoid-rich but possesses no cytotoxic effect is indeed rather surprising. Nonetheless, following repeated chromatographic separation, the crude extract of the hybrid species yielded three prenylflavonoids, cudraflavone C **(13)**, cycloheterophyllin **(15)** and artonin J **(16)**, which were shown to possess improved anti-proliferative activity as compared to the crude extract (Tables 4.1 and 4.2). This observation could potentially be due to the presence of other secondary metabolites present within the extract that might have caused antagonistic interactions with the biologically active flavonoids. For instance, unwanted interactions due to tannins within a herbal concoction were previously found to hinder absorption of active constituents, thus affecting the overall bioavailability and resulting in a negative impact on the therapeutic effect.[192]

Of the three prenylflavonoids tested, **13** showed the most potent activity (IC_{50} values range from 2.80 – 4.15 μg/mL, followed by **15** (IC_{50} values range from 8.85 – 25.6 μg/mL) while **16** is essentially inactive. Although cudraflavone C **(13)** seems to possess appreciable cytotoxicity, the SI values calculated show **13** to be a non-selective anti-proliferative agent based on the four cancer cell lines and the non-cancerous MRC-5 cell line tested. Previously, **13** have also been found to show cytotoxicity against hepatocellular carcinoma (SMMC-7721), gastric carcinoma (BGC-823 and SGC-7901) and B-16 melanoma carcinoma cell lines.[55,193] The anti-proliferative activities shown by flavonoids **13**, **15** and **16** broadly confirm the SAR proposed by Arung et al., [55] which suggested the importance of the prenyl side chain at C-3 for activity. The presence of an intact prenyl side chain at C-3 in **13** is consistent with its superior anti-proliferative

activity compared to **15** and **16**, in which the prenyl side chains at C-3 are part of the pyranoflavone and furanoxanthone ring systems, respectively.

The crude extract of *M. hypoleuca* showed weak anti-proliferative activity against MCF-7 and A549, while the two quercetin-3-*O*-*α*-L-arabinopyranoside **(18)** and quercetin-3-*O*-*β*-D-galactoside **(20)** tested are devoid of anti-proliferative activity against all the tested cell lines. The lack of activity for both **18** and **20** can be attributed to the presence of the sugar substituents in the molecules where the sugar moieties were believed to have significantly reduced the hydrophobicity of the molecules and hence reduce their ability to permeate through the cellular membrane.[91,107] Therefore, it can be assumed that the growth inhibition observed for the crude extract was not due to flavonoid glycosides but the cumulative effects of the aglycones, such as quercetin and kaempherol, present within the extract of *M. hypoleuca*.

Overall, this screening effort has identified three phenanthroindolizidine alkaloids (**4**, **5** and **6**) and flavonoid **13** to be most potent in cancer cell growth inhibition among the tested compounds. These compounds were generally found to be especially active towards MCF-7 and HCT-116 cell lines and were therefore selected for further apoptotic study using these two cell lines the two most succeptible cell lines, MCF-7 and HCT-116.

Table 4.1: Anti-proliferative activity of selected isolated pure compounds using the NR uptake assay against selected cancer cell lines.

Compounds	Mean IC_{50} values (µg/mL)				
	A549	MCF-7	MDA-MB-231	HCT 116	MRC-5
1	37.30 ± 5.28	24.70 ± 0.46	41.00 ± 3.75	12.20 ± 1.50	-
2	**0.45 ± 0.03 (3.0)**	**0.18 ± 0.01 (6.9)**	**1.15 ± 0.01 (1.0)**	**0.13 ± 0.02 (9.6)**	**1.21 ± 0.28**
4	**7.39 ± 0.58 (8.0)**	**3.69 ± 0.45 (4.5)**	**4.62 ± 1.59 (3.6)**	**3.46 ± 0.35 (4.8)**	16.5 ± 5.37
5	**7.33 ± 0.59 (2.9)**	**5.27 ± 0.68 (4.1)**	**8.54 ±0.52 (2.8)**	**4.70 ± 0.67 (4.6)**	16.3 ± 3.96
6	**0.056 ± 0.003 (0.7)**	**0.0003 ± 0.0001 (190)**	**0.015 ± 0.003 (2.6)**	**0.006 ± 0.001 (6.3)**	**0.038 ± 0.008**
10	> 50.0	> 50.0	> 50.0	25.20 ± 6.42	-
11	> 50.0	33.80 ± 3.85	29.60 ± 5.71	25.20 ± 2.74	-
12	> 50.0	> 50.0	25.20 ± 6.48	> 50.0	-
13	**3.76 ± 0.15 (0.7)**	**2.80 ± 0.13 (0.9)**	**4.15 ± 0.16 (0.7)**	**3.68 ± 0.84 (0.7)**	**2.70 ± 0.28**
15	18.60 ± 5.04	20.40 ± 0.34	25.60 ± 4.89	**8.85 ± 0.40**	-
16	> 50.0	> 50.0	> 50.0	> 50.0	-
18	> 50.0	> 50.0	> 50.0	Nil	-
20	> 50.0	> 50.0	> 50.0	Nil	-
Vinblastine (positive control)	**0.009 ± 0.001 (229)**	**0.0010 ± 0.0001 (206)**	**0.0010 ± 0.0001 (206)**	**(0.400 ± 0.003) x 10^{-5} (515000)**	**2.070 ± 0.800**

Nil: no inhibition; Selectivity index (SI) value indicated in brackets. Data represents mean IC_{50} values ± SE, n = 3 and selectivity index (SI) where applicable. Bold values indicate isolated pure compound with good – moderate potency which conforms to NCI guidelines as shown in Figure 4.1.

Table 4.2: Anti-proliferative activity of crude extracts using the NR uptake assay against selected cancer cell lines.

Plant extracts	Mean IC_{50} values (µg/mL)			
	A549	MCF-7	MDA-MB-231	HCT 116
A. heterophyllus x integer (Bark)	279.0 ± 68.7	471.0 ± 3.5	841.0 ± 193.0	186.0 ± 7.4
M. hypoleuca (Leaves)	30.05 ± 4.81	**14.40 ± 2.78**	92.30 ± 6.89	**36.20 ± 2.67**
F.fistulosa (Leaves)	**0.025 ± 0.003**	**0.012 ± 0.002**	**0.161 ± 0.05**	**0.007 ± 0.002**
F. fistulosa (Bark)	**0.060 ± 0.010**	**0.033 ± 0.006**	**1.410 ± 0.089**	**0.027 ± 0.006**
F. hispida (Leaves)	**0.047 ± 0.003**	**0.003 ± 0.001**	**0.168 ± 0.032**	**0.011 ± 0.004**
F. hispida (Bark)	**0.047 ± 0.003**	**0.003 ± 0.001**	**0.167 ± 0.033**	**0.010 ± 0.003**
F. schwarzii (Leaves)	**0.297 ± 0.085**	**5.270 ± 3.500**	**0.060 ± 0.014**	**0.051 ± 0.001**

Data represents mean IC_{50} values ± SE, $n = 3$. Bold values indicate crude extracts with good – moderate potency which conforms to NCI guidelines as shown in Figure 4.1.

4.3 Morphological observation of apoptosis

Apoptosis is an ordered and orchestrated cellular process that occurs in physiological and pathological conditions. It is one of the most studied topics among cell biologists. In this study, the anti-proliferative effect evaluated by the NR assay in the previous section, showed concentration dependent growth inhibition with treatment of the active compounds (Table 4.1, Appendices 71-72). On the basis of these data, morphological observation of the cellular nuclei was carried out to determine if the growth inhibitory effects upon treatment with the active compounds, i.e., **4**, **5**, **6** and **13**, were associated with apoptosis.

The induction of apoptosis was determined by acridine orange-ethidium bromide (AO/EB) double staining of untreated cells (control) and cells treated with the four selected active compounds for 24 hours. AO/EB double staining can distinguish apoptotic cells from viable and necrotic cells on the basis of membrane integrity. Acridine orange permeates through the cell membrane and emits a green fluorescence when intercalated with cellular DNA in viable cells, while ethidium bromide is only taken up by necrotic cells with compromised membrane integrity, which then emits a red fluorescence. Therefore, viable cells will appear uniformly dull green, while the onset of apoptosis is indicated by the presence of bright green spots in cells due to morphological changes such as nuclear condensation and fragmentation.[194,195] On the other hand, necrotic cells will have uniform red or orange nucleus morphology.[194,195] Other morphological hallmarks that can be observed which are associated with apoptosis include cell shrinkage, membrane blebbing and disassembly of apoptotic bodies.[194,196]

HCT-116 and MCF-7 cells were treated with compounds **4**, **5, 6** and **13** at two concentrations, namely, IC_{50} and 2 x IC_{50} (Table 5.3), for 24 hours to determine if these

compounds induced apoptosis compared to the untreated cells. Cells treated with vinblastine were used as a positive control. Vinblastine was selected as a suitable control because it is an anti-cancer drug derived from plant alkaloid and is well documented for its cytotoxic activity.

Upon observation, chromatin condensation and membrane blebbing was seen in HCT-116 treated population among viable cells (Figures 4.2 - 4.5a,b). Similarly was observed in MCF-7 treated cells however, without the occurrence of membrane blebbing (Figures 4.2 – 4.4d,e). Although these are notable characteristics of apoptosis, cells treated with **4**, **5** and **6** did not show a stark contrast when compared to the control population, with only a minute number of treated cells expressing such traits. Higher treatment concentrations (2 x IC_{50}) with these compounds did show more cells displaying apoptotic changes however, the emergence of cells undergoing necrosis was also observed among the treated populations. Although unfavorable, literature states that apoptosis and necrosis may coexist depending on the concentration of the anti-cancer agents, where lower and higher concentrations induce apoptosis and necrosis, respectively.[197] Similar biphasic response was also reported in prominent anti-cancer drugs such as Taxol® (paclitaxel).[198] This is in contrast to HCT-116 and MCF-7 cells treated with **13** where chromatin condensation was clearly observable in cells treated at IC_{50} concentrations and 2 x IC_{50} without the presence of necrotic cells.

Although observations resembling the presence of apoptotic characteristic such as chromosome condensation and membrane blebbing were made, the amount of cells exhibiting these changes were not substantial when compared to the control. Therefore, the induction of apoptosis by compounds **4**, **5** and **6** were not conclusive. Furthermore, the lack of apoptotic bodies which are the end product and the concluding factor of apoptosis are not present within the treated population renders the induction of apoptosis by compounds **4**, **5** and **6** ambiguous. Moreover, literature suggests that the

induction of apoptosis may not necessarily be the primary mode of growth inhibition for compounds **4**, **5** and **6** as phenanthroindolizidines have been reported to be generally non-apoptotic.[116,199] This comes to suggest of the possibility of non-apoptotic chromosome condensation[200] and membrane blebbing[201] as a result of stress-induced response.

In regards to **13**, apoptotic bodies were also not observed however, AO/EB staining showed strong characteristics of chomatin condensation and membrane blebbing (HCT-116 cells) almost comparable to apoptotic changes seen on vinblastine treated cells. The absence of apoptotic bodies in cells treated with **13** could be due to insufficient treatment time for the completion of the apoptotic process. Figure 4.5b shows membrane blebs packed with condensed chromatin (seen as bright green) ready to be disposed, which may later appear as apoptotic bodies. This is not the argument for cells treated with **4**, **5** and **6** because of the emergence of necrotic cells even at 24 hours treatment.

Out of the four tested compounds, **13** appears to be the best potential as an apoptotic agent as literature have acknowledged flavonoids for their anti-cancer activities through the induction of apoptosis.[112,120–122] Further assessment of apoptosis is needed to confirm the induction of apoptosis by **13** and to determine if the apoptotic traits observed is indeed apoptotic related.

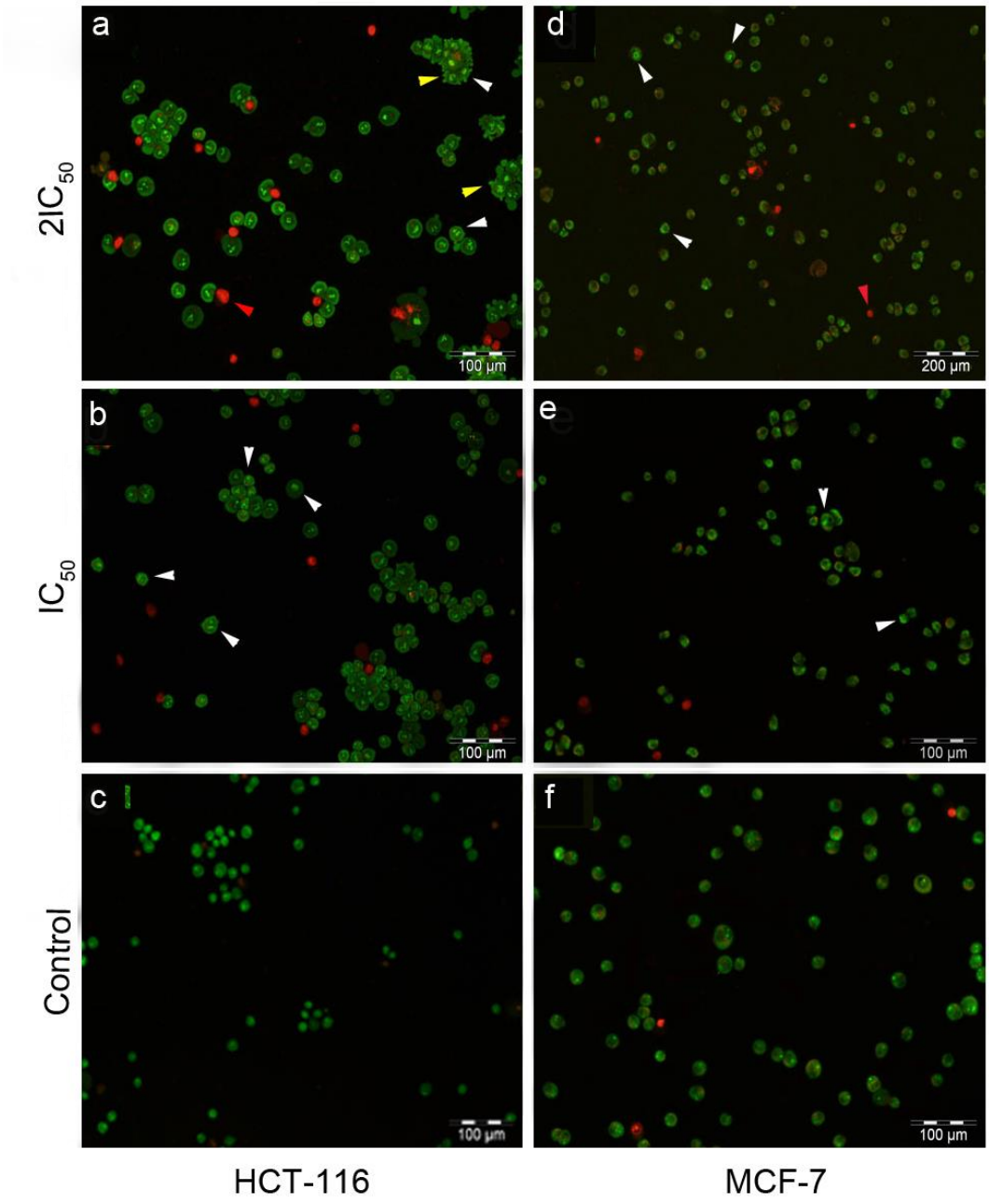

Figure 4.2: Morphological observation with AO/EB double staining by flourescence microscope (200 x) of control cells and cells treated with fistulopsine A (4) for 24 hours. Cells showing condensed chromatin, membrane blebbing and necrosis within the observed population are indicated by white, yellow and red arrowheads, respectively. Images are representative of one of three similar experiments. Chromatin condensation and membrane blebbing at higher magnification are shown in Appendix 73.

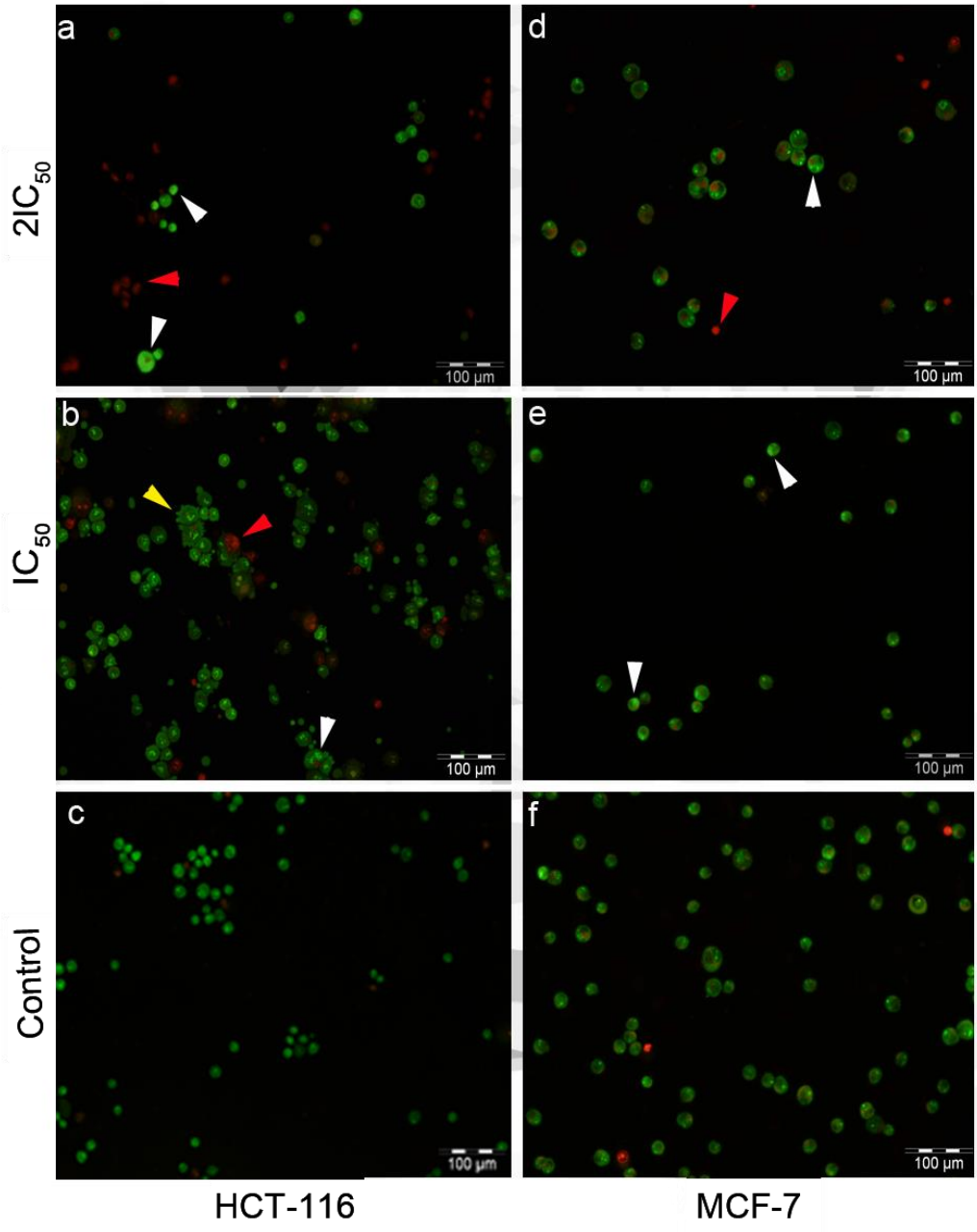

Figure 4.3: Morphological observation with AO/EB double staining by fluorescence microscope (200 x) of control cells and cells treated with fistulopsine B (5) for 24 hours. Cells showing condensed chromatin, membrane blebbing and necrosis within the observed population are indicated by white, yellow and red arrowheads, respectively. Images are representative of one of three similar experiments. Chromatin condensation and membrane blebbing at higher magnification are shown in Appendix 74.

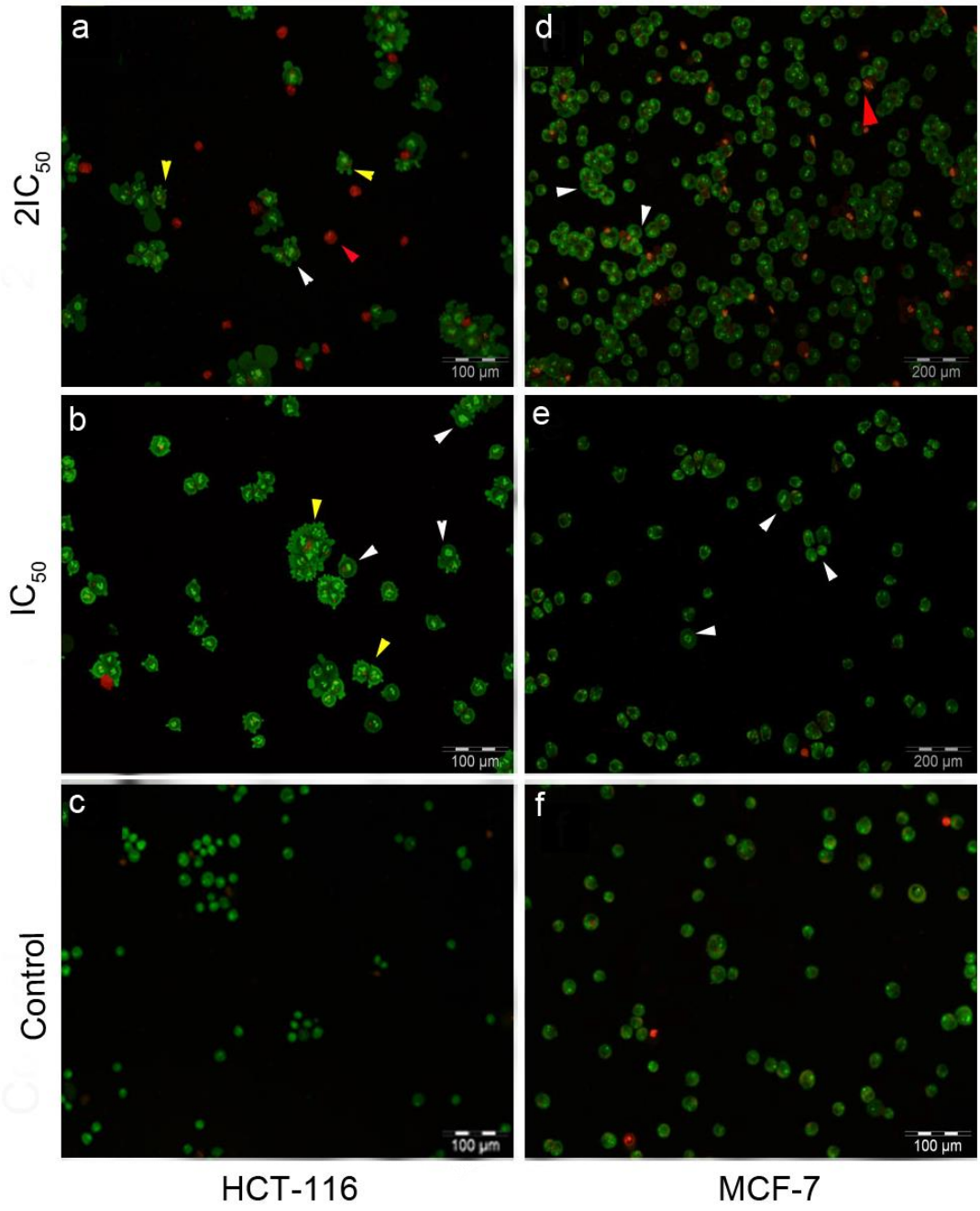

Figure 4.4: Morphological observation with AO/EB double staining by fluorescence microscope (200 x) of control cells and cells treated with 13a(*R*)-(-)-3,6-didemethylisotylocrebrine (6) for 24 hours. Cells showing condensed chromatin, membrane blebbing and necrosis within the observed population are indicated by white, yellow and red arrowheads, respectively. Images are representative of one of three similar experiments. Chromatin condensation and membrane blebbing at higher magnification are shown in Appendix 75.

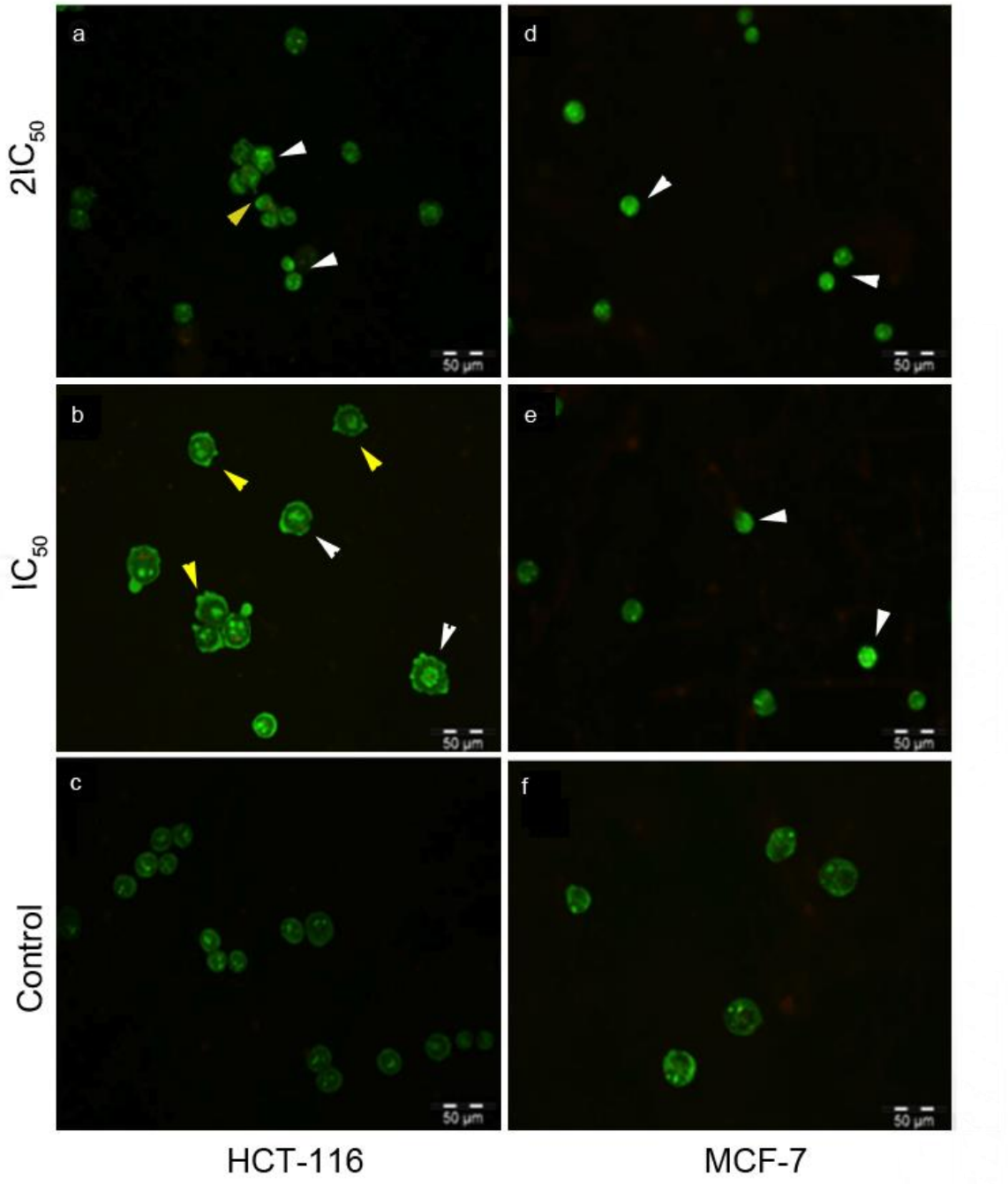

Figure 4.5: Morphological observation with AO/EB double staining by fluorescence microscope (200 x) of control cells and cells treated with cudraflavone C (13) for 24 hours. Cells showing condensed chromatin, membrane blebbing and necrosis within the observed population are indicated by white, yellow and red arrowheads, respectively. Images are representative of one of three similar experiments. Population of cells showing chromatin condensation and membrane blebbing in different viewing fields are shown in Appendix 76.

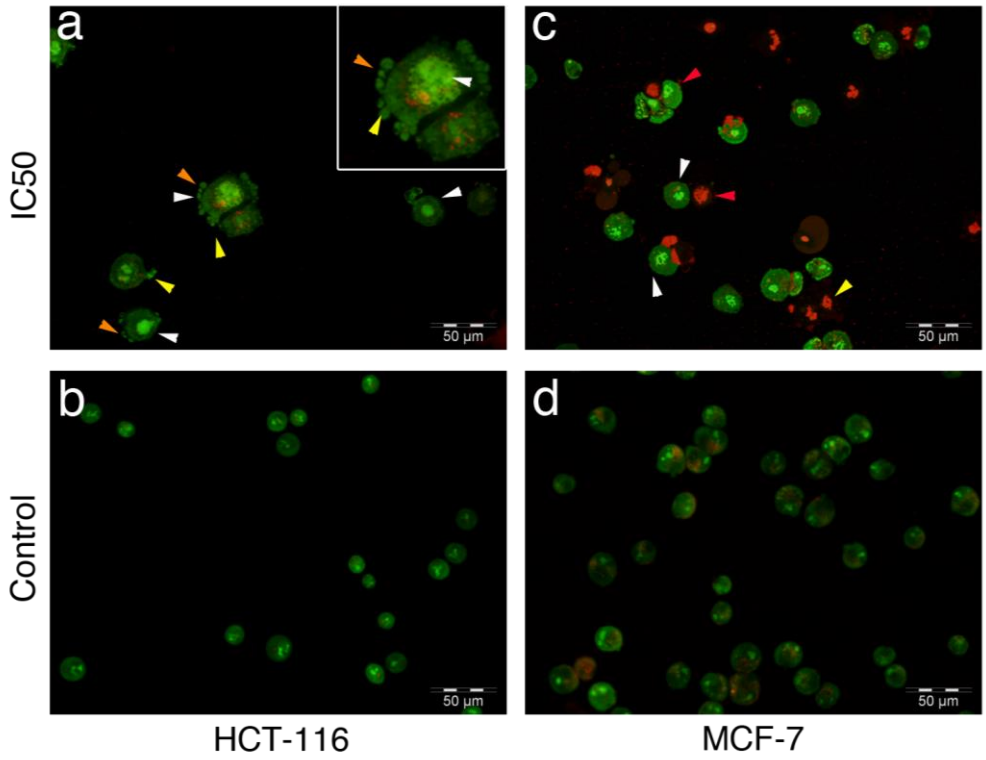

Figure 4.6: Morphological observation with AO/EB double staining by fluorescence microscope (200 x) of control cells and cells treated with vinblastine for 24 hours. Cells showing condensed chromatin, membrane blebbing, apoptotic bodies and necrosis are indicated by white, yellow, brown and red arrowheads, respectively. (a) Inset shows digital magnification of apoptotic features indicated by respective colored arrows. Images are representative of one of three similar experiments.

4.4 Cell cycle analysis

The cell cycle is a series of events that takes place in a cell leading to its division and duplication. The cell cycle consists of four phases: G1, S, G2 and M and is mediated by growth factors (Figure 4.7). Progression through the cell cycle involves checkpoint pathways that monitor for DNA damage (G1, S and G2 checkpoints), proper chromosome replication (G2 checkpoint) and chromosome attachment to the spindle (M checkpoint, between metaphase and anaphase), transiently halting progression through the cell cycle at various points if conditions are not suitable for continuing. The driving force for ongoing proliferation can be traced to defective cell cycle control in cancer cells, largely by excessive production of growth factor signaling components coupled by the loss of restriction point control and failures in checkpoint pathway[202]

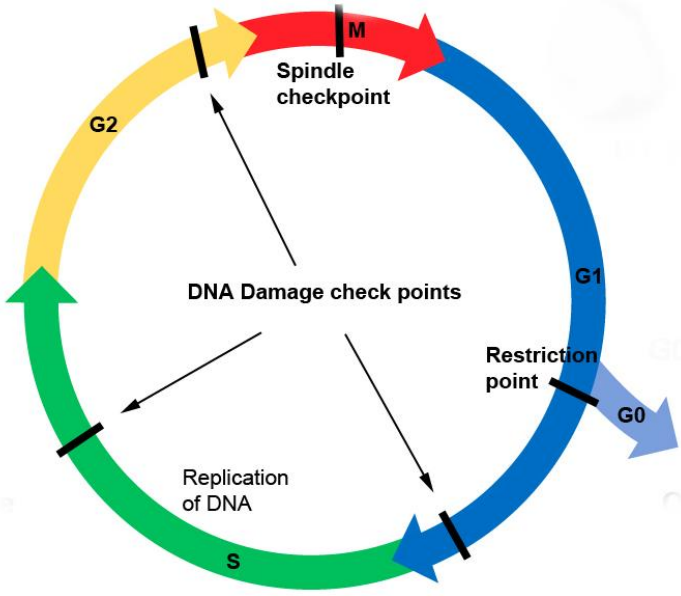

Figure 4.7: Cell cycle phases and checkpoints.
(Diagram adapted from Kleinsmith, L. J. 2005[202])

The analysis of different phases in the cell cycle was made possible by using flow cytometry. This approach of analysis of cellular DNA content following staining with intercalating DNA dye such as propidium iodide (PI), which fluoresces when

bound to DNA, reveals distribution of cells in three major phases of the cell cycle (G1 *vs* S *vs* G2/M). This is under the assumption that the DNA content of an individual cell is proportional to the fluorescence intensity of the excited PI (blue laser 488 nm). All cells in G1 have uniform DNA content, as do cells in G2/M where the latter is described as having twice the normal G1 DNA content. Apoptotic cells are also detected with its fractional DNA content (fragmented low MW DNA) represented on the histogram by "sub-G1" peak. A histogram of DNA content of cells in a population can be used to derive the percentage of cells in each phase of the cell cycle and any perturbation caused by the test compounds.

Due to time constrain, cell cycle analysis was focused on novel compounds fistulopsines A **(4)** and B **(5)**. Herein, cell cycle perturbation of the two novel phenanthroindolizidine alkaloids, fistulopsines A **(4)** and B **(5)**, were studied by flow cytometry on HCT-116 and MCF-7 cell lines following treatment at approximate IC_{50} concentration (Table 5.3) of these compounds at 24, 48 and 72 hours. Figures 4.8 and 4.9 show the effects of **4** and **5** on the cell cycle of the two cell lines. As shown in Figures 4.8 and 4.9, the treatment with **4** and **5** for 24, 48, and 72 hours resulted in significant increase of cells in the G1 phase of the cell cycle, accompanied by reduction of cells in the S and G2/M phases of the cell cycle in both cell lines. Taken together, these data suggest that the induction of G1 arrest in HCT-116 and MCF-7 cells by **4** and **5** might be responsible for cell growth inhibition.[116] Cell cycle arrest at G1 is commonly associated with the modulation of multiple cell cycle regulatory proteins. Among the regulatory proteins which is associated with G1 arrest is the downregulation of CDK2, CDK4 and CDK6, cyclins D1 and D2, and the upregulation of CDK inhibitors p21 and p27.[116,203–205]

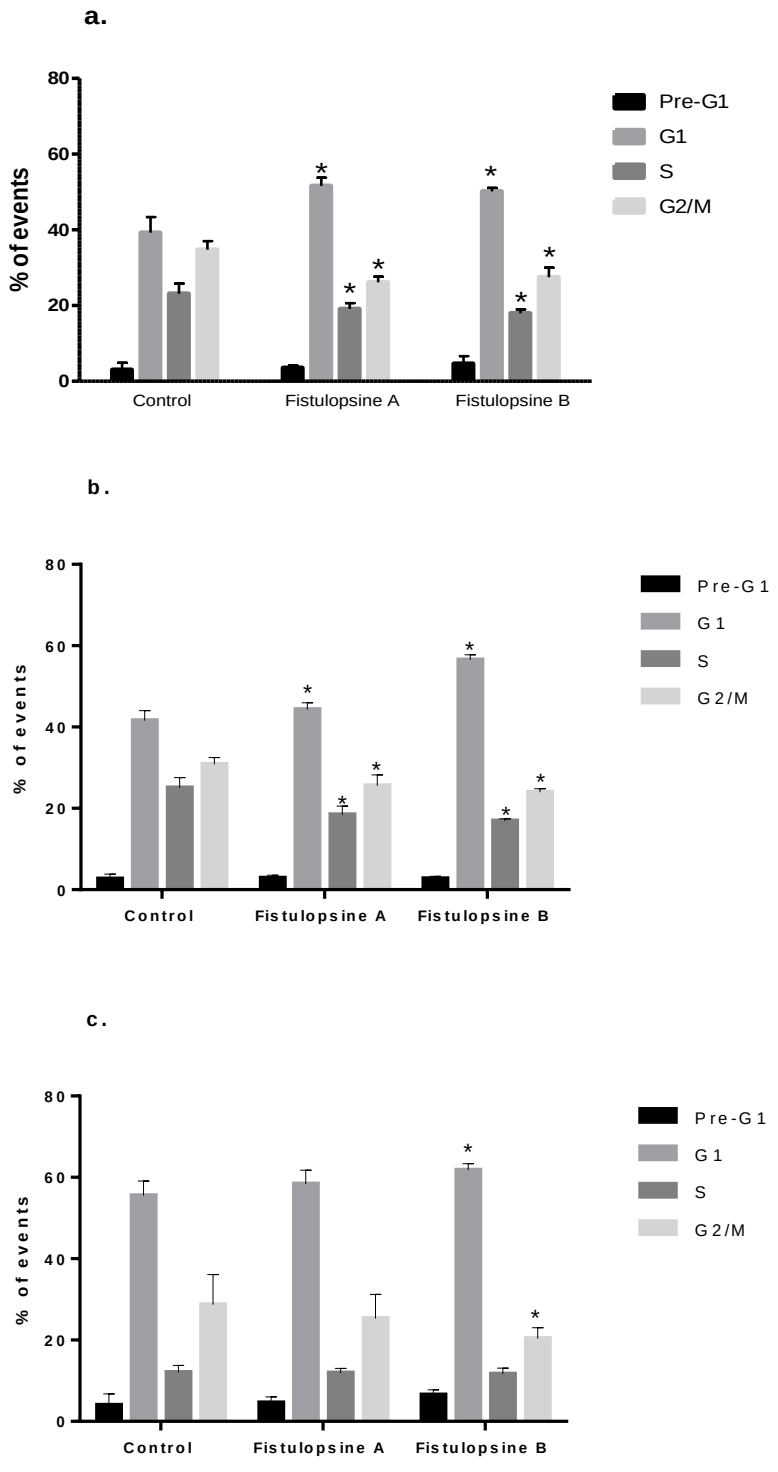

Figure 4.8: Effects of fistulopsines A **(4)** and B **(5)** at IC_{50} concentration on the cell cycle of HCT-116 cells after 24 (a), 48 (b) and 72 (c) hours treatment. Data are representative of three experiments. Significant differences were compared between control and treated cells - asterisk indicates significant ($p<0.05$) increase or decrease in events with respect to control (Appendix 77 and 78).

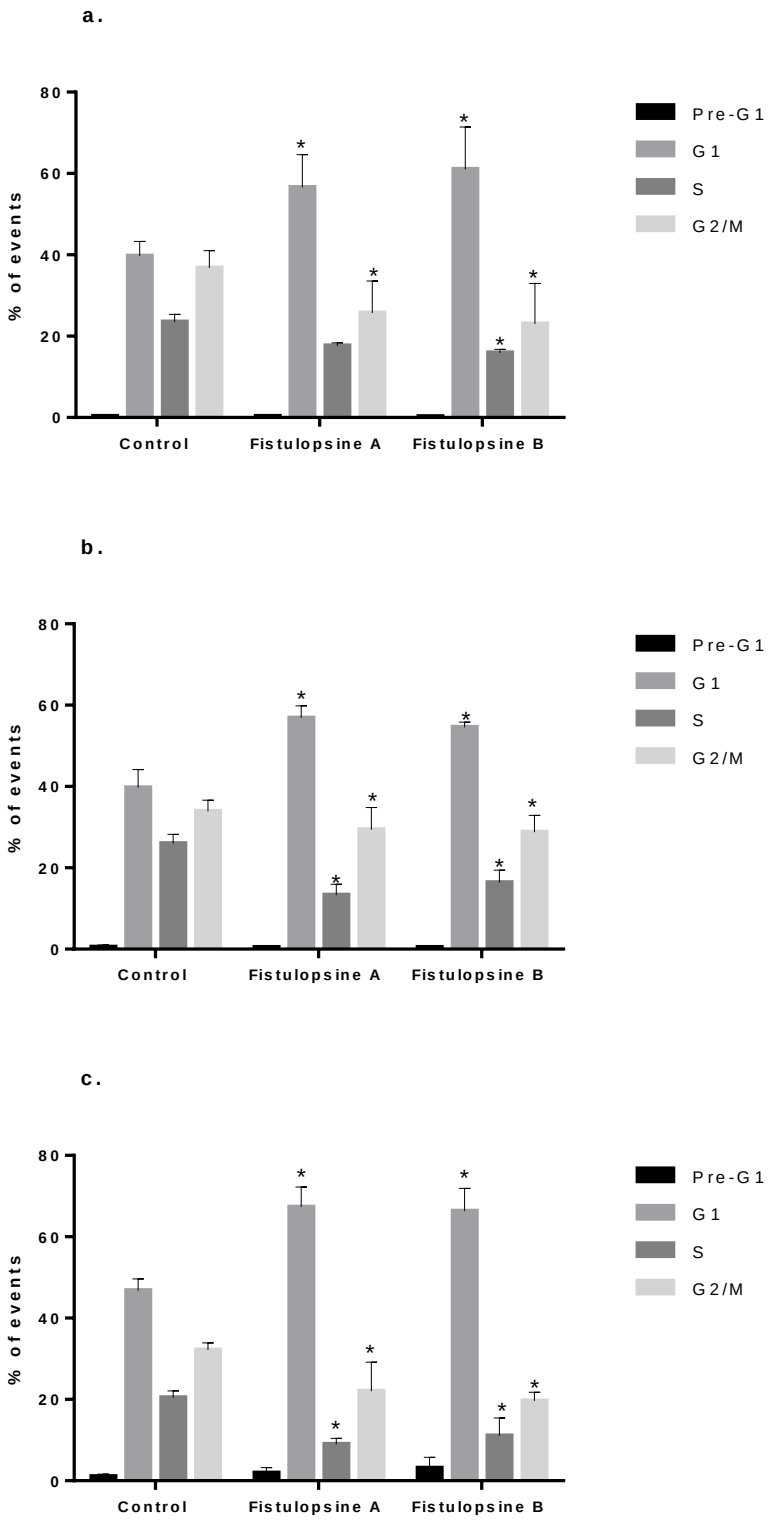

Figure 4.9: Effects of fistulopsines A **(4)** and B **(5)** at IC_{50} concentration on the cell cycle of MCF-7 cells after 24 (a), 48 (b) and 72 (c) hours treatment. Data are representative of three experiments. Significant differences were compared between control and treated cells - asterisk indicates significant ($p<0.05$) increase or decrease in events with respect to control (Appendix 77 and 79).

Additionally, HCT-116 showed trends of recovery from the G1 arrest induced by fistulopsine A **(4)** (Figure 4.8c) at 72h where the treated cells did not show any significant difference in cell population as compared to the control. At the same time point, HCT- 116 cells treated with fistulopsine B **(5)** still showed significant increase in G1 cell population. However, the reduction in S phase cell population was no longer significant hence suggesting that the onset of recovery from the G1 arrest is underway (Figure 4.8c). Literature states that this observation could be attributed to the decrease in intracellular drug accumulation and/or loss of cell sensitivity.[206] A higher concentration of **4** and **5** could circumvent this problem and prevent recovery at least for the 72 hour time exposure.

It was also interesting to note that the two cell lines did not exhibit significant accumulation of pre-G1 events, which is indicative of apoptosis. These results are in agreement with those obtained from the AO/EB double staining which did not show the presence of apoptotic bodies among the observed cell population as a conclusive indicator of apoptosis. Furthermore, the findings of this study is supported by previous studies on structurally similar compounds such as tylophorine **(8)**[116] and antofine **(50)**[199] which rendered this class of compounds as generally non-apoptotic.

Taken together, the NR results from this study found that phenanthroindolizidine alkaloids **4** and **5** are growth inhibitory agents. Growth inhibition may be cytostatic or cytotoxic through apoptosis or necrosis. Although morphological observation for apoptosis by AO/EB staining showed signs of chromosome condensation and membrane blebbing, the lack of apoptotic bodies among the observed population rendered the induction of apoptosis by **4** and **5** as inconclusive. It is however apparent that these compounds induced their growth inhibitory effect through cytostasis by G1 phase arrest in the cell cycle.

Majority of the genetic mutation in cancers involve genes that regulate progression through G1 phase in the cell cycle.[207,208] Key regulators for progression through G1 to S phase are cyclins D and E. The roles in which these proteins play in regulating the transition of cells throughout the G1/S phase is shown in Figure 4.10

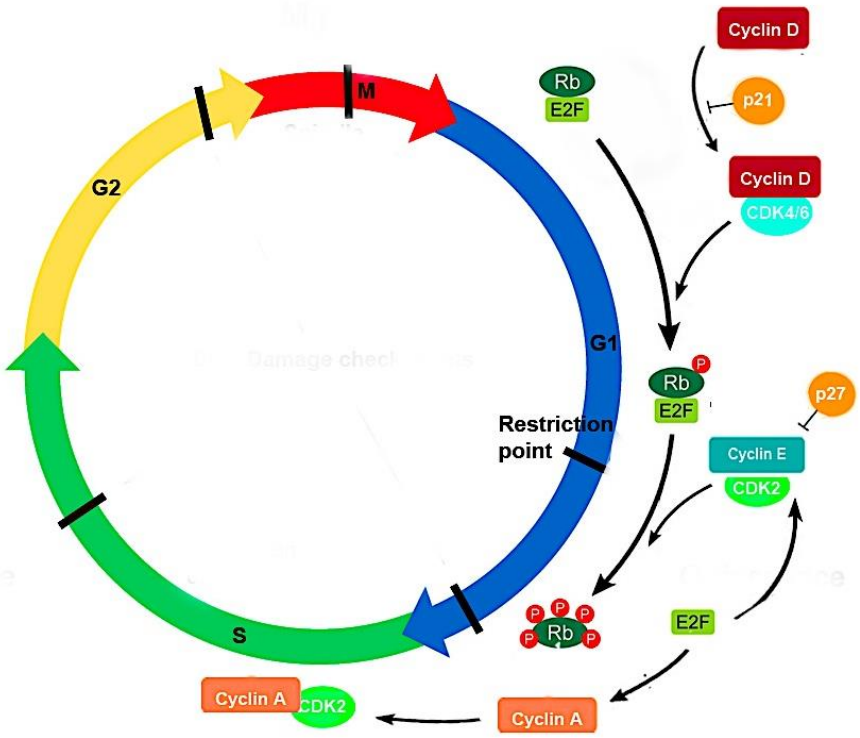

Figure 4.10: Regulation of G1 cell cycle progression.
(Diagram adapted from Kleinsmith, L. J., 2005[202] and Foster, D. A. *et al.*, 2010[207])

G1 cell cycle progression is triggered by the coupling of Cyclin D with CDK4 or CDK6 and cyclin E with CDK2 to form complexes which initiate the phosphorylation of retinoblastoma tumor suppressor protein (Rb) to its hyperphosphorylated state.[208] Prior to this, Rb in its unphosphorylated form is associated with transcription factor, E2F to form a Rb-E2F complex which keeps E2F in an inactive state.[207] When Rb is hyperphosporylated, E2F disassociates from Rb and is able to activate genes that are necessary for progression into the S phase.[207] Among the

genes activated by E2F include cyclin E[209], which generates a positive feedback loop allowing cells to move past the G1 restriction point and simultaneously increasing the production of cyclin A2[210,211] which facilitates the transition of cells from G2 to M phase in the cell cycle. Cell cycle progression can be inhibited by cyclin-dependent kinase inhibitors (CKIs) such as p21[212] and p27[213] which are involved in cell cycle arrest at G1 phase.

As in the case of compounds **4** and **5**, tylophorine **(8)** was previously found to induce G1 arrest in HepG2, HONE-1 and NUGC-3 carcinoma cells, which was linked to the suppression of cyclin A2 expression.[116] Therefore, given that compounds **4**, **5** and **8** share structural similarities, it is possible that compounds **4** and **5** exhibit its G1 phase arrest in a similar manner as **8**. Therefore, the effect of compounds **4** and **5** on CKIs, cyclins D and E, CDKs 2, 4, or 6, which may eventually lead to the downregulation of cyclin A2 and G1 phase arrest cannot be ruled out.

Chapter 5: Experimental

5.1 General experimental procedures

Melting points were determined on a Stuart SMP-10 melting point apparatus and were uncorrected. Optical rotations were determined on a JASCO P-1020 automatic digital polarimeter. IR spectra were recorded on a Perkin Elmer Spectrum RX1 FT-IR Spectrophotometer. UV spectra were obtained on a GE Ultrospec 8000 spectrophotometer. CD spectra were obtained on a J-815 Circular Dichroism Spectrometer. ^{1}H and ^{13}C NMR spectra were recorded in $CDCl_3$ or acetone-d_6 using TMS as internal standard on a JEOL JNL-LA400, JNM-ECA 400 or Bruker Avance III 400 spectrometers, at 400 and 100 Hz, respectively or on a Bruker Avane III 600 spectrometer at 600 and 150 MHz, respectively. Coupling constants (*J*) were reported in Hz and chemical shifts (δ) in ppm. X-ray diffraction analysis was carried out on a Bruker SMART APEX II CCD area detector system equipped with a graphite monochromator and a Mo Kα fine-focus sealed tube (λ=0.71703 Å), at 100K. The structure was solved by direct methods (SHELXS-97) and redefined with full-matrix least-squares on F^2 (SHELXL-97). ESIMS and HRESIMS were obtained on an Agilent 6530 Q-TOF mass spectrometer. Fluorescent microscopic images were viewed using Nikon Eclipse 80i (Nikon, NY). NMR, X-ray diffraction, ESIMS and HRESIMS was carried out by collaborators at the Chemistry Department of University Malaya under the supervision of Prof. T. S. Kam.

5.2 Chromatographic methods

5.2.1 Column chromatography

Column chromatography was performed using silica gel 60 (Merck 9385, 230-400 mesh) unless otherwise stated. The weight ratio of silica gel to sample was approximately 30:1 for crude samples. The gel was made into slurry with the eluting solvent system before being packed into a glass column. In separations by size exclusion, LH-20 sephadex gel was soaked in MeOH overnight to allow the gel to expand prior to column packing. Fractions collected were monitored by TLC and similar fractions were combined and subjected to further separation by column or preparative centrifugal thin layer chromatography where needed.

5.2.2 Thin layer chromatography (TLC)

TLC was used for detection and monitoring of targeted flavonoids and alkaloids in the crude extracts and fractions. The samples were loaded on to a TLC aluminum sheet pre-coated with silica gel 60 F_{254} 0.20 mm thickness and developed in saturated chromatographic chambers with appropriate solvent systems. The developed spots were visualized by examination of the TLC plates under UV_{254}, followed by spraying with Dragendroff's reagent (Section 5.3.1) or 1% ethanolic aluminium chloride solution (Section 5.3.2). Flavonoids appeared as bright yellow spots under UV_{365} while orange spots formed by reaction with Dragendroff's reagent indicated the presence of alkaloids.

5.2.3 Preparative Centrifugal TLC (CTLC)

Preparative centrifugal TLC was carried out using a round chromatographic plate measuring 24 cm in diameter. Preparation of the chromatographic plate was carried out by securing the edge of the plate with cellophane tape to form a mould.

Sillica gel slurry (Merck 7759, 50g in 110 mL cold distilled water) was then poured on to the previously prepared mould while rotating the plate to obtain an even setting. The plate was then left to air dry prior to being dried in an oven at 80 °C overnight. The newly prepared plate was then shaved to the desired thickness of 1, 2 or 4 mm before being attached to a centrifugal thin layer apparatus (Chromatotron).

Separation of compounds was carried out by dissolving the sample in a minimum volume of a suitable solvent and loaded on the centre of the spinning silica plate to form a thin band. Elution was then carried out with the appropriate solvent system. Fractions were collected, concentrated by rotary evaporation, monitored by TLC and combined where appropriate. Solvents systems used as eluents were:

1. Chloroform
2. Chloroform : Hexanes
3. Chroloform saturated in ammonia vapor
4. Chroloform : Methanol
5. Diethyl ether
6. Diethyl ether : Hexanes
7. Diethyl ether : Methanol
8. Diethyl ether saturated in ammonia vapor
9. Ethyl acetate
10. Ethyl acetate : Hexanes
11. Ethyl acetate : Methanol
12. Ethyl acetate saturated in ammonia vapor
13. Acetone
14. Acetone : Hexanes

5.3 Spraying Reagent

5.3.1 Dragendorff's Reagent

Solution A: 0.85 g of bismuth nitrate was dissolved in a mixture of 10 mL glacial acetic acid and 40 mL of distilled water.

Solution B: 8 g of potassium iodine was dissolved in 20 mL of distilled water.

A stock solution was prepared by mixing equal volumes of solutions A and B. One mL of stock solution was then mixed with 2 mL of glacial acetic acid and 10 mL of distilled water.

5.3.2 Aluminium chloride solution

Aluminium chloride spray reagent was prepared by dissolving 5 g aluminium chloride hexahydrate into 500 mL absolute ethanol.

5.4 Plant materials

Plant materials were collected from various locations in Malaysia and were authenticated by Dr Yong Kien Thai (Institute of Biological Sciences, University of Malaya (UM), and Kuala Lumpur). Voucher specimens were deposited at the Herbarium University of Malaya, Kuala Lumpur.

Table 5.1: Source and authentication of plant materials

Specimen No.	Locality	Plant species	Date of collection	Herbarium
UNMC 60	Melaka	*Artocarpus heterophyllus x integer*	Aug 2009	UM
UNMC 70	Semenyih, Selangor	*Macaranga hypoleuca*	June 2011	UM
UNMC 68	Rawang, Selangor	*Ficus fistulosa*	Dec 2011	UM
UNMC 77	Semenyih, Selangor	*Ficus hispida*	July 2012	UM
UNMC 87	Gombak, Selangor	*Ficus schwarzii*	July 2013	UM

5.5 Extraction of plant material

The stem-bark and leaves (3 kg each) of *F. hispida* were extracted with 95% EtOH (40 L). The concentrated ethanolic extracts were slowly added into 3% tartaric acid solution with constant stirring. The acidic solutions were then filtered through kieselguhr to remove the non-alkaloidal substances and then basified with concentrated NH_3 to approximately pH 10. The liberated alkaloids were exhaustively extracted with $CHCl_3$, washed with water, dried over anhydrous Na_2SO_4 and concentrated to furnish the crude alkaloidal mixtures (0.67 g; 0.02% and 1.67 g; 0.06%, respectively). The stem-bark and leaves of *F. fistulosa* (8 kg each) and leaves of *F. schwarzii* (4 kg) were extracted in the same manner as described for *F. hispida* to produce the crude alkaloidal mixtures (1.87 g; 0.02%, 8.38 g; 0.1%, and 0.88 g; 0.02% respectively).

The dried ground bark (4 kg) of *A. heterophyllus x integer* was sequentially extracted with *n*-hexane (30 L) followed by ethyl acetate (30 L) and then 95% ethanol (30 L) at room temperature (25 °C) for 72 hours. The ethyl acetate extracts were filtered and the extractions were repeated twice by adding fresh ethyl acetate and soaked for 24

hours at 25 °C. The ethyl acetate filtrates were combined and concentrated to dryness under reduced pressure using a rotary evaporator to afford the ethyl acetate crude extract (60 g; 1.5%).

The dried and ground leaf material of *M. hypoleuca* (2.2 kg) was sequentially extracted with *n*-hexane (20 L), ethyl acetate (20 L) and 95% ethanol (20 L). The three different extracts were concentrated to dryness under reduced pressure using a rotary evaporator. The concentrated ethyl acetate extract was re-dissolved in minimal amount of methanol and then partitioned with hexane to afford a hexane soluble syrup and methanol soluble syrup. The methanol soluble syrup was evaporated to dryness under reduced pressure using a rotary evaporator to afford 54 g (2.45%) of ethyl acetate crude extract.

5.6 Isolation of alkaloids

5.6.1 General procedure

The crude mixture obtained from the extraction procedure was initially frationated by vacuum liquid chromatography over silica gel. The column was eluted with chloroform, followed by a step-wise increase of methanol gradient. Based on TLC, the fractions obtained were pooled into several major fractions which were then subjected to further fractionation by vacuum liquid chromatography or CTLC.

5.6.2 Isolation of alkaloids from the bark and leaves of *F. hispida*

The stem-bark crude alkaloid mixture (0.67 g) was initially fractionated by silica gel column chromatography (4 x 20 cm) eluted with $CHCl_3$ with increasing proportions of MeOH to afford eight combined fractions. Fraction-3 (F3) was re-chromatographed using preparative centrifugal thin layer chromatography (CTLC) eluted with $CHCl_3$

(NH_3-saturated) followed by CH_2Cl_2/MeOH (NH_3-saturated) to yield 13a(*R*)-(+)-deoxypergularinine **(3)** (5 mg; 0.0002%). Fraction-8 (F-8) was re-chromatographed using centrifugal preparative TLC (CTLC) with $CHCl_3$ (NH_3-saturated) to yield hispidacine **(1)** (33 mg; 0.001%).

The leaf crude alkaloid mixture (1.67 g) was initially fractionated by silica gel column chromatography (4 x 20 cm) eluted with $CHCl_3$ with increasing proportions of MeOH to afford six combined fractions. Fraction-4 (F4) was re-chromatographed using CTLC eluted with CH_2Cl_2/MeOH (NH_3-saturated) followed by EtOAc/Hexane (NH_3-saturated) to yield hispilosine **(2)** (7 mg; 0.0002%).

5.6.3 Triacetate derivative of hispidacine (1a)

A mixture of hispidacine **(1)** (5 mg, 0.010 mmol), acetic anhydride (10 mole eq.), pyridine (10 mole eq.), 4-dimethylaminopyridine (cat. amount) in CH_2Cl_2 (3 mL) was stirred under N_2 at (25 °C) temperature for 20 min. The mixture was then poured into saturated Na_2CO_3 solution and extracted with CH_2Cl_2. Removal of the solvent, followed by purification by preparative centrifugal TLC over silica gel (Et_2O-MeOH) afforded 4 mg (65%) of the triacetate derivative **1a.**

5.6.4 Isolation of alkaloids from the bark and leaves of *F. fistulosa*

The stem-bark crude alkaloid mixture of *F. fistulosa* (1.87 g) was initially fractionated by silica gel column chromatography (2.5 x 20 cm), eluted with $CHCl_3$-$CHCl_3$/MeOH (4:1) (in the order of gradual increase in polarity) to produce ten fractions (F1 – F10). Fraction-3 (F3) (0.48 g) was re-chromatographed using CTLC eluted with Et_2O/Hexane (1:2) (NH_3-saturated) to yield 13a(*S*)-(+)-tylocrebrine **(7)** (4 mg; 0.00005%). Fraction-4 (F4) (1.77 g) was re-chromatographed by column

chromatography (4 x 12 cm) eluted with CH_2Cl_2 and CH_2Cl_2/MeOH (NH_3-saturated) and further purified by CTLC using Et_2O/Hex (4:1) to yield 13a(*S*)-(+)-septicine **(9)** (5.9 mg; 0.00007%). Fraction-5 (F5) (0.11 g) was re-chromatographed by CTLC eluted with $CHCl_3$/Hex (1:1) to yield fistulopsine A **(4)** (7.1 mg; 0.00009%).

The leaf crude alkaloid mixture (8.38 g) was subjected to silica gel column chromatography (7 x 20 cm) eluted with CH_2Cl_2 and CH_2Cl_2/MeOH (4:1) (in the order of gradual increase in polarity) to produce 11 fractions (F1 - F11). Fraction-2 (F2) (0.05 g) was purified by CTLC using Et_2O (NH_3-saturated) to yield 13a(*S*)-(+)-tylophorine **(8)** (11.8 mg; 0.0001%) as white precipitate. Fraction-5 (F-5) (0.75 g) was re-chromatographed by CTLC, eluted with CH_2Cl_2/Hex (1:1) (NH_3-saturated) to yielded eight sub-fractions (F5-1 – F5-8). F5-1 yielded vomifoliol **(10)** (7 mg; 0.00006%) as colourless needles. F5-5 (0.13 g) formed precipitates which was further purified by CTLC, eluted with CH_2Cl_2 (NH_3-saturated) to yield fistulopsine B **(5)** (20.9 mg; 0.0003%) and 13a(*R*)-(-)-3,6-didemethylisotylocrebrine **(6)** (24.9 mg; 0.0003%). Crystallisation of **10** and **5** occurred spontaneously upon isolation of these compounds.

5.6.5 Isolation of alkaloids from the leaves of *F. schwarzii*

The leaf crude alkaloid mixture (0.88 g) was initially fractionated by silica gel column chromatography (4 x 20 cm) eluted with $CHCl_3$/Hexane (3:7) and $CHCl_3$/MeOH (19:1) to afford nine semi-purified fractions. Fraction-1 (F1) (0.28 g) was re-chromatographed using CTLC eluted with Et_2O/Hexane (NH_3-saturated) to yield schwarzinicine A **(11)** (106.3 mg; 0.003%). Fraction-4 (F4) (0.11 g) was re-chromatographed using CTLC eluted with Et_2O (NH_3-saturated) to yield schwarzinicine B **(12)** (213.8 mg; 0.005%).

5.7 Isolation of flavonoids

5.7.1 General procedure

The ethyl acetate crude extracts of *A. heterophyllus x integer* and *M. hypoleuca* was fractionated by vacuum chromatography over silica gel eluted with EtOAc/hexane, followed by a step-wise decrease of hexane and continually a gradual increase of methanol gradient. Fractions obtained were pooled into several major fractions based on the TLC profiles and was then subjected to further fractionation by vacuum chromatography or CTLC.

5.7.2 Isolation of flavonoids from the bark of *A. heterophyllus x integer*

The ethyl acetate bark extract of *A. heterophyllus x integer* (60 g) was subjected to silica gel column chromatography (8 x 12 cm), eluted with EtOAc/hexane (5:1) and EtOAc/MeOH (4:1) (in the order of gradual increase in polarity) to produce 12 fractions. Fraction-5 (F5) (2.6 g) was re-chromatographed using CTLC eluted with EtOAc/Hex(1:4) (in the order of gradual increase in polarity) to produce 11 sub-fractions (F5-1 –F5-11). Sub-fraction F5-5 (0.4 g) was purified by CTLC eluted with $CHCl_3$/hexane (1:1) to yield cycloheterophyllin **(15)** (45.3 mg; 0.001%). Sub-fraction F5-6 was re-chromatographed using CTLC, eluted with Et_2O/Hex (2:1) followed by Acetone/hexane (1:4) with gradual decrease of hexane to yield lichexanthone crystals **(17)** (1.7 mg; 0.00004%). Fraction-7 (F7) (4.48 g) was re-chromatographed by column chromatography (4 x 12 cm) eluted with EtOAc/hexane (1:4) and EtOAc/MeOH (4:1) to afford one flavonoid containing sub-fraction which was further purified by CTLC eluted with Et_2O/hexane (1:1) and Et_2O/MeOH (4:1) followed by acetone/hexane (1:1) to produce artonin J as yellowish crystals **(16)** (100 mg; 0.003%). Fraction-9 (F9) (4.5 g) was chromatographed by column chromatography (4 x 12 cm) to afford four

flavonoid containing sub-fractions (F9-2 to F9-5). Sub-fraction F9-2 was purified by CTLC eluted with $CHCl_3$/hexane (4:1) and $CHCl_3$/MeOH (4:1) to yield cudraflavone C **(13)** (20 mg; 0.0005%), while sub-fraction F9-5 was re-chromatographed by CTLC eluted with $CHCl_3$/MeOH (4:1) followed by purification by LH-20 sephadex column chromatography (1 x 44 cm, MeOH) to yield artocarpetin A **(14)** (4 mg; 0.0001%). Crystallisation of **16** and **17** occurred spontaneously upon isolation of these compounds.

5.7.3 Isolation of flavonoids from the leaves of *M. hypoleuca*

The ethyl acetate leaf extract of *M. hypoleuca* (54 g) was subjected to silica gel column chromatography (8 x 12 cm) eluted with EtOAc/hexane (1:4) and EtOAc/MeOH (4:1) (in the order of gradual increase in polarity) to produce 11 fractions. Fraction-2 (F2) (3.4 g) was re-chromatographed by CTLC, eluted with $CHCl_3$/hexane (1:4) and $CHCl_3$/MeOH (4:1) to yield 3-*epi*-taraxerol **(24)** (3.0 mg; 0.0001%) as colorless crystals and a flavonoid containing sub-fraction (F2-7) which was purified by LH-20 sephadex column chromatography to produce 5,7-dihydroxy-2-(4-methoxyphenyl)-8-(3-methylbut-2-en-1-yl)chroman-4-one **(23)** (2.3 mg; 0.0001%). Fraction-6 (2.6 g) was re-chromatographed by CTLC and eluted with $CHCl_3$ to produce quercetin **(21)** (17.1 mg; 0.0008%) and kaempherol **(22)** (38 mg; 0.002%). Fraction-9 (F9) (4.6 g) produced yellow needles which were identified as quercetin-3-*O*-α-L-arabinopyranoside **(18)** (22.5 mg; 0.001%). Re-chromatography of fraction-10 (F10) (4.5 g) by CTLC, eluted with $CHCl_3$ afforded two flavonoid containing sub-fractions (F10-2 and F10-3). Precipitation of sub-fraction F10-2 was identified as quercetin-3-*O*-α-L-arabinofuranoside **(19)** (26.2 mg; 0.001%) while purification of sub-fraction F10-3 by LH-20 sephadex column chromatography produced quercetin-3-*O*-β-D-galactoside **(20)** (40.0 mg; 0.002%). Crystallisation of **18** and **24** occurred spontateously upon isolation of these compounds.

5.8 Compound data

Hispidacine (1): Light yellowish oil; $[\alpha]_D^{25}$ +20 (*c* 0.28, $CHCl_3$); CD (CH_3CN, 0.058 nM), λ (Δε): 206 (+1.29), 237 (-2.58), 273 (+1.55) nm; UV (EtOH) λ_{max} (log ε) 228 (3.86), 271 (3.60) nm; IR (dry film) ν_{max} 3385, 1585, 1505 cm^{-1}; ^{13}C NMR and ^{1}H NMR data, see Table 2.2; ESIMS *m/z* 494 $[M + H]^+$; HRESIMS *m/z* 494.2380 (calcd for $C_{25}H_{35}NO_9 + H^+$, 494.2390).

Triacetate derivative of hispidacine (1a): Light yellowish oil; CD (CH_3CN, 0.046 nM), λ (Δε): 204 (+1.32), 235 (-5.79), 275 (+3.48) nm; IR (dry film) ν_{max} 3325, 1738, 1585, 1505 cm^{-1}; ^{13}C NMR and ^{1}H NMR data, see Table 2.2; ESIMS *m/z* 620 $[M + H]^+$; HRESIMS *m/z* 620.2691 (calcd for $C_{31}H_{41}NO_{12} + H^+$, 620.2707).

Hispiloscine (2): Light yellowish oil; $[\alpha]_D^{25}$ +1 (*c* 0.40, $CHCl_3$); UV (EtOH) λ_{max} (log ε) 260 (3.67), 286 (3.51), 313 (3.06), 338 (2.66) nm; IR (dry film) ν_{max} 1736 cm^{-1}; ^{13}C NMR and ^{1}H NMR data, see Table 2.3; ESIMS *m/z* 422 $[M + H]^+$; HRESIMS *m/z* 422.1957 (calcd for $C_{25}H_{27}NO_5 + H^+$, 422.1968).

13a(*S*)-(+)-Deoxypergularinine (3): Colourless oil; $[\alpha]_D^{25}$+3 (*c* 0.11, $CHCl_3$); UV (EtOH) λ_{max} (log ε) 228 (3.63), 261 (3.88), 287 (3.80) nm; IR (dry film) ν_{max} 2963, 1609, 1512 cm^{-1}; ^{1}H NMR data, see Table 2.4; HRESIMS *m/z* 364.1909 $[M + H]^+$ (calcd. for $C_{23}H_{25}NO_3 + H^+$, 364.1913).

Fistulopsine A (4): Colourless oil; $[\alpha]_D^{25}$ = -47 (c 0.30, $CHCl_3$); UV (EtOH) λ_{max} (log ε) 225 (4.16), 265 (3.94) and 282 (3.86) nm; UV (EtOH + NaOH) λ_{max} (log ε) 226 (4.18), 247 (4.02), 269 (3.93) and 280 (3.88) nm; IR (KBr) ν_{max} 3375 (OH), 1583, 1515 cm^{-1}; ^{1}H NMR and ^{13}C NMR data, see Table 2.5; HRESIMS *m/z* 412.2099 $[M + H]^+$ (calcd. for $C_{24}H_{29}NO_5 + H^+$, 412.2125).

Fistulopsine B (5): Colourless needles ($CHCl_3$/MeOH); mp: 209-210˚C; $[\alpha]_D^{25}$ +18 (*c* 0.32, MeOH); UV (EtOH) λ_{max} (log ε) 225 (4.11), 239 (4.01), 263 (3.90), and 286 (3.89) nm; UV (EtOH + NaOH) λ_{max} (log ε) 226 (4.15), 250 (4.02), and 300 (3.87) nm; IR (KBr) ν_{max} 3350 (OH), 1594, 1508 cm^{-1}; ^1H NMR and ^{13}C NMR data, see Table 2.5; HRESIMS *m/z* 368.1868 $[M + H]^+$ (calcd. for $C_{22}H_{25}NO_4 + H^+$, 368.1862).

Crystalographic data of fistulopsine B (5): Colourless needles, $C_{22}H_{25}NO_4$, *M*r = 367.24, monoclinic, space group $P2_1/n$, a = 10.5986(17) Å, b = 11.447(2) Å, c = 15.756(3) Å, α = γ = 90°, β = 102.895(3)°, V = 1863.4(5) $Å^3$, T = 100 k, Z = 4, D_{cald}= 1.170 g/cm^3, crystal size 0.39 × 0.26 × 0.19 mm, F(000) = 700. The final R_1 value is 0.1781 (wR_2 = 0.4323) for 4663 reflections [$I \geq 2\sigma(I)$].

13a(*R*)-(-)-3,6-Didemethylisotylocrebrine (6): Light yellowish oil, with $[\alpha]_D^{25}$ -113 (*c* 0.13, $CHCl_3$/MeOH). UV (EtOH) λ_{max} (log ε) 262 (4.81), 279 (4.43), 304 (4.04), and 317 (4.03) nm; IR (KBr) ν_{max} 3385 cm^{-1}(OH), 1601, 1514; ^1H NMR and ^{13}C NMR data , see Table 2.6; HRESIMS *m/z* 366.1690 $[M + H]^+$ (calcd. for $C_{22}H_{23}NO_4 + H^+$, 366.1705).

13a(*S*)-(-)-Tylocrebrine (7): Light yellowish oil; $[\alpha]_D^{25}$ +19 (*c* 0.15, $CHCl_3$); UV (EtOH) λ_{max} (log ε) 244(3.21), 264 (3.57), 276 (1.29), 309 (3.03), 321 (2.31); IR (KBr) ν_{max} 1600, 1515 cm^{-1}; ^1H NMR and ^{13}C NMR data, see Table 2.6; HRESIMS *m/z* 394.1938 $[M + H]^+$ (calcd. for $C_{24}H_{27}NO_4 + H^+$, 394.2018).

13a(*S*)-(+)-Tylophorine (8): White amorphous; mp: 290-295˚C; $[\alpha]_D^{25}$ +44 (*c* 0.12, $CHCl_3$); UV (EtOH) λ_{max} (log ε) 240 (3.21), 257 (3.61), 288 (3.34), 304 (3.07) and 399 (3.87) nm; IR (KBr) ν_{max} 1619, 1515 cm^{-1}; ^1H NMR and ^{13}C NMR data, see Table 2.7; HRESIMS *m/z* 394.2011 $[M + H]^+$ (calcd. for $C_{24}H_{27}NO_4 + H^+$, 394.2018).

13a(*S*)-(+)-Septicine (9): Light yellowish oil; $[\alpha]_D^{25}$ +7 (*c* 0.28, $CHCl_3$); UV (EtOH) λ_{max} (log ε) 204(3.83), 235(3.89), 263 (3.94), 280 (3.97), 353 (4.07) nm; ^{1}H NMR and ^{13}C NMR data , see Table 2.7; HRESIMS *m/z* 396.2152 $[M + H]^+$ (calcd. for $C_{24}H_{29}NO_4$ + H^+, 396.2175).

Vomifoliol (10): Colourless needles; mp: 98-104˚C; $[\alpha]_D^{25}$ +117 (*c* 0.41, $CHCl_3$); UV (EtOH) λ_{max} (log ε) 237 (3.78) nm; IR (KBr) ν_{max} 3369, 1663 cm^{-1} ; ^{1}H NMR and ^{13}C NMR data , see Table 2.8; HRESIMS *m/z* 225.1505 $[M + H]^+$ (calcd. for $C_{13}H_{20}O_3$ + H^+, 255.1491).

Schwarzinicine A (11): Light yellowish oil; $[\alpha]_D^{25}$ +24 (*c* 0.50, $CHCl_3$); UV (EtOH) λ_{max} (log ε) 228 (3.30), 280 (3.85) nm; ^{1}H NMR and ^{13}C NMR data, see Table 2.9; HRESIMS *m/z* 524.3006 $[M + H]^+$ (calcd. for $C_{31}H_{41}NO_6$ + H^+, 524.3012).

Schwarzinicine A (12): Light yellowish oil; $[\alpha]_D^{25}$ +2 (*c* 0.45, $CHCl_3$); UV (EtOH) λ_{max} (log ε) 230 (3.09), 281 (2.66) nm; IR (KBr) ν_{max} 3587 cm^{-1}; ^{1}H NMR and ^{13}C NMR data, see Table 2.9; HRESIMS *m/z* 396.2152 $[M + H]^+$ (calcd. for $C_{30}H_{39}NO_6$ + H^+, 510.2856).

Cudraflavone C (13): Light orange oil, UV (EtOH) λ_{max} (log ε) 201 (4.51), 232 (4.21), 261 (4.49), 314 (3.93) nm; IR (KBr) ν_{max} 3364, 1649 cm^{-1}; ^{1}H NMR and ^{13}C NMR data, see Table 3.2; HRESIMS *m/z* 423.1811 $[M + H]^+$ (calcd. for $C_{25}H_{26}O_6$ + H^+, 423.1808).

Artocarpetin A (14): Light yellowish powder, mp: 268-273 ˚C; UV (EtOH) λ_{max} (log ε) 208 (4.21), 253 (3.65), 269 (3.89), 286 (3.62) and 360 (3.83) nm; IR (KBr) ν_{max} 3400, 1651, 1602 cm^{-1}; ^{1}H NMR and ^{13}C NMR data, see Table 3.2; HRESIMS *m/z* 369.1348 $[M + H]^+$ (calcd. for $C_{21}H_{21}O_6$ + H^+, 369.1338).

Cycloheterophyllin (15): Light yellowish powder; mp: 220-222 °C; UV (EtOH) λ_{max} (log ε): 273 (3.99), 299 (4.15), and 405 (3.88); IR (KBr) ν_{max}: 3346, 1652, 1375 and 1346 cm^{-1}; ^{1}H NMR and ^{13}C NMR data, see Table 3.3; ESIMS *m/z* 501.2 $[M - H]^-$ (calcd. for $C_{30}H_{30}O_7 - H^+$, 501.1913).

Artonin J (16): Light yellowish crystals; mp: 280-285 °C; UV (EtOH) λ_{max} (log ε): 380 (3.41), 264 (3.84), 231 (3.98) and 210 (4.20); IR (KBr) ν_{max}: 3399, 1713, 1651 cm^{-1}; ^{1}H NMR and ^{13}C NMR data, see Table 3.3; ESIMS *m/z* 437.3 $[M + H]^+$ (calcd. for $C_{25}H_{24}O_7 + H^+$, 437.1600).

Crystallographic data of artnoin J (16): Light yellowish crystals, $C_{25}H_{24}O_7$, *M*r = 340.36, monoclinic, space group $P2_1/c$, a = 7.0568(4) Å, b = 17.6285(8) Å, c = 18.3043(8) Å, α = γ = 90°, β = 97.818(3)°, V = 2255.90(19) $Å^3$, T = 100 k, Z = 4, D_{cald}= 1.002 g/cm^3, crystal size 0.62 × 0.22 × 0.12 mm, F(000) = 720. The final R_1 value is 0.1001 (wR_2 = 0.2534) for 16953 reflections [$I \geq 2\sigma(I)$]

Lichexanthone (17): Yellow needles; mp: 185-190 °C, ^{1}H NMR (400MHz, $CDCl_3$): δ_H 2.83 (3H, s, H-8), 3.84 (3H, s, OMe), 3.88 (3H, s, OMe). 6.28 (1H, d, J = 2.8 Hz, H-2), 6.31 (1H, d, J = 2.8 Hz, H-4), 6.64 (1H, s, H-5), δ 6.66 (1H, s, H-7).

Crystallographic data of Lichexanthone (17): Colourless needles, $C_{16}H_{14}O_5$, *M*r = 286.27, monoclinic, space group $P2_1/c$, a = 11.6219(4) Å, b = 7.5059(2) Å, c = 15.1606(5) Å, α = γ = 90°, β = 102.282(2)°, V = 477.62(11) $Å^3$, T = 100 K, Z = 4, D_{cald}= 1.471 g/cm^3, crystal size 0.48 × 0.08 × 0.04 mm, F(000) = 600. The final R_1 value is 0.0478 (wR_2 = 0.1119) for 11753 reflections [$I \geq 2\sigma(I)$].

Quercetin-3-*O*-α-L-arabinopyranoside (18): Yellow needles; mp: 242-244 °C; UV (EtOH) λ_{max} (log ε): 256 (4.21), 357 (4.47); IR (KBr) ν_{max}: 3476, 2903, 1654, 1618,

1508 cm^{-1}; ^{1}H NMR and ^{13}C NMR data, see Table 3.5; HRESIMS *m/z* 435.0922 $[M + H]^+$ (calcd. for $C_{20}H_{18}O_{11} + H^+$, 435.0927).

Crystalographic data of Quercetin-3-*O*-α-L-arabinopyranoside (18): Yellow needles, $C_{20}H_{18}O_{11}.2H_2O$, *M*r = 470.246, triclinic, space group *P*1, *a* = 4.7435(6) Å, *b* = 10.2235(13) Å, *c* = 11.1721(14) Å, α = 109.622(11)°, β = 100.161(10)°, γ = 103.176(10)°, *V* = 477.62(11) $Å^3$, T = 100 K, *Z* = 1, D_{cald}= 1.673 g/cm^3, crystal size 0.10 × 0.02 × 0.01 mm, *F*(000) = 241.0. The final R_1 value is 0.2664 (wR_2 = 0.6524) for 3512 reflections [$I \geq 2\sigma(I)$].

Quercetin-3-*O*-α-L-arabinofuranoside (19): Yellow amorphous; mp: 204-206 °C; UV (EtOH) λ_{max} (log ε): 258 (4.61), 292 (4.14), 358 (4.52); IR (KBr) ν_{max}: 3400, 2920, 1613, 1594, 1460 cm^{-1}; ^{1}H NMR and ^{13}C NMR data, see Table 3.5; HRESIMS *m/z* 435.0877 $[M + H]^+$ (calcd. for $C_{20}H_{18}O_{11} + H^+$, 435.0927).

Quercetin-3-*O*-β-D-galactoside (20): Yellow amorphous; mp: 229-231 °C; UV (EtOH) λ_{max} (log ε): 258 (4.0), 306 (4.05), 316 (3.55), 363 (3.94); IR (KBr) ν_{max}: 3400, 1608, 1496, 1363, 1300, 1201 cm^{-1}; ^{1}H NMR and ^{13}C NMR data, see Table 3.5; HRESIMS *m/z* 465.1030 $[M + H]^+$ (calcd. for $C_{21}H_{20}O_{12} + H^+$, 465.1033).

Quercetin (21): Yellow powder; mp: 279-283 °C; UV (EtOH) λ_{max} (log ε): 257 (4.61), 303 (4.31), 374 (4.76); IR (KBr) ν_{max}: 3476, 1614, 1519 cm^{-1}; ^{1}H NMR and ^{13}C NMR data, see Table 3.6; HRESIMS *m/z* 303.0498 $[M + H]^+$ (calcd. for $C_{15}H_{10}O_7 + H^+$, 303.0505).

Kaempherol (22): Yellow powder; mp: 274-279 °C; UV (EtOH) λ_{max} (log ε): 265 (294), 367 (322); IR (KBr) ν_{max} 3476, 1614 cm^{-1}; ^{1}H NMR and ^{13}C NMR data, see Table 3.6; ESIMS *m/z* 287.1 $[M + H]^+$ (calcd. for $C_{15}H_{10}O_6 + H^+$, 287.0556).

5,7-Dihydroxy-2-(4-methoxyphenyl)-8-(3-methylbut-2-en-1-yl)chroman-4-one (23): Yellow crystals, mp: 215-218 °C; UV (EtOH) λ_{max} (log ε): 219 (4.69), 296 (4.48), 336 (3.87); IR (KBr) ν_{max}: 3241, 1643, 1516 cm^{-1}; ^{1}H NMR and ^{13}C NMR data, see Table 3.7; HRESIMS *m/z* 355. 1504 $[M + H]^+$ (calcd. for $C_{21}H_{22}O_5 + H^+$, 355.1546).

3-*Epi*-taraxerol (24): Colourless crystals; mp: 260-263 °C; IR (KBr) ν_{max}: 3400, 848 cm^{-1}; ^{1}H NMR (400MHz, $CDCl_3$): δ_H 0.81(3H, s, H-24), 0.86 (3H, s, H-28), 0.91(3H, s, H-30), 0.94 (3H, s, H-27), 0.95 (3H, s, H-29), 1.09 (3H, s, H-23), 1.25 (3H, s, H-20), 3.40 (1H, t , *J* = 2.28 Hz, H-3), 5.50 (H, dd, *J* = 8.2, 3.1 Hz, H-15).

Crystalographic data of 3-*epi*-taraxerol (24): Colourless needles, $C_{30}H_{50}O$, *M*r = 426.70, triclinic, space group *P*1, *a* = 6.2860(4) Å, *b* = 13.5426(9) Å, *c* = 15.7104(10) Å, α = 110.801(4)°, β = 90.366(4)°, γ = 93.318(4)°, *V* = 1247.62(14) $Å^3$, T = 100 K, *Z* = 2, D_{cald}= 1.136 g/cm^3, crystal size 0.52 × 0.41 × 0.23 mm, *F*(000) = 476. The final R_1 value is 0.0641 (wR_2 = 0.1530) for 11001 reflections [$I \geq 2\sigma(I)$].

5.9 Cell culture

Human cell lines used in this study were A549 (human lung carcinoma), MCF-7 (human breast adenocarcinoma-estrogen receptor positive), MDA-MB-231 (human breast adenocarcinoma-estrogen receptor negative), HCT-116 (human colon carcinoma) and MRC-5 (normal human lung fibroblast), which were purchased from American Type Culture Collection (ATCC), USA. A549 and MRC-5 were cultured in RPMI 1650 medium supplemented with sodium pyruvate (Sigma, UK), MCF-7 and MDA-MB-231 cells were cultured in Dubelcco's modified Eagle's medium (DMEM) (Sigma, UK), whereas HCT-116 was cultured in McCoy's 5A medium (Sigma, UK). All media were supplemented with 10% (v/v) fetal bovine serum (Gibco, USA), 100 U/mL of

penicillin, 100 µg/mL streptomycin and 50 µg/mL amphotericin B (Gibco, UK). All cells were maintained at 37°C in a humidified 5% CO_2 incubator (ESCO, USA).

5.9.1 Preparation of treatment extracts and test compounds

Stock crude extract and test compounds were dissolved in DMSO to a concentration of 20 mg/mL and 10 mg/mL, respectively. The stock solutions were then further diluted to the required concentrations (Table 5.2) with culture media.

5.9.2 Neutral red uptake assay

Neutral red (NR) uptake assay was carried out according to methods reported by Guillermo *et al.*[188] Ninety- six well plates (Nunc, Denmark) were seeded with 5 x 10^3 cells per well and allowed to adhere for 24 hours prior to treatment with test samples. Seeded cells were treated with test samples at concentrations of 10-1000 µg/mL for crude extracts, while pure compounds were treated within the range as indicated in Table 5.2 for the duration of 72 hours. Wells containing untreated cells were regarded as a negative control, while cells treated with vinblastine (1 x 10^{-2} – 1 x 10^{-7} µg/mL) served as a positive control.

After 72 hours, the media in the wells were replaced with NR medium (50 µg/mL NR stock in culture media) and allowed to incubate for 3 hours. Then, the NR medium was removed and the wells were rinsed with (phosphate Buffered Saline; pH7.4) PBS. The dye accumulated within the cells was extracted with a solution containing acetic acid, ethanol and water (1:50:49). Absorbance (A) was measured at 540 nm using a multiwall plate reader (Thermo Fisher Scientific, USA).

Table 5.2: NR treatment concentrations for isolated compounds.

Compounds	A549, MCF-7, MDA-MB-231, HCT-116	MRC-5
	Treatment range (µg/mL)	
1, **10**, **11**, **12**, **15**, **18**, and **20**	3.25 – 50.0	1.5 -25.0
2, **4**, **5**, and **13**	0.01 – 10.0	
6	1×10^{-5} – 0.1	1×10^{-5} – 0.1

Percentage of inhibition was expressed as NR uptake of treated cells as compared to untreated cells, calculated as: $[(A_{untreated} - A_{treated})/(A_{untreated}) \times 100\%]$.[195] Results were presented as mean ± SE of triplicate wells from three independent experiments. IC_{50} (concentration required to reduce the growth by 50% as illustrated in Figure 5.1) values were then calculated by Prism Graphpad software (Version 5.0, GraphPad Software, Inc., California USA). Dose response curves in which IC_{50} values were derived from are shown in Appendices 70-72. Compounds deemed active (IC_{50} less than 5 µg/ml) were tested against the non-cancerous cell line, MRC-5, to investigate cell type selectivity. The selectivity index (SI) was calculated as IC_{50} against MRC-5 cells/IC_{50} against cancer cells) where samples with SI greater than 3 were considered highly selective towards cancer cells.[191]

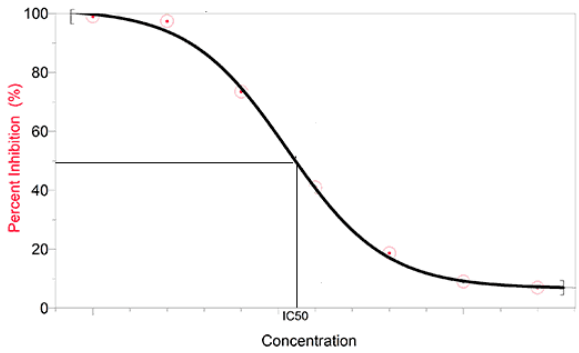

Figure 5.1: Illustration of concentration-response graph indicating the definitive values of IC_{50}

5.9.3 Acridine orange-ethidium bromide staining

Cell morphological changes were assessed by differential staining using DNA-intercalate fluorescent dyes, acridine orange (AO) and ethidium bromide (EB). Cells (HCT-116 and MCF-7) were seeded into six-well tissue culture plates (7 x 10^4 cells/well) for 24 hours prior to treatment with relevant compounds at approximate IC_{50} and two times IC_{50} concentrations for 24 hours (Table 5.3). Untreated cells served as a negative control while cells treated with vinblastine at IC_{50} served as a positive control. After incubation, the control and treated cells were detached, pelleted and suspended in 25 µL of PBS pH 7.4. Prior to microscopic viewing, one µL of AO/EB solution (1% AO in PBS; 1 % EB in PBS) was added to each sample. The stained cell suspension (15 µg/mL) was then placed on a glass slide and covered with a glass coverslip. The slide was then observed under a microscope (Nikon, Japan) and photographed under fluorescent illumination (FITC, Cy3 and DAPI filters). Images were analysed by Nikon's imaging software, NIS-Elements.

Table 5.3: Approximate IC_{50} and 2 IC_{50} treatment concentrations (µg/mL) for tested compounds.

Compounds	IC_{50}		$2IC_{50}$	
	MCF-7	HCT-116	MCF-7	HCT-116
4	3	6	3	6
5	0.002	0.004	0.006	0.012
6	6	12	4	8
13	2	4	4	8

5.9.4 Cell cycle analysis by flow cytometry

Cell cycle analysis was carried out by a collaborator at the Centre for Biomolecular Sciences, University of Nottingham, UK according to the method by Nicoletti *et al.*[214] A total of 1 x 10^6 cells (HCT-116 and MCF-7) were seeded into a six-

well plate and incubated for 24 hours at 37 ^{o}C, after which treatment with compounds **4** and **5** were applied at approximate IC_{50} concentration (Table 5.3) for 24, 48 and 72 hours. At the end of the designated time point, the medium was collected into individual centrifuge tubes and the adherent cells were rinsed with PBS, detached and pelleted by centrifugation at 1200 rpm (5 minutes, 4 ^{o}C). Cell pellet obtained was re-suspended in 0.4 ml fluorochrome solution (50 μg/mL of propidium iodide (PI), 0.1 mg/mL of ribonuclease A, 0.1% v/v Triton X-100, and 0.1% w/v sodium citrate in dH_2O) and stored overnight in the dark at 4 ^{o}C. A single cell suspension was achieved by passing the cells through a 23 g needle immediately prior to analysis by flow cytometry machine (Beckamn Coulter Ltd, UK) for cell cycle analysis. Data was analysed using EXPO 32 software (Beckman Coulter Ltd, UK).

5.9.5 Statistical analysis

Statistical calculations of cell cycle analysis were carried out with Prism Graphpad 6 software. Results are expressed as mean ± SD of 3 independent experiments. Significant differences between untreated (control) and treated groups at varying time points were determined by using the two-way analysis of variance (ANOVA) with significant differences between groups determined by Duncan's multiple range tests (DMRT) at 95 % significant difference (p>0.05) using Graphpad Prism software (Version 5.0, GraphPad Software, Inc., California USA).

Chapter 6: Research Limitations, Future Studies and Conclusion

6.1 Research Limitations

The research has successfully yielded six new and 18 known compounds, some of which were shown to possess interesting biological activity, several limitations and difficulties encountered throughout the research period need to be considered and are discussed as follows:

1. The phytochemical investigation of the leaves of *F. schwarzii* was only carried out on preliminary basis and as such only a very small amount of plant material was used. This study has resulted in the isolation of two novel tri-*nor*-sesquilignan alkaloids **11** and **12**, which are the major alkaloids present in the alkaloid crude extract. Several minor alkaloids that were faintly noticeable by TLC were however not isolable due to insufficient amount of the alkaloid crude extract. Furthermore, due to limited resources and time constraints the absolute configuration of **11** and **12** was also not established.
2. Several of the new and known compounds were only isolated in minute amounts, which in many instances have hindered further biological evaluation. This can be overcome by re-collecting the plant materials at a larger scale so that more pure compounds can be obtained for further studies.
3. It was unexpected that the research was unable to uncover any new flavonoids from *A. heterophyllus x integer* and *M. hypoleuca* although screening efforts (total flavonoid content, TLC) showed that the crude extracts are rich in flavonoids. However, the many flavonoids present in the extracts are believed to be in minute quantities hence not all were isolable.

4. Preliminary biological evaluations found that some of the compounds isolated showed compelling bioactivity, however limitations due to unavailability of equipment and time constrains have limited the depth of study for the bioactive compounds.
5. The time taken to carry out structure elucidation has been longer than expected mainly due to the unavailability of NMR facility within the University of Nottingham Malaysia Campus. NMR spectra for pure compounds were acquired from Chemistry Department, University of Malaya.

6.2 Future studies

The novel oxyneolignan alkaloid hispidacine **(1)** and tri-*nor*-sesquilignan alkaloids, schwarzinicines A **(11)** and B **(12)** did not show any cytotoxic effect towards the tested cancer cells but were however found in a separate study by Dr K. N. Ting's research group (School of Biomedical Sciences, University of Nottingham Malaysia) that these alkaloids exhibited potent vasorelaxant activity (unpublished data). A detailed investigation to uncover the underlying mechanism that is responsible for the observed effect is underway. Findings from this study may be potentially useful for the treatment of asthma, cardiovascular and other related diseases. On the other hand, a more thorough phytochemical study on the leaves of *Ficus schwarzii* will be implemented by Dr K. H. Lim's group with the intention to uncover more schwarzinicine-type alkaloids which may also possess useful vasorelaxant activity.

Fistulopsines A **(4)** and B **(5)** showed potentially active anti-cancer properties that can be further exploited. This study found that compounds **4** and **5** induced cell cycle perturbation at G1 phase of the cell cycle. Based on literature, phenanthroindolizidine tylophorine **(8)** also showed G1 phase cell cycle arrest, which was linked to the down regulation of cyclin A2. However, the point of initiation that led

to this was not explored. Given that **4** and **5** are of the same class of metabolites as **8**, it is highly possible that these two compounds share similar modes of action. The down regulation of cyclin A2 is a downstream event that occurred as a result of perturbation in the G1 phase machinery which encompasses many other players particularly cyclins D and E. As both these regulatory cyclins are activated independently of each other, it is advantageous to explore the specific targets in which these compounds exert its effects. As majority of genetic mutation that occur in human cancers encodes proteins that regulate through the G1 phase of the cell cycle[207,208], understanding the key regulatory points of potential cytostatic agents may allow rational targeting of regulatory sites in G1 phase of the cell cycle in most cancers, if not all.

The anti-cancer potential of cudraflavone C **(13)** has yet to be fully explored even though there were several previous studies that reported the cytotoxicity of it towards B16 melanoma cells, hepatocellular and gastric cancer cells.[55,193] In a recent collaborative effort with Dr C. W. Mai and Dr C. O. Leong from International Medical University (IMU), it has been disclosed that **13** showed selective inhibition towards colon cancer cell proliferation but not towards normal colon epithelial cells (unpublished data). This has further sparked the interest on this compound to explore the underlying anti-cancer mechanism at the molecular and genomic levels. Among the proposed studies include identification of gene expression as well as genomic mapping of inter-related genes involved in the activity by means of qPCR and microarray analysis, followed by quantification of the protein of interest by immunoblotting.

6.3 Conclusion

A total of 11 alkaloids, six of which are new, were isolated from three *Ficus* species, namely, *Ficus hispida*, *F. fistulosa* and *F. schwarzii*. As far as alkaloid content is concerned only phenanthroindolizidine and aminocaprophenone alkaloids were previously reported from three *Ficus* species, namely *F. septica*, *F. fistulosa* and *F. hispida*.

The novel alkaloid hispidacine **(1)** was isolated from the stem-bark of *F. hispida* as an 8,4'-oxyneolignan that has unusually incorporated a 2-hydroxyethylamine moiety and therefore represents the third alkaloid class isolated from *Ficus*. Hispiloscine **(2)**, which was obtained from the leaves of *F. hispida*, represents the first naturally occurring phenanthroindolizidine alkaloid with acetoxy substitution and exhibited appreciable anti-proliferative activity against breast, lung and colon cancer cell lines.

The two new alkaloids obtained from *Ficus fistulosa*, namely, fistulopsines A **(4)** and B **(5)**; represent the second and third septicine-type alkaloids to be isolated from the same species. Fistulopsines A **(4)** and B **(5)**, showed appreciable *in vitro* anti-proliferative activities in HCT-116 and MCF-7 cell lines with IC_{50} ranging from 2 – 7 μg/ml. Furthermore, these alkaloids were found to predominantly arrest cells at G1 phase of the cell cycle without the induction of apoptosis. The known phenanthroindolizidine alkaloid 13a(*R*)-(-)-3,6-didemethylisotylocrebrine **(6)** also isolated from *Ficus fistulosa* was shown to be potent anti-proliferative agents with IC_{50} values in the nanogram range towards the cell lines tested. As in the case of **4**, **5** and 13a(*S*)-(+)-tylophorine **(8)**, it could be assumed that **6** exerted its growth inhibitory activity by means of cell cycle arrest.

Ficus schwarzii, which was chemically, investigated for the first time, yielded two new alkaloids, namely, schwarzinicines A **(11)** and B **(12)**, which represents the

first members of a novel class of plant alkaloids, i.e., tri-*nor*-sesquilignan alkaloids. Schwarzinicines A **(11)** and B **(12)** did not show any growth inhibitory effect against cancer cell lines. However, a separate study carried out by our collaborators found that these alkaloids showed pronounced relaxation effects on rat isolated aorta and trachea.

Four known prenylated flavonoids and a known xanthone were obtained from the bark of *A. heterophyllus x integer*. On the other hand, the leaves of *M. hypoleuca* provided seven known compounds, of which three are flavonoid glycosides, three flavonoid aglycones and one triterpenoid compound. Of the flavonoids tested for growth inhibitory activity, only the known prenylflavonoid cudraflavone C (**13**) showed appreciable activity against the cancer cell lines tested, while cycloheterophyllin **(15)** was only shown to be weakly active.

References

(1) Sissi Wachtel-Galor; Iris F. F. Benzie. In *Herbal Medicine: Biomolecular and Clinical Aspects*; Iris F. F. Benzie; Sissi Wachtel-Galor, Eds.; CRC Press: Florida, 2011; p. 2.

(2) Chin, Y. C.; Balunas, M. J.; Chai, H. B.; M., K. *AAPS J.* **2006**, *8*, E239–E253.

(3) Amin, A.; Gali-Muhtasib, H.; Ocker, M.; Schneider-Stock, R. *Int. J. Biomed. Sci.* **2009**, *5*, 1–11.

(4) Cragg, G. M.; Newman, D. J. *Biochim. Biophys. Acta - Gen. Subj.* **2013**, *1830*, 3670–3695.

(5) Stevigny, C.; Bailly, C.; Quetin-Leclercq. *Curr. Med. Chem. Agents* **2005**, *5*, 173–182.

(6) Kennedy, D. O.; Wightman, E. L. *Adv. Nutr. An Int. Rev. J.* **2011**, *2*, 32–50.

(7) Harborne, J. B. *Introduction to Ecological Biochemistry*; 4th ed.; Academic Press Limited: London, 1993.

(8) Koehn, F. E.; Carter, G. T. *Nat. Rev. Drug Discov.* **2005**, *4*, 206–220.

(9) Hesse, M. In *Alkaloids: Nature's Curse or Blessing?*; Wallimann, P. M.; Kisakurek, V., Eds.; Verlag Helvetica Chimica Acta: Zurich, Switzerland, 2002; pp. 1–9.

(10) Waterman, P. G. In *Alkaloids: Biochemistry, Ecology,and Medicinal Applications*; Roberts, M. F.; Wink, M., Eds.; Plenum Press: New York, 1998; p. 87.

(11) Hesse, M. In *Alkaloids: Nature's Curse or Blessing?*; Wallimann, P.; Kisakirek V., Eds.; Verlag Helvetica Chimica Acta: Zurich, Switzerland, 2002; pp. 283–312.

(12) Lewis, W. H.; Elvin-Lewis, M. P. F. *Medical Botany, Plants affecting human health*; 2nd ed.; John Wiley & Sons, Inc.: Hoboken , NewJersey, 2003.

(13) Fester, K. In *Encyclopedia of Life Sciences (eLS)*; John Wiley & Sons, Inc., 2010; pp. 1–11.

(14) Roberts, M. F.; Wink, M. In *Alkaloids: Biochemistry, Ecology,and Medicinal Applications*; Roberts, M. F.; Wink, M., Eds.; Plenum Press: New York, 1998; pp. 1–7.

(15) Bruneton, J. *Pharmacognosy, Phytochemistry, Medicinal Plants*; 2nd ed.; Lavoisier: Paris, 1999.

(16) Hesse, M. In *Alkaloids: Nature's Curse or Blessing?*; Wallimann, P.; Kisakirek, V., Eds.; Verlag Helvetica Chimica Acta: Zurich, Switzerland, 2002; pp. 185–202.

(17) Hesse, M. In *Alkaloids: Nature's Curse or Blessing?*; Wallimann, P.; V. Kisakirek, Eds.; Verlag Helvetica Chimica Acta: Zurich, Switzerland, 2002; pp. 11–114.

(18) Stærk, D.; Christensen, J.; Lemmich, E.; Duus, J. Ø.; Olsen, C. E.; Jaroszewski, J. W. *J. Nat. Prod.* **2000**, *63*, 1584–1586.

(19) Damu, A. G.; Kuo, P. C.; Shi, L. S.; Li, C. Y.; Su, C. R.; Wu, T. S. *Planta Med.* **2009**, *75*, 1152–1156.

(20) Chemler, S. R. *Curr. Bioact. Compd.* **2009**, *5*, 2–19.

(21) Damu, A. G.; Kuo, P. C.; Shi, L. S.; Li, C. Y.; Kuoh, C. S.; Wu, P. L.; Wu, T. S. *J. Nat. Prod.* **2005**, *68*, 1071.

(22) Gellert, E. *J. Nat. Prod.* **1982**, *45*, 50–73.

(23) Kumar, S.; Abhay K. Pandey. *Sci. World J.* **2013**, *2013*, Article ID 162750.

(24) Agrawal, A. D. *Int. J. Pharm. Sci. Nanotechnol.* **2011**, *4*, 1394–1398.

(25) Pietta, P. G. *J. Nat. Prod.* **2000**, *63*, 1035–1042.

(26) Terao, J. *Forum Nutr.* **2009**, *61*, 87–94.

(27) Iwashina, T. *J. Plant Res.* **2000**, *113*, 287–299.

(28) Harrison, R. D. *Bioscience* **2005**, *55*, 1053.

(29) Berg, C. C.; Corner, E. J. H. *Flora Malesiana, Series I. Volume 12 part 2.*; Steenis, C., Ed.; Nationaal Herbarium Nederland.: Leiden, 2005.

(30) Chaudhary, L. B.; Sudhakar, J. V. A. K.; Bajpai, O.; Tiwari, R. G.; Murthy, V. S. *Taiwania* **2012**, *57*, 193–216.

(31) Shanahan, M.; So, S.; Gompton, S. G.; Gorlett, R. *Biol. Rev.* **2001**, *76*, 529–572.

(32) Singh, A. P. *Ethnobot. Leafl.* **2006**, *10*, 329–335.

(33) Lim, T. K. *Edible Medicinal and Non Medicinal Plants: Volume 3: Fruits*; Springer Science & Business Media, 2012.

(34) Lansky, E. P.; Paavilainen, H. M.; Pawlus, A. D.; Newman, R. A. *J. Ethnopharmacol.* **2008**, *119*, 195–213.

(35) Simon, P. N.; Chaboud, A.; Darbour, N.; Di Pietro, A.; Dumontet, C.; Lurel, F.; Raynaud, J.; Barron, D. *Anticancer Res.* **2001**, *21*, 1023–1027.

(36) Sheu, Y. W.; Chiang, L. C.; Chen, I. S.; Chen, Y. C.; Tsai, I. L. *Planta Med.* **2005**, *71*, 1165–1167.

(37) Chang, M. S.; Yang, Y. C.; Kuo, Y. C.; Kuo, Y. H.; Chang, C.; Chen, C. M.; Lee, T. H. *J. Nat. Prod.* **2005**, *68*, 11–13.

(38) Tuyen, N. V; Kim, D. S. H. L.; Fong, H. S.; Soejarto, D. D.; Khanh, T. C.; Tri, M. V; Xuan, L. T. *Phytochemistry* **1999**, *50*, 467–469.

(39) Stærk, D.; Lykkeberg, A. K.; Christensen, J.; Budnik, B. A.; Abe, F.; Jaroszewski, J. W. *J. Nat. Prod.* **2002**, *65*, 1299–1302.

(40) Peraza-Sánchez, S. R.; Chai, H. B.; Shin, Y. G.; Santisuk, T.; Reutrakul, V.; Farnsworth, N. R.; Cordell, G. A.; Pezzuto, J. M.; Kinghorn, A. D. *Planta Med.* **2002**, *68*, 186–188.

(41) Subramaniam, G.; Ang, K. K. H.; Ng, S.; Buss, A. D.; Butler, M. S. *Phytochem. Lett.* **2009**, *2*, 88–90.

(42) Ueda, J.; Takagi, M.; Shin-ya, K. *J. Nat. Prod.* **2009**, *72*, 2181–2183.

(43) Jagtap, U. B.; Bapat, V. A. *J. Ethnopharmacol.* **2010**, *129*, 142–166.

(44) Panthong, K.; Tohdee, K.; Hutadilok-Towatana, N.; Voravuthikunchai, S. P.; Chusri, S. *J. Braz. Chem. Soc.* **2013**, *24*, 1656–1661.

(45) Hakim, E. H.; Juliawaty, L. D.; Syah, Y. M.; Achmad, S. A. *Mol. Divers.* **2005**, *9*, 149–158.

(46) Hakim, E. H.; Achmad, S. A.; Juliawaty, L. D.; Makmur, L.; Syah, Y. M.; Aimi, N.; Kitajima, M.; Takayama, H.; Ghisalberti, E. L. *J. Nat. Med.* **2007**, *61*, 229.

(47) Widyawaruyanti, A.; Kalauni, S. K.; Awale, S.; Nindatu, M.; Zaini, N. C.; Syafruddin, D.; Asih, P. B. S.; Tezuka, Y.; Kadota, S. *J. Nat. Med.* **2007**, *61*, 410–413.

(48) Achmad, S. A.; Hakim, E. H.; Juliawaty, L. D.; Makmur, L.; Aimi, N.; Ghisalberti, E. L. *J. Nat. Prod.* **1996**, *59*, 878–879.

(49) Hakim, E. H.; Fahriyati, A.; Kau, M. S.; Achmad, S. A.; Makmur, L.; Ghisalberti, E. L.; Nomura, T. *J. Nat. Prod.* **1999**, *62*, 613–615.

(50) Syah, Y. M.; Achmad, S. A.; Ghisalberti, E. L.; Hakim, E. H.; Makmur, L.; Mujahidin, D. *Phytochemistry* **2002**, *61*, 949–953.

(51) Syah, Y. M.; Achmad, S. A.; Ghisalberti, E. L.; Hakim, E. H.; Mujahidin, D. *Fitoterapia* **2004**, *75*, 134–140.

(52) Syah, Y. M.; Juliawaty, L. D.; Achmad, S. A.; Hakim, E. H.; Ghisalberti, E. L. *J. Nat. Med.* **2006**, *60*, 308–312.

(53) Musthapa, I.; Juliawaty, L. D.; Syah, Y. M.; Hakim, E. H.; Latip, J.; Ghisalberti, E. L. *Arch. Pharm. Res.* **2009**, *32*, 191–194.

(54) Arung, E. T.; Shimizu, K.; Kondo, R. *Biol. Pharm. Bull.* **2006**, *29*, 1966–1969.

(55) Arung, E. T.; Yoshikawa, K.; Shimizu, K.; Kondo, R. *Fitoterapia* **2010**, *81*, 120–123.

(56) Wei, B. L.; Weng, J. R.; Chiu, P. H.; Hung, C. F.; Wang, J. P.; Lin, C. N. *J. Agric. Food Chem.* **2005**, *53*, 3867–3871.

(57) Fang, S. C.; Hsu, C. L.; Yu, Y. S.; Yen, G. C. *J. Agric. Food Chem.* **2008**, *56*, 8859–8868.

(58) Lin, K. W.; Liu, C. H.; Tu, H. Y.; Ko, H. H.; Wei, B. L. *Food Chem.* **2009**, *115*, 558–562.

(59) Suhartati, T.; Achmad, S. A.; Aimi, N.; Hakim, E. H.; Kitajima, M.; Takayama, H.; Takeya, K. *Fitoterapia* **2001**, *72*, 912–918.

(60) Seo, E. K.; Lee, D.; Shin, Y. G.; Chai, H. B.; Navarro, H. A.; Kardono, L. B. S.; Rahman, I.; Cordell, G. A.; Farnsworth, N. R.; Pezzuto, J. M.; Kinghorn, A. D.; Wani, M. C.; Wall, M. E. *Arch. Pharm. Res.* **2003**, *26*, 124–127.

(61) Namdaung, U.; Aroonrerk, N.; Suksamrarn, S.; Danwisetkanjana, K.; Saenboonrueng, J.; Arjchomphu, W.; Suksamrarn, A. *Chem. Pharm. Bull. (Tokyo).* **2006**, *54*, 1433–1436.

(62) Ren, Y.; Kardono, L. B. S.; Riswan, S.; Chai, H.; Farnsworth, N. R.; Soejarto, D. D.; Carcache de Blanco, E. J.; Kinghorn, A. D. *J. Nat. Prod.* **2010**, *73*, 949–955.

(63) Lin, C. N.; Lu, C. M.; Huang, P. L. *Phytochemistry* **1995**, *39*, 1447–1451.

(64) Zheng, Z. P.; Cheng, K. W.; To, J. T. K.; Li, H.; Wang, M. *Mol. Nutr. Food Res.* **2008**, *52*, 1530–1538.

(65) Hano, Y.; Aida, M.; Shiina, M.; Nomura, T.; Kawai, T.; Ohe, H.; Kagei, K. *Heterocycles* **1989**, *29*, 1447–1453.

(66) Aida, M.; Shinomiya, K.; Hano, Y.; Nomura, T. *Heterocycles* **1993**, *36*, 575–583.

(67) Aida, M.; Shinomiya, K.; Matsuzawa, K.; Hano, Y.; Nomura, T. *Heterocycles* **1994**, *39*, 847–858.

(68) Shamaun, S. S.; Rahmani, M.; Hashim, N. M.; Ismail, H. B. M.; Sukari, M. A.; Lian, G. E. C.; Go, R. *J. Nat. Med.* **2010**, *64*, 478–481.

(69) Hsu, C. L.; Chang, F. R.; Tseng, P. Y.; Chen, Y. F.; El-Shazly, M.; Du, Y. C.; Fang, S. C. *Planta Med.* **2012**, *78*, 995–1001.

(70) Likhitwitayawuid, K.; Chaiwiriya, S.; Sritularak, B.; Lipipun, V. *Chem. Biodivers.* **2006**, *3*, 1138–1143.

(71) Whitmore, T. C. *Biol. J. Linn. Soc.* **1969**, *1*, 223–231.

(72) Siregar, M.; Sambas, E. N. In *International Symposium on Tropical Peatlands*; 1999; pp. 153–164.

(73) Davies, S. J. *Ecology* **1998**, *79*, 2292–2308.

(74) Joseph, J. M. *J. Med. Plants Res.* **2014**, *8*, 489–503.

(75) Nick, A.; Rali, T.; Sticher, O. *J. Ethnopharmacol.* **1995**, *49*, 147–156.

(76) Grosvenor, P. W.; Gothard, P. K.; McWilliam, N. C.; Supriono, A.; Gray, D. O. *J. Ethnopharmacol.* **1995**, *45*, 75–95.

(77) Eswani, N.; Abd Kudus, K.; Nazre, M.; Awang Noor, A. G.; Ali, M. *J. Agric. Sci.* **2010**, *2*, 189–210.

(78) Yoder, B. J.; Cao, S.; Norris, A.; Miller, J. S.; Ratovoson, F.; Razafitsalama, J.; Andriantsiferana, R.; Rasamison, V. E.; Kingston, D. G. I. *J. Nat. Prod.* **2007**, *70*, 342–346.

(79) Kawakami, S.; Harinantenaina, L.; Matsunami, K.; Otsuka, H.; Shinzato, T.; Takeda, Y. *J. Nat. Prod.* **2008**, *71*, 1872–1876.

(80) Agustina, W.; Juliawati, L. D.; Hakim, E. H.; Shah, Y. M. *ITB J. Sci.* **2012**, *44*, 13–18.

(81) Jang, D. S.; Cuendet, M.; Hawthorne, M. E.; Kardono, L. B. S.; Kawanishi, K.; Fong, H. H. S.; Mehta, R. G.; Pezzuto, J. M.; Kinghorn, A. D. *Phytochemistry* **2002**, *61*, 867–872.

(82) Syah, Y. M.; Ghisalberti, E. L. *Nat. Prod. Commun.* **2010**, *5*, 219–222.

(83) Tanjung, M.; Hakim, E. H.; Mujahidin, D.; Hanafi, M.; Syah, Y. M. *J. Asian Nat. Prod. Res.* **2009**, *11*, 929–932.

(84) Trinh Thi Thanh, V.; Doan Thi Mai, H.; Pham, V. C.; Litaudon, M.; Dumontet, V.; Guéritte, F.; Nguyen, V. H.; Chau, V. M. *J. Nat. Prod.* **2012**, *75*, 2012–2015.

(85) Jang, D. S.; Cuendet, M.; Pawlus, A. D.; Kardono, L. B. S.; Kawanishi, K.; Farnsworth, N. R.; Fong, H. H. S.; Pezzuto, J. M.; Kinghorn, A. D. *Phytochemistry* **2004**, *65*, 345–350.

(86) Rakoff-Nahoum, S. *Yale J. Biol. Med.* **2006**, *79*, 123–130.

(87) Ricciotti, E.; FitzGerald, G. A. *Arterioscler. Thromb. Vasc. Biol.* **2011**, *31*, 986–1000.

(88) Jang, M.; Cai, L.; Udeani, G. O.; Slowing, K. V; Thomas, C. F.; Beecher, C. W.; Fong, H. H.; Farnsworth, N. R.; Kinghorn, A. D.; Mehta, R. G.; Moon, R. C.; Pezzuto, J. M. *Science* **1997**, *275*, 218–220.

(89) Su, B. N.; Cuendet, M.; Hawthorne, M. E.; Kardono, L. B. S.; Riswan, S.; Fong, H. H. S.; Mehta, R. G.; Pezzuto, J. M.; Kinghorn, A. D. *J. Nat. Prod.* **2002**, *65*, 163–169.

(90) Wada, S.; Tanaka, R. *Chem. Biodivers.* **2006**, *3*, 473–479.

(91) Depeint, F.; Gee, J. M.; Williamson, G.; Johnson, I. T. *Proc. Nutr. Soc.* **2002**, *61*, 97–103.

(92) Kamei, H.; Koide, T.; Kojimam, T.; Hasegawa, M.; Terabe, K.; Umeda, T.; Hashimoto, Y. *Cancer Biother. Radiopharm.* **1996**, *11*, 193–196.

(93) Brownson, D. M.; Azios, N. G.; Fuqua, B. K.; Dharmawardhane, S. F.; Mabry, T. J. *J. Nutr.* **2002**, *132*, 3482S – 3489S.

(94) Sutthivaiyakit, S.; Unganont, S.; Sutthivaiyakit, P.; Suksamrarn, A. *Tetrahedron* **2002**, *58*, 3619–3622.

(95) Tseng, M. H.; Chou, C. H.; Chen, Y. M.; Kuo, Y. H. *J. Nat. Prod.* **2001**, *64*, 827–828.

(96) Phommart, S.; Sutthivaiyakit, P.; Chimnoi, N.; Ruchirawat, S.; Sutthivaiyakit, S. *J. Nat. Prod.* **2005**, *68*, 927–930.

(97) Versiani, M. A.; Diyabalanage, T.; Ratnayake, R.; Henrich, C. J.; Bates, S. E.; McMahon, J. B.; Gustafson, K. R. *J. Nat. Prod.* **2011**, *74*, 262–266.

(98) Zakaria, I.; Ahmat, N.; Jaafar, F. M.; Widyawaruyanti, A. *Fitoterapia* **2012**, *83*, 968–972.

(99) Zakaria Ishak; Ahmat, N.; Ahmad, R.; Mohd Jaafar, F.; Ab Ghani, N.; Khamis, S. *World Appl. Sci. J.* **2010**, *9*, 103–1007.

(100) Yana M. Syah; Ghisalberti, E. L. *Nat. Prod. J.* **2012**, *2*, 45–49.

(101) Li, X.; Xu, L.; Wu, P.; Xie, H.; Huang, Z.; Ye, W.; Wei, X. *Chem. Pharm. Bull. (Tokyo).* **2009**, *57*, 495–498.

(102) Suffness, M.; Cordell, G. A. *Alkaloids Chem. Pharmacol.* **1985**, *25*, 1–355.

(103) Chahar, M. K.; Sharma, N.; Dobhal, M. P.; Joshi, Y. C. *Pharmacogn. Rev.* **2011**, *5*, 1–12.

(104) Kanadaswami, C.; Lee, L. T. A.; Lee, P. P. H.; Hwang, J. J.; Ke, F. C.; Huang, Y. T.; Lee, M. T. *In Vivo (Brooklyn).* **2005**, *19*, 895–909.

(105) Senderowicz, A. M. *Invest. New Drugs* **1999**, *17*, 313–320.

(106) Wang, Z.; Wu, M.; Wang, Y.; Li, Z.; Wang, L.; Han, G.; Chen, F.; Liu, Y.; Wang, K.; Zhang, A.; Meng, L.; Wang, Q. *Eur. J. Med. Chem.* **2012**, *51*, 250–258.

(107) Lopez-Lazaro, M. *Curr. Med. Chem. Agents* **2002**, *2*, 691–714.

(108) Agullo, G.; Gamet-Payrastre, L.; Fernandez, Y.; Anciaux, N.; Demigné, C.; Rémésy, C. *Cancer Lett.* **1996**, *105*, 61–70.

(109) Donaldson, G. R.; Atkinson, M. R.; Murray, A. W. *Biochem. Biophys. Res. Commun.* **1968**, *31*, 104–109.

(110) Huang, M. T.; Grollman, A. P. *Mol. Pharmacol.* **1972**, *8*, 538–550.

(111) Ueno, S.; Yamazaki, R.; Ikeda, T.; Yaegashi, T.; Matsuzaki, T. *Anticancer Res.* **2014**, *34*, 3391–3398.

(112) Ren, W.; Qiao, Z.; Wang, H.; Zhu, L.; Zhang, L. *Med. Res. Rev.* **2003**, *23*, 519–534.

(113) Chang, W. S.; Lee, Y. J.; Lu, F. J.; Chiang, H. C. *Anticancer Res. 13*, 2165–2170.

(114) Mutoh, M.; Takahashi, M.; Fukuda, K.; Komatsu, H.; Enya, T.; Matsushima-Hibiya, Y.; Mutoh, H.; Sugimura, T.; Wakabayashi, K. *Jpn. J. Cancer Res.* **2000**, *91*, 686–691.

(115) Lee, S. K.; Nam, K. A.; Heo, Y. H. *Planta Med.* **2003**, *69*, 21–25.

(116) Wu, C. M.; Yang, C. W.; Lee, Y. Z.; Chuang, T. H.; Wu, P. L.; Chao, Y. S.; Lee, S. J. *Biochem. Biophys. Res. Commun.* **2009**, *386*, 140–145.

(117) Choi, J. A.; Kim, J. Y.; Lee, J. Y.; Kang, C. M.; Kwon, H. J.; Yoo, Y. D.; Kim, T. W.; Lee, Y. S.; Lee, S. J. *Int. J. Oncol.* **2001**, *19*, 837–844.

(118) Cho, H. J.; Park, J. H. Y. *J. Cancer Prev.* **2013**, *18*, 257–263.

(119) Zi, X.; Feyes, D. K.; Agarwal, R. *Clin. Cancer Res.* **1998**, *4*, 1055–1064.

(120) Shukla, S.; Gupta, S. *Mol. Carcinog.* **2004**, *39*, 114–126.

(121) Yi, L.; Zongyuan, Y.; Cheng, G.; Lingyun, Z.; Guilian, Y.; Wei, G. *Cancer Sci.* **2014**, *105*, 520–527.

(122) Li, W.; Du, B.; Wang, T.; Wang, S.; Zhang, J. *Chem. Biol. Interact.* **2009**, *177*, 121–127.

(123) Gao, W.; Lam, W.; Zhong, S.; Kaczmarek, C.; Baker, D. C.; Cheng, Y. C. *Cancer Res.* **2004**, *64*, 678.

(124) Saraswati, S.; Kanaujia, P. K.; Kumar, S.; Kumar, R.; Alhaider, A. A. *Mol. Cancer* **2013**, *12*, 82.

(125) Fotsis, T.; Pepper, M.; Adlercreutz, H.; Fleischmann, G.; Hase, T.; Montesano, R.; Schweigerer, L. *Proc. Natl. Acad. Sci.* **1993**, *90*, 2690–2694.

(126) Hoeben, A.; Landuyt, B.; Highley, M. S.; Wildiers, H.; Van Oosterom, A. T.; De Bruijn, E. A. *Pharmacol. Rev.* **2004**, *56*, 549–580.

(127) Yap, V. A.; Loong, B. J.; Ting, K. N.; Loh, S. H. S.; Yong, K. T.; Low, Y. Y.; Kam, T. S.; Lim, K.-H. *Phytochemistry* **2015**, *109*, 96–102.

(128) Moss, G. P. *Pure Appl. Chem.* **2000**, *72*, 1493–1523.

(129) Gan, M.; Zhang, Y.; Lin, S.; Liu, M.; Song, W.; Zi, J.; Yang, Y.; Fan, X.; Shi, J.; Hu, J.; Sun, J.; Chen, N. *J. Nat. Prod.* **2008**, *71*, 647–654.

(130) Herrera Braga, A. C.; Zacchino, S.; Badano, H.; Sierra, M. G.; Rúveda, E. A. *Phytochemistry* **1984**, *23*, 2025–2028.

(131) Huo, C.; Liang, H.; Zhao, Y.; Wang, B.; Zhang, Q. *Phytochemistry* **2008**, *69*, 788–795.

(132) Huang, X. X.; Zhou, C. C.; Li, L. Z.; Li, F. F.; Lou, L. L.; Li, D. M.; Ikejima, T.; Peng, Y.; Song, S. J. *Bioorg. Med. Chem. Lett.* **2013**, *23*, 5599–5604.

(133) Wallis, A. F. A. *Aust. J. Chem.* **1973**, *26*, 85–594.

(134) Arnoldi, A.; Merlini, L. *J. Chem. Soc. Perkin Trans. 1* **1985**, 2555–2557.

(135) Govindachari, T. R. *J. Indian Chem. Soc.* **1973**, *50*, 1–9.

(136) Govindachari, T. R.; Viswanathan, N.; Radhakrishnan, J.; Pai, B. R.; Natarajan, S.; Subramaniam, P. S. *Tetrahedron* **1973**, *29*, 891–897.

(137) Zhen, Y. Y.; Huang, X. S.; Yu, D.-Q.; Yu, S. S. *Acta Bot. Sin.* **2002**, *44*, 349–353.

(138) Mulchandani, N. B.; Venkatachalam, S. R. *Phytochemistry* **1976**, *15*, 1561–1563.

(139) Abe, F.; Iwase, Y.; Yamauchi, T.; Honda, K.; Hayashi, N. *Phytochemistry* **1995**, *39*, 695–699.

(140) Abe, F.; Hirokawa, M.; Yamauchi, T.; Honda, K.; Hayashi, N.; Ishii, M.; Imagawa, S.; Iwahana, M. *Chem. Pharm. Bull. (Tokyo).* **1998**, *46*, 767–769.

(141) Huang, X.; Shan, Y. S.; Liang, X. *Chinese Chem. Lett.* **2002**, *13*, 61–64.

(142) Haasnoot, C. A. G.; de Leeuw, F. A. A. M.; Altona, C. *Tetrahedron* **1980**, *36*, 2783–2792.

(143) Wu, P. L.; Rao, K. V.; Su, C. H.; Kuoh, C. S.; Wu, T. S. *Heterocycles* **2002**, *57*, 2401–2408.

(144) Hirano, T.; Abe, K.; Gotoh, M.; Oka, K. *Br. J. Cancer* **1995**, *72*, 1380–1388.

(145) Buckley, T. F.; Henry, R. *J. Org. Chem.* **1983**, *48*, 4222–4232.

(146) Lee, Y. Z.; Huang, C. W.; Yang, C. W.; Hsu, H. Y.; Kang, I. J.; Chao, Y. S.; Chen, I. S.; Chang, H. Y.; Lee, S. J. *Planta Med.* **2011**, *77*, 1932–1938.

(147) Nordlander, J. E.; Njoroge, F. G. *J. Org. Chem.* **1987**, *52*, 1627–1630.

(148) Stoye, A.; Peez, T. E.; Opatz, T. *J. Nat. Prod.* **2013**, *76*, 275–278.

(149) Su, C. R.; Damu, A. G.; Chiang, P. C.; Bastow, K. F.; Morris-Natschke; L, S.; Lee, K. H.; Wu, T. S. *Bioorg. Med. Chem.* **2008**, *16*, 6233–6241.

(150) Budzianowski, J.; Morozowska, M.; Wesołowska, M. *Phytochemistry* **2005**, *66*, 1033–1039.

(151) Jarevång, T.; Nilsson, M.-C.; Wallstedt, A.; Odham, G.; Sterner, O. *Phytochemistry* **1998**, *48*, 893–896.

(152) Li, C.; Yao, Z. H.; Qin, Z. F.; Zhang, J. B.; Cao, R. Y.; Dai, Y.; Yao, X. S. *Fitoterapia* **2014**, *97*, 92–97.

(153) Niphakis, M. J.; Georg, G. I. *Org. Lett.* **2011**, *13*, 196–199.

(154) Bhakuni, D. S.; Mangla, V. K. *Tetrahedron* **1981**, *37*, 401–407.

(155) Govindachari, T. R.; Viswanathan, N. *Tetrahedron* **1970**, *26*, 715–719.

(156) Comins, D. L.; Chen, X.; Morgan, L. A. *J. Org. Chem.* **1997**, *62*, 7435–7438.

(157) Yamano, Y.; Ito, M. *Chem. Pharm. Bull. (Tokyo).* **2005**, *53*, 541–546.

(158) Bhandari, S. P. S.; Babu, U. V.; Garg, H.S. *Phytochemistry* **1998**, *47*, 1435–1436.

(159) Shoeb, M.; MacManus, S. M.; Kumarasamy, Y.; Jaspars, M.; Nahar, L.; Thoo-Lin, P. K.; Nazemiyeh, H.; Sarker, S. D. *Phytochemistry* **2006**, *67*, 2370–2375.

(160) Wang, Y. H.; Hou, A. J.; Chen, L.; Chen, D. F.; Sun, H. D.; Zhao, Q. S.; Bastow, K. F.; Nakanish, Y.; Wang, X. H.; Lee, K. H. *J. Nat. Prod.* **2004**, *67*, 757–761.

(161) Yoshio Hano; Matsumoto, Y.; Shinohara, K.; Sun, J. Y.; Nomura, T. *Heterocycles* **1990**, *31*, 1339.

(162) Micheletti, A. C.; Beatriz, A.; Lima, D. P.; Honda, N. K.; Pessoa, C. Ó.; Moraes, M. O.; Lotufo, L. V; Magalhães, H. I. F.; Carvalho, N. C. P. *Quim. Nova* **2009**, *32*, 12–20.

(163) Buitrago, A.; Rojas, J.; Valentina, C.; Bruno-Colmenarez, J.; de Delagado, G. D. *Boletín Latinoam. y del Caribe Plantas Med. y Aromáticas* **2010**, *9*, 470–474.

(164) Letcher, R. M. *Org. Mass Spectrom.* **1968**, *1*, 551–561.

(165) Prabu, G. R.; Gnanamani, A.; Sadulla, S. *J. Appl. Microbiol.* **2006**, *101*, 487–495.

(166) Fraisse, D.; Heitz, A.; Carnat, A.; Carnat, A. P.; Lamaison, J. L. *Fitoterapia* **2000**, *71*, 463–464.

(167) Kaouadji, M.; Thomasson, F.; Bennini, B.; Chulia, A. J. *Phytochemistry* **1992**, *31*, 2483–2486.

(168) Agrawal, P. K. *Phytochemistry* **1992**, *31*, 3307–3330.

(169) Vvedenskaya, I. O.; Rosen, R. T.; Guido, J. E.; Russell, D. J.; Mills, K. A.; Vorsa, N. *J. Agric. Food Chem.* **2004**, *52*, 188–195.

(170) Markham, K. R.; Geiger, H. In *The flavonoids: Advances in research since 1984*; Harborne, J. B., Ed.; Chapman & Hall/CRC: Florida, 1994; pp. 441–497.

(171) Yan, X.; Murphy, B. T.; Hammond, G. B.; Vinson, J. A.; Neto, C. C. *J. Agric. Food Chem.* **2002**, *50*, 5844–5849.

(172) Alavi, S.; Yassa, N.; Hajiaghaee, R.; Matin Yekta, M.; Rezaei Ashtiani, N.; Ajani, Y.; Hadjiakhondi, A. *Iran. J. Pharm. Res.* **2010**, 71–75.

(173) Angyal, S. J. *Carbohydr. Res.* **1979**, *77*, 37–50.

(174) Colquhoun, I. J.; Morris, V. J.; Sutherland, I. W. *Carbohydr. Res.* **1989**, *187*, 103–115.

(175) Gorin, P. A. J.; Mazurek, M. *Can. J. Chem.* **1975**, *53*, 1212–1223.

(176) Berardini, N.; Schieber, A.; Klaiber, I.; Beifuss, U.; Carle, R.; Conrad, J. *Zeitschrift für Naturforsch. B* **2005**, *60*, 801–804.

(177) Ulubelen, A.; Topcu, G.; Kolak, U. In *Studies in Natural Products Chemistry*; Atta-ur-Rahman, Ed.; Studies in Natural Products Chemistry; Elsevier: Amsterdam, 2005; Vol. 30, pp. 233–302.

(178) Syah, Y. M.; Achmad, S. A.; Ghisalberti, E. L.; Hakim, E. H.; Makmur, L.; Mujahidin, D. *Fitoterapia* **2001**, *72*, 765–773.

(179) Granica, S.; Czerwińska, M. E.; Zyżyńska-Granica, B.; Kiss, A. K. *Fitoterapia* **2013**, *91*, 180–188.

(180) Komatsu, M.; Yokoe, I.; Shirataki, Y. *Chem. Pharm. Bull. (Tokyo).* **1978**, *26*, 3863–3870.

(181) Parsons, I. C.; Gray, A. I.; Waterman, P. G.; Hartley, T. G. *J. Nat. Prod.* **1993**, *56*, 46–53.

(182) Ray, T. K.; Misra, D. R.; Khastgir, H. N. *Phytochemistry* **1975**, *14*, 1876–1877.

(183) Chen, K.; Chang, F.; Chia, Y.; Wu, T.; Wu, Y. *J. Chinese Chem. Soc.* **1998**, *45*, 103–110.

(184) Markstädter, C.; Federle, W.; Jetter, R.; Riederer, M.; Hölldobler, B. *Chemoecology* **2000**, *10*, 33–40.

(185) Liu, K. C.; Yen, C. Y.; Wu, R. S. C.; Yang, J. S.; Lu, H. F.; Lu, K. W.; Lo, C.; Chen, H. Y.; Tang, N. Y.; Wu, C. C.; Chung, J. G. *Environ. Toxicol.* **2014**, *29*, 428–439.

(186) Zhang, Y.; Chen, A. Y.; Li, M.; Chen, C.; Yao, Q. *J. Surg. Res.* **2008**, *148*, 17–23.

(187) Ko, F. N.; Cheng, Z. J.; Lin, C. N.; Teng, C. M. *Free Radic. Biol. Med.* **1998**, *25*, 160–168.

(188) Repetto, G.; del Peso, A.; Zurita, J. L. *Nat. Protoc.* **2008**, *3*, 1125–1131.

(189) Shoemaker, R. H. *Nat. Rev. Cancer* **2006**, *6*, 813–823.

(190) Boik, J. *Natural compounds in cancer therapy*; Oregon Medical Press Princeton, NJ, 2001.

(191) Mahavorasirikul, W.; Viyanant, V.; Chaijaroenkul, W.; Itharat, A.; Na-Bangchang, K. *BMC Complement. Altern. Med.* **2010**, *10*, 1–8.

(192) Williamson, E. M. *Phytomedicine* **2001**, *8*, 401–409.

(193) Ma, J.-P.; Qiao, X.; Pan, S.; Shen, H.; Zhu, G. F.; Hou, A. J. *J. Asian Nat. Prod. Res.* **2010**, *12*, 586–592.

(194) Baskić, D.; Popović, S.; Ristić, P.; Arsenijević, N. N. *Cell Biol. Int.* **2006**, *30*, 924–932.

(195) Ramasamy, S.; Abdul Wahab, N.; Zainal Abidin, N.; Manickam, S.; Zakaria, Z. *PLoS One* **2012**, *7*, e34793.

(196) Lim, S. W.; Ting, K. N.; Bradshaw, T. D.; Zeenathul, N. A.; Wiart, C.; Khoo, T. J.; Lim, K. H.; Loh, H. S. *J. Ethnopharmacol.* **2011**, *138*, 616–623.

(197) Zong, W. X.; Thompson, C. B. *Genes Dev.* **2006**, *20*, 1–15.

(198) Yeung, T. K.; Germond, C.; Chen, X.; Wang, Z. *Biochem. Biophys. Res. Commun.* **1999**, *263*, 398–404.

(199) Min, H. Y.; Chung, H. J.; Kim, E. H.; Kim, S.; Park, E. J.; Lee, S. K. *Biochem. Pharmacol.* **2010**, *80*, 1356–1364.

(200) Plehn-Dujowich, D.; Bell, P.; Ishov, A. M.; Baumann, C.; Maul, G. G. *Chromosoma* **2000**, *109*, 266–279.

(201) Huot, J.; Francois, H.; Rousseau, S.; Drschesnes, R. G.; Shah, G. M.; Landry, J. *J. Cell Biol.* **1998**, *143*, 1361–1373.

(202) Kleinsmith, L. J. *Principles of cancer biology*; Winslow, S., Ed.; 1st ed.; Benjamin Cummings: San Fransisco, California, 2005.

(203) Wang, L.; Wang, G.; Yang, D.; Guo, X.; Xu, Y.; Feng, B.; Kang, J. *Mol. Med. Rep.* **2013**, *8*, 1279–1285.

(204) Pan, M. H. *Carcinogenesis* **2002**, *23*, 1677–1684.

(205) Wang, Y.; Zhou, Y.; Zhou, H.; Jia, G.; Liu, J.; Han, B.; Cheng, Z.; Jiang, H.; Pan, S.; Sun, B. *PLoS One* **2012**, *7*, e43826.

(206) Svihálková-Sindlerová, L.; Foltinová, V.; Vaculová, A.; Horváth, V.; Soucek, K.; Sova, P.; Hofmanová, J.; Kozubík, A. *Anticancer Res.* **2010**, *30*, 1183–1188.

(207) Foster, D. A.; Yellen, P.; Xu, L.; Saqcena, M. *Genes and cancer* **2010**, *1*, 1124–1131.

(208) Ho, A.; Dowdy, S. F. *Curr. Opin. Genet. Dev.* **2002**, *12*, 47–52.

(209) Harbour, J. W.; Luo, R. X.; Dei Santi, A.; Postigo, A. A.; Dean, D. C. *Cell* **1999**, *98*, 859–869.

(210) Yam, C. H.; Fung, T. K.; Poon, R. Y. C. *Cell. Mol. Life Sci.* **2002**, *59*, 1317–1326.

(211) Henglein, B.; Chenivesse, X.; Wang, J.; Eick, D.; Bréchot, C. *Proc. Natl. Acad. Sci. U. S. A.* **1994**, *91*, 5490–5494.

(212) Gartel, A. L.; Radhakrishnan, S. K. *Cancer Res.* **2005**, *65*, 3980–3985.

(213) Hwang, H. C.; Clurman, B. E. *Oncogene* **2005**, *24*, 2776–2786.

(214) Nicoletti, I.; Migliorati, G.; Pagliacci, M. C.; Grignani, F.; Riccardi, C. *J. Immunol. Methods* **1991**, *139*, 271–279.

(215) Ainsworth, E. A.; Gillespie, K. M. *Nat. Protoc.* **2007**, *2*, 875–877.

(216) Miliauskas, G.; Venskutonis, P. R.; van Beek, T. A. *Food Chem.* **2004**, *85*, 231–237.

Appendices

Appendix 1: Comparison of total phenolic content and total flavonoid content among *Artocarpus* and *Macaranga* plants.

Table 1a: Total phenolic content (TPC) using Folin-Ciocalteu reagent [215]

Plant (ethyl acetate extracts)	Part	Total Phenolics (mg quercetin equivalents/ g plant extract)
A. heterophyllus x integer	Bark	29.60 ± 0.06
M. hypoleuca	Leaves	50.34 ± 0.01

Total phenolic compounds was determined from regression equation of calibration curve (y = 0.0582x + 0.0151, R^2= 0.98) and expressed in mg gallic acid equivalents. Data represent mean ± SD of 5 replicates (n=5).

Table 1b: Total flavonoid content (TFC) using ethanolic aluminium chloride solution[216]

Plant (ethyl acetate extracts)	Part	Total flavonoids (mg quercetin equivalents/ g plant extract)
A. heterophyllus x integer	Leaves	8.63±0.04
	Bark	46.23±0.05
A. heterophyllus	Leaves	8.81±0.06
	Bark	52.96±0.03
A. integer	Leaves	1.28±0.01
	Bark	17.63±0.04
M. hypoleuca	Leaves	47.68 ± 0.09
M. griffithiana	Leaves	18.018. ± 0.19

Total content of flavonoid compounds was determined from regression equation of calibration curve (y = 0.00166x + 0.0731, R^2= 0.9769) and expressed in mg quercetin equivalents. Data represent mean ± SD of 5 replicates (n=5).

Appendix 2: Comparison of anti-proliferative activity of the ethyl acetate bark extracts of *A. heterophyllus*, *A. integer* and the hybrid *A. heterophyllus x integer*

Table 2: Anti-proliferative activity of crude extracts against various cell lines using MTT assay

Plant extracts	Mean IC_{50} values (µg/ml)			
	A549	MCF-7	MDA-MB-231	HCT 116
A. heterophyllus x integer	46.77	60.26	>100	34.67
A. heterophyllus	2.11	10.96	>100	3.39
A. integer	6.81	20.89	>100	15.49

Data represents mean of IC_{50} values of triplicate samples conducted in three independent experiments

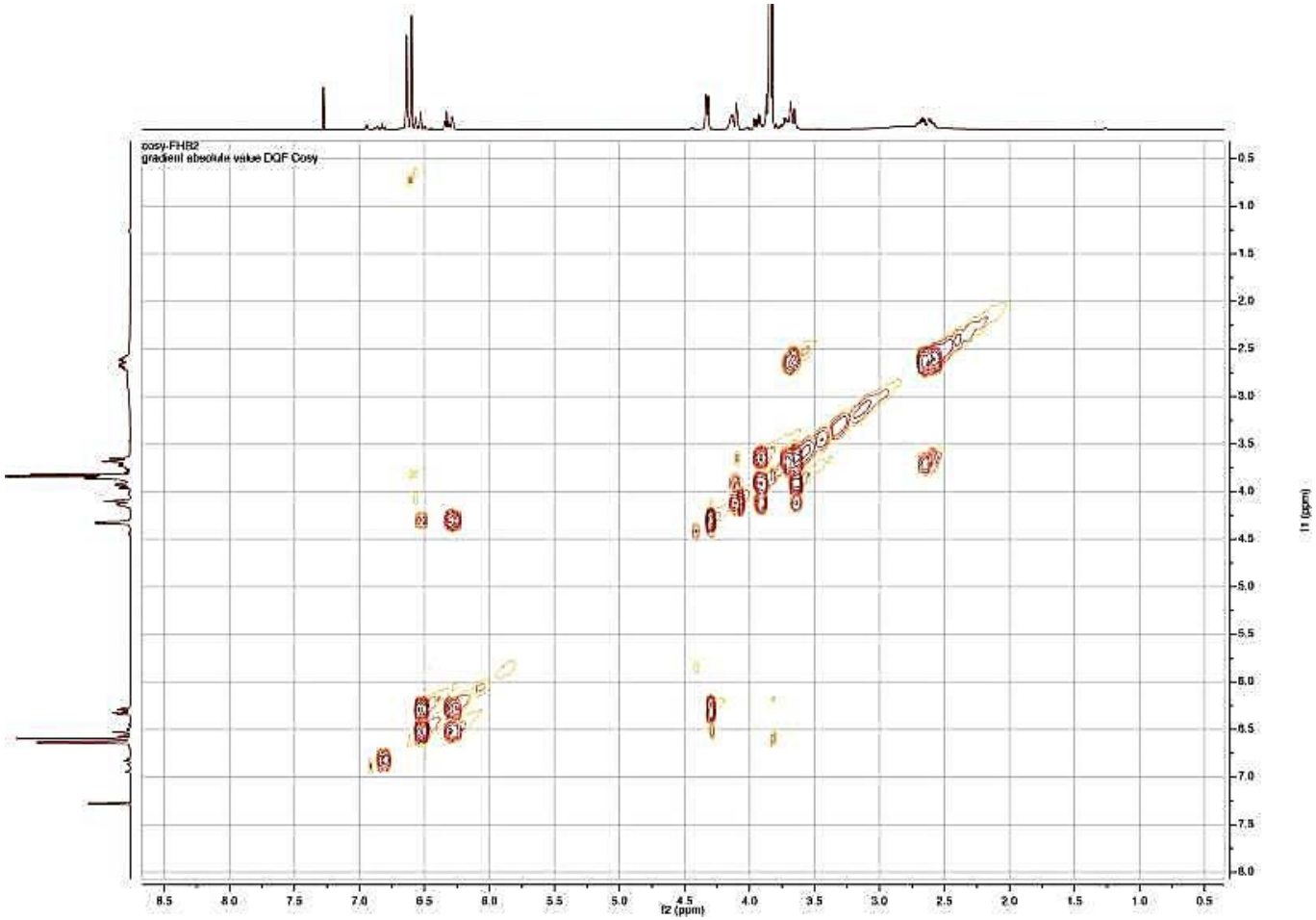

Appendix 3: COSY spectrum of hispidacine **(1)**

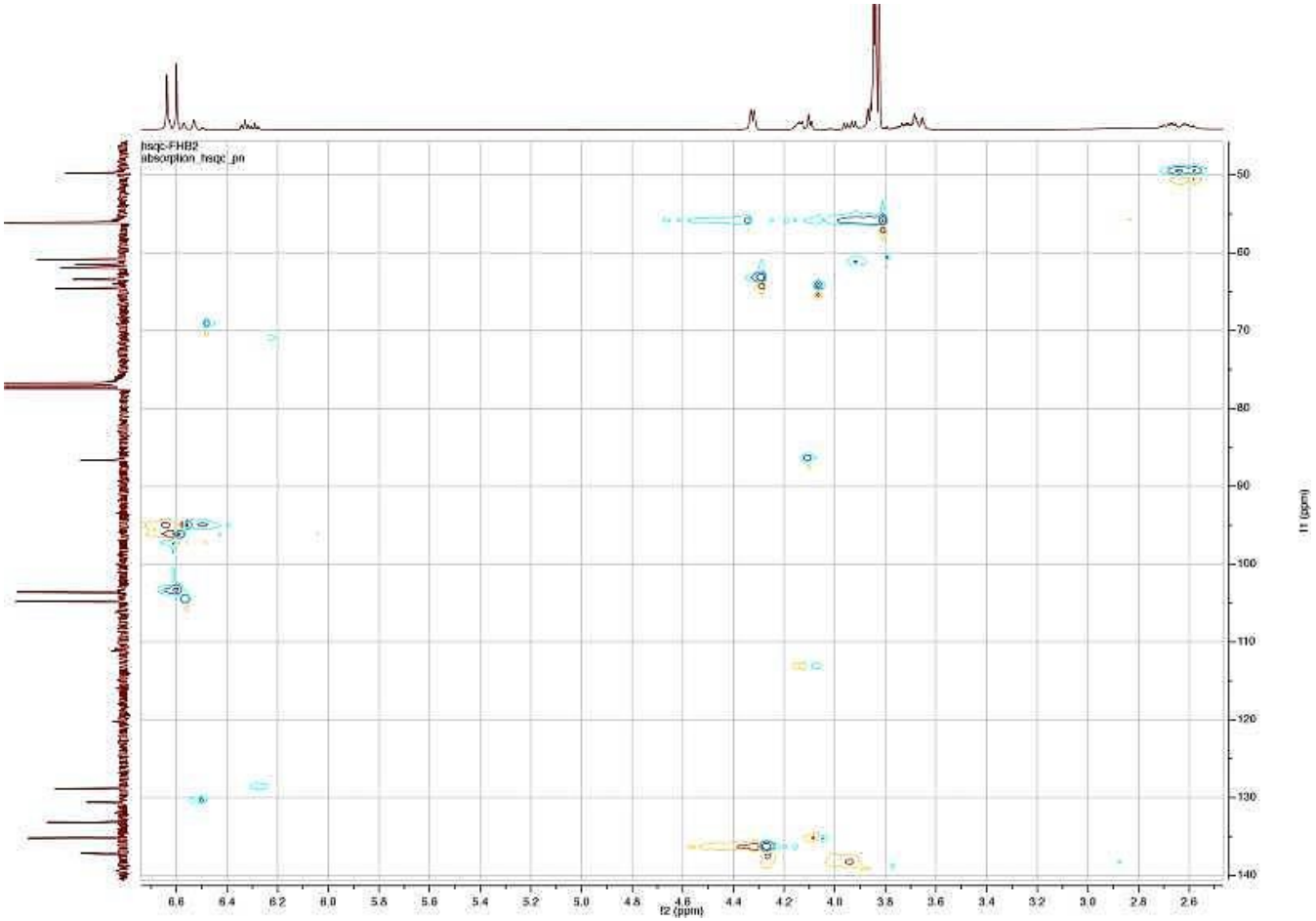

Appendix 4: HSQC spectrum of hispidacine **(1)**

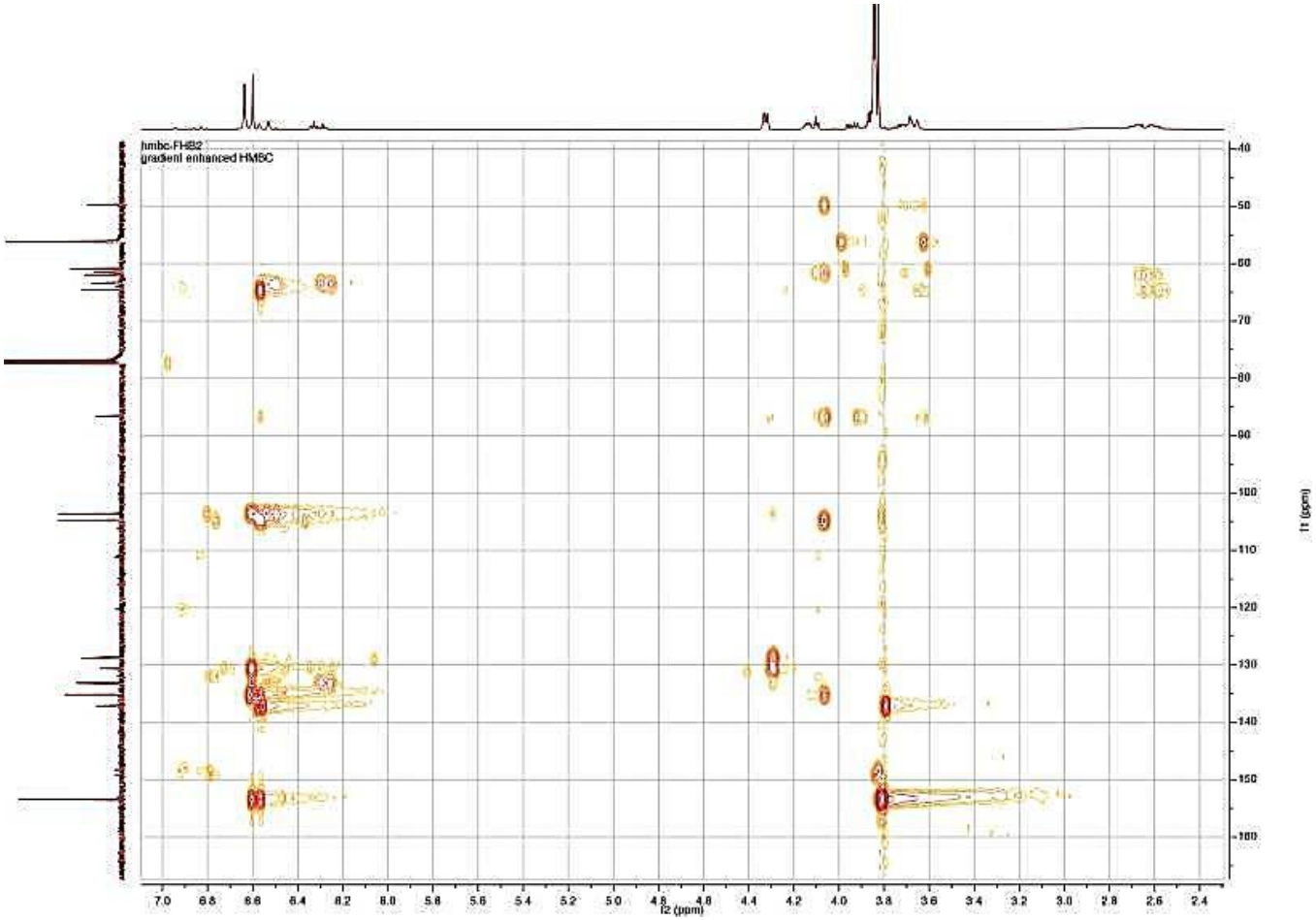

Appendix 5: HMBC spectrum of hispidacine **(1)**

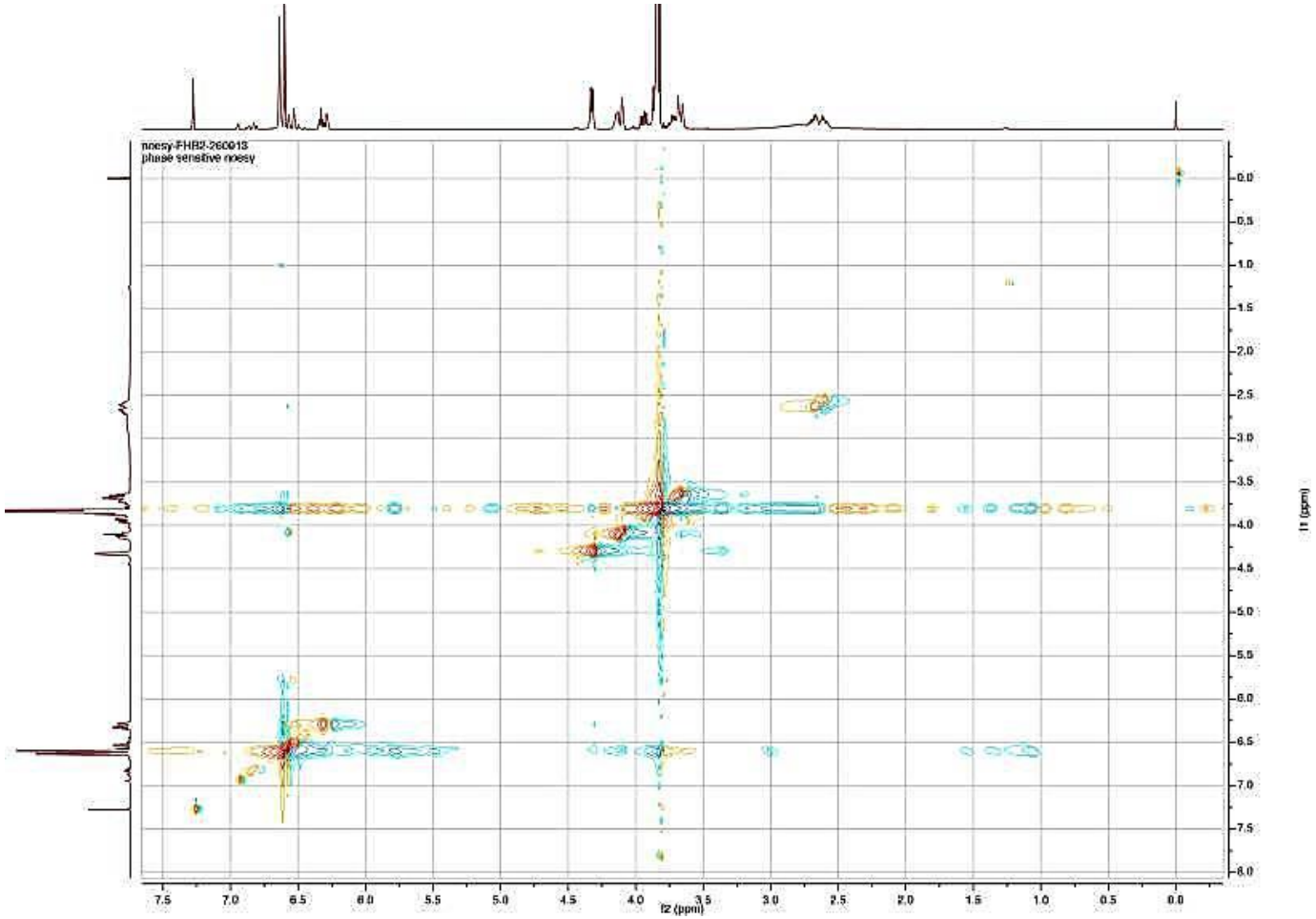

Appendix 6: NOESY spectrum of hispidacine **(1)**

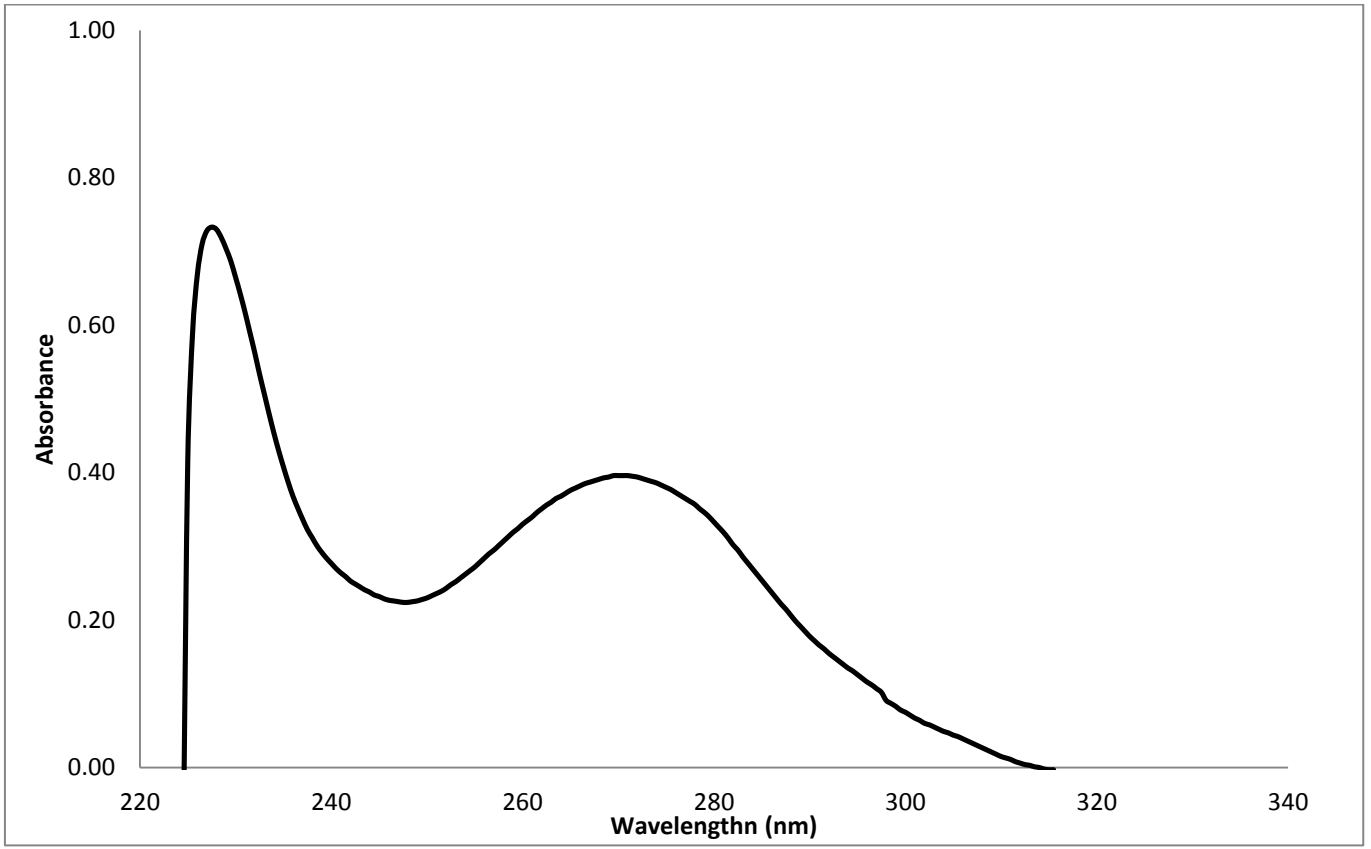

Appendix 7: UV spectrum of hispidacine **(1)**

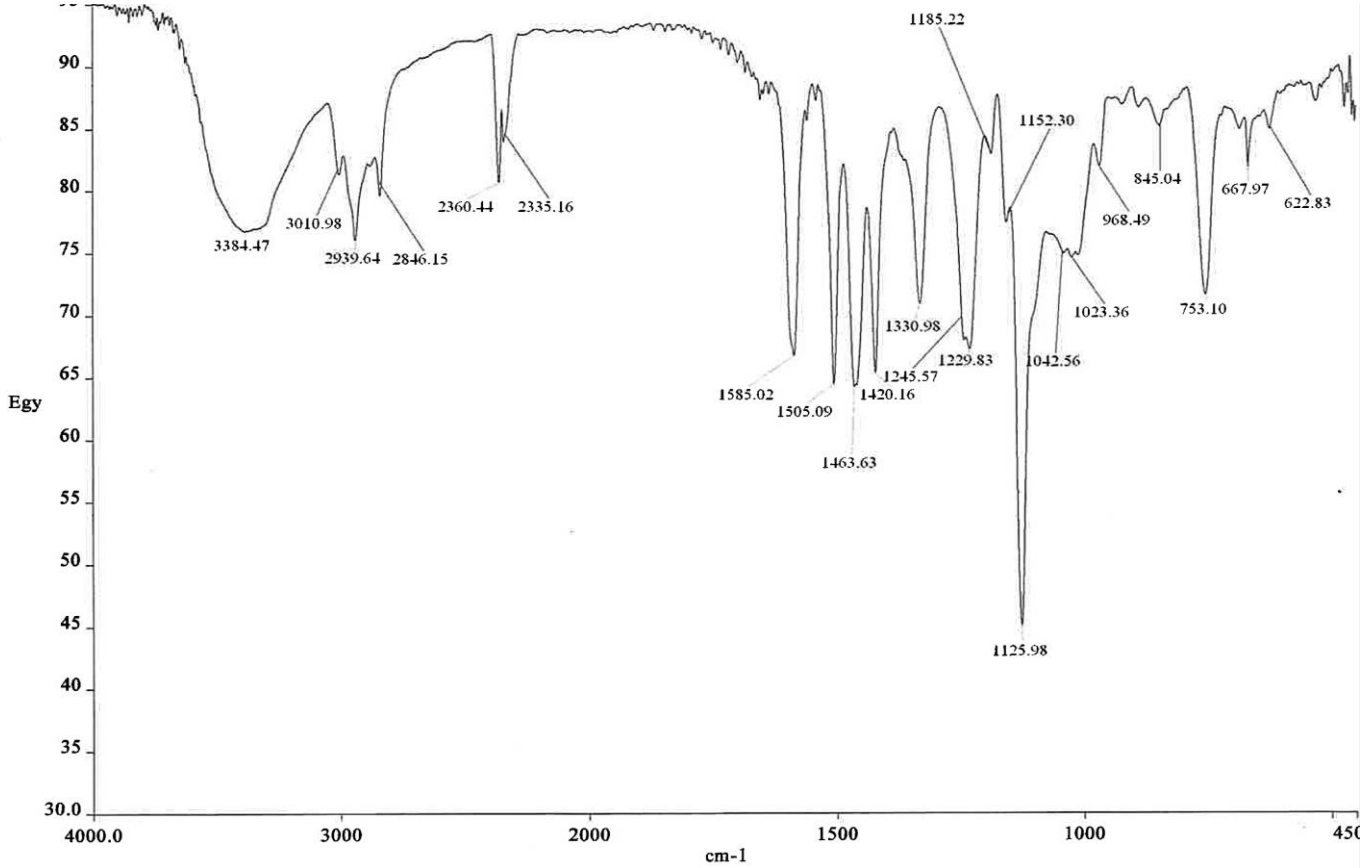

Appendix 8: IR spectrum of hispidacine **(1)**

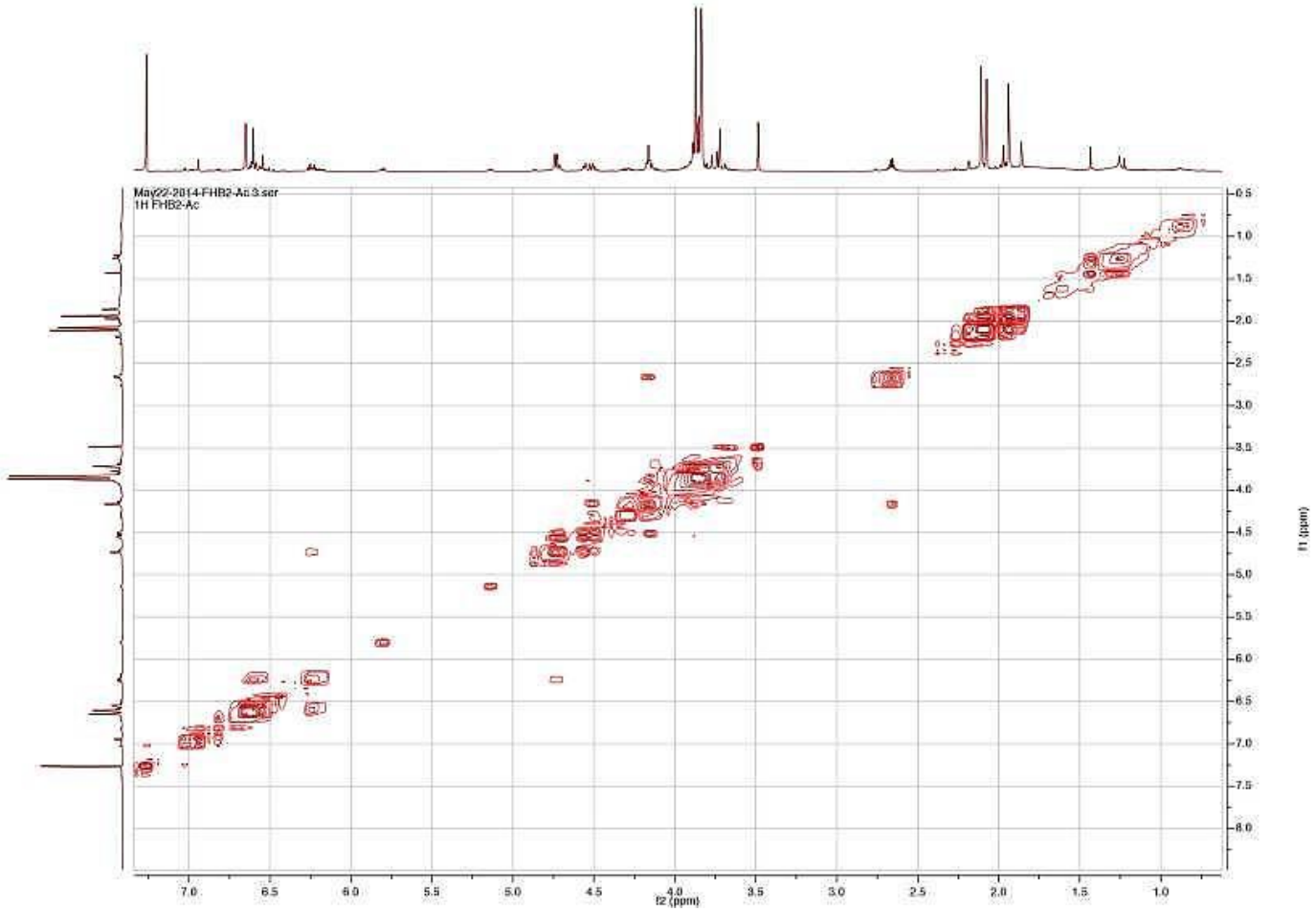

Appendix 9: COSY spectrum of hispidacine triacetate **(1a)**

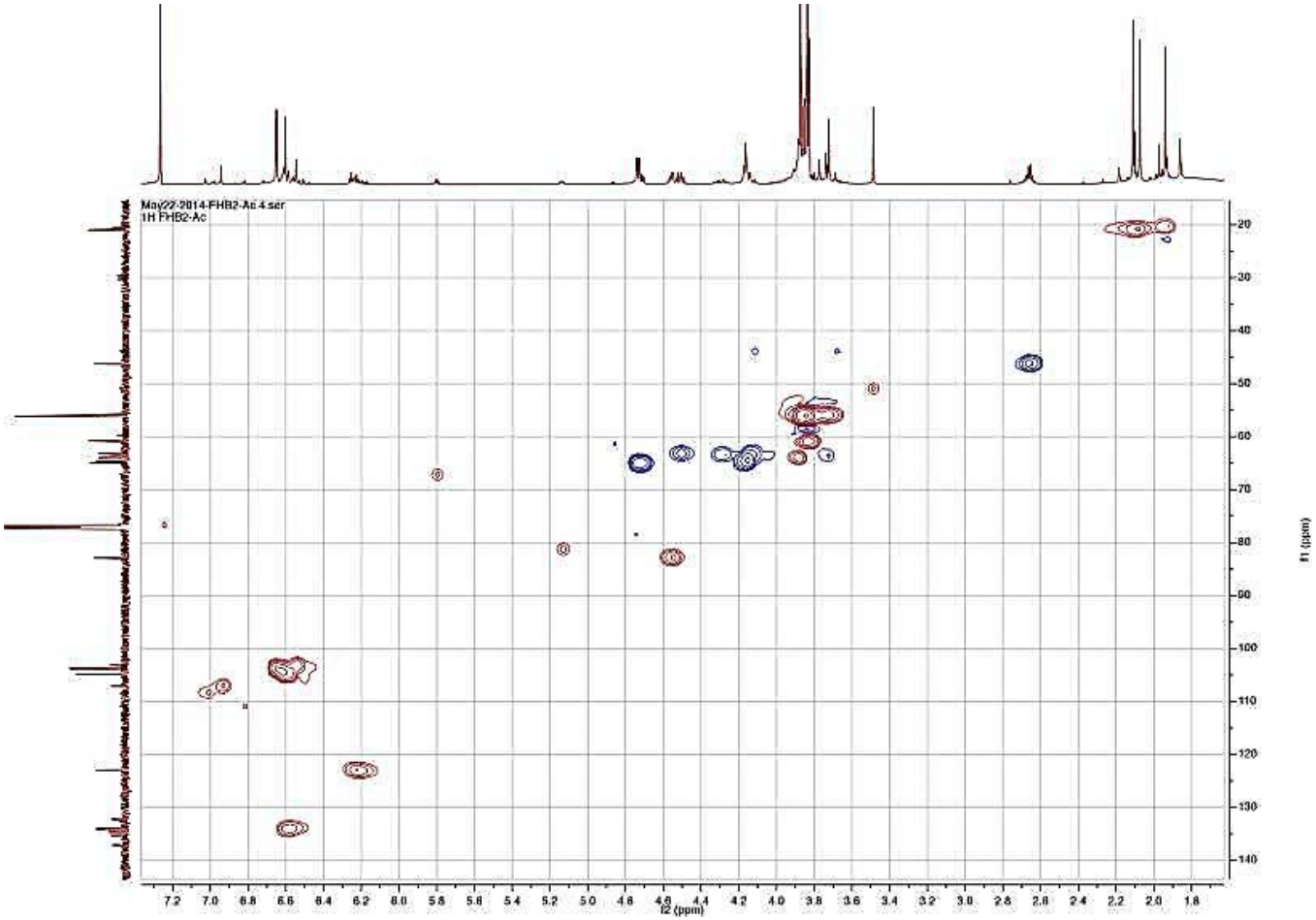

Appendix 10: HSQC spectrum of hispidacine triacetate **(1a)**

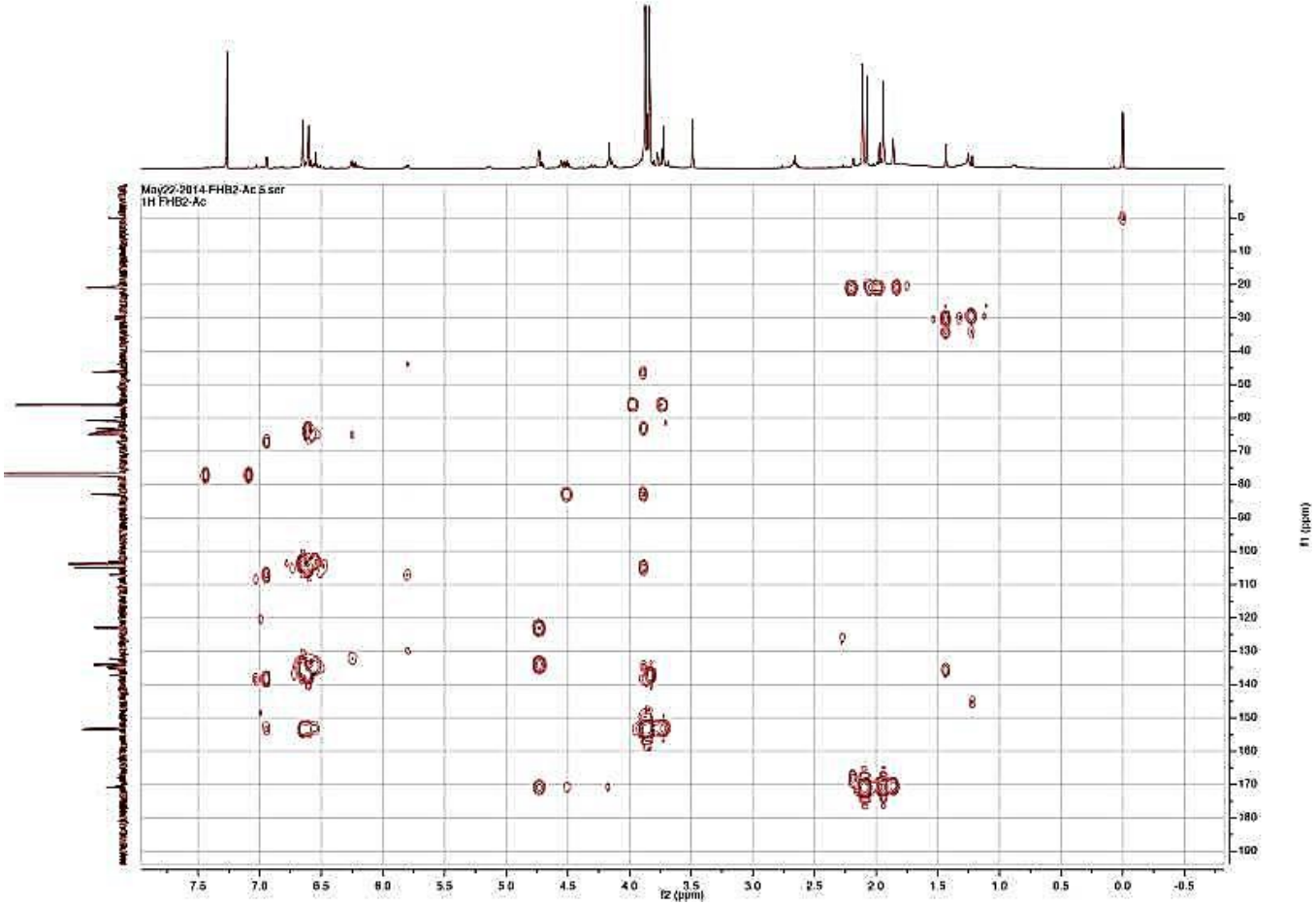

Appendix 11: HMBC spectrum of hispidacine triacetate **(1a)**

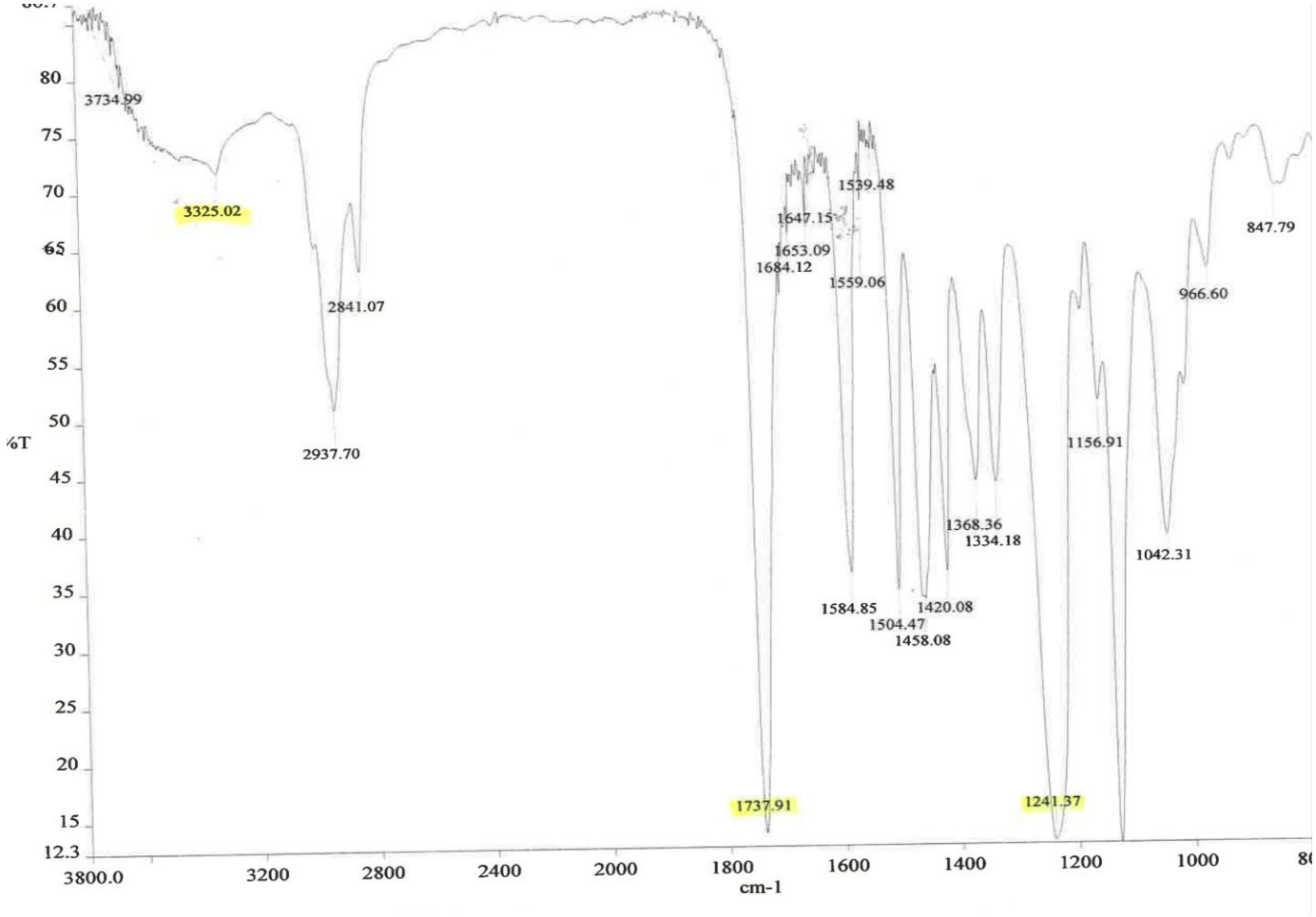

Appendix 12: IR spectrum of hispidacine triacetate **(1a)**

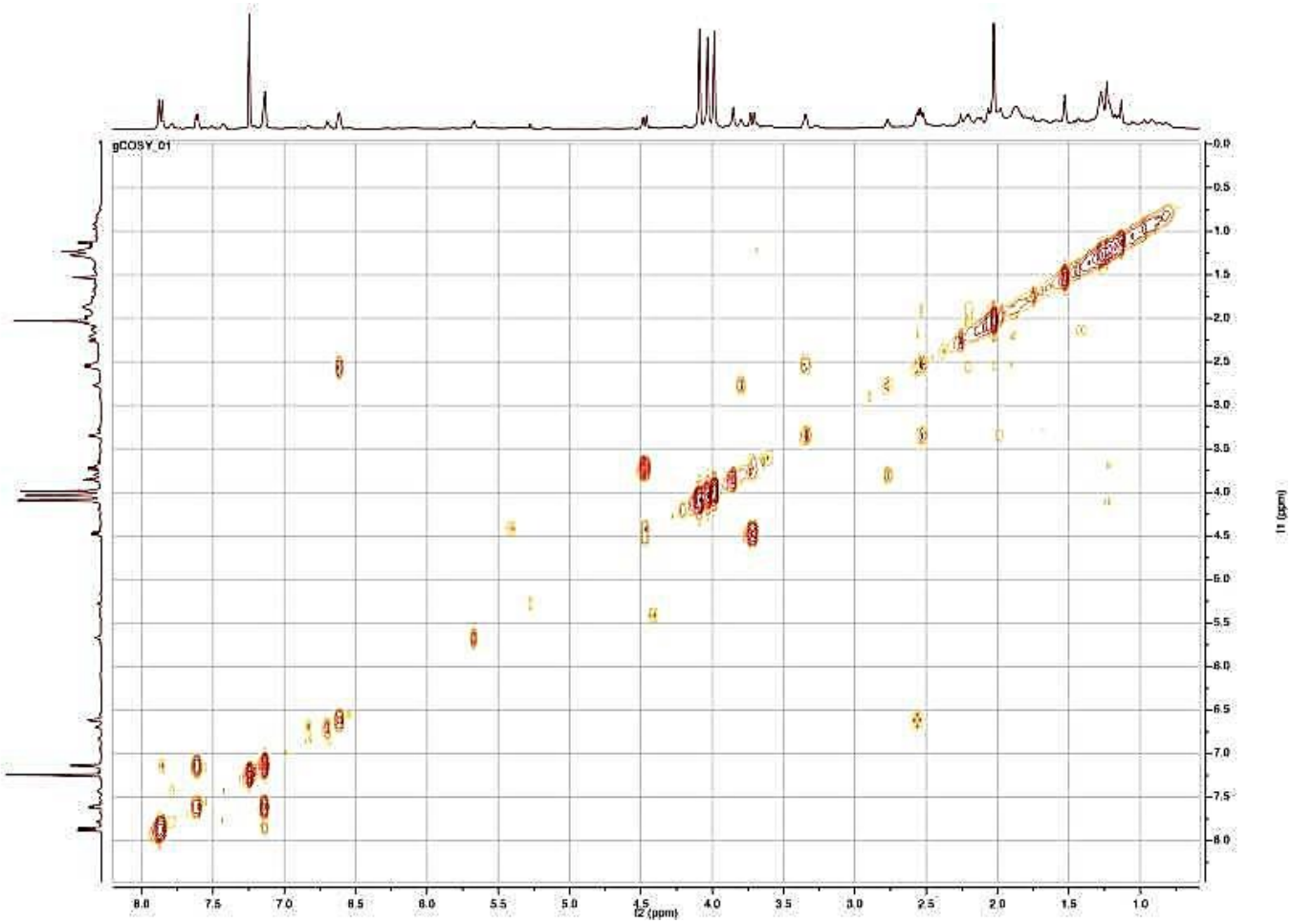

Appendix 13: COSY spectrum of hispiloscine **(3)**

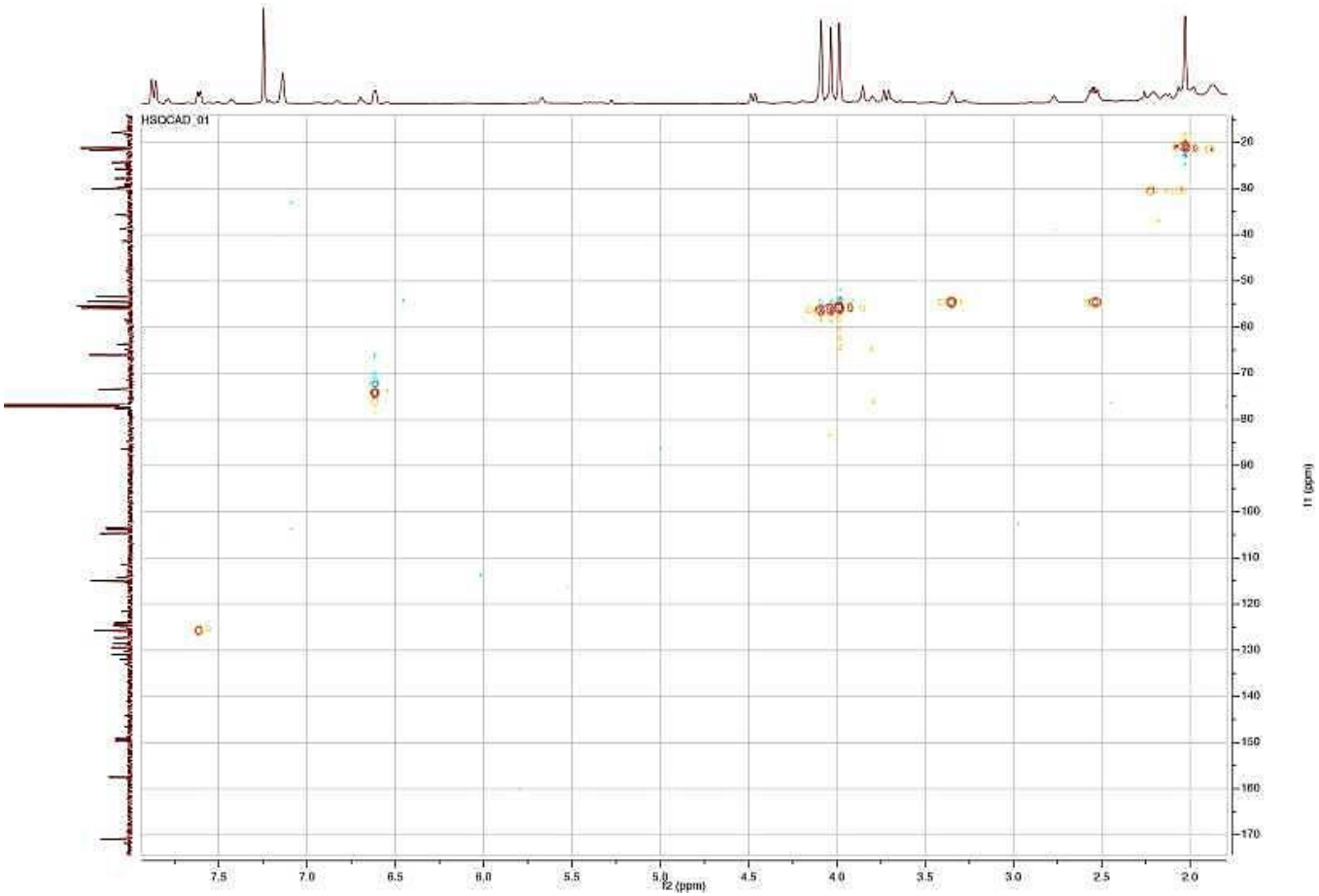

Appendix 14: HSQC spectrum of hispiloscine **(3)**

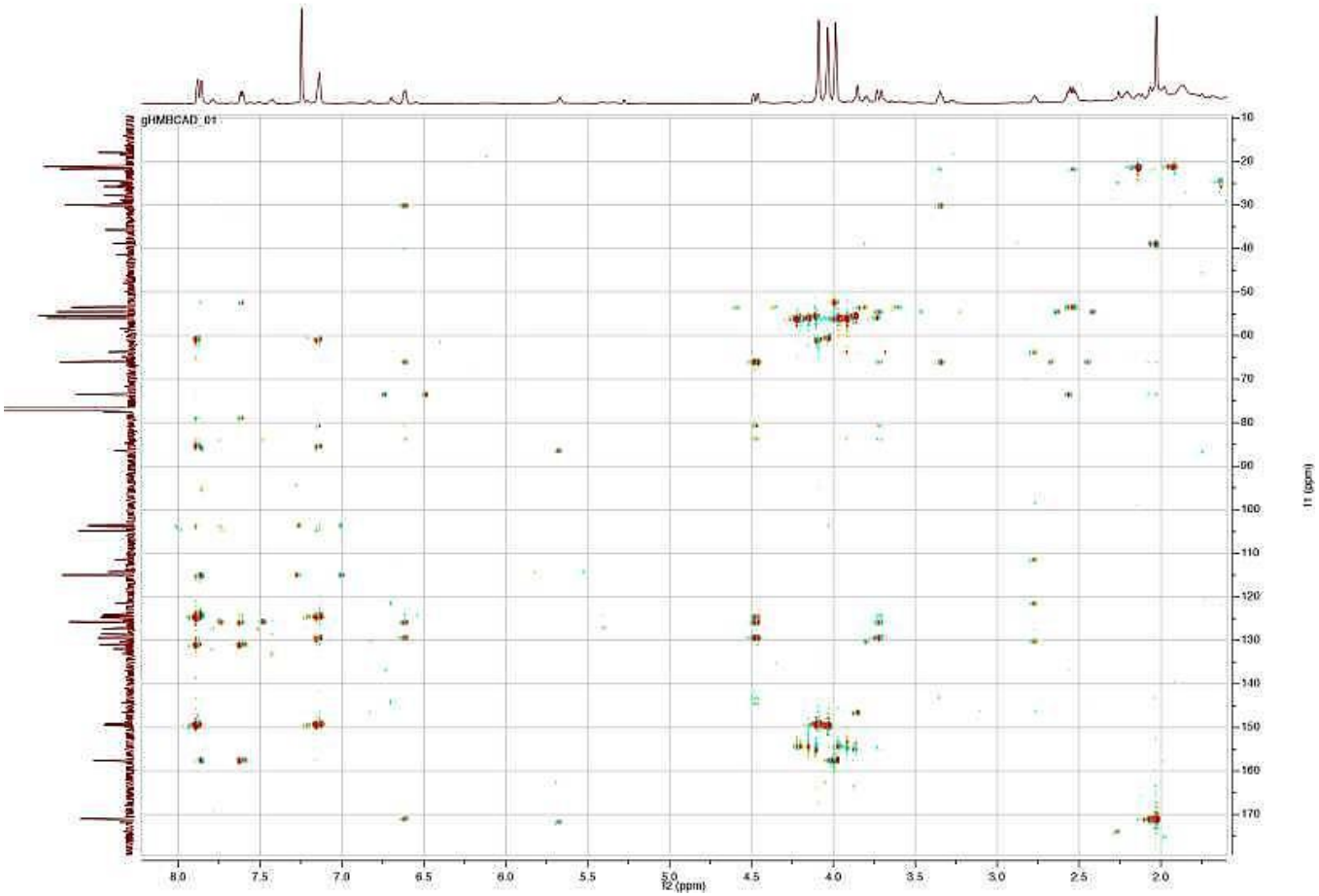

Appendix 15: HMBC spectrum of hispiloscine **(3)**

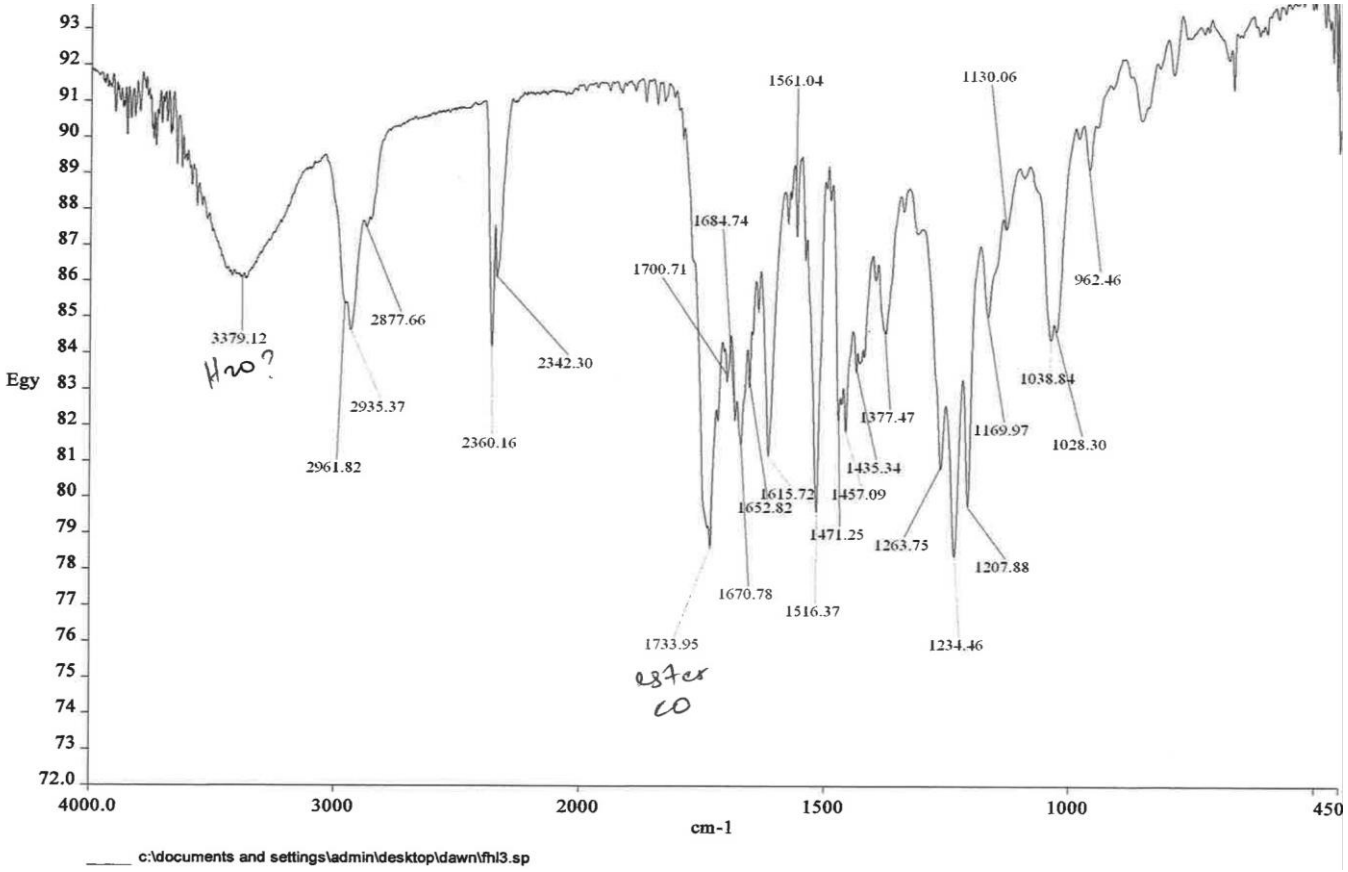

Appendix 16: IR spectrum of hispiloscine **(3)**

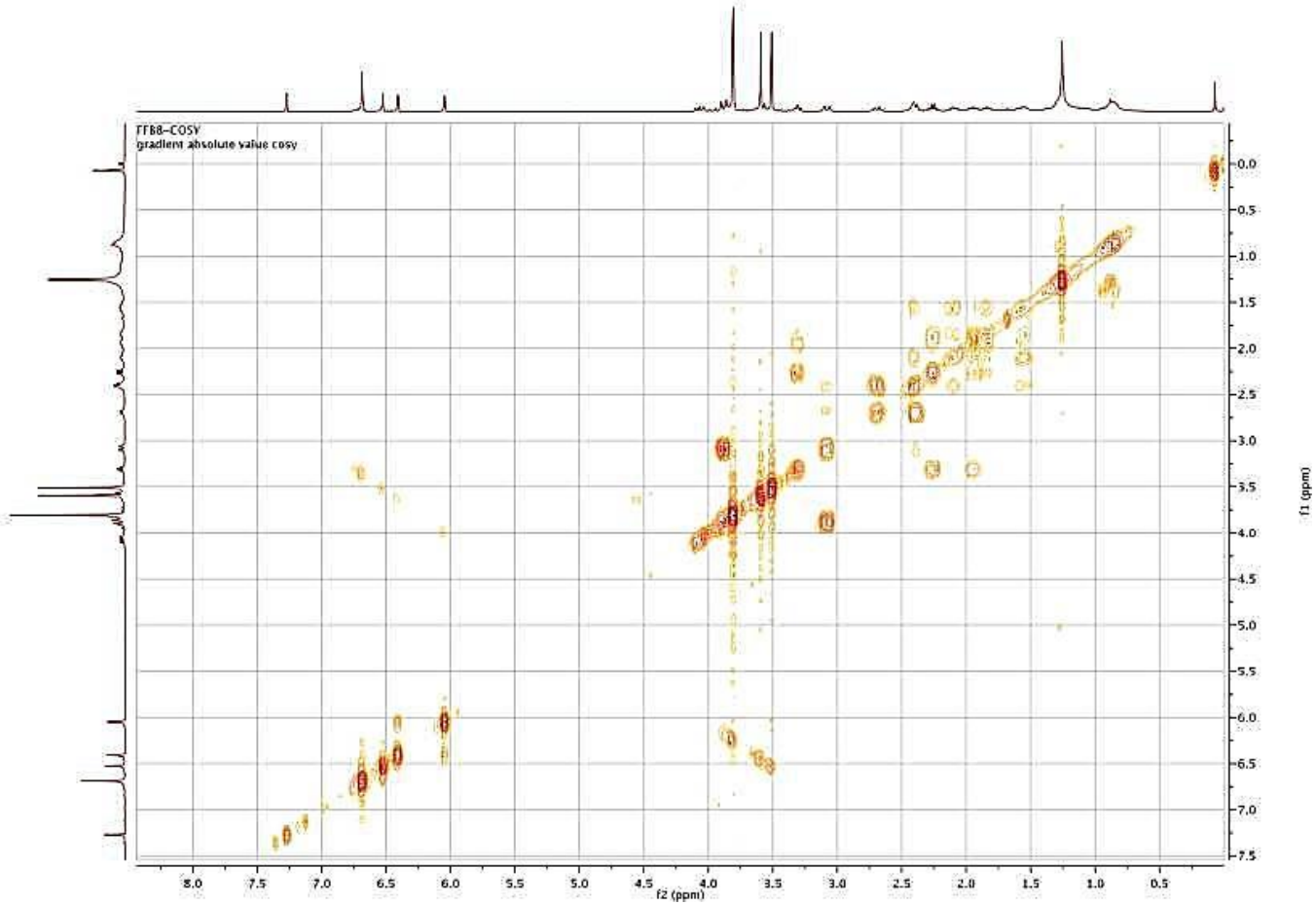

Appendix 17: COSY spectrum of fistulopsine A **(4)**

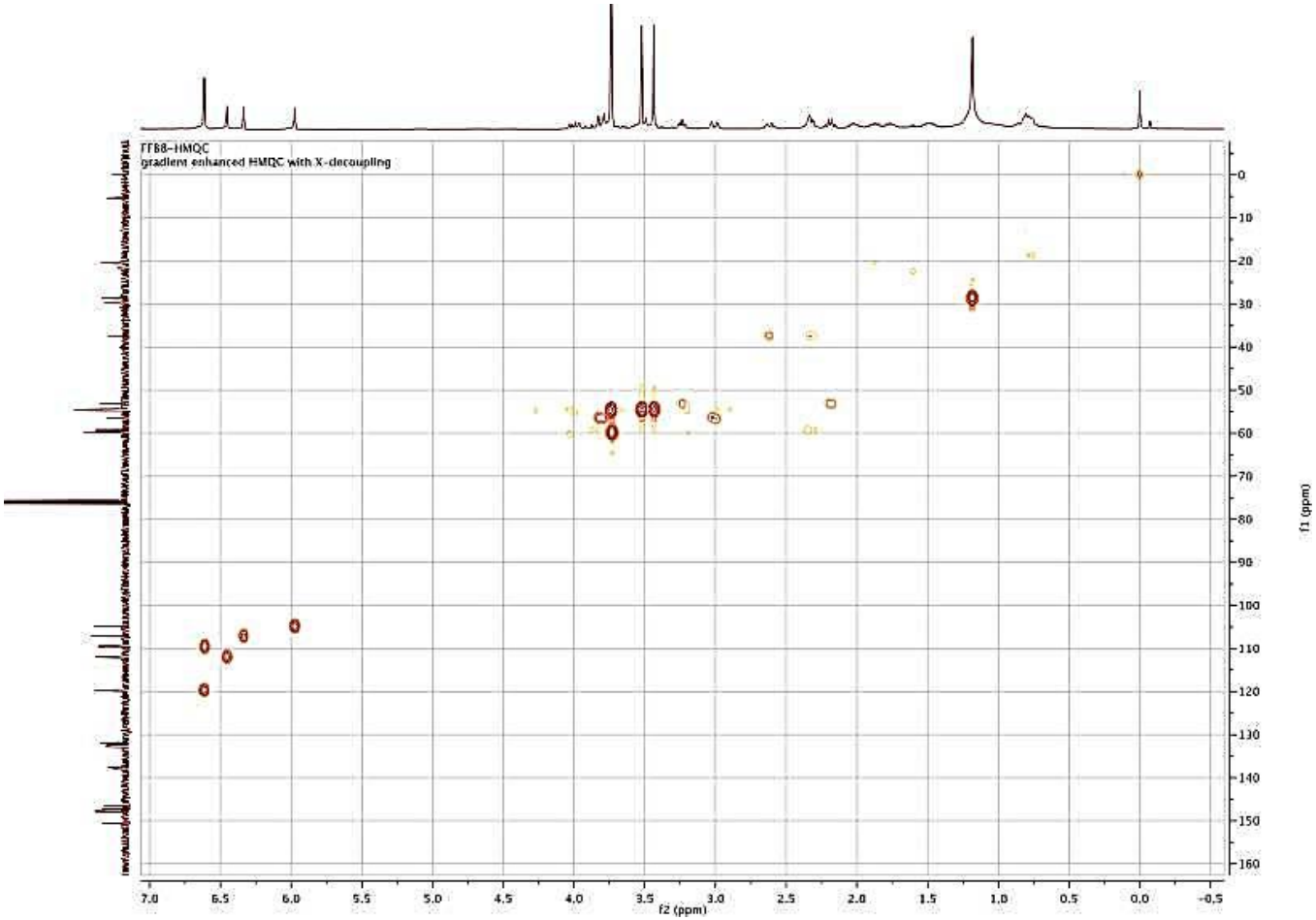

Appendix 18: HSQC spectrum of fistulopsine A **(4)**

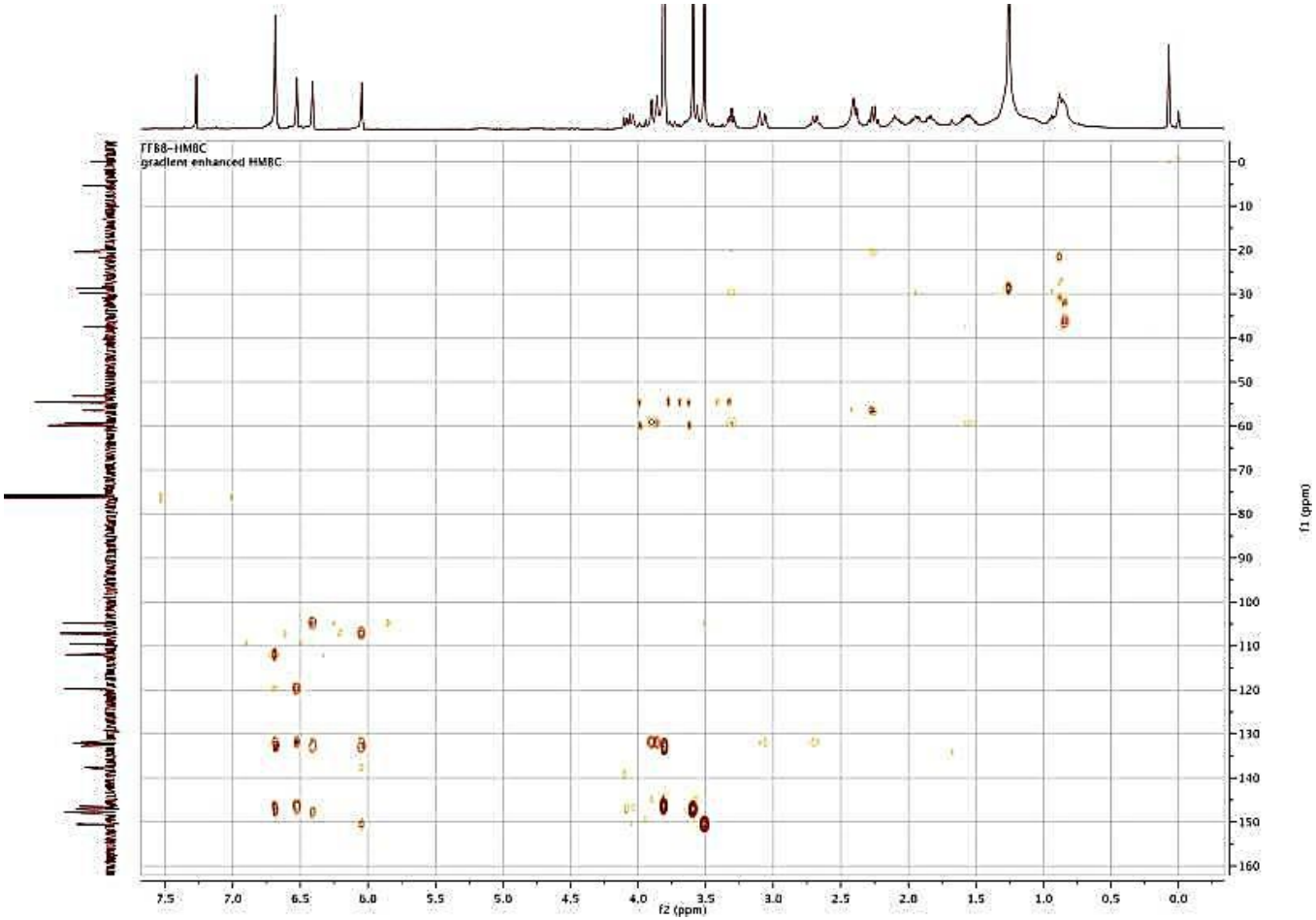

Appendix 19: HMBC spectrum of fistulopsine A **(4)**

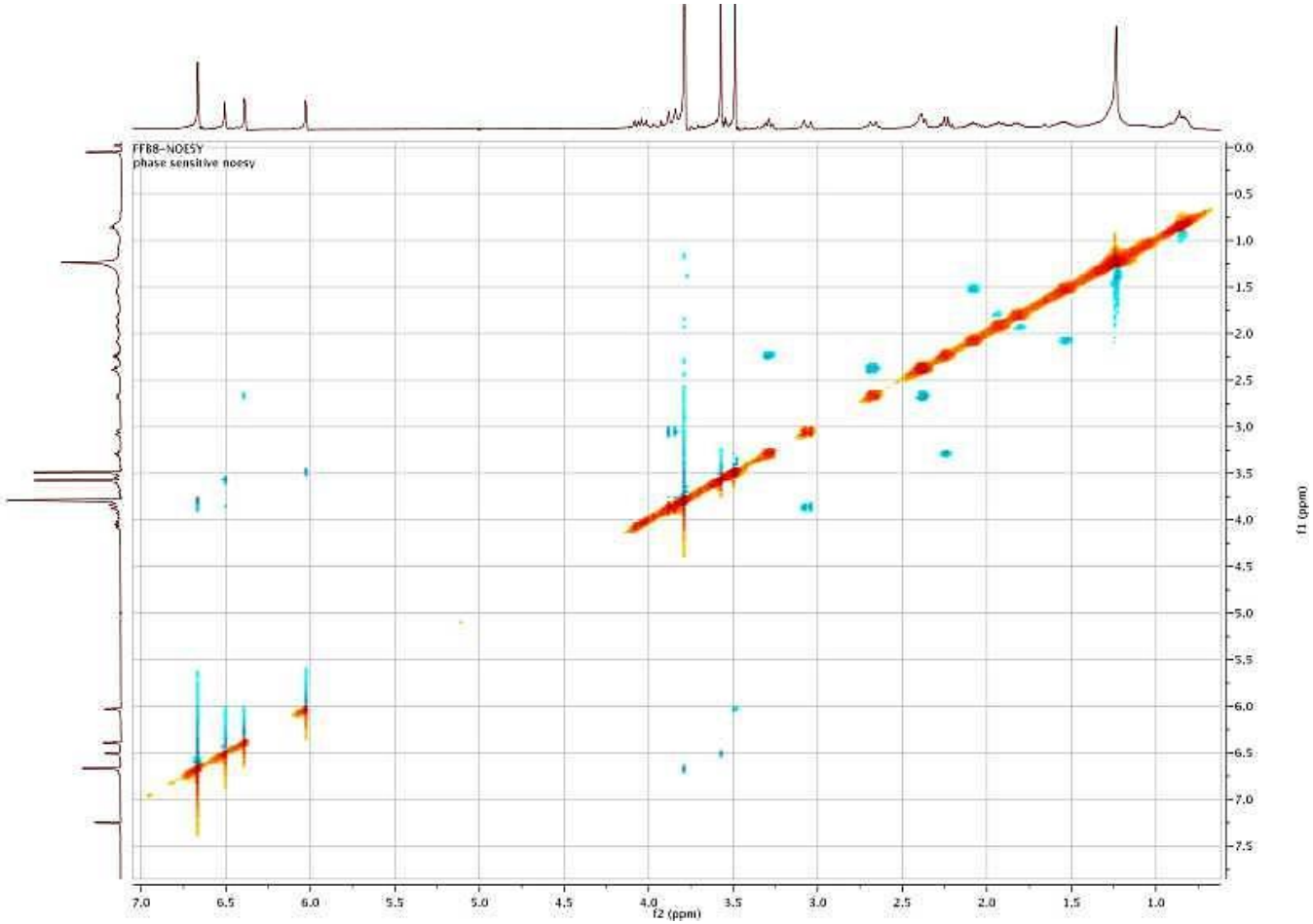

Appendix 20: NOESY spectrum of fistulopsine A **(4)**

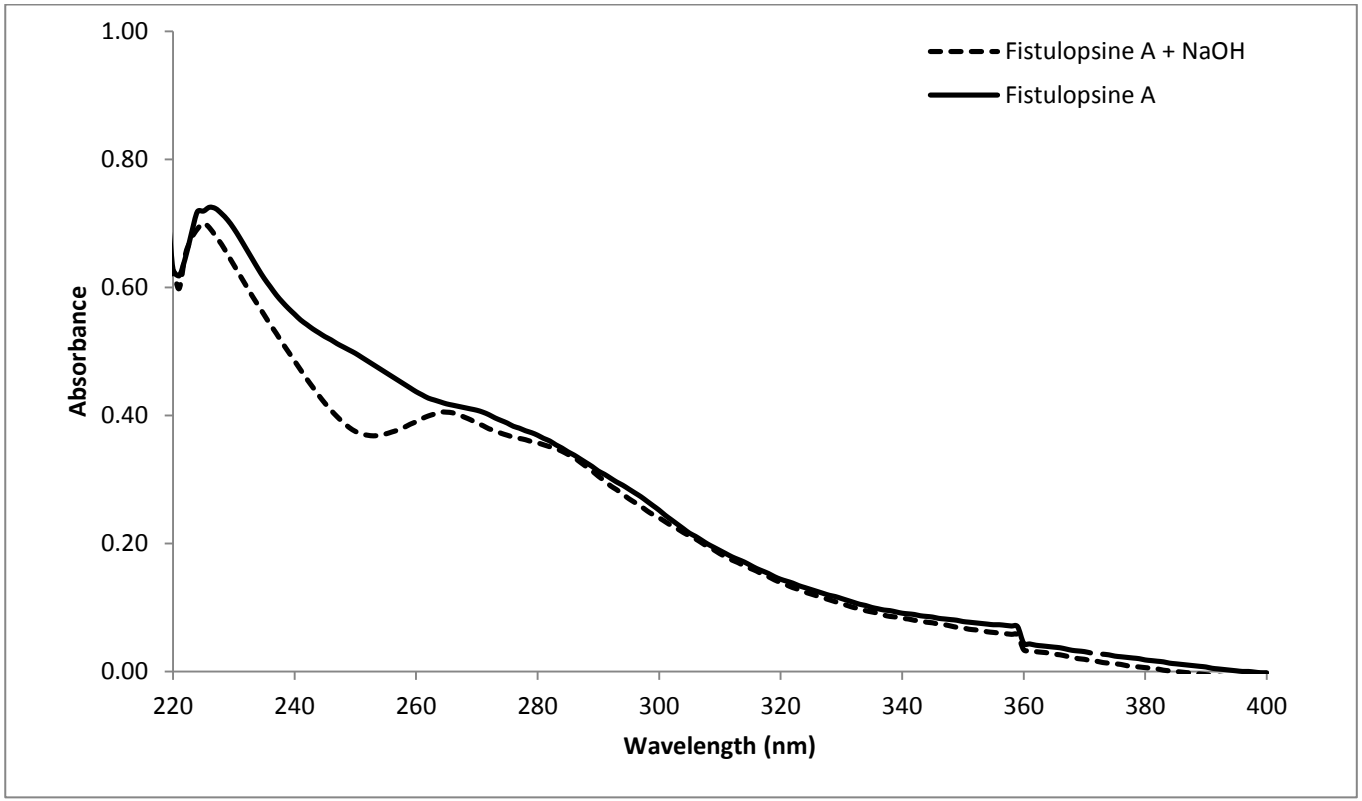

Appendix 21: UV spectrum of fistulopsine A **(4)**

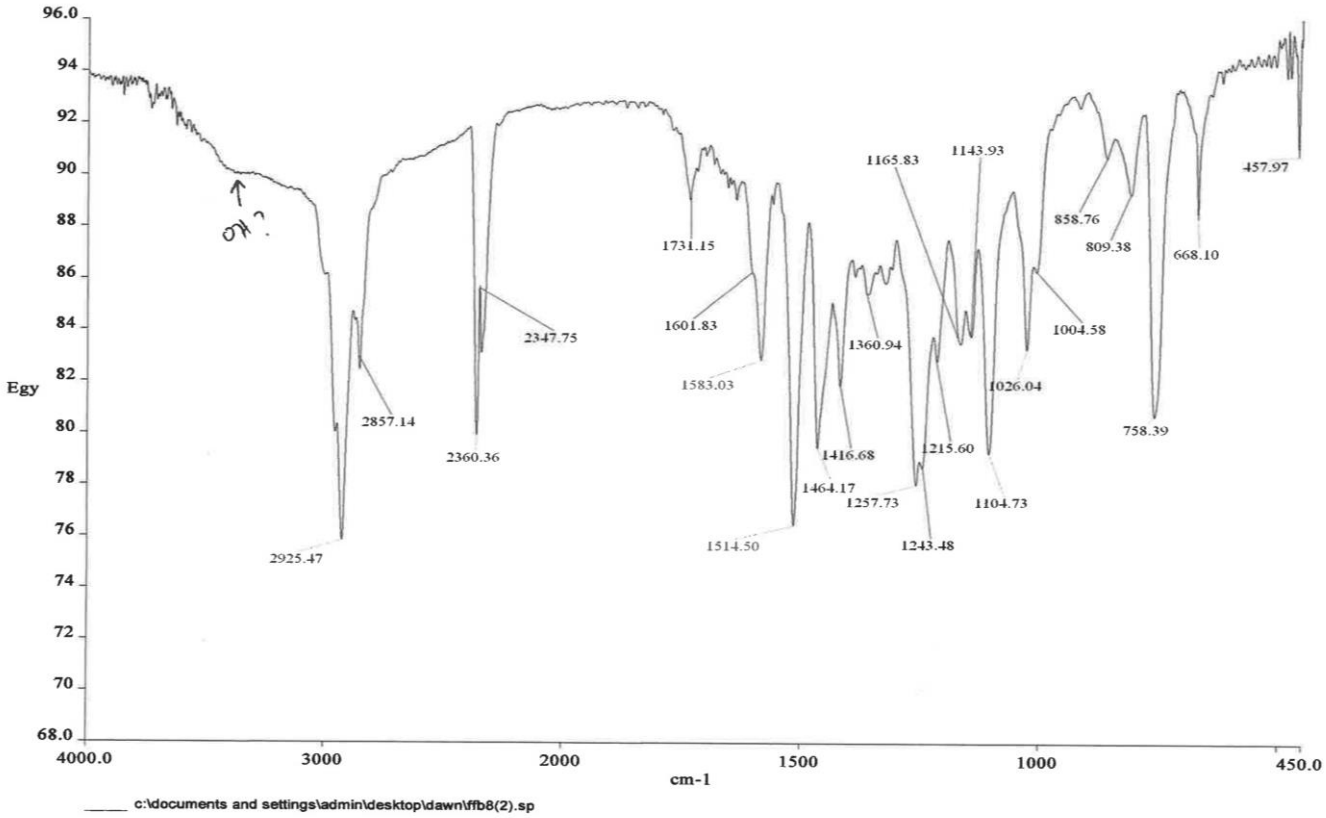

Appendix 22: IR spectrum of fistulopsine A **(4)**

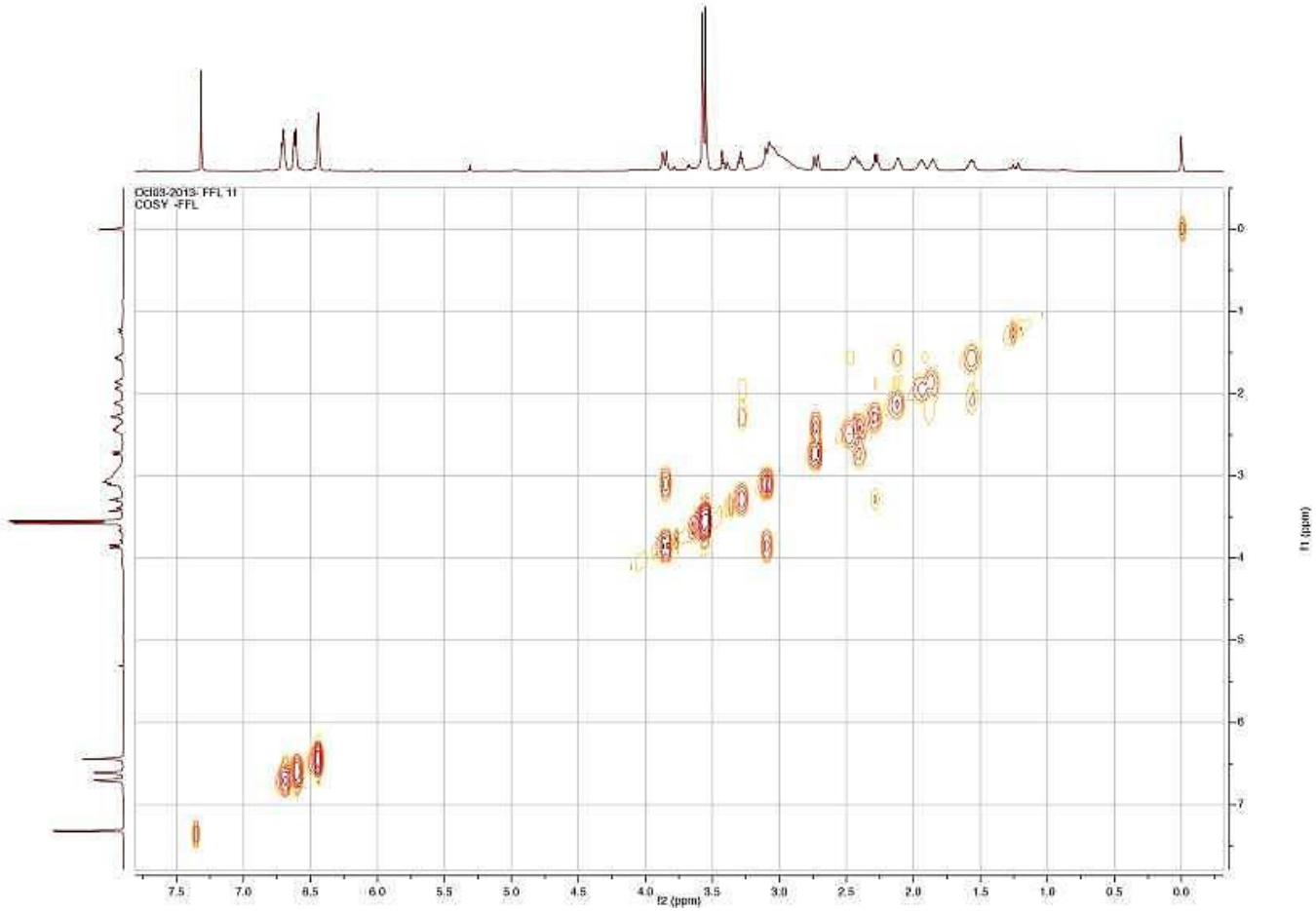

Appendix 23: COSY spectrum of fistulopsine B **(5)**

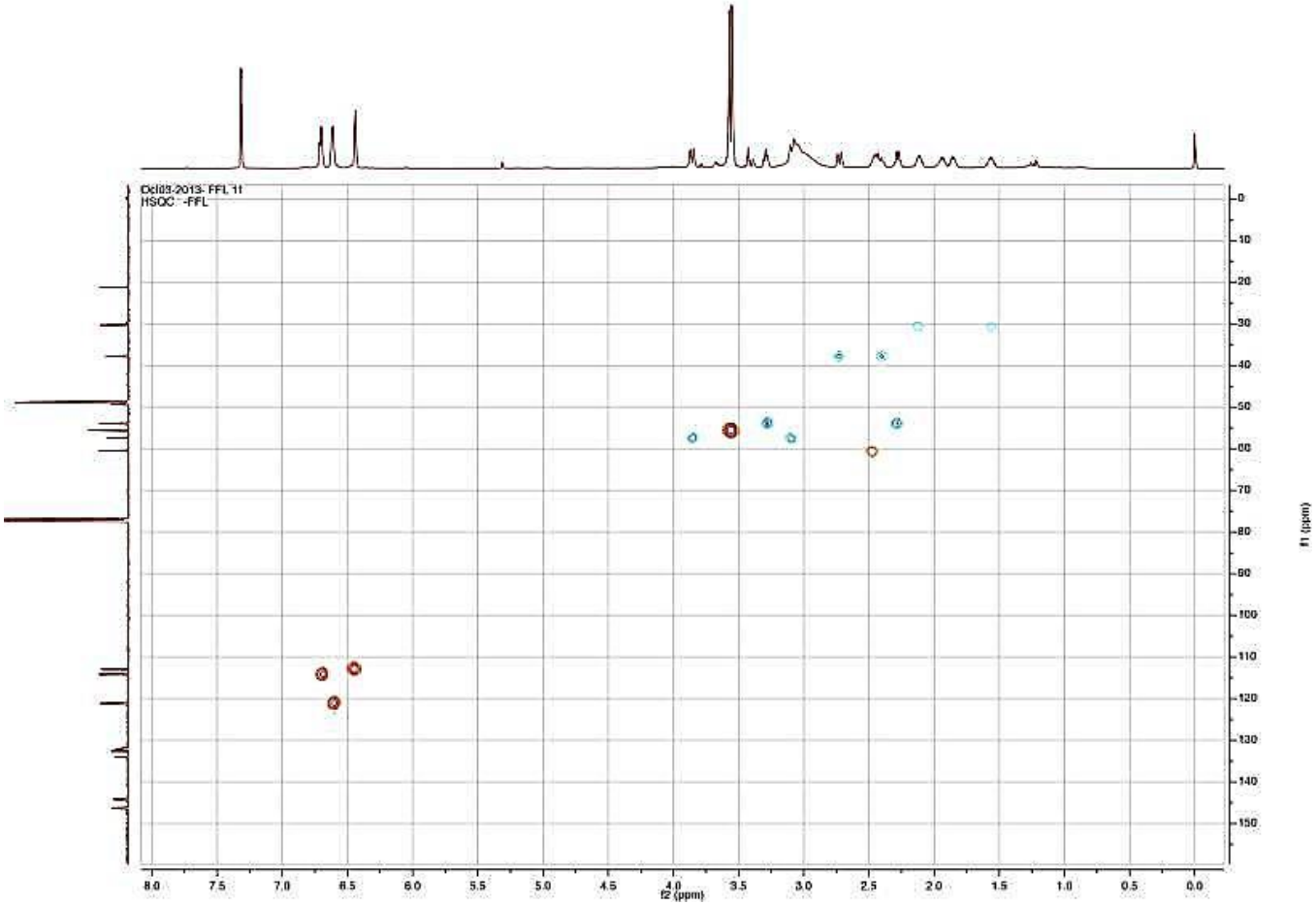

Appendix 24: HSQC spectrum of fistulopsine B **(5)**

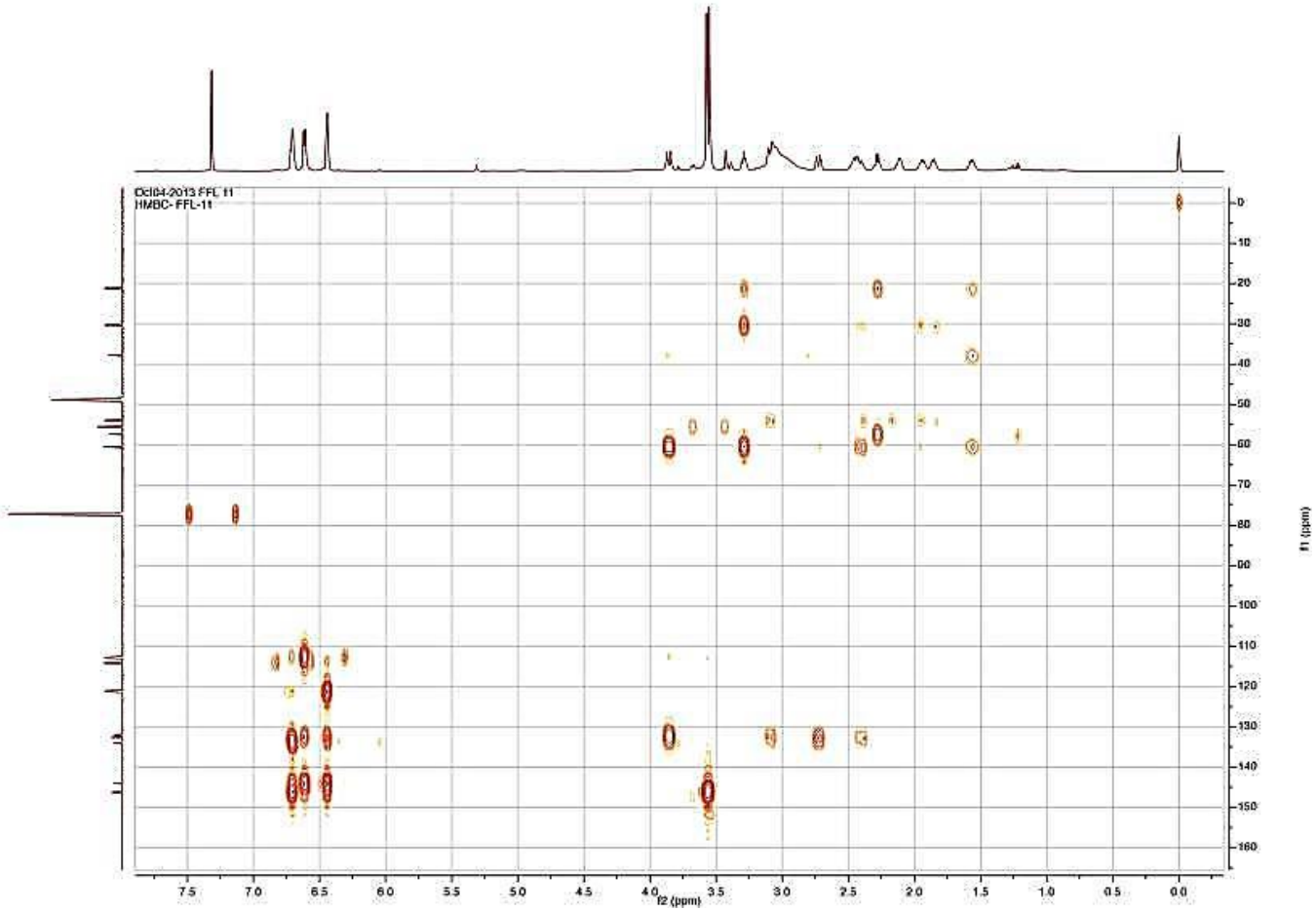

Appendix 25: HMBC spectrum of fistulopsine B **(5)**

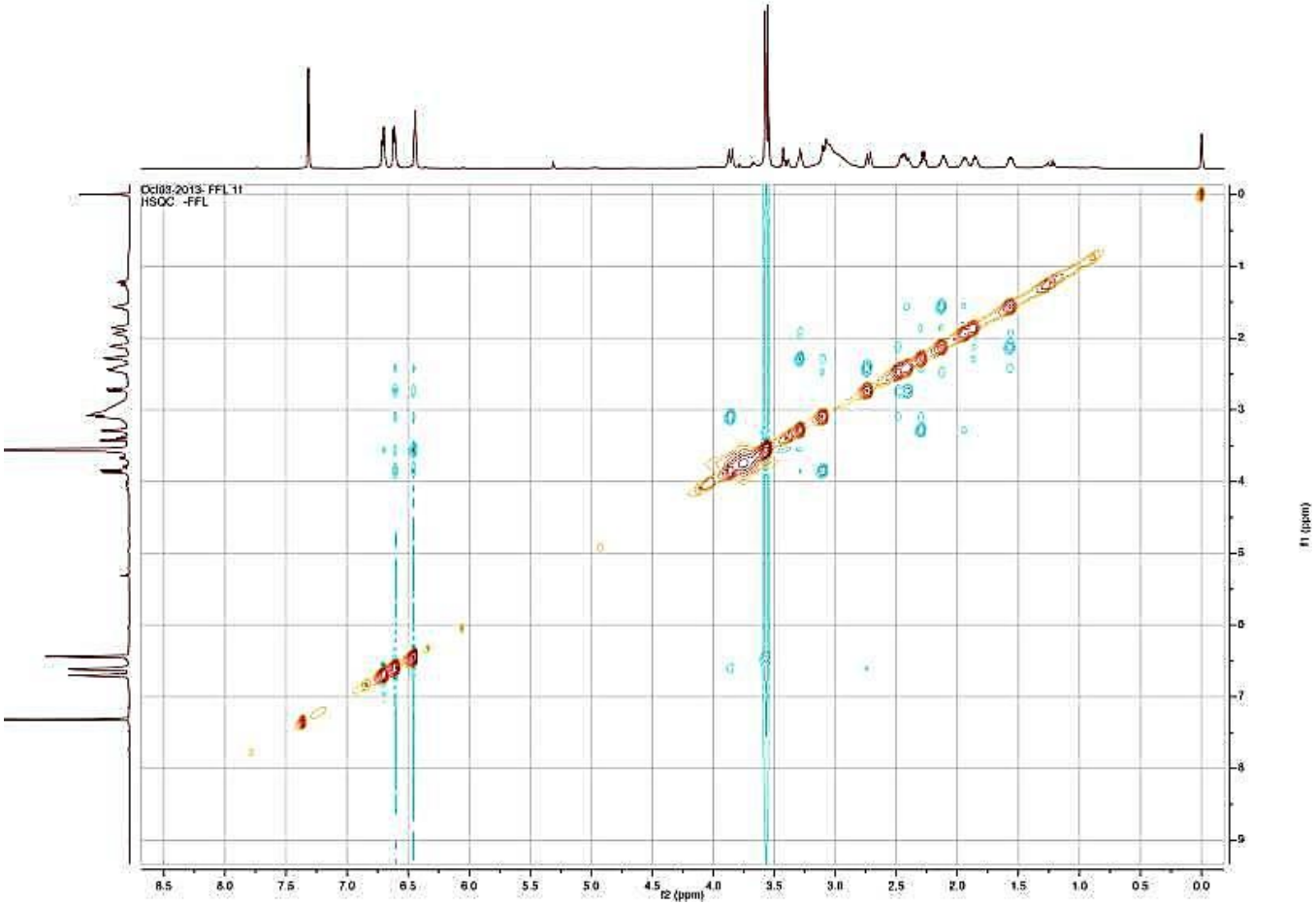

Appendix 26: NOESY spectrum of fistulopsine B **(5)**

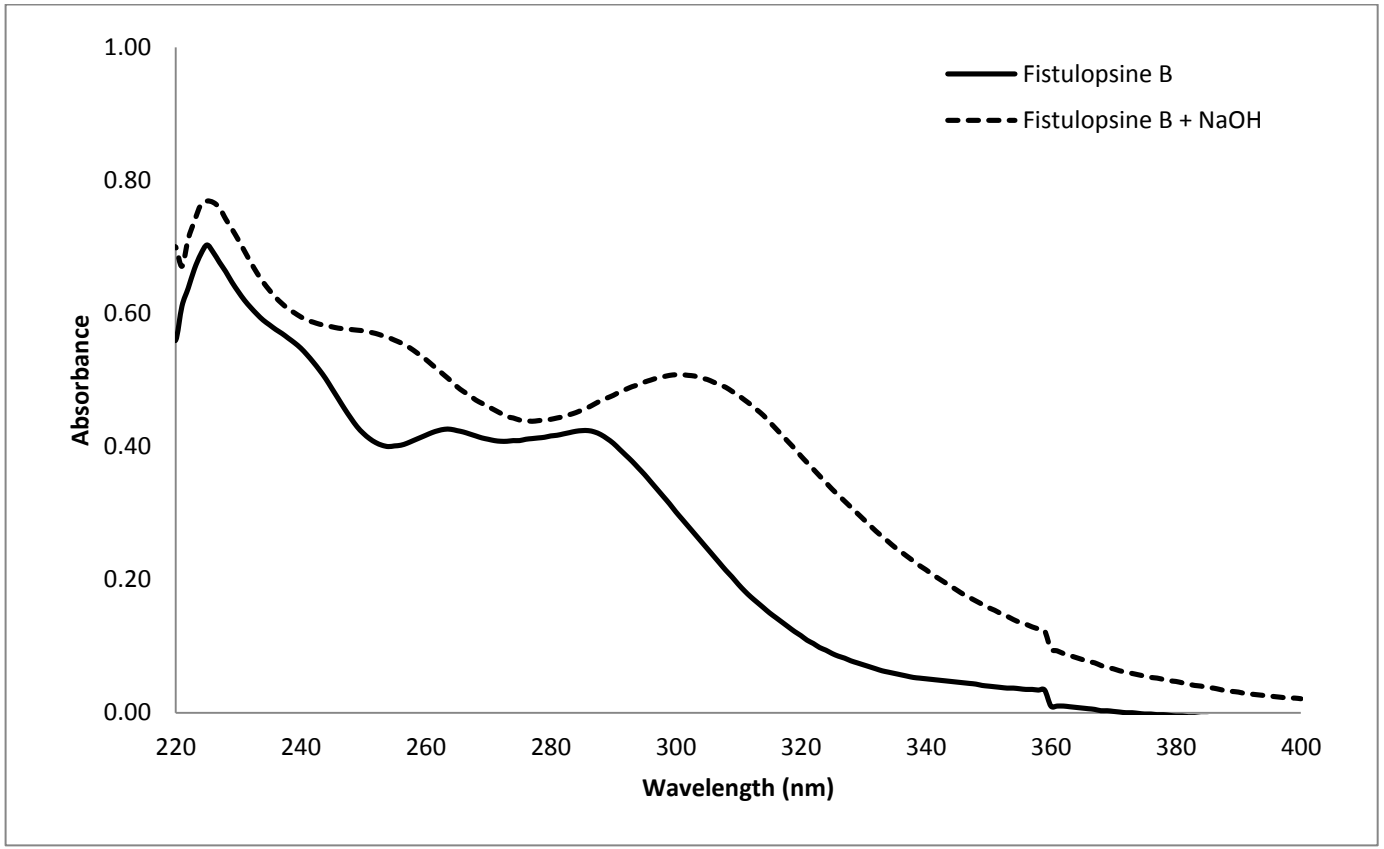

Appendix 27: UV spectrum of fistulopsine B **(5)**

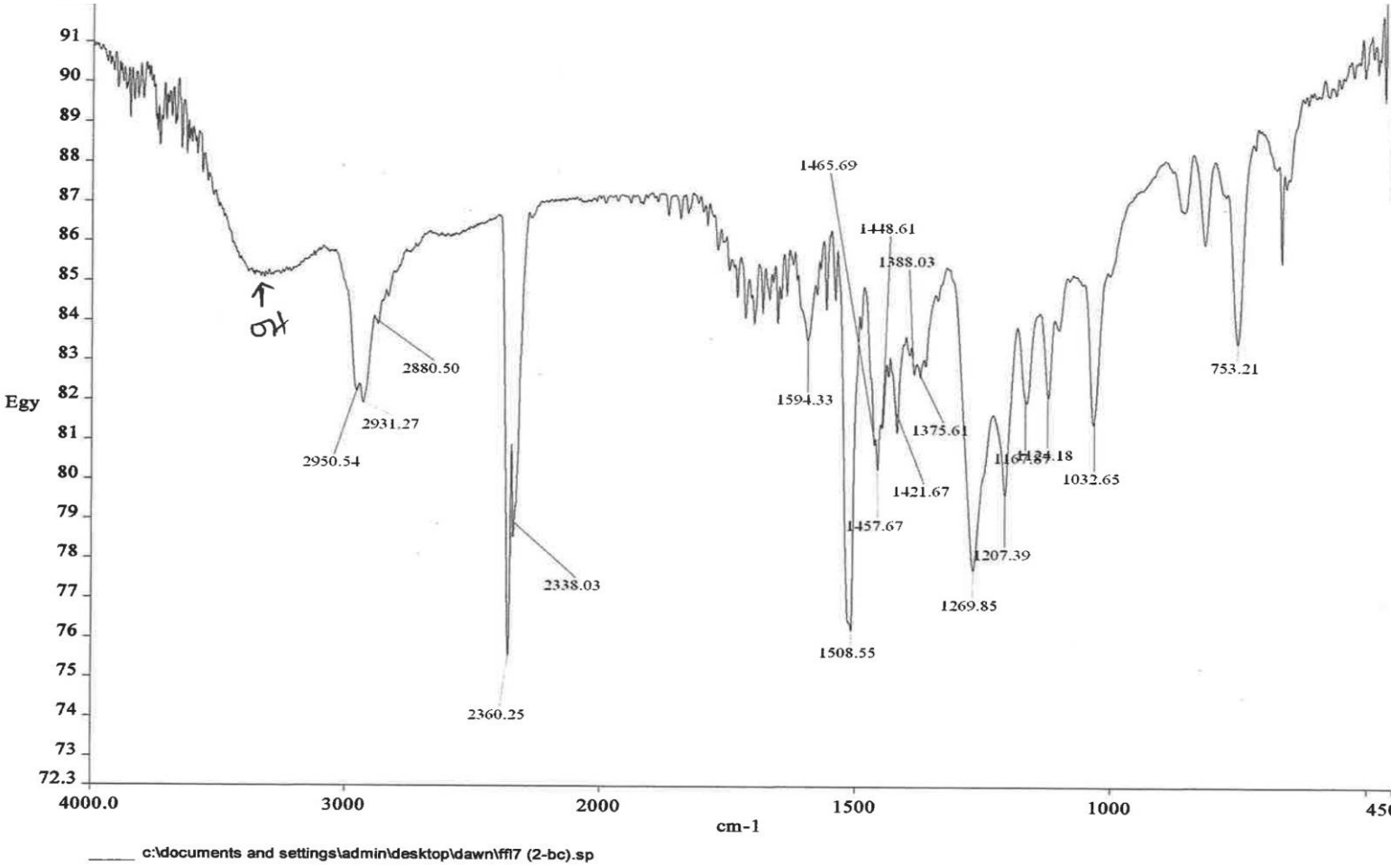

Appendix 28: IR spectrum of fistulopsine B **(5)**

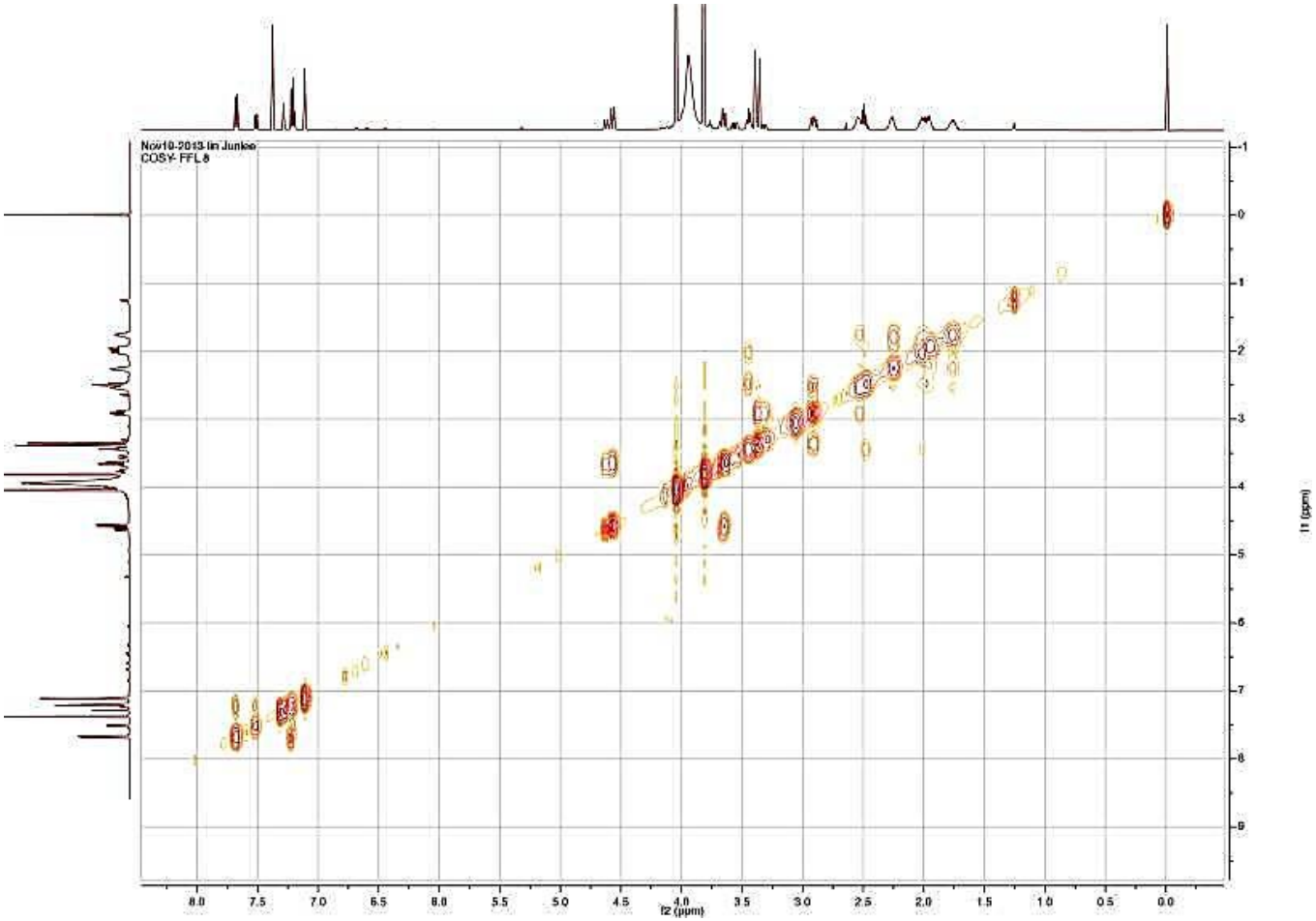

Appendix 29: COSY spectrum of 13a(*R*)-(-)-3,6-didemethylisotylocrebrine **(6)**

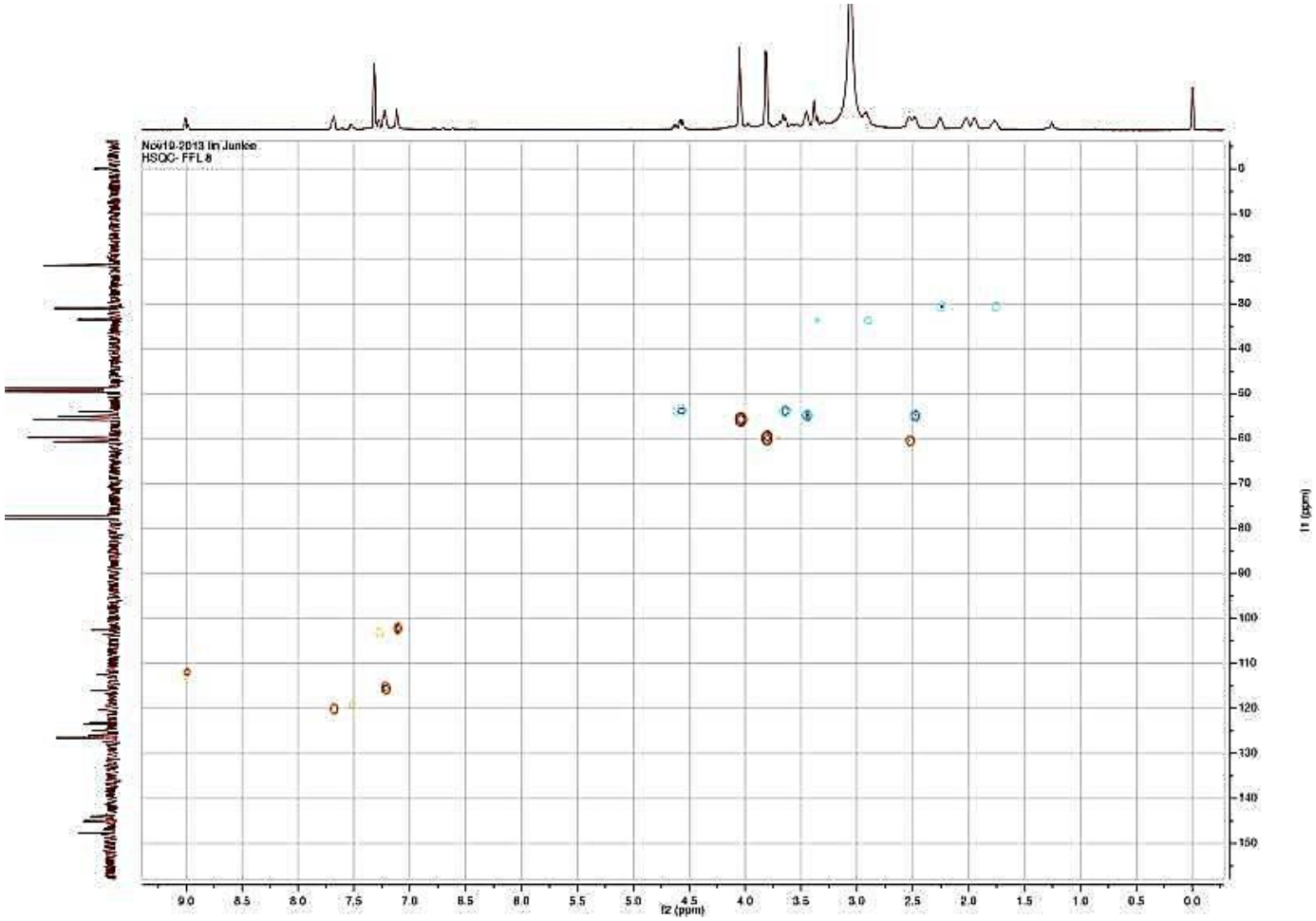

Appendix 30: HSQC spectrum of 13a(*R*)-(-)-3,6-didemethylisotylocrebrine **(6)**

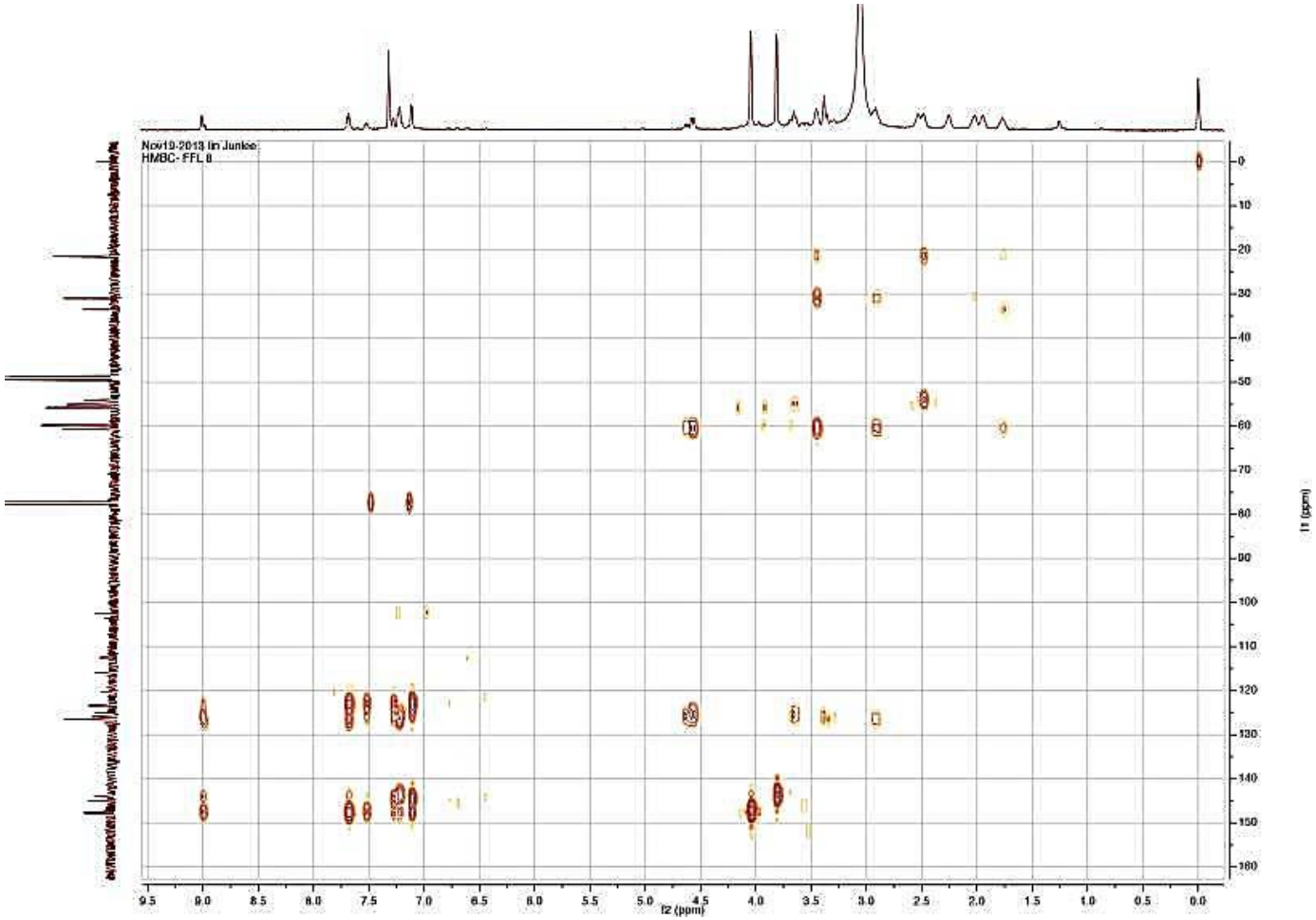

Appendix 31: HMBC spectrum of 13a(*R*)-(-)-3,6-didemethylisotylocrebrine **(6)**

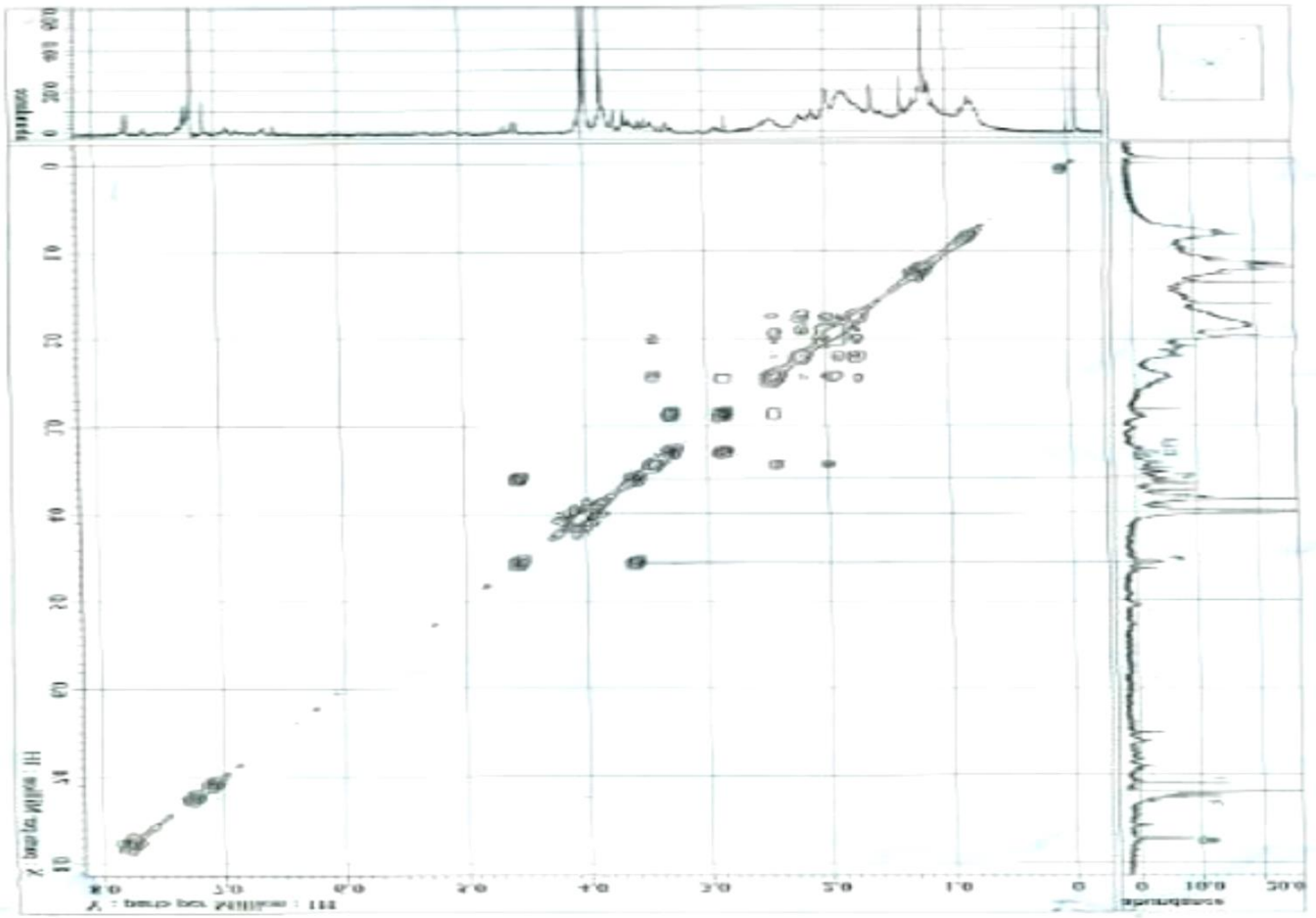

Appendix 32: COSY spectrum of 13a(*S*)-(+)-tylocrebrine **(7)**

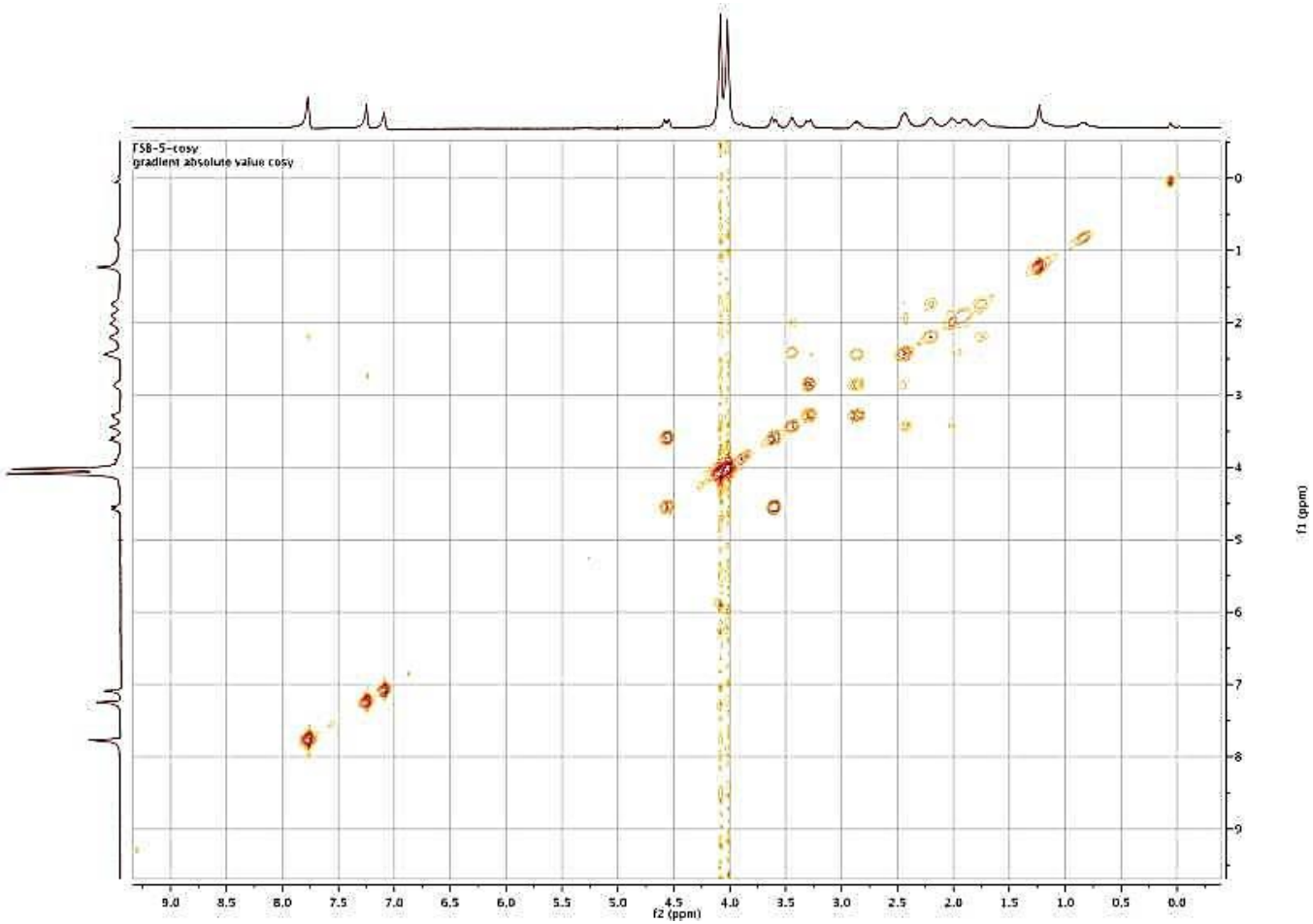

Appendix 33: COSY spectrum of 13a(*S*)-(+)-tylophorine **(8)**

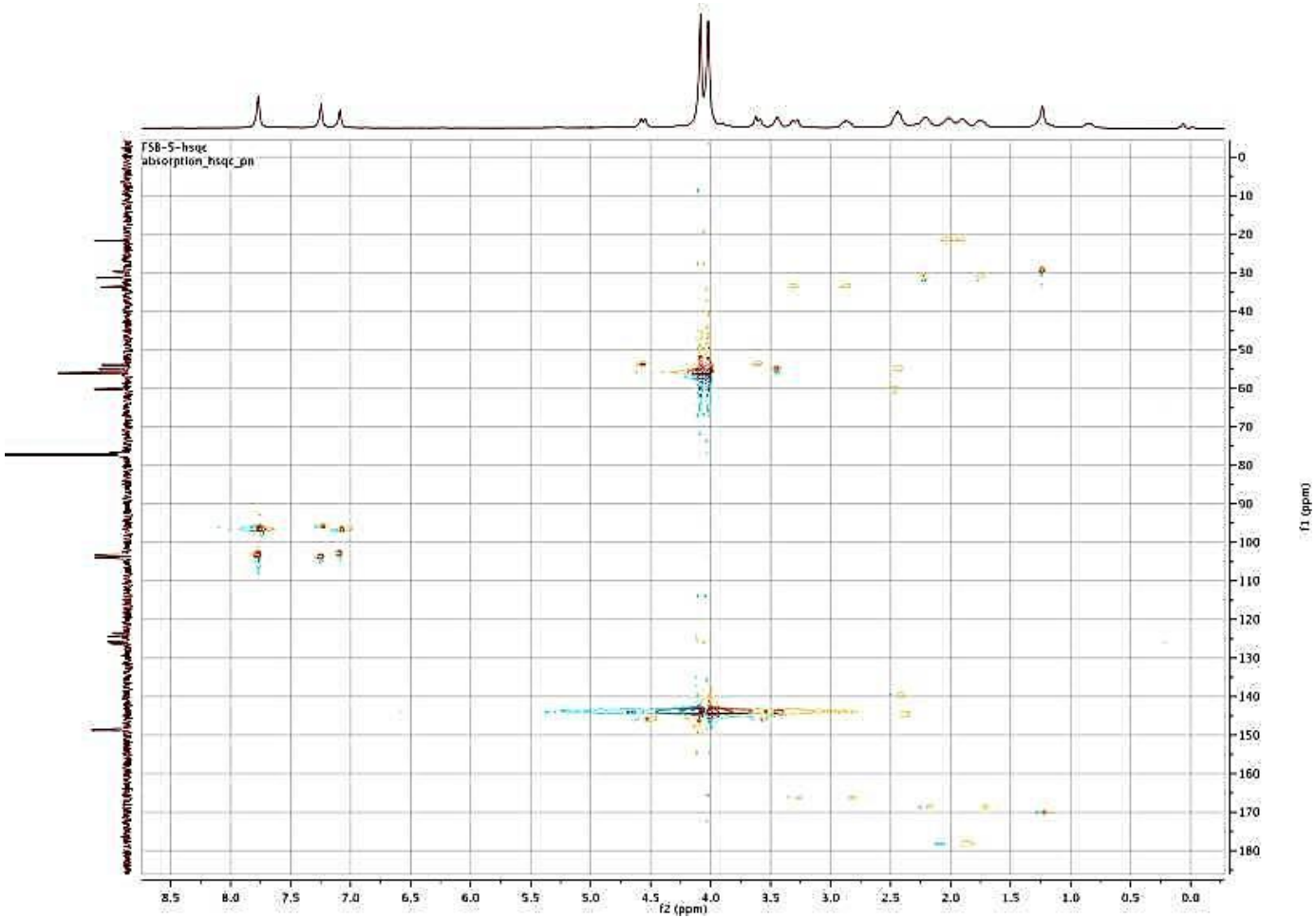

Appendix 34: HSQC spectrum of 13a(*S*)-(+)-tylophorine **(8)**

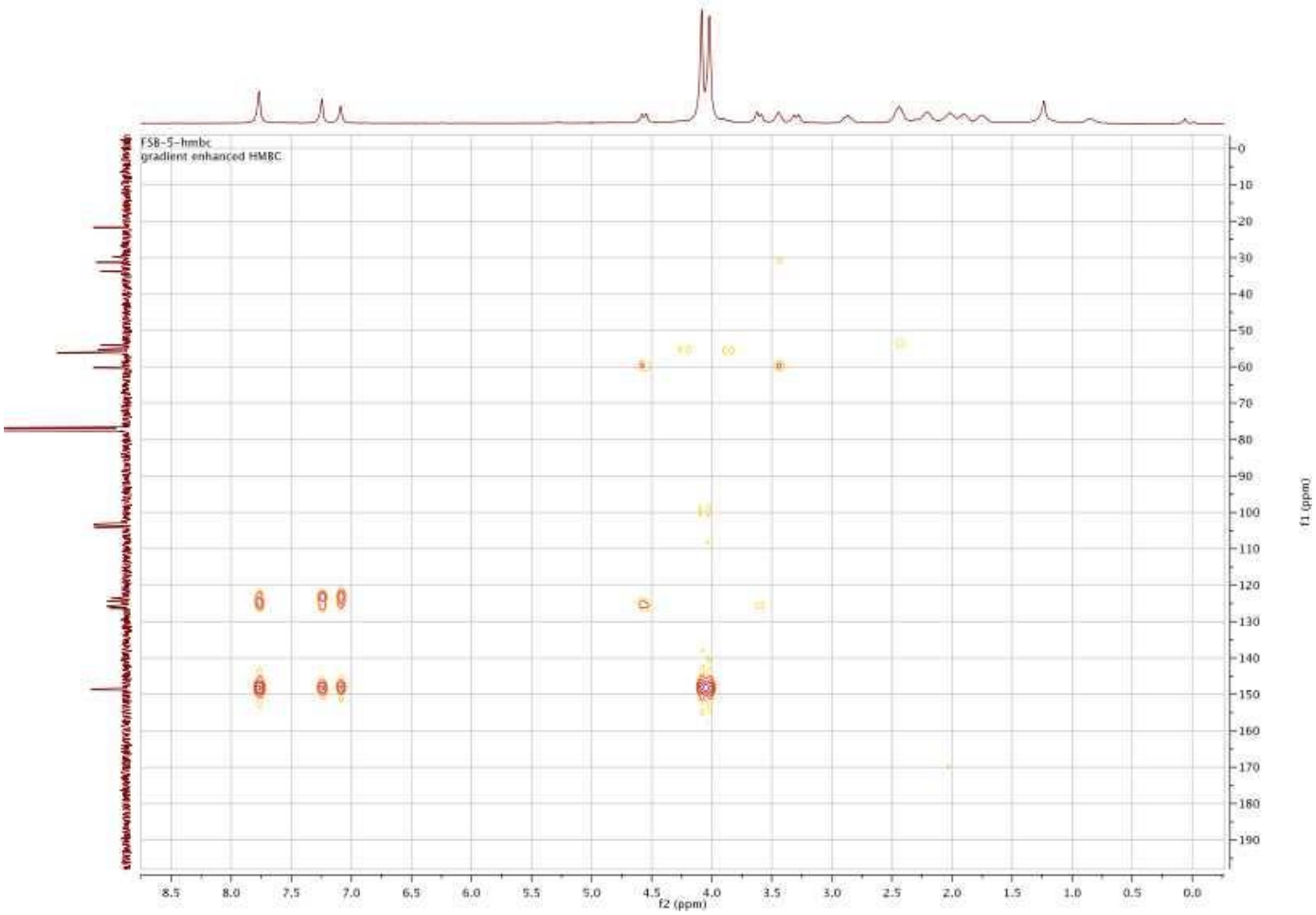

Appendix 35: HMBC spectrum of 13a(*S*)-(+)-tylophorine **(8)**

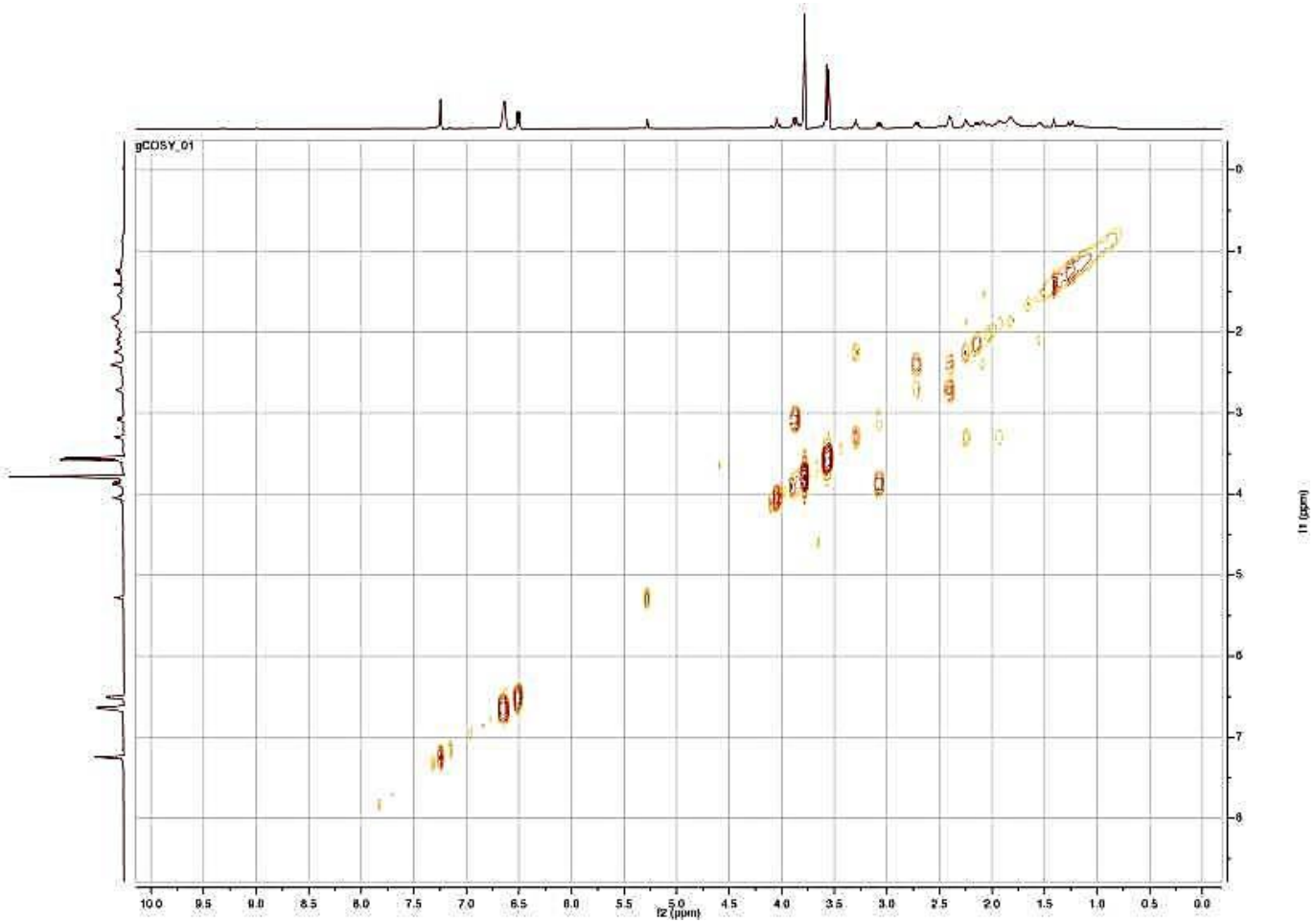

Appendix 36: COSY spectrum of 13a(*S*)-(+)-septicine **(9)**

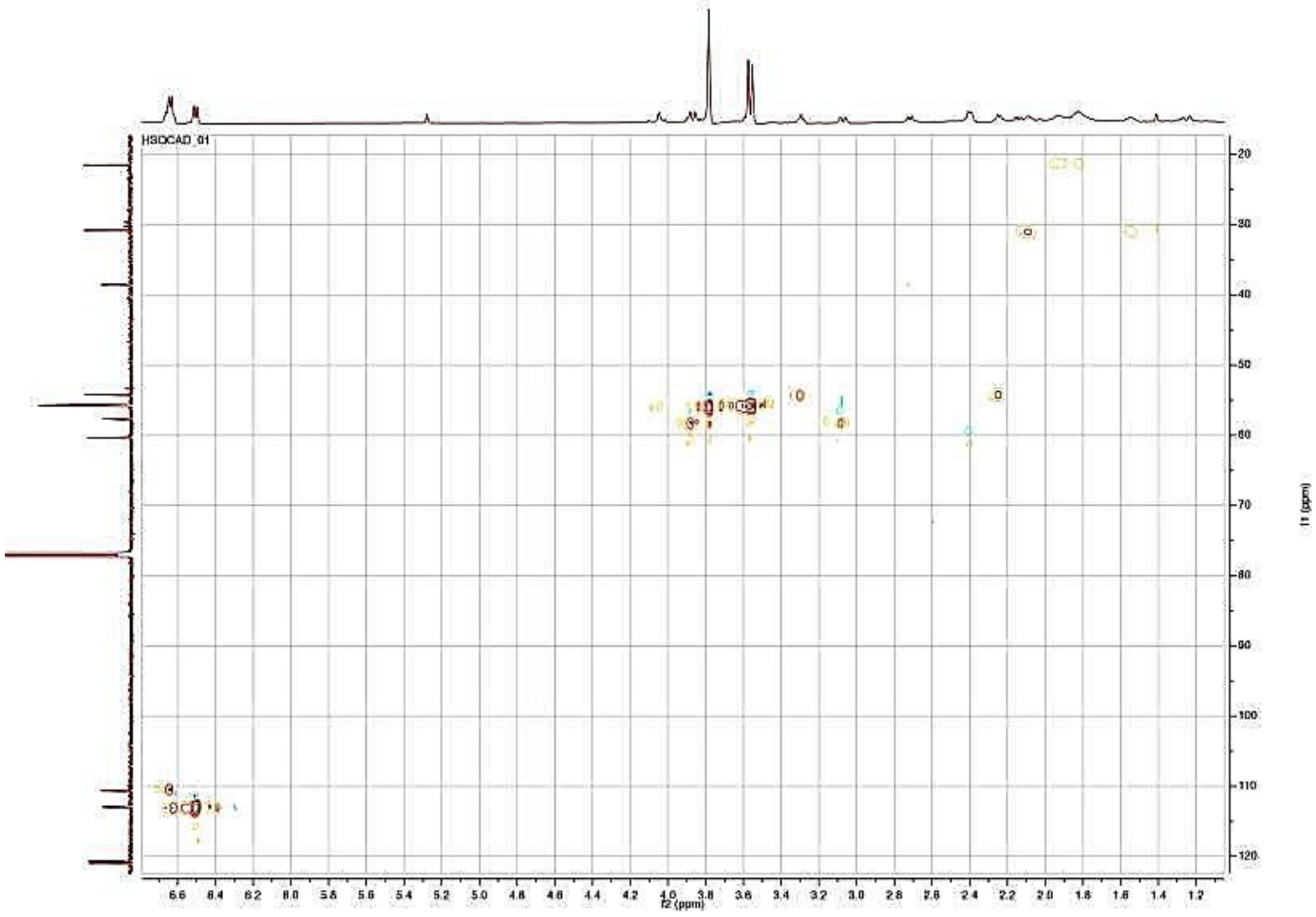

Appendix 37: HSQC spectrum of 13a(*S*)-(+)-septicine **(9)**

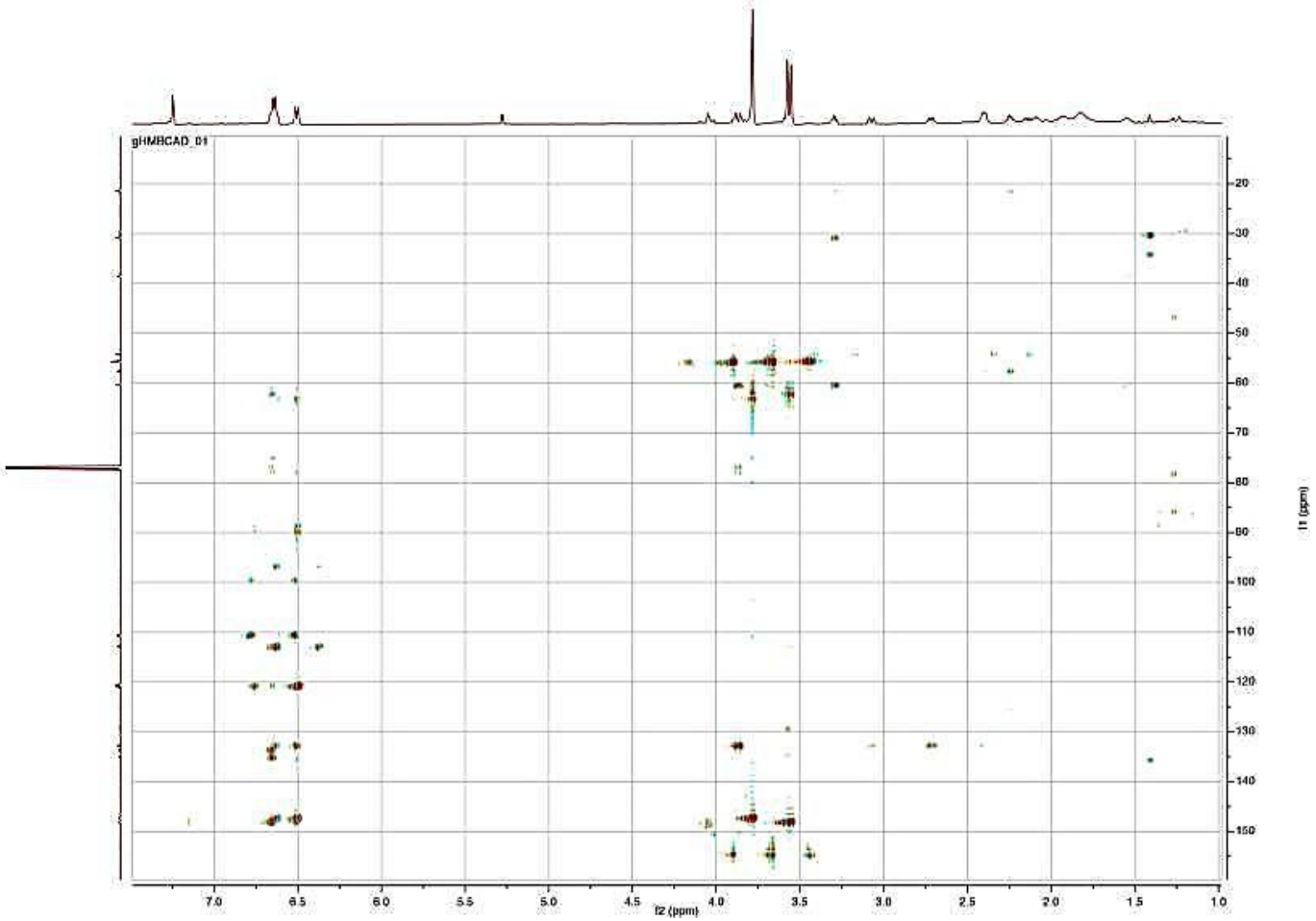

Appendix 38: HMBC spectrum of 13a(*S*)-(+)-septicine **(9)**

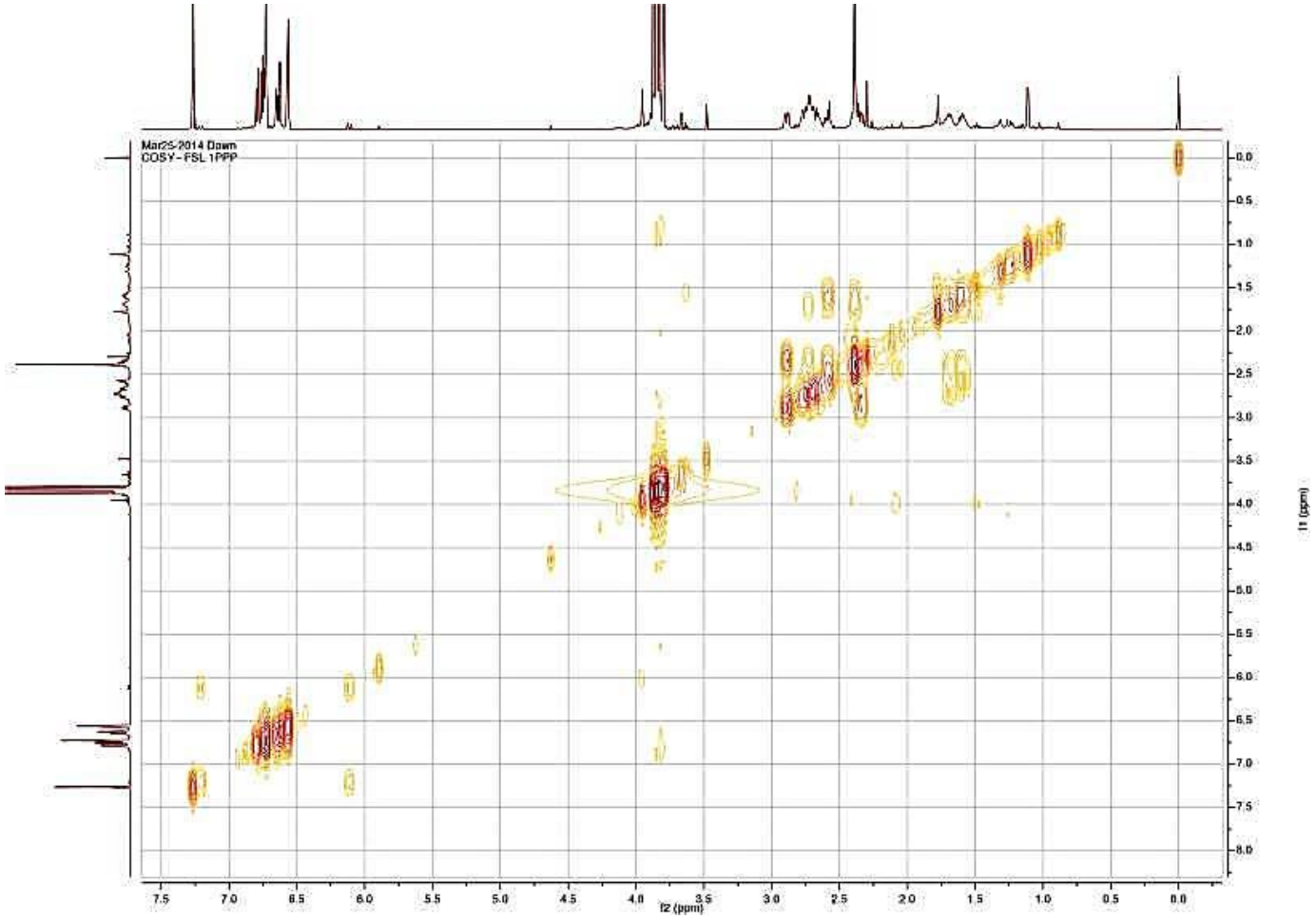

Appendix 39: COSY spectrum of schwarzinicine A **(11)**

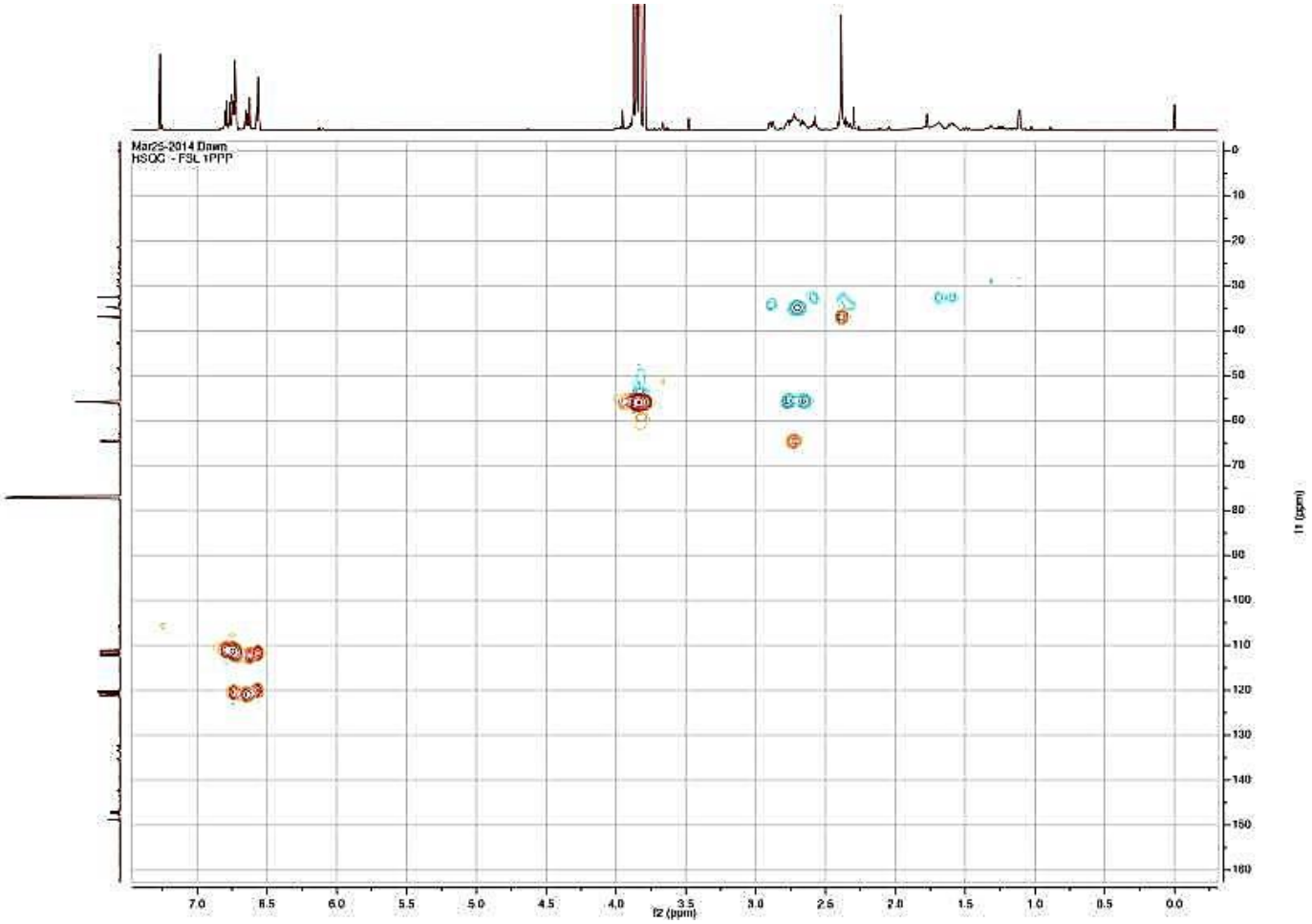

Appendix 40: HSQC spectrum of schwarzinicine A **(11)**

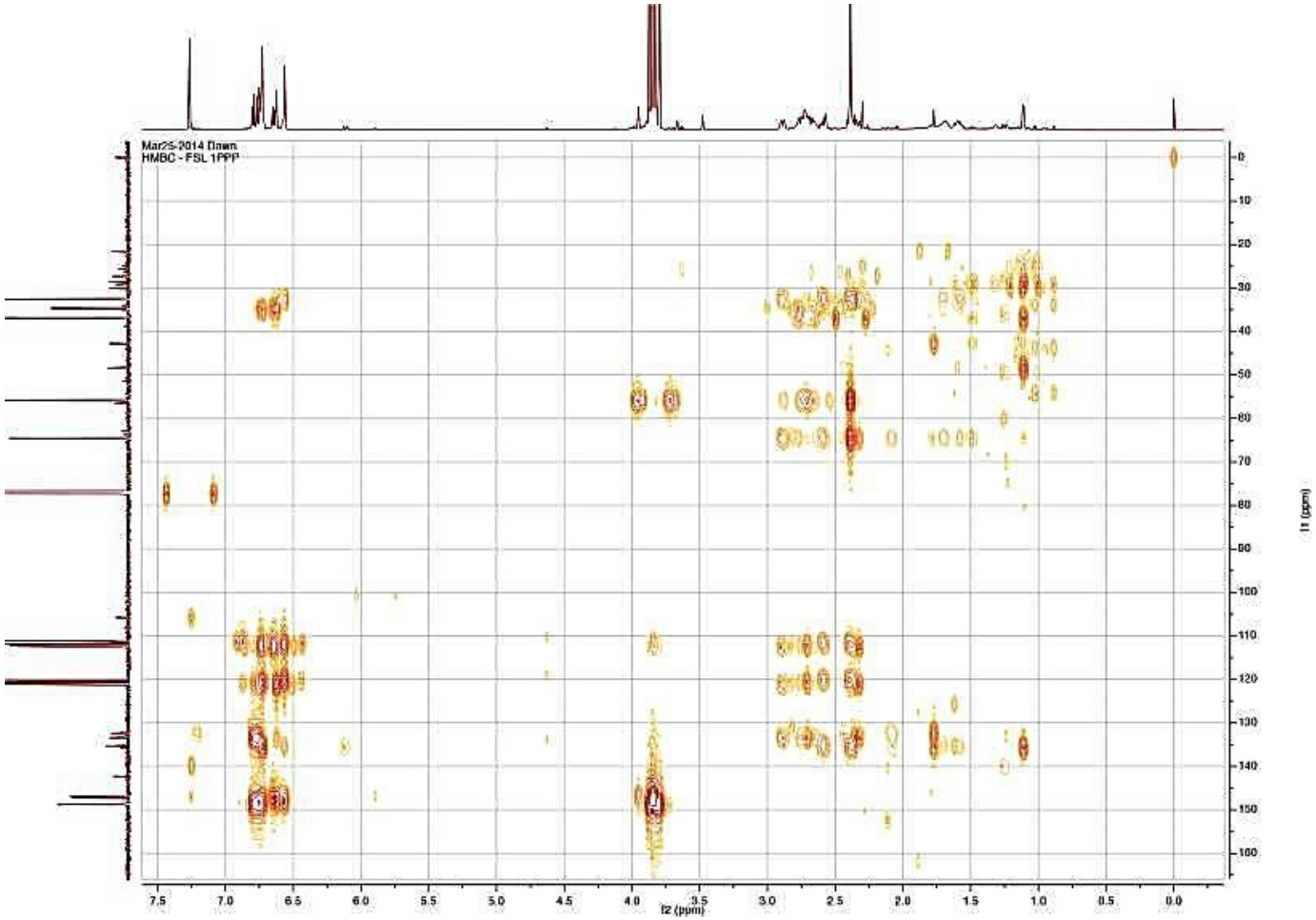

Appendix 41: HMBC spectrum of schwarzinicine A **(11)**

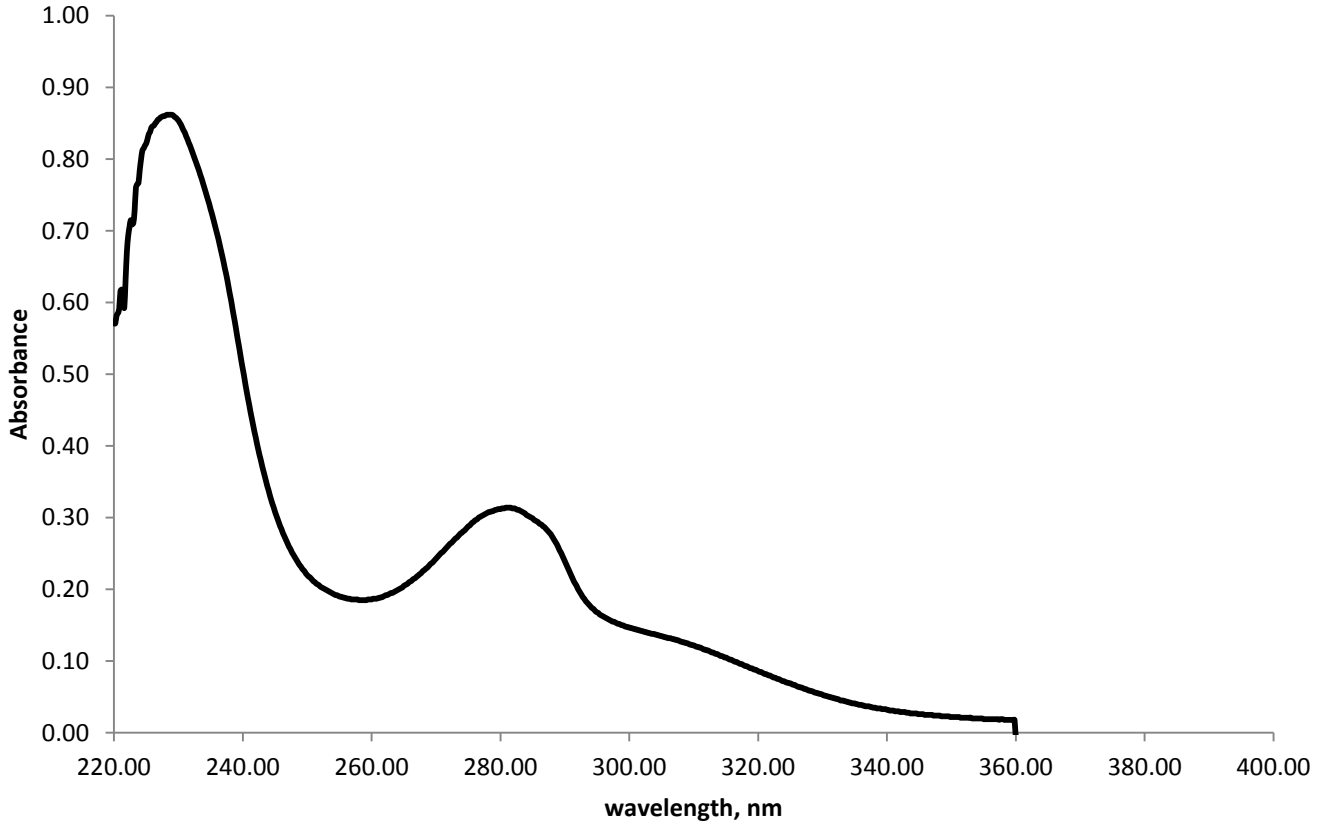

Appendix 42: UV spectrum of schwarzinicine A **(11)**

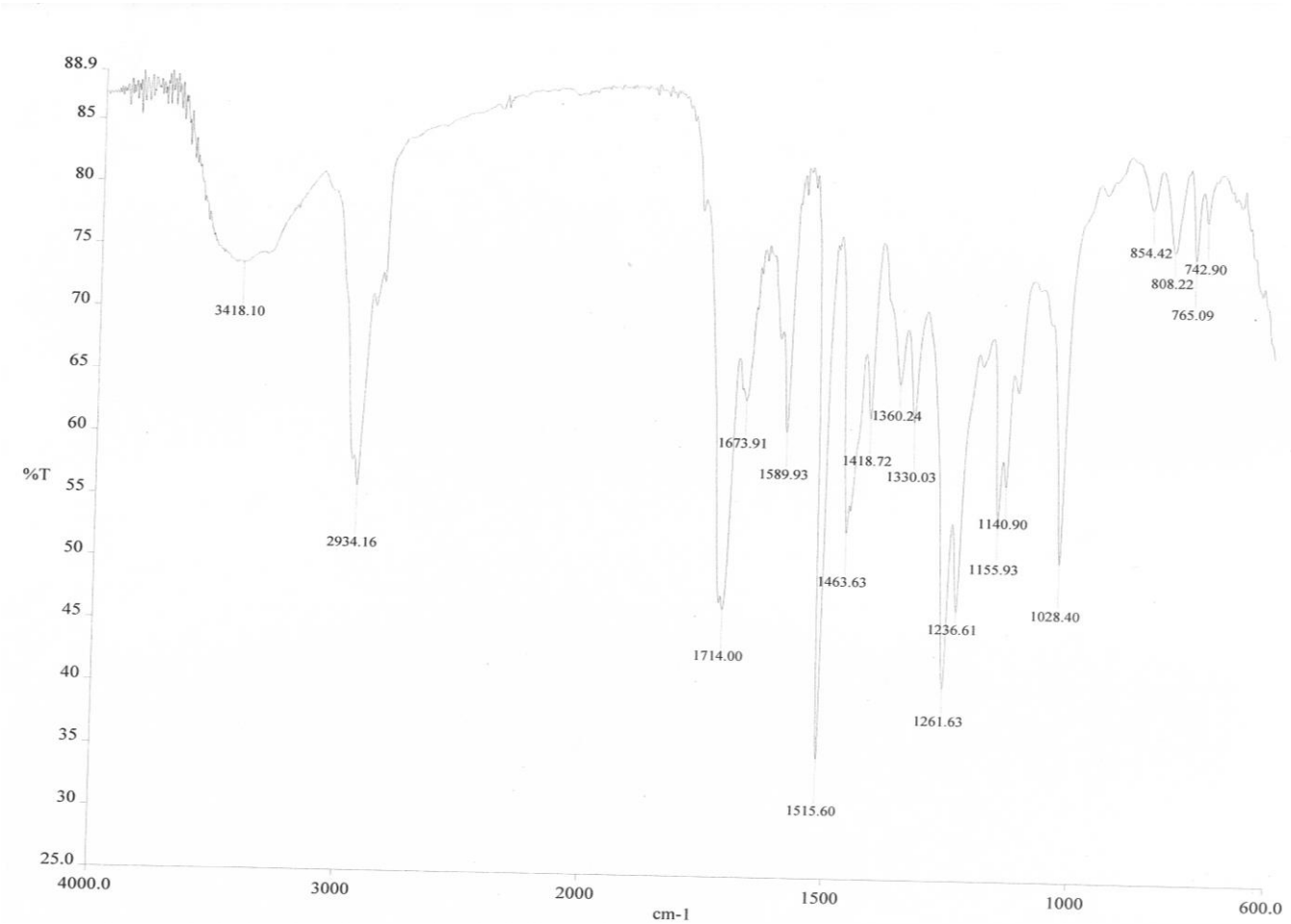

Appendix 43: IR spectrum of schwarzinicine A **(11)**

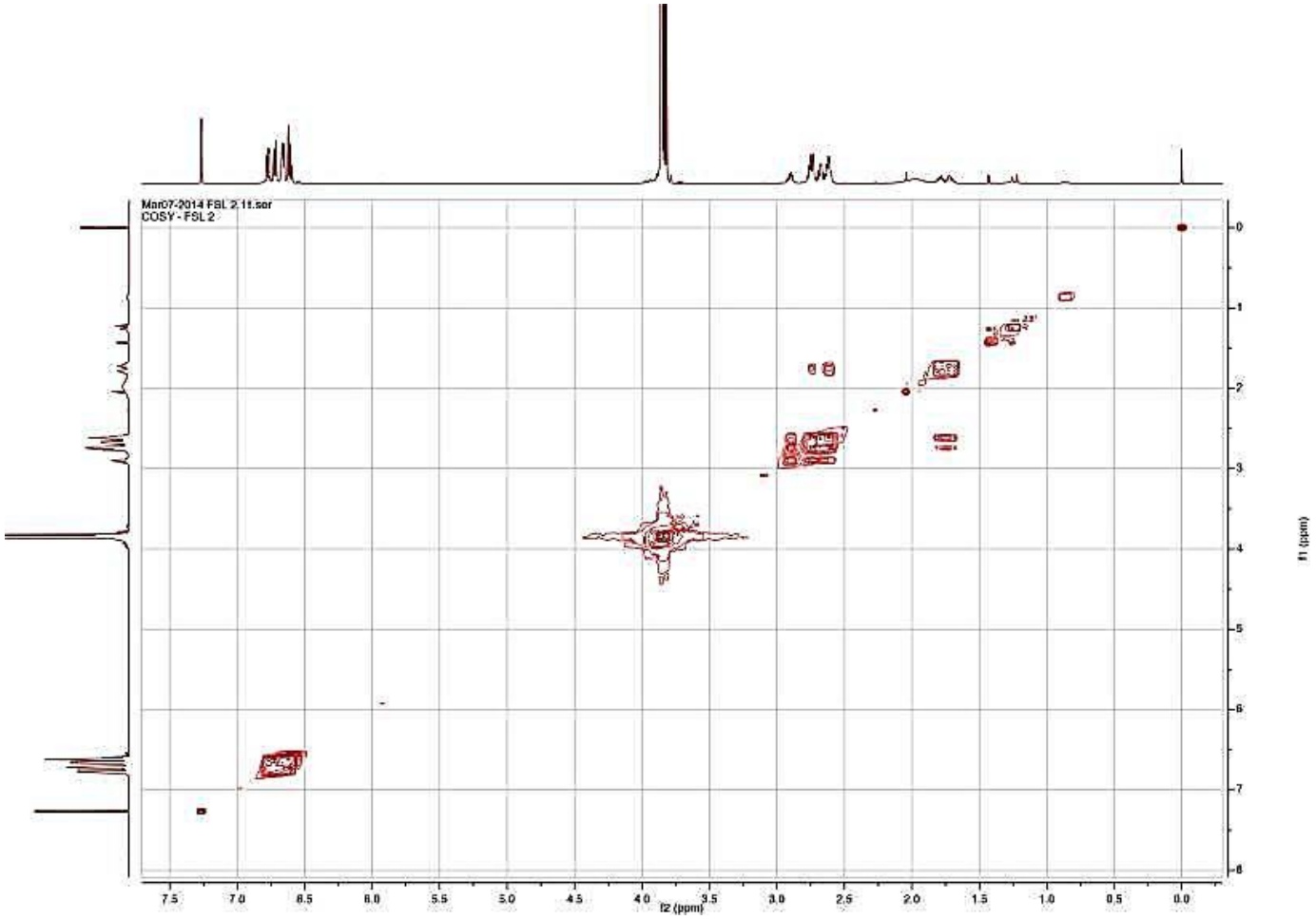

Appendix 44: COSY spectrum of schwarzinicine B **(12)**

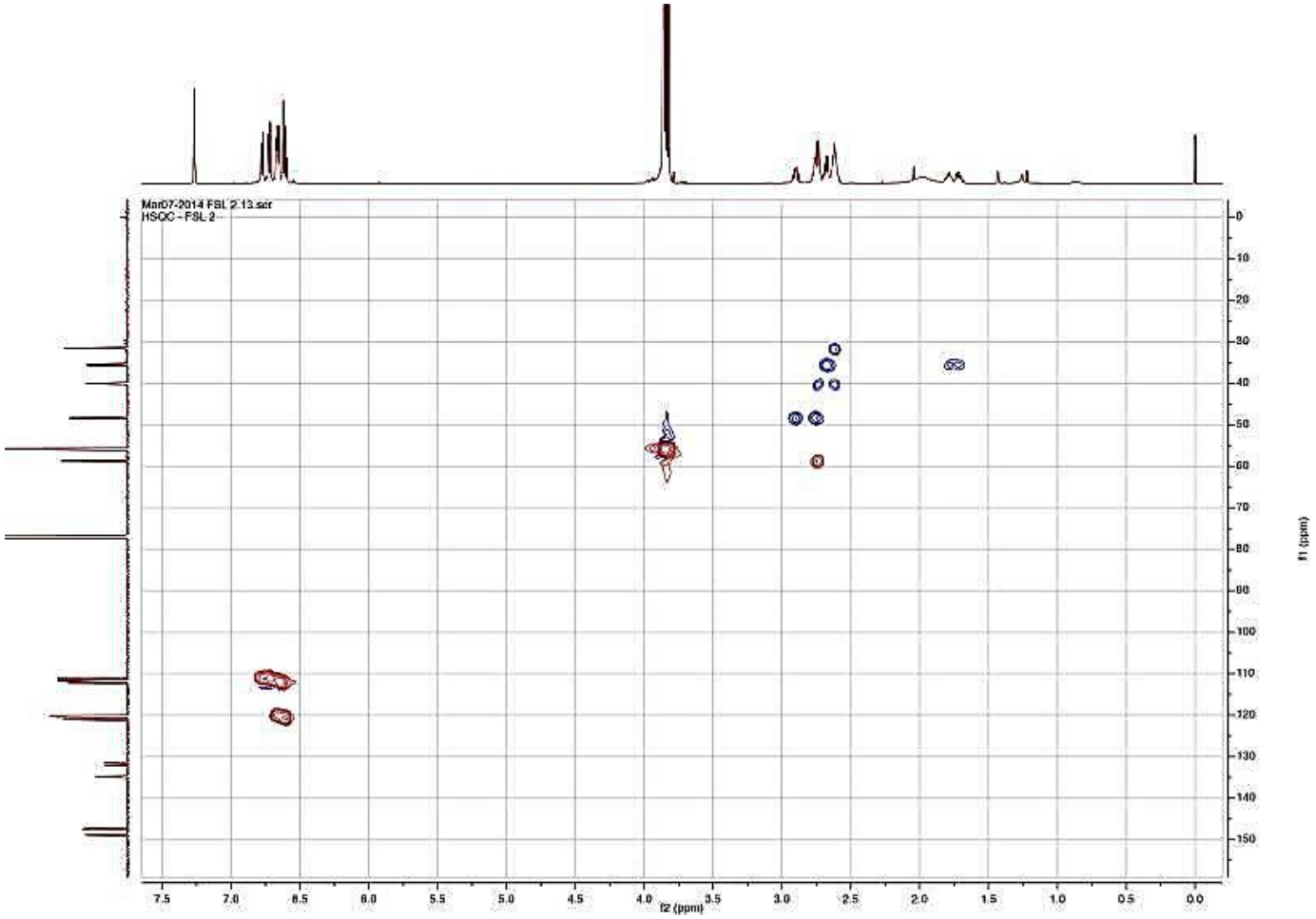

Appendix 45: HSQC spectrum of schwarzinicine B **(12)**

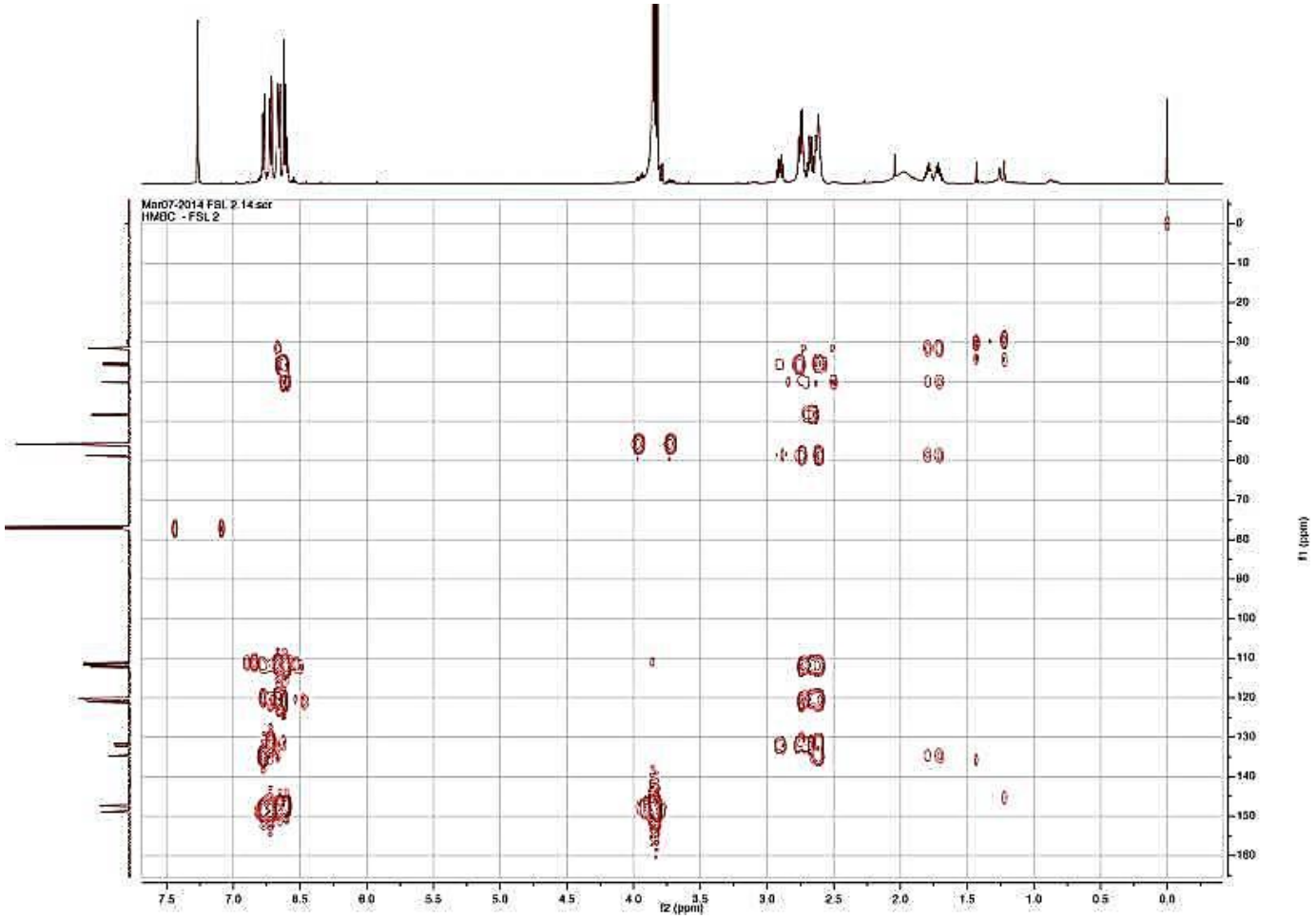

Appendix 46: HMBC spectrum of schwarzinicine B **(12)**

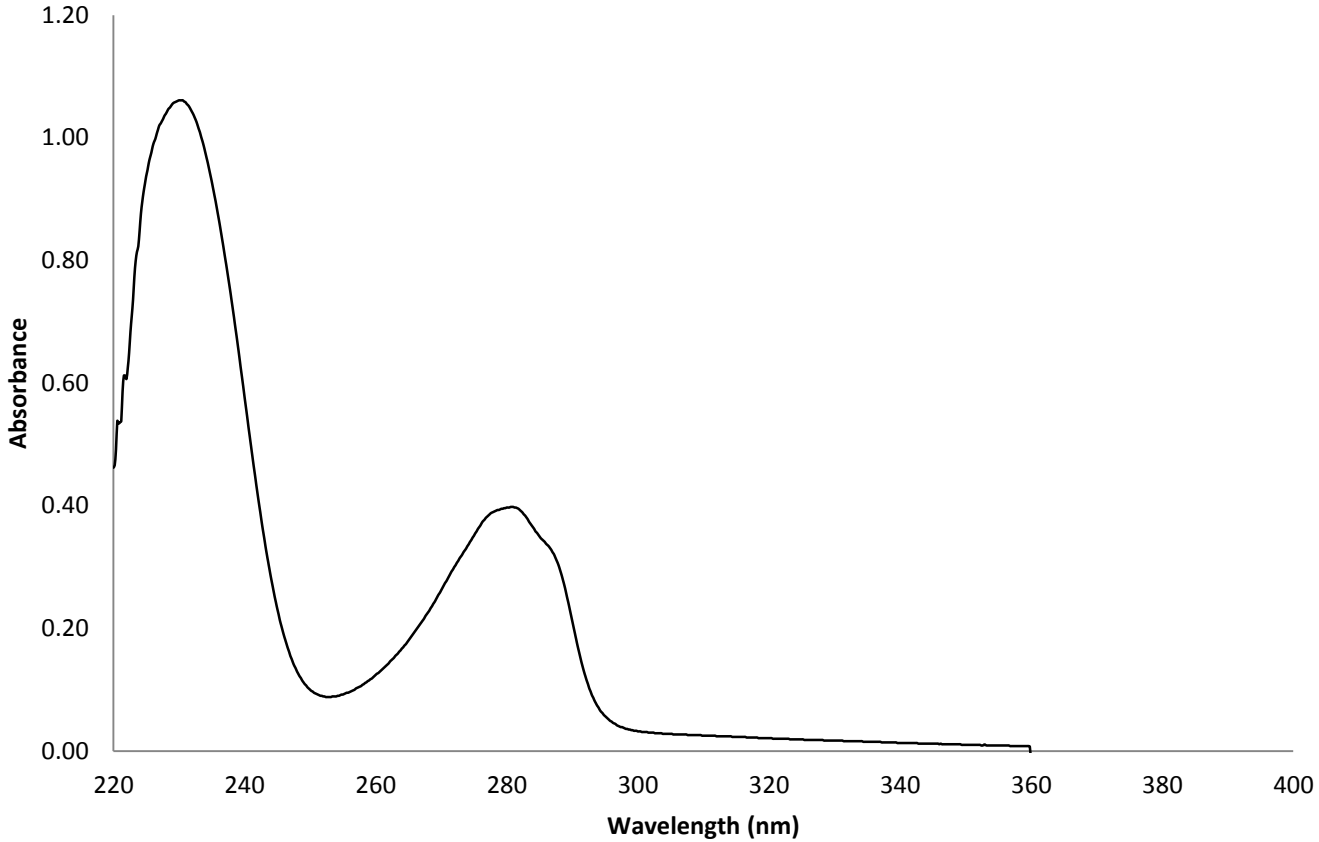

Appendix 47: UV spectrum of schwarzinicine B **(12)**

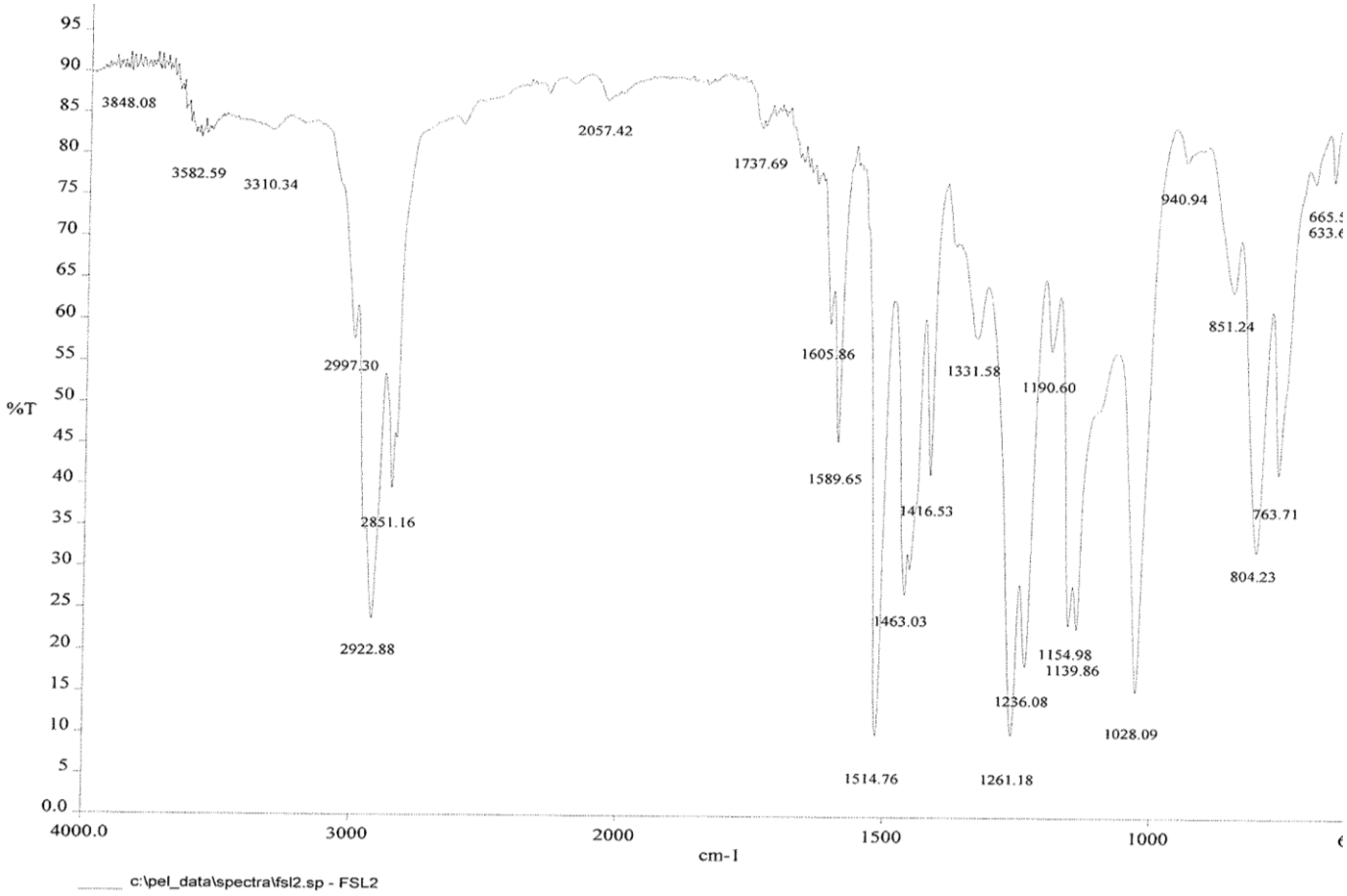

Appendix 48: IR spectrum of schwarzinicine B **(12)**

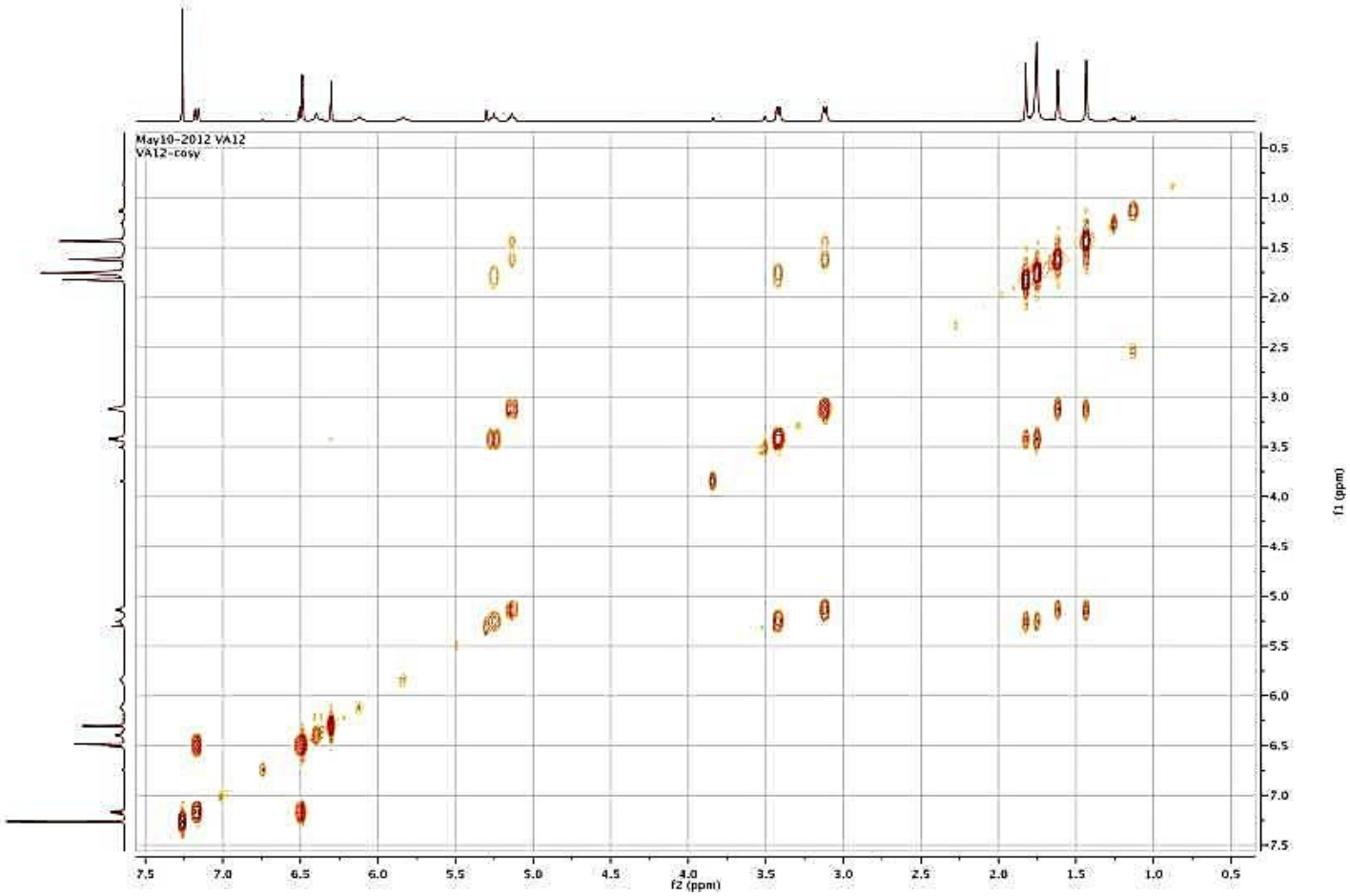

Appendix 49: COSY spectrum of cudraflavone C **(13)**

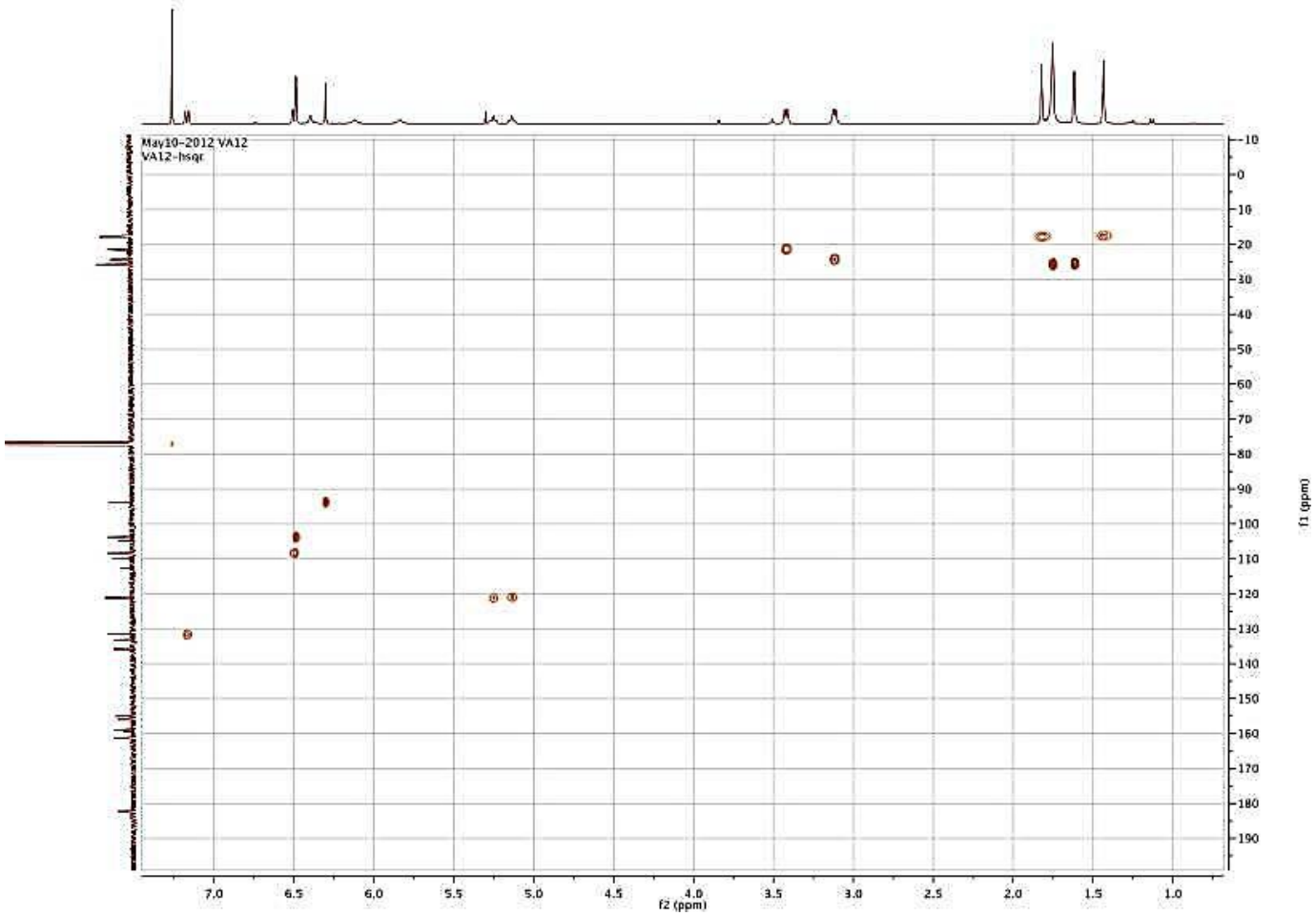

Appendix 50: HSQC spectrum of cudraflavone C **(13)**

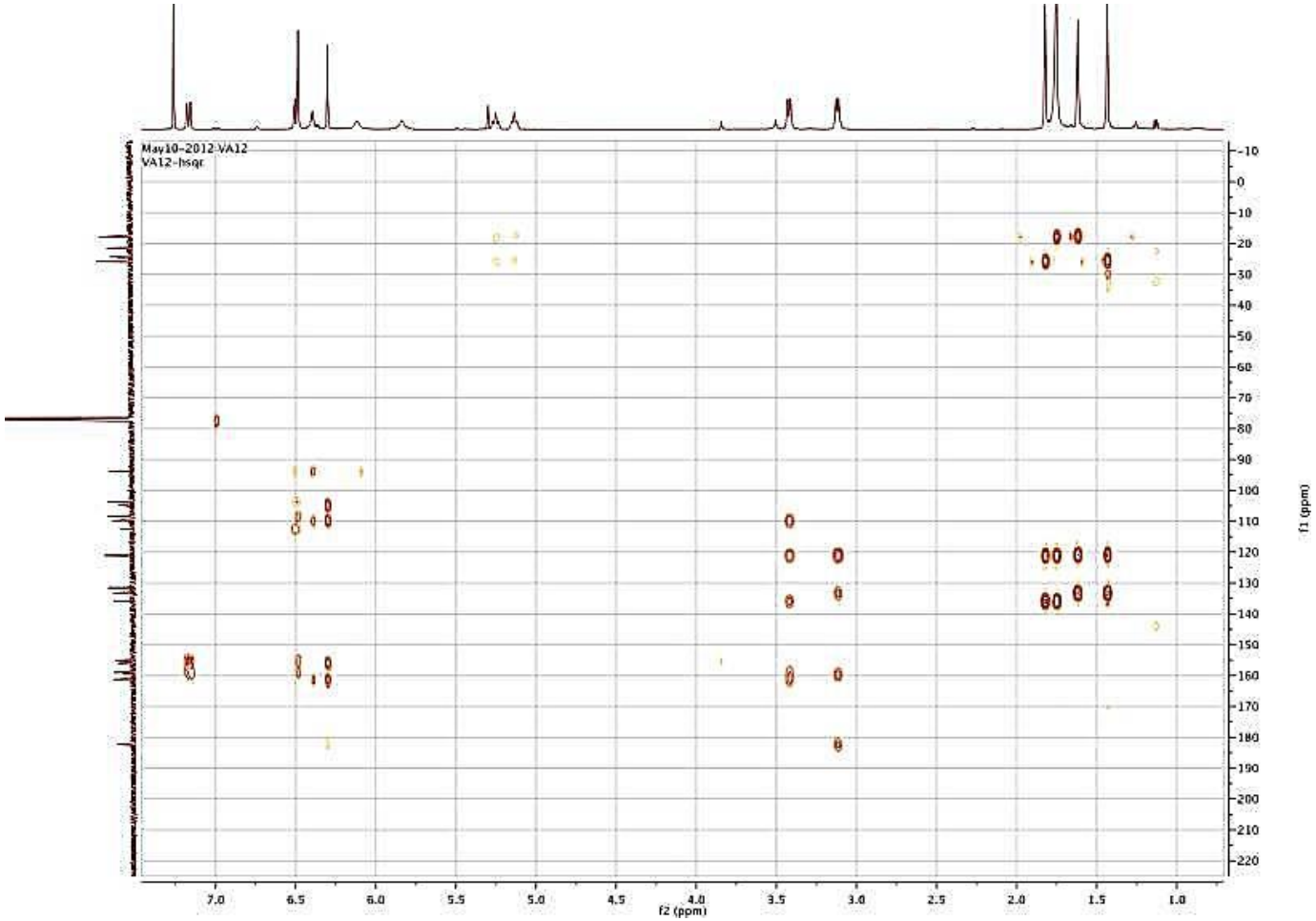

Appendix 51: HMBC spectrum of cudraflavone C **(13)**

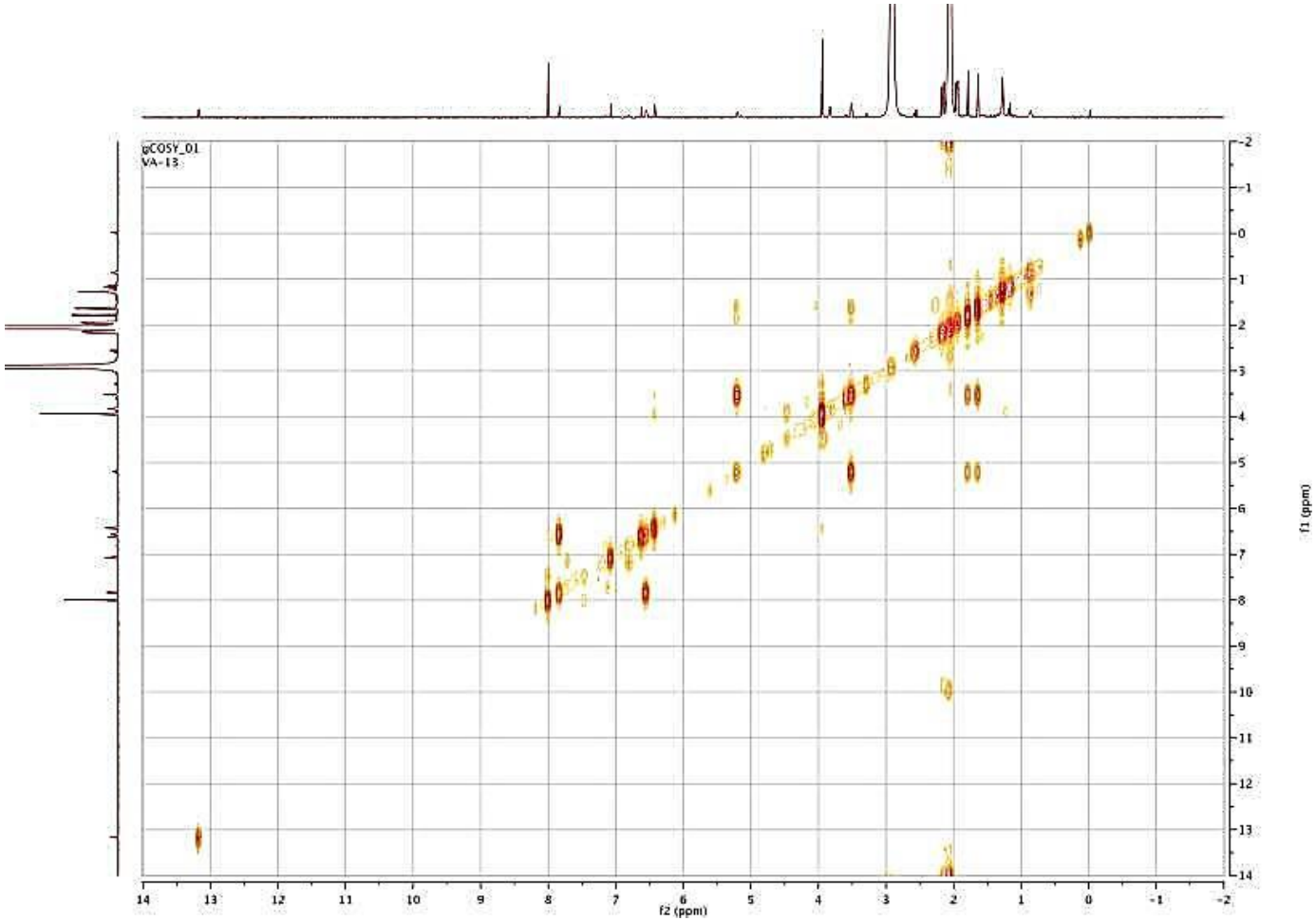

Appendix 52: COSY spectrum of artocarpetin A **(14)**

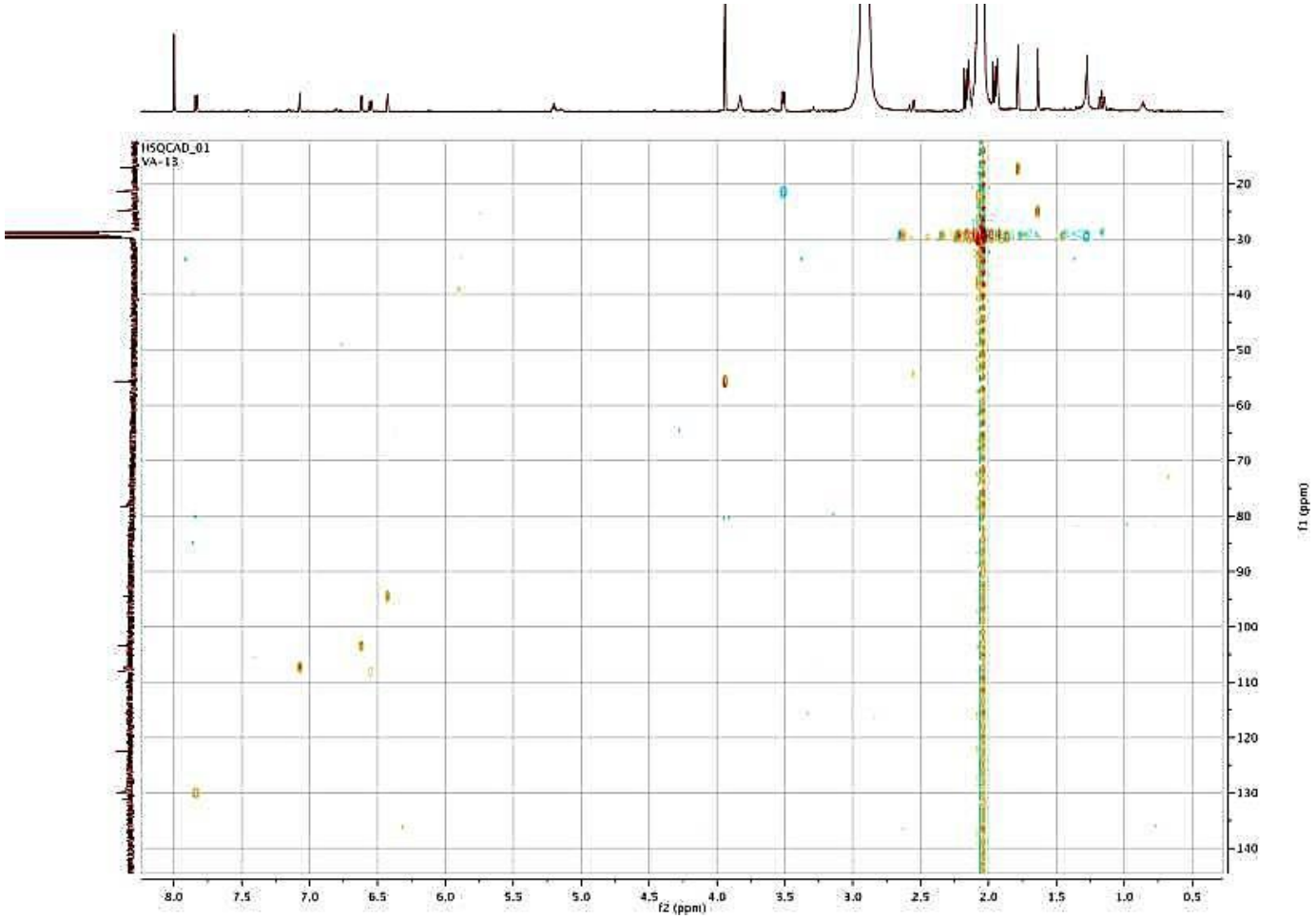

Appendix 53: HSQC spectrum of artocarpetin A **(14)**

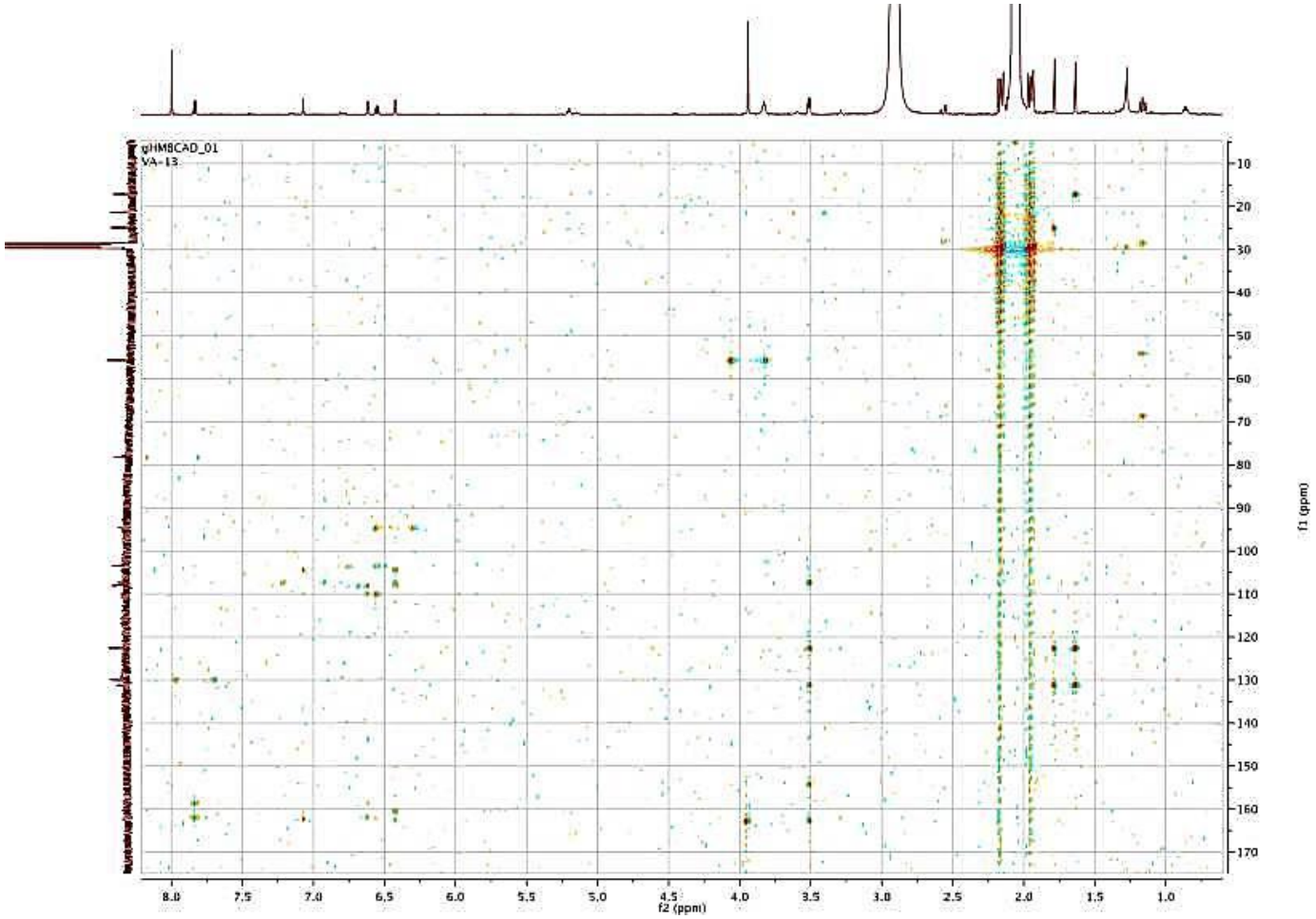

Appendix 54: HMBC spectrum of artocarpetin A **(14)**

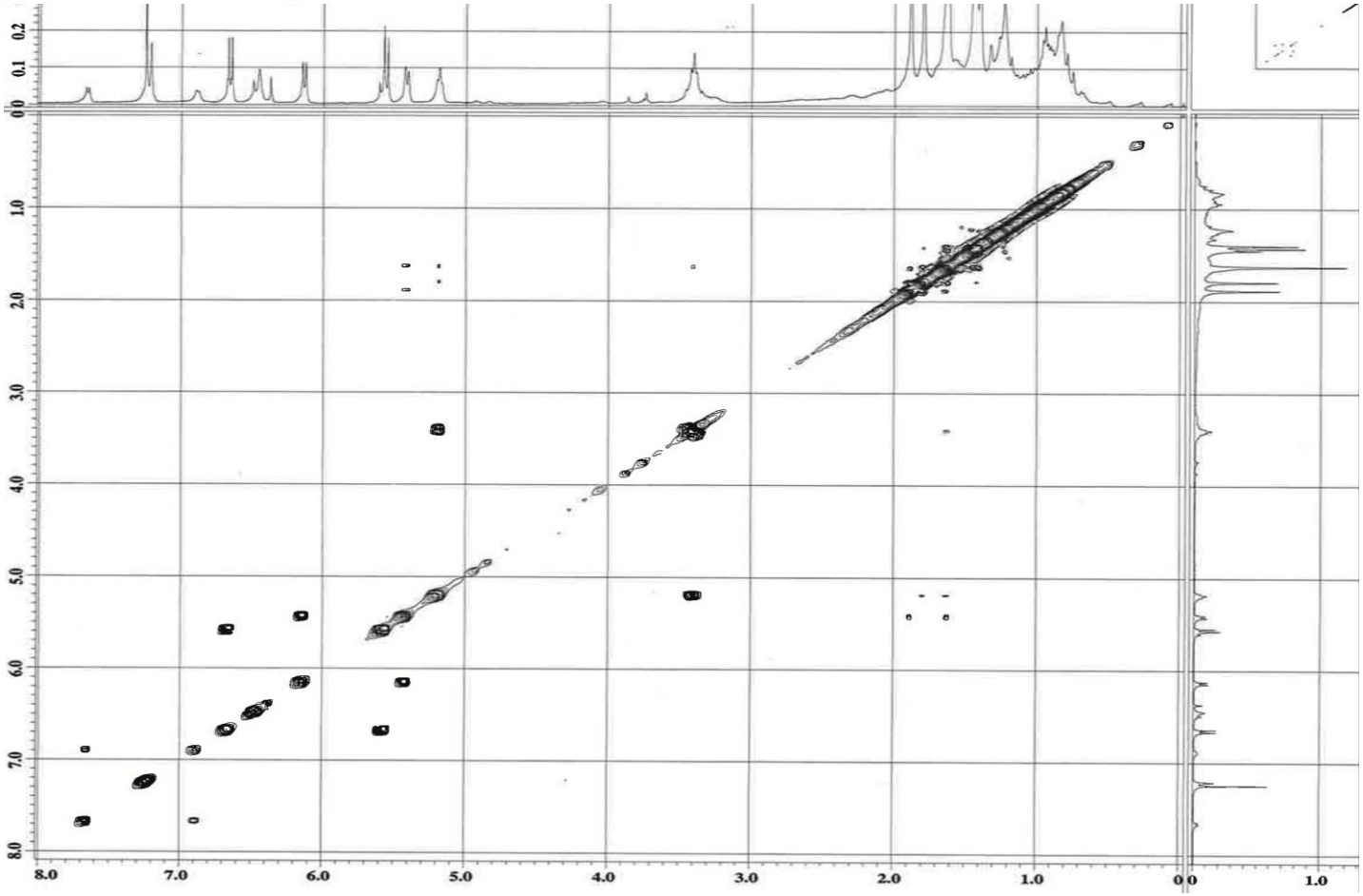

Appendix 55: COSY spectrum of cycloheterophyllin **(15)**

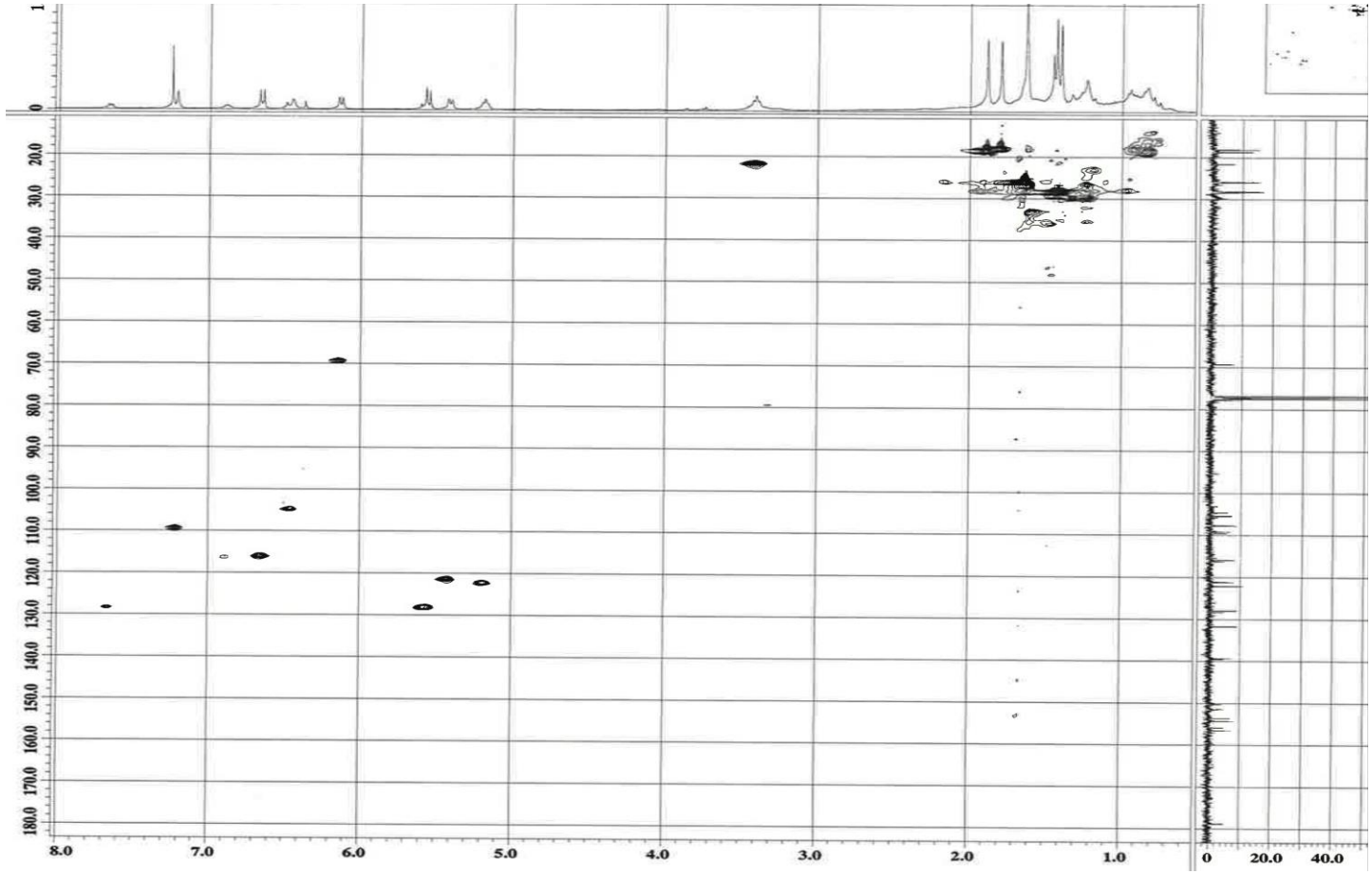

Appendix 56: HSQC spectrum of cycloheterophyllin **(15)**

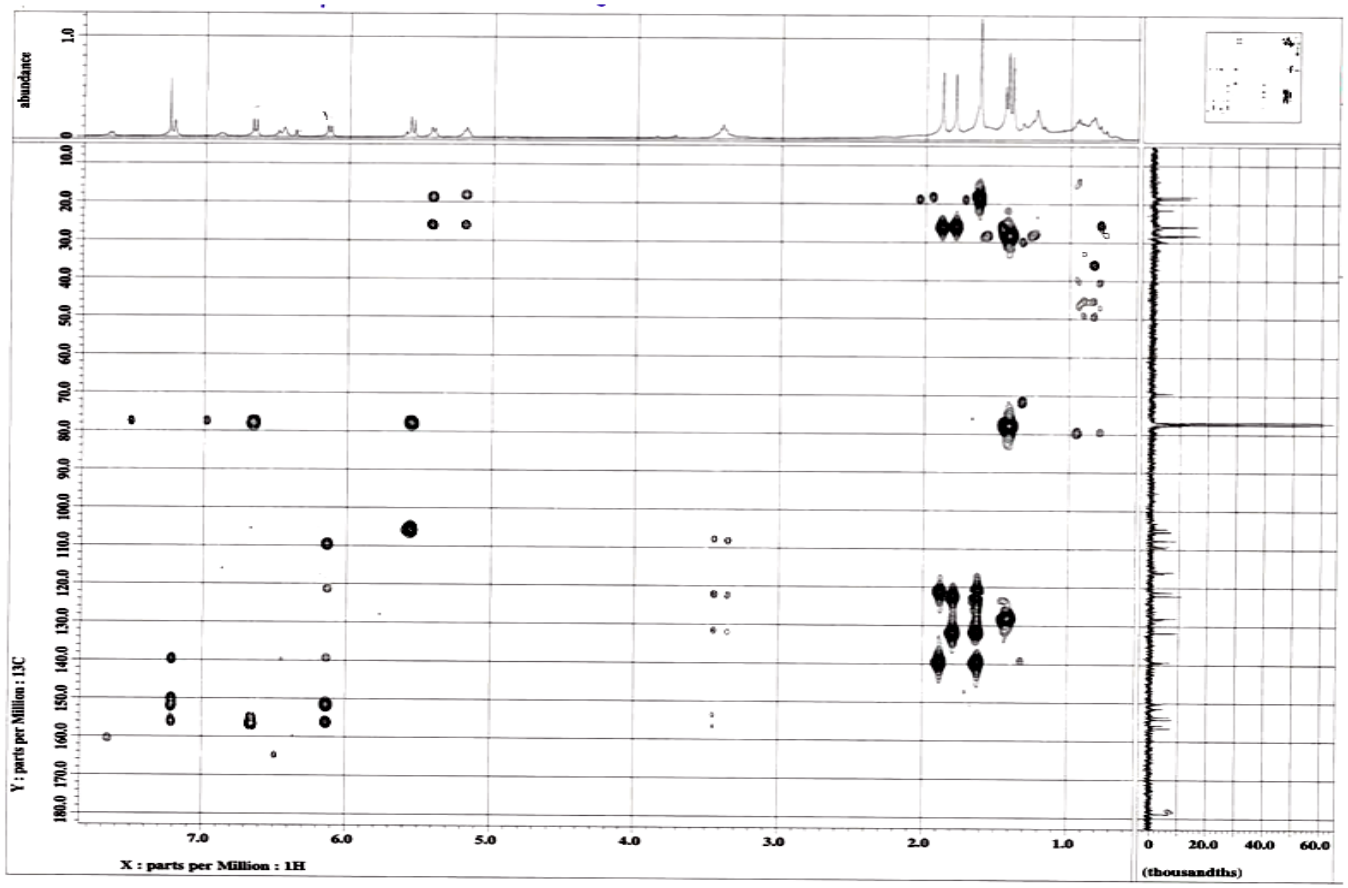

Appendix 57: HMBC spectrum of cycloheterophyllin **(15)**

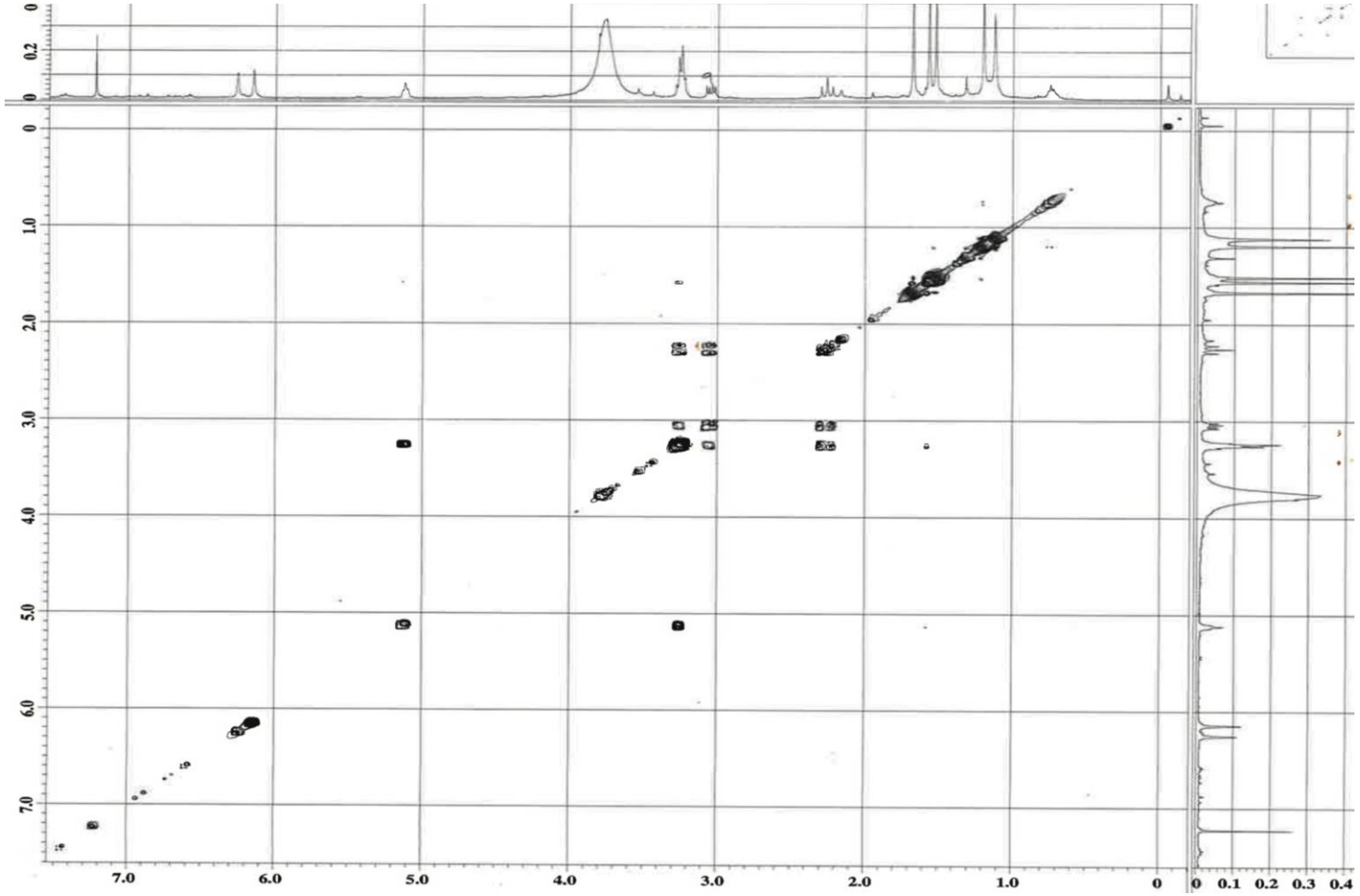

Appendix 58: COSY spectrum of artonin J **(16)**

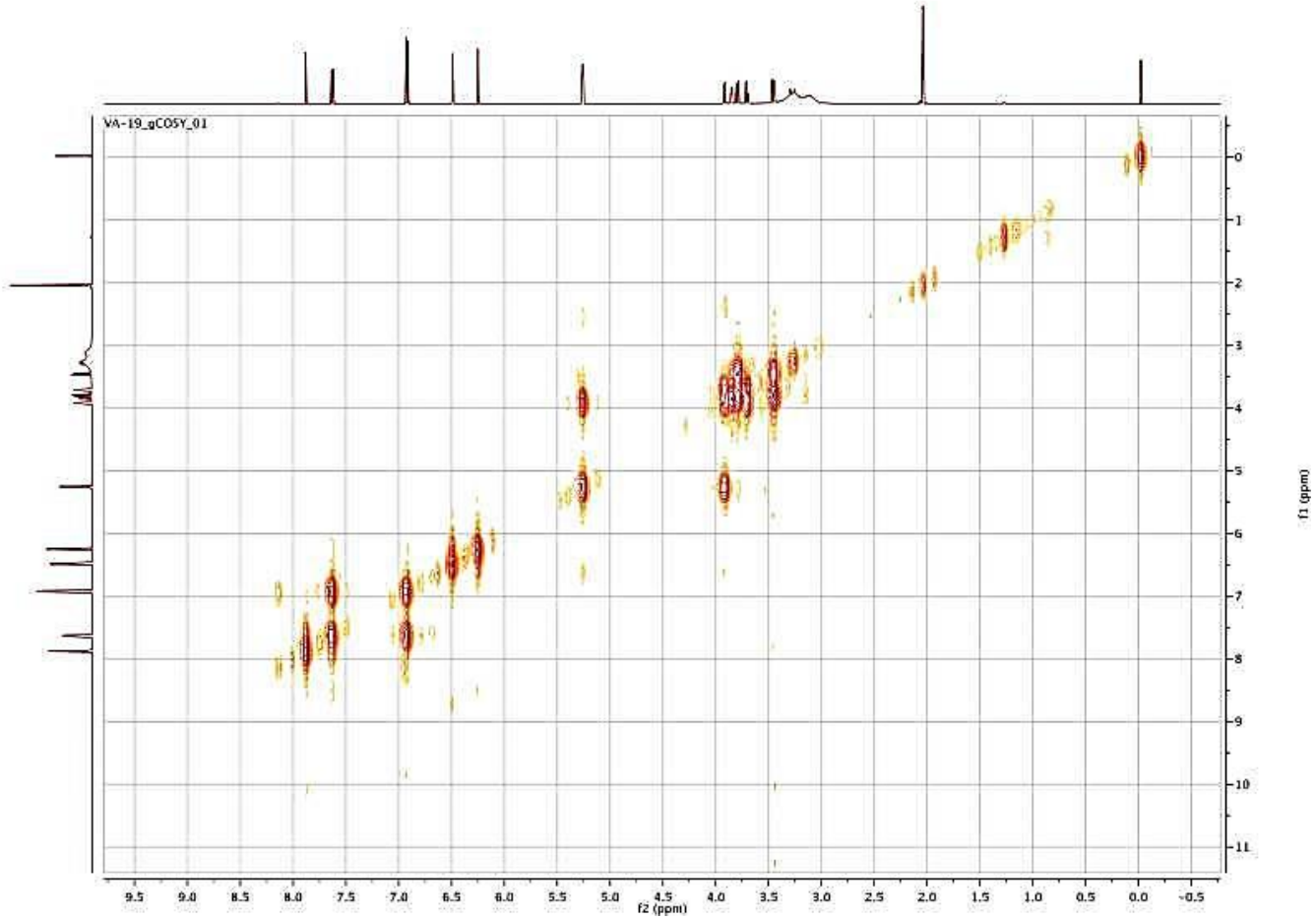

Appendix 59: COSY spectrum of quercetin-3-*O*-α-L-arabinopyranoside **(18)**

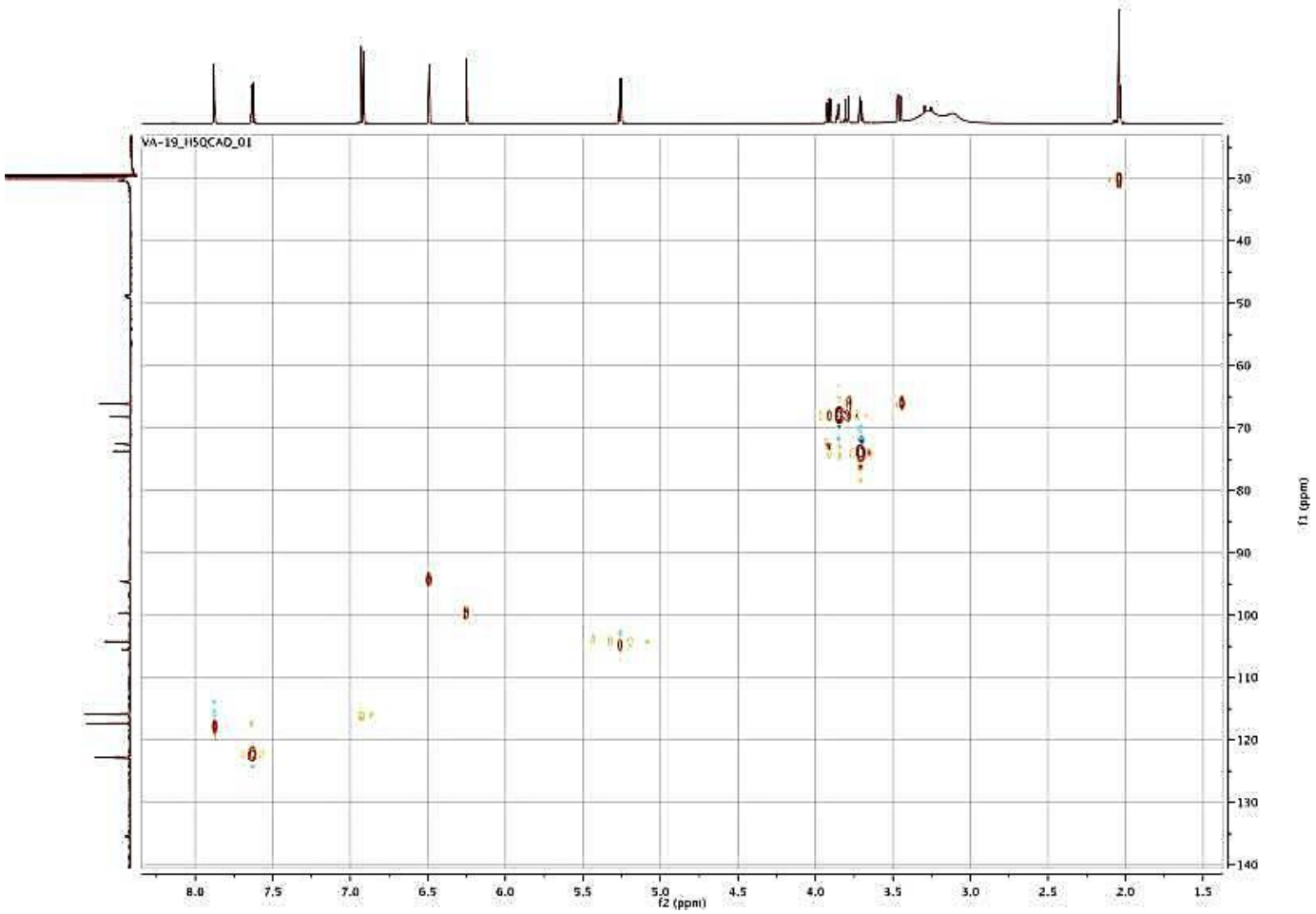

Appendix 60: HSQC spectrum of quercetin-3-*O*-α-L-arabinopyranoside **(18)**

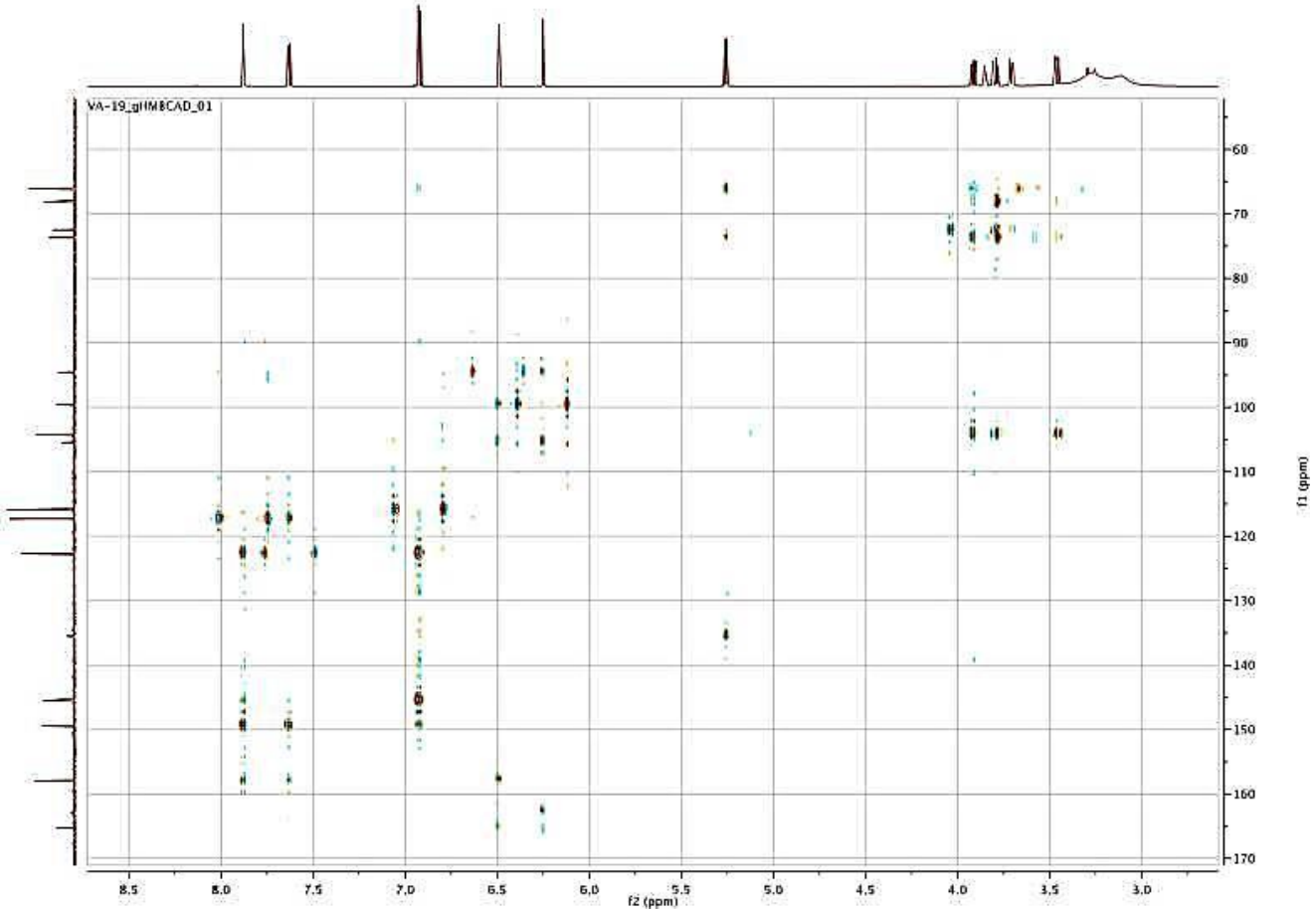

Appendix 61: HMBC spectrum of quercetin-3-*O*-α-L-arabinopyranoside **(18)**

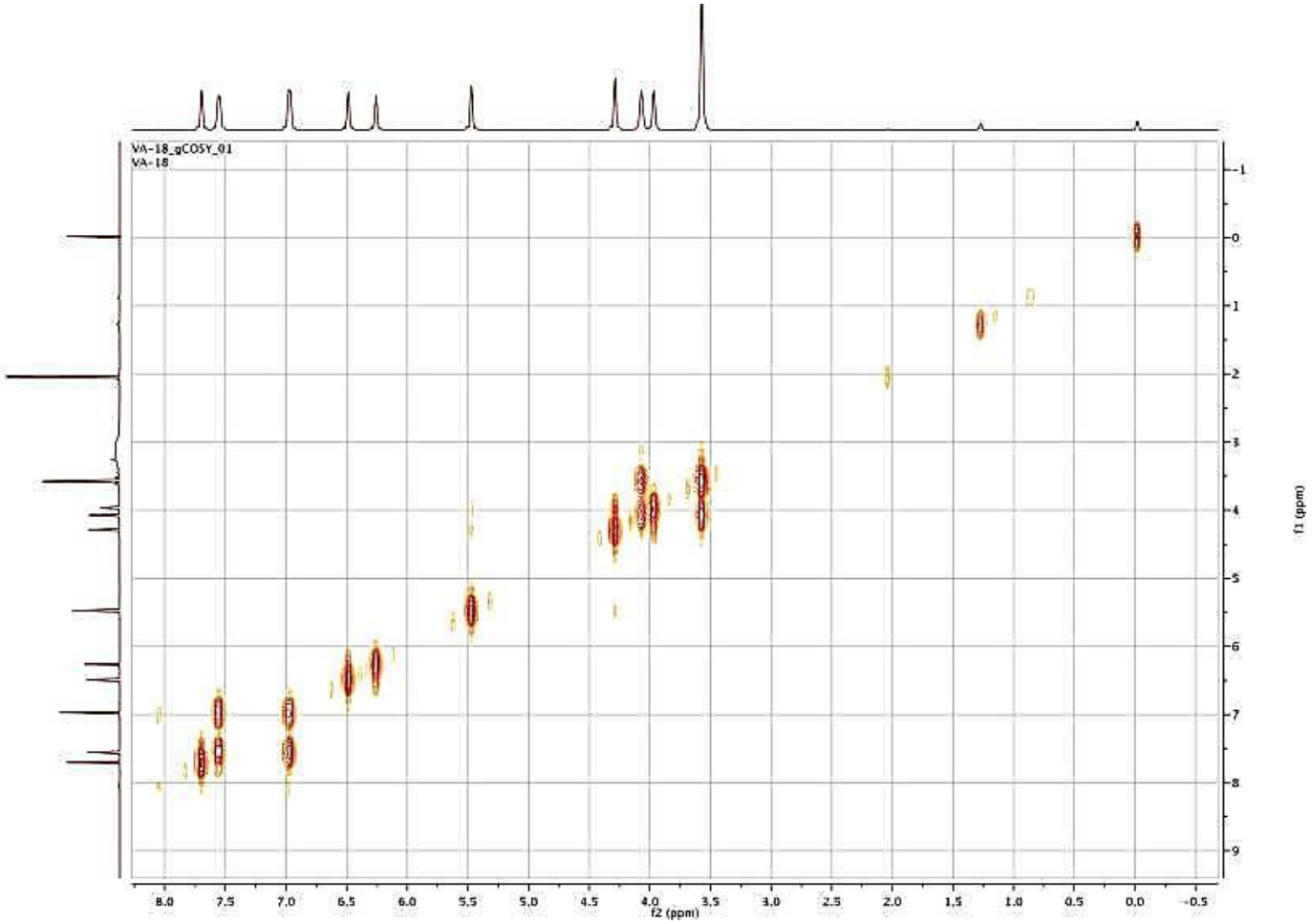

Appendix 62: COSY spectrum of quercetin-3-*O*-α-L-arabinoanofuranoside **(19)**

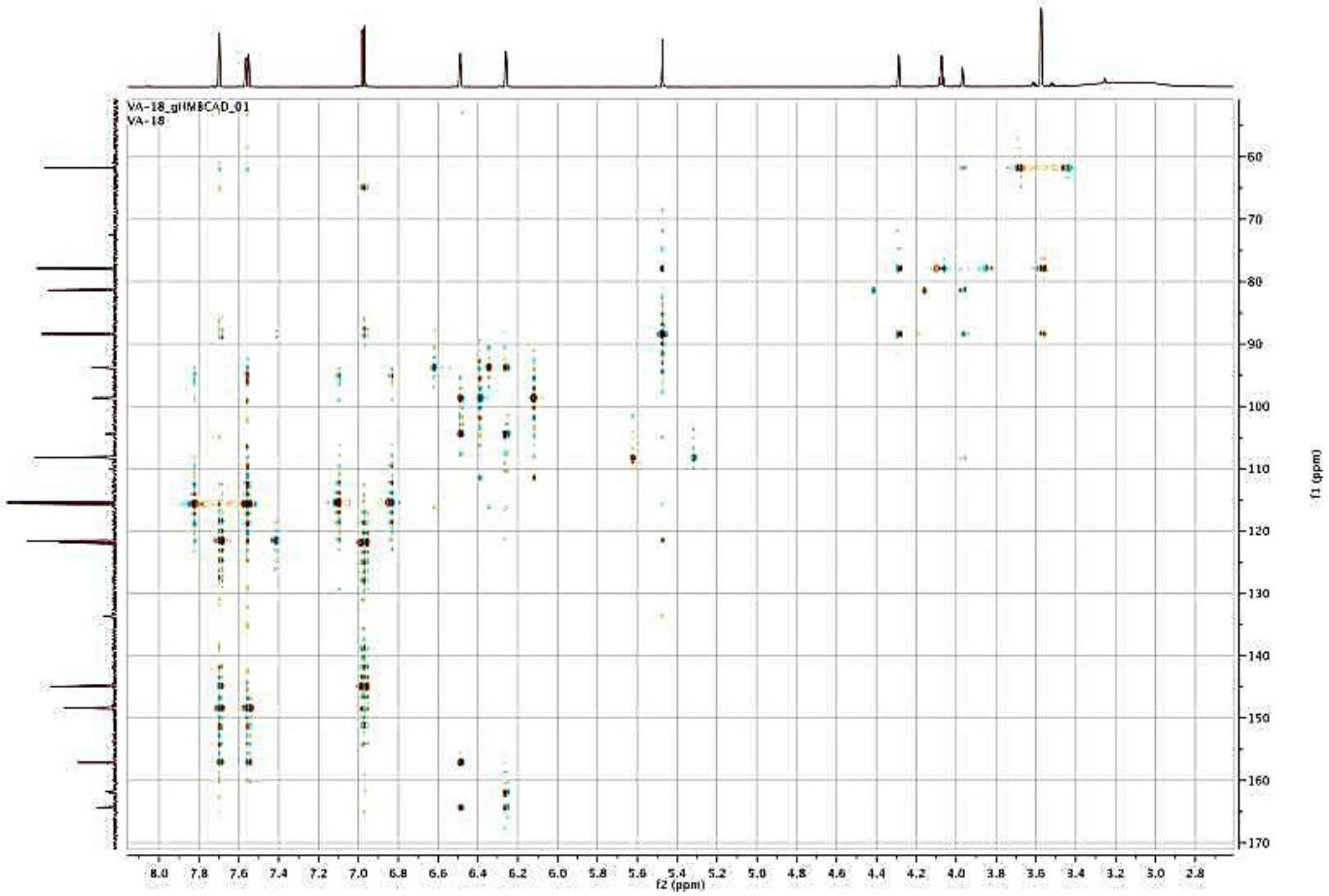

Appendix 63: HMBC spectrum of quercetin-3-*O*-α-L-arabinoanofuranoside **(19)**

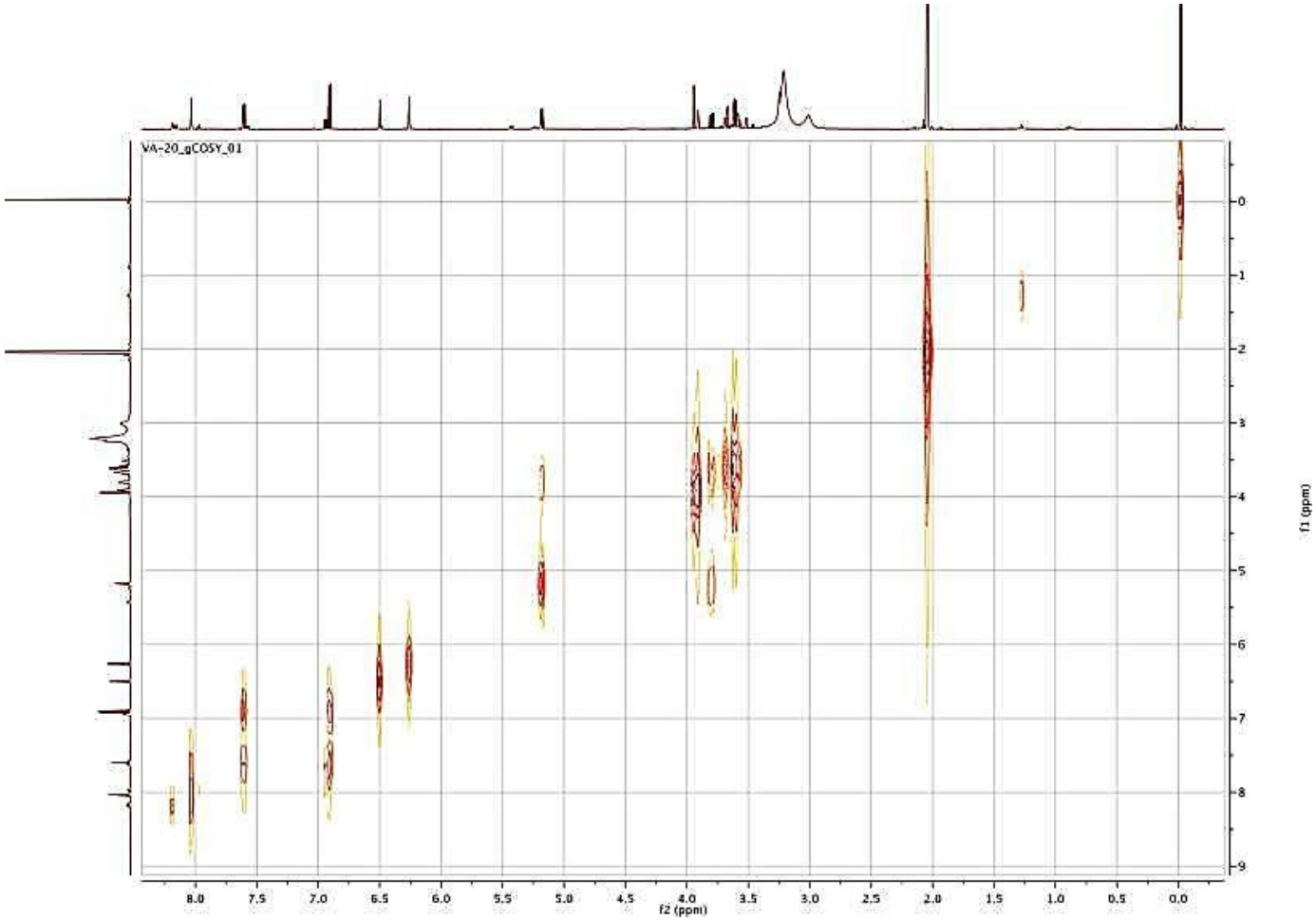

Appendix 64: COSY spectrum of quercetin-3-*O*-β-D-galactopyranoside **(20)**

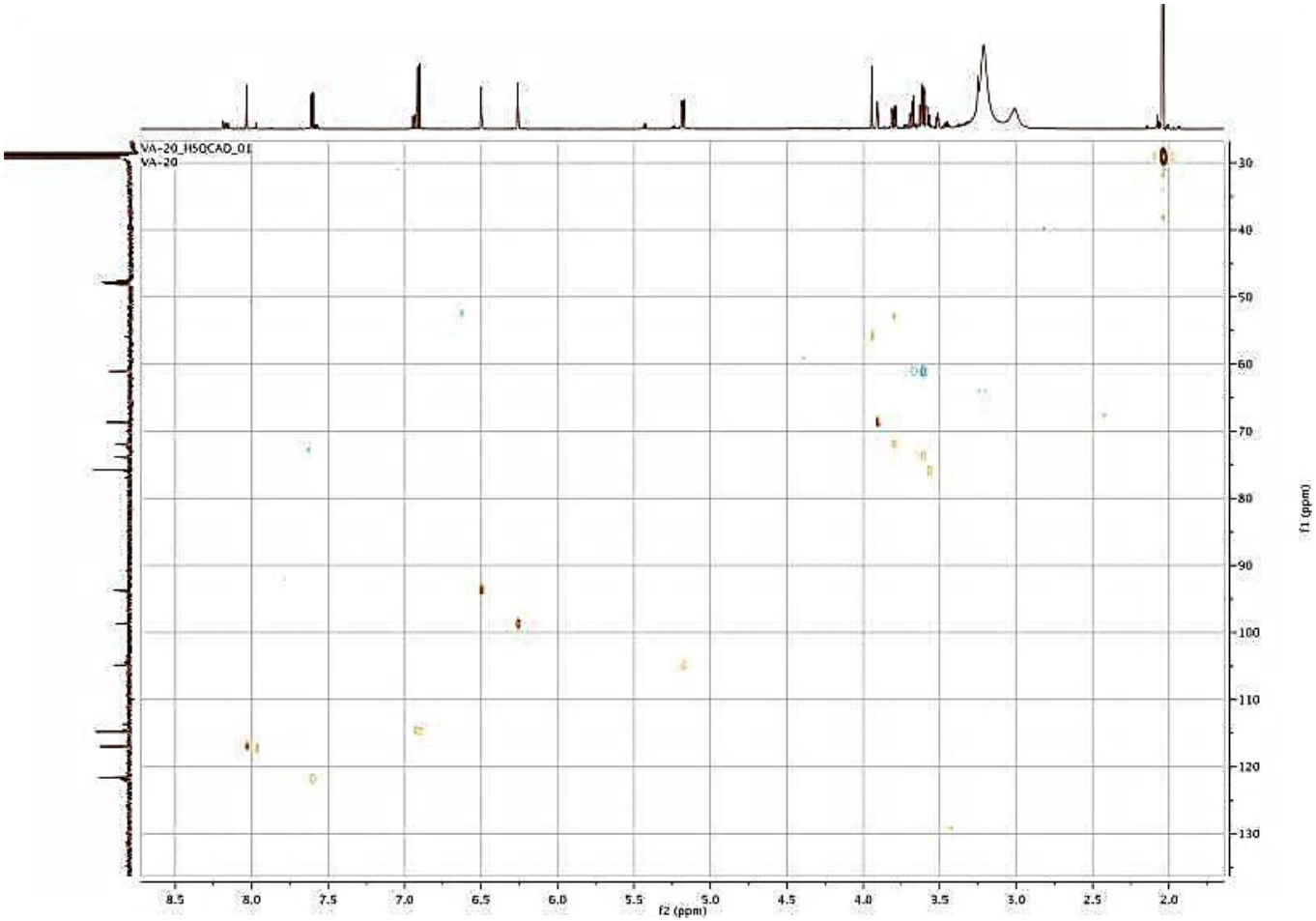

Appendix 65: HSQC spectrum of quercetin-3-*O*-β-D-galactopyranoside **(20)**

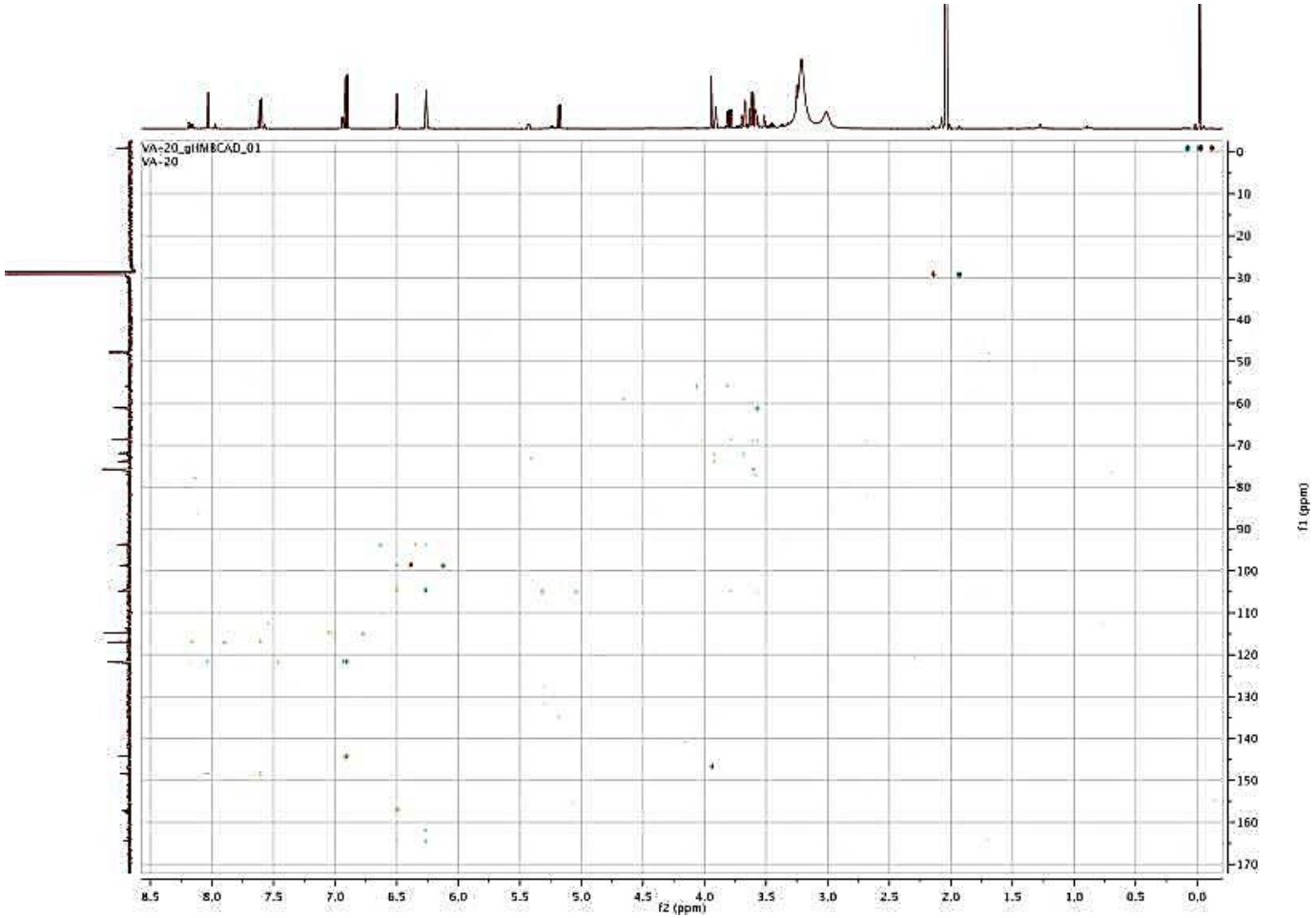

Appendix 66: HMBC spectrum of quercetin-3-*O*-β-D-galactopyranoside **(20)**

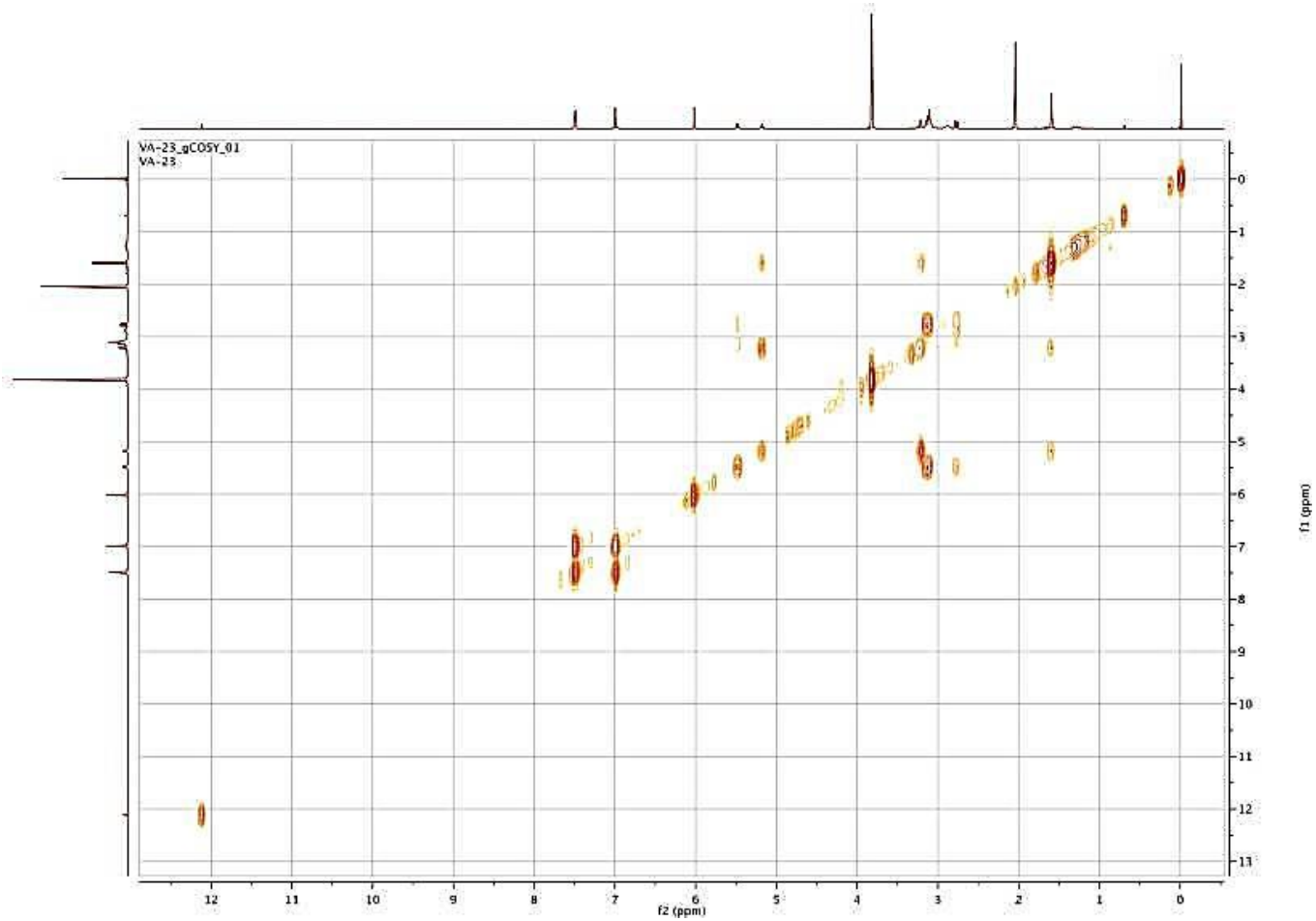

Appendix 67: COSY spectrum of 5,7-dihydroxy-2-(4-methoxyphenyl)-8-(3-methylbut-2-en-1-yl)chroman-4-one **(23)**

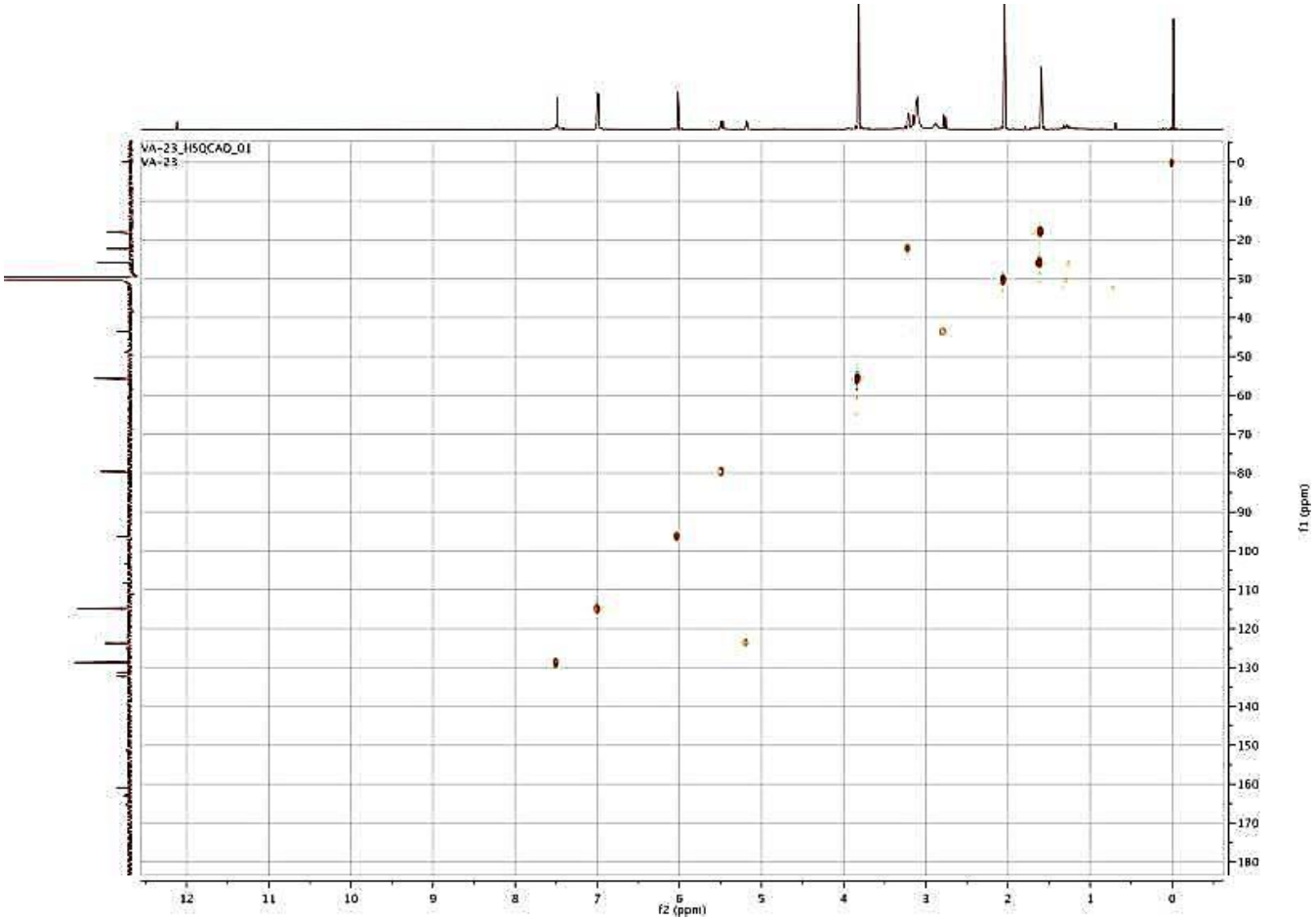

Appendix 68: HSQC spectrum of 5,7-dihydroxy-2-(4-methoxyphenyl)-8-(3-methylbut-2-en-1-yl)chroman-4-one **(23)**

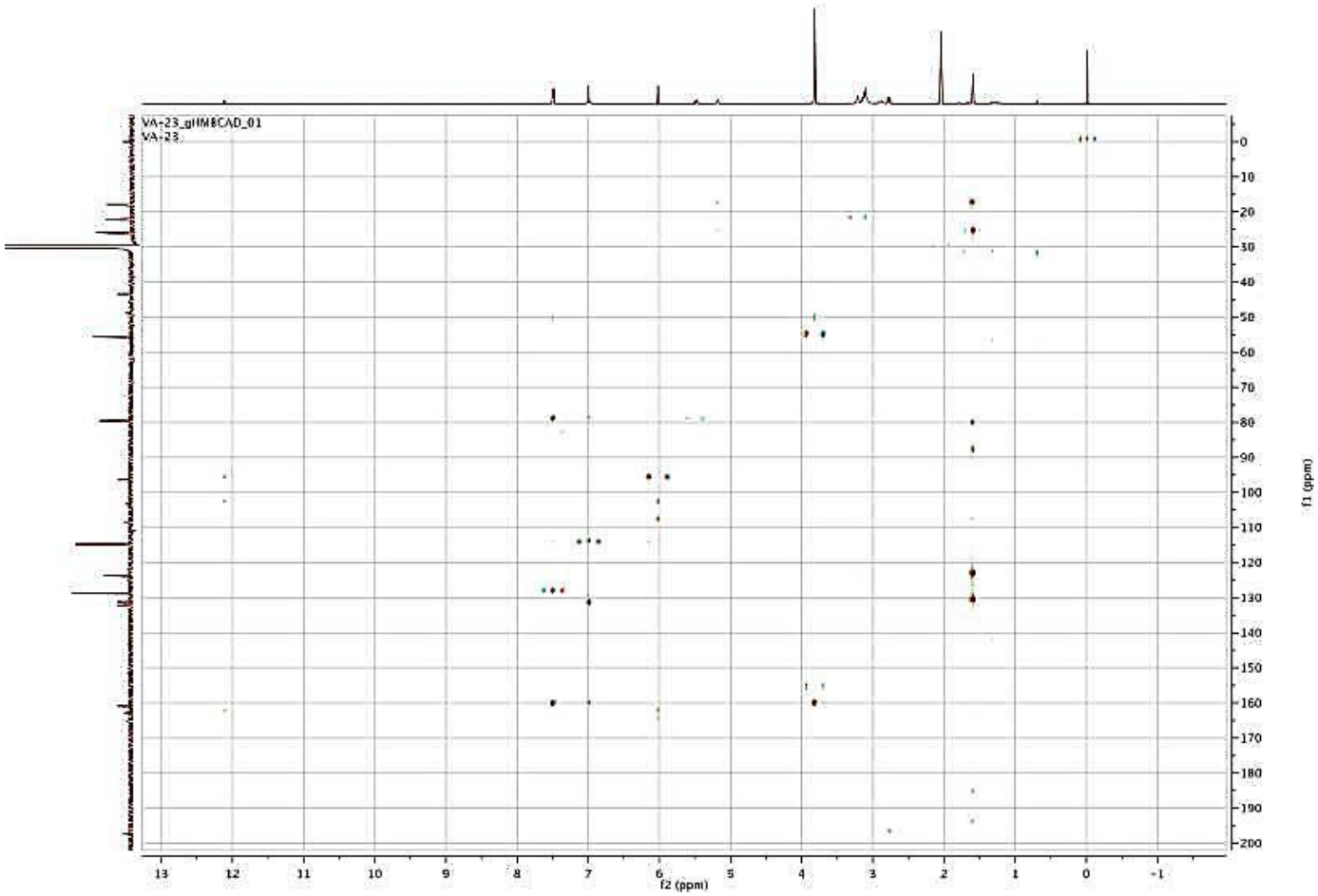

Appendix 69: HMBC spectrum of 5,7-dihydroxy-2-(4-methoxyphenyl)-8-(3-methylbut-2-en-1-yl)chroman-4-one **(23)**

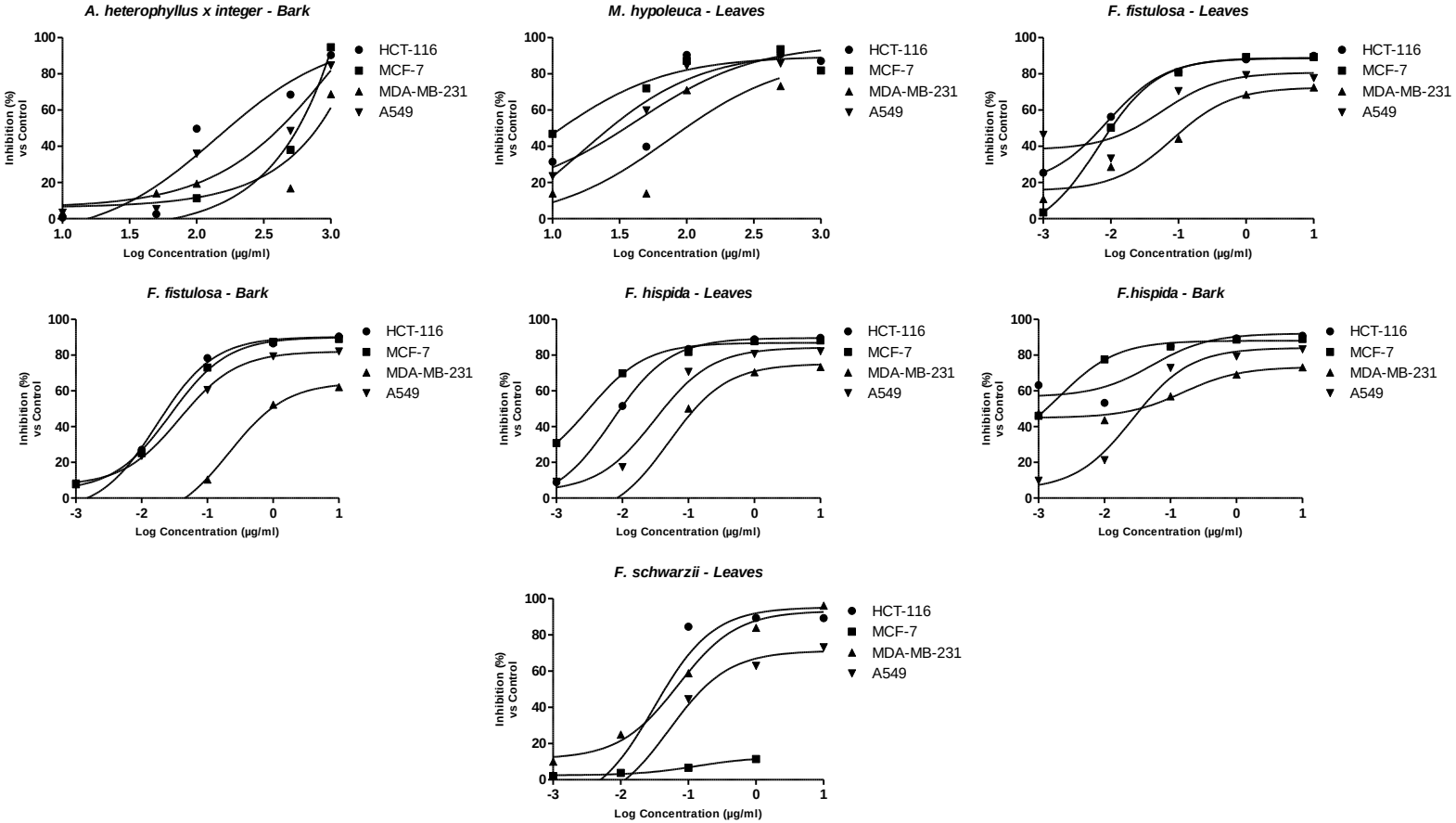

Appendix 70: Concentration-response curves of crude extracts against selected cancer cell lines.

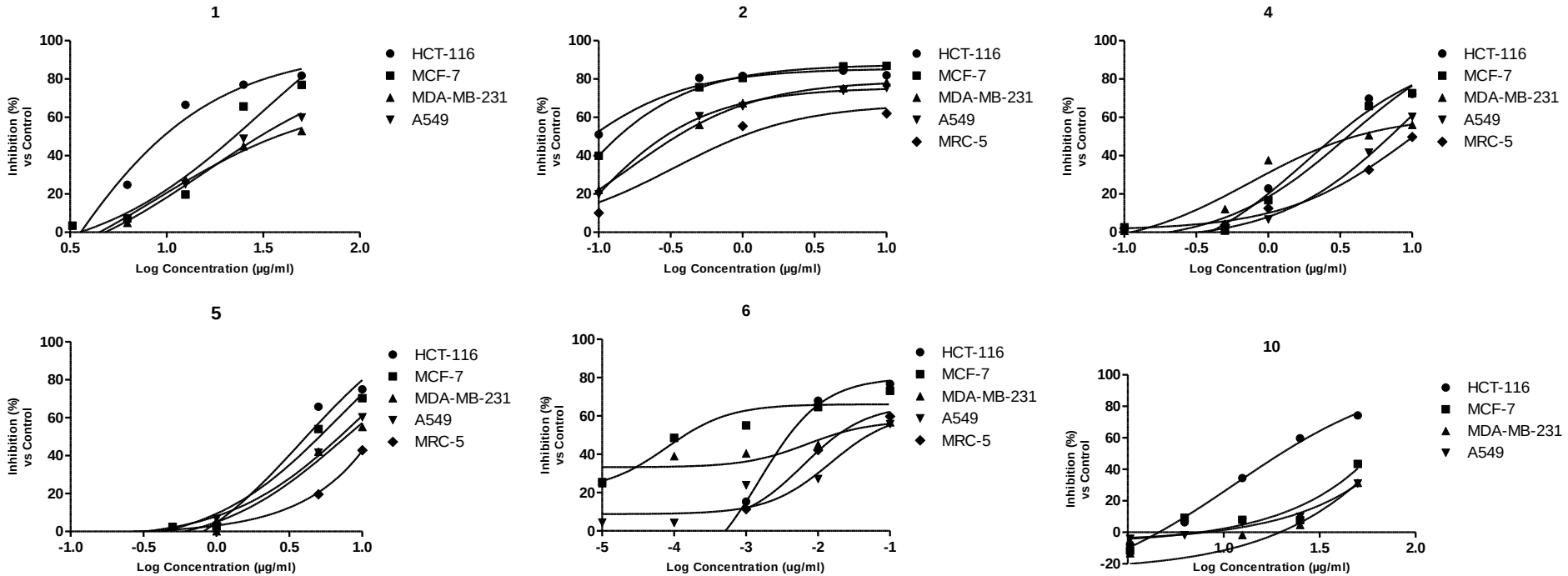

Appendix 71: Concentration-response curves of isolated compounds **(1-10)** against selected cancer cell lines.

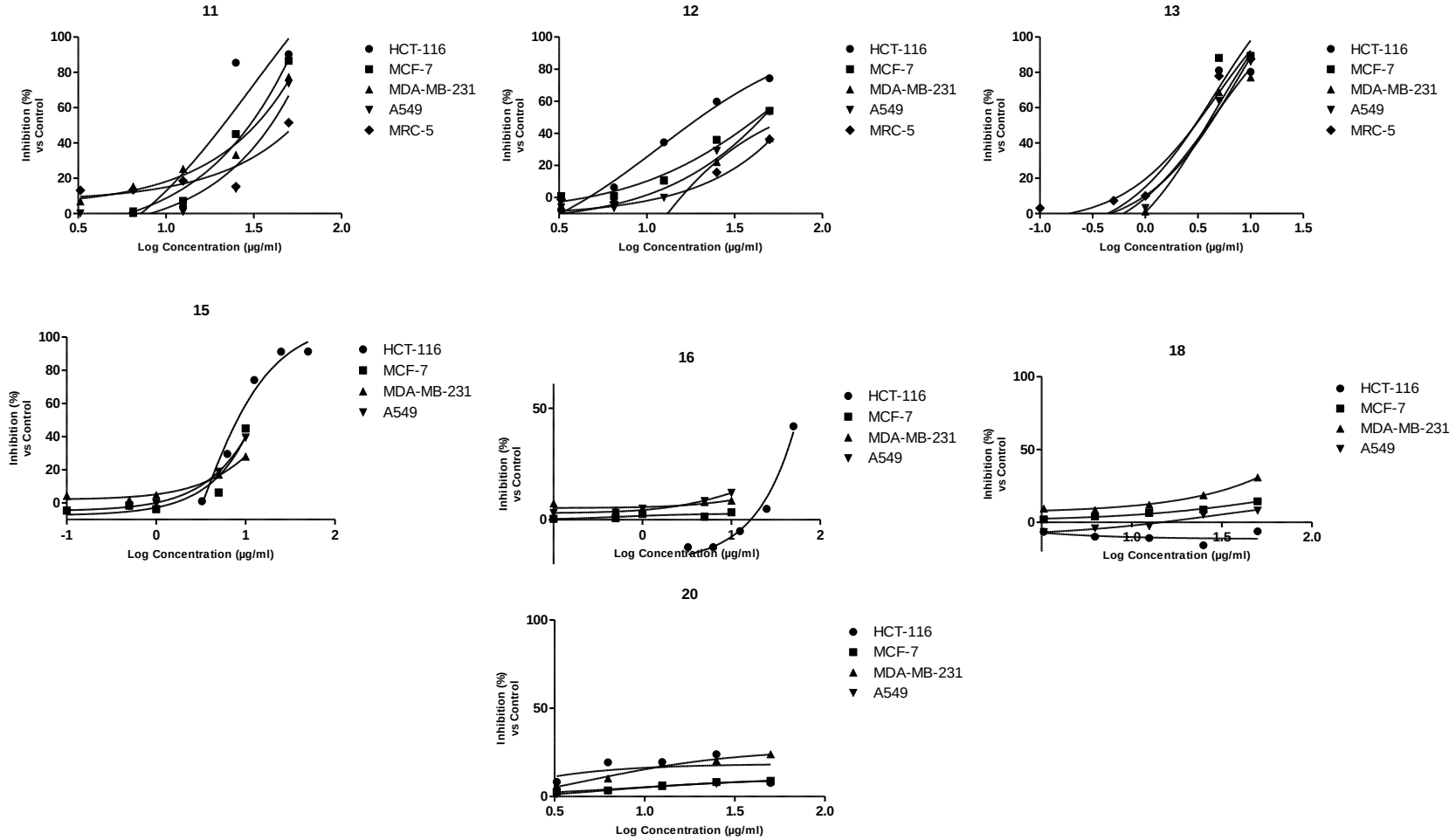

Appendix 72: Concentration-response curves of isolated compounds **(10-20)** against selected cancer cell lines.

Appendix 73: HCT-116 and MCF-7 cells observed with AO/EB double staining after 24 hours treatment with fistulopsine A **(4)** in comparison to untreated cells as control.

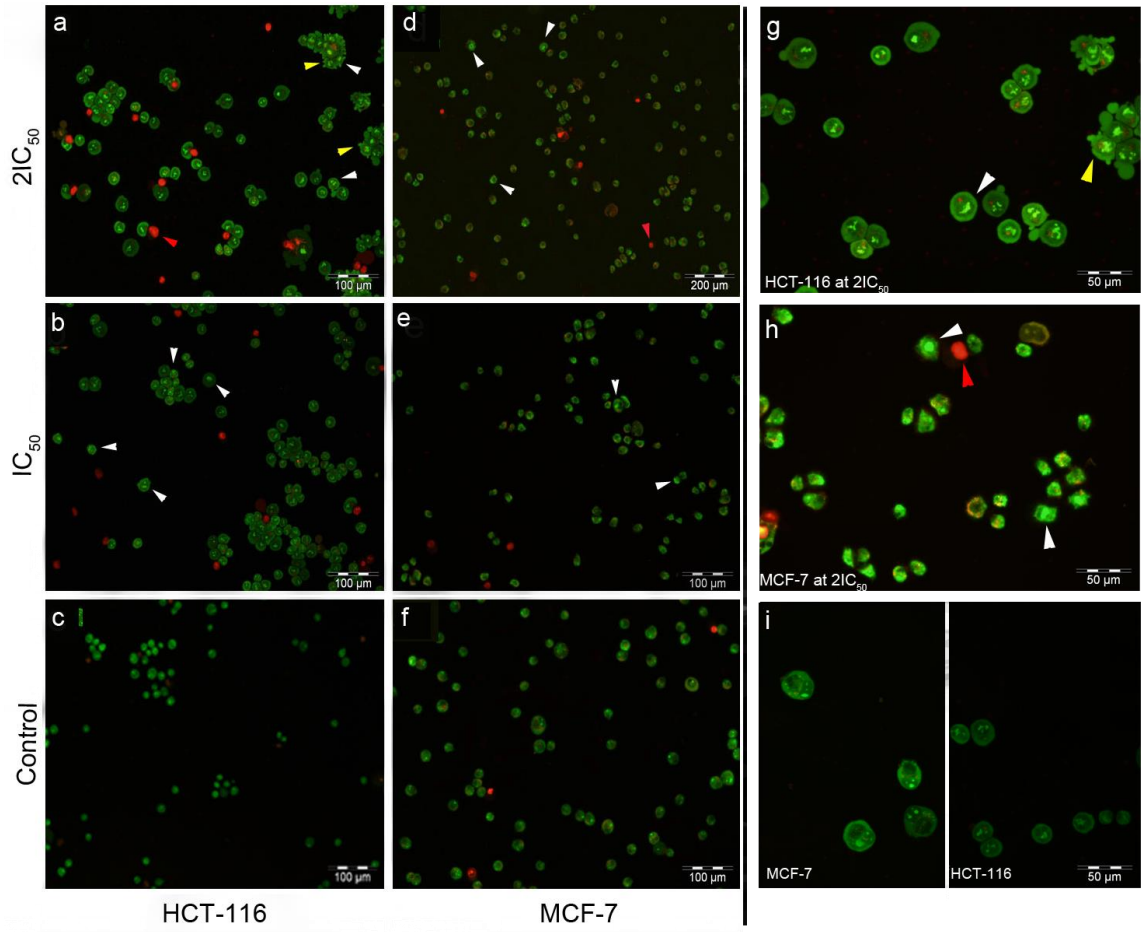

(a)-(f): Treated and control cells at 200x magnification; (g)-(h): Treated cells showing apoptotic features under 400x magnification. Cells showing condensed chromatin, membrane blebbing, apoptotic bodies and necrosis are indicated by white, yellow and red arrowheads, respectively; (i): Untreated/control cells as comparison under 400 x magnifications. Images are representative of one of three similar experiments.

Appendix 74: HCT-116 and MCF-7 cells observed with AO/EB double staining after 24 hours treatment with fistulopsine B **(5)** in comparison to untreated cells as control.

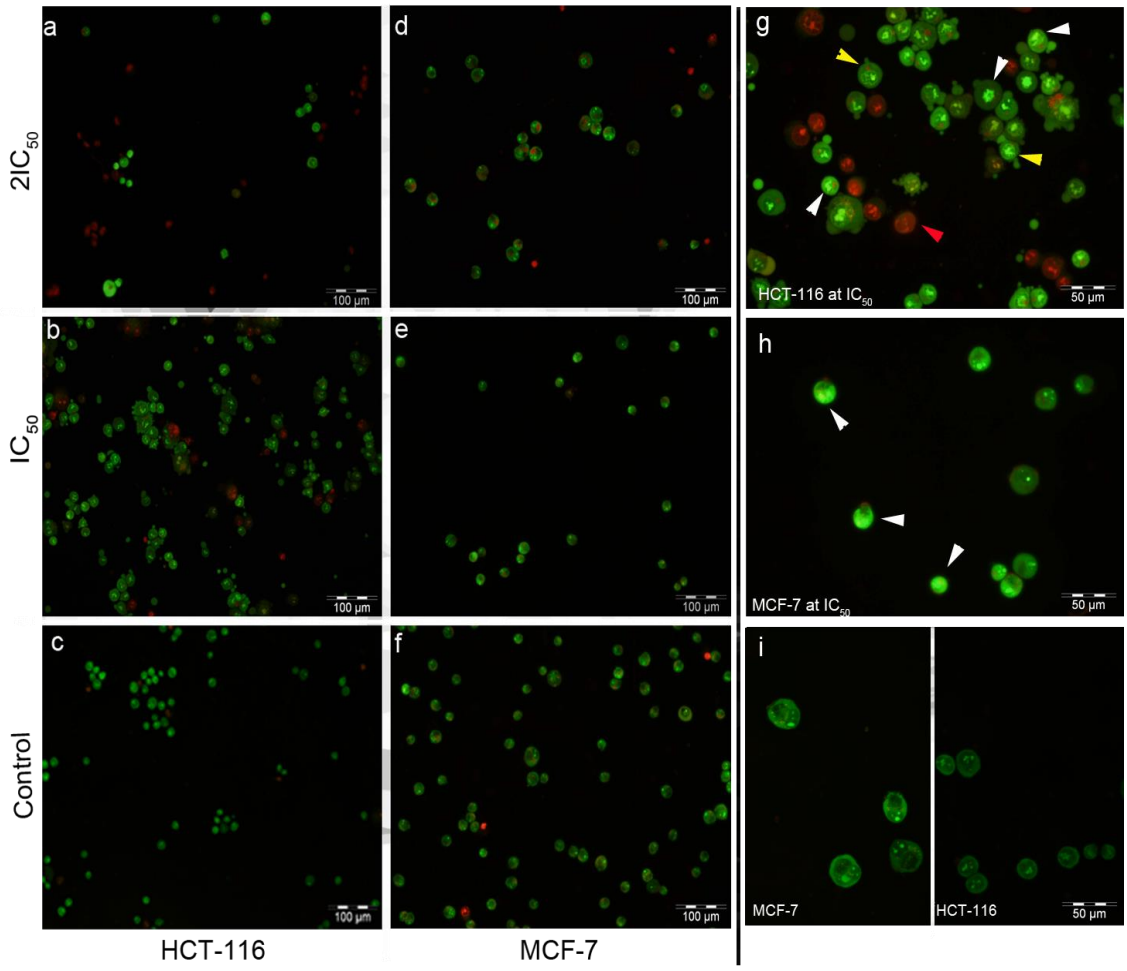

(a)-(f): Treated and control cells at 200x magnification; (g)-(h): Treated cells showing apoptotic features under 400x magnification. Cells showing condensed chromatin, membrane blebbing, apoptotic bodies and necrosis are indicated by white, yellow and red arrowheads, respectively; (i): Untreated/control cells as comparison under 400 x magnifications. Images are representative of one of three similar experiments.

Appendix 75: HCT-116 and MCF-7 cells observed with AO/EB double staining after 24 hours treatment with 13a(*R*)-(-)-3,6-didemethylisotylocrebrine **(6)** in comparison to untreated cells as control.

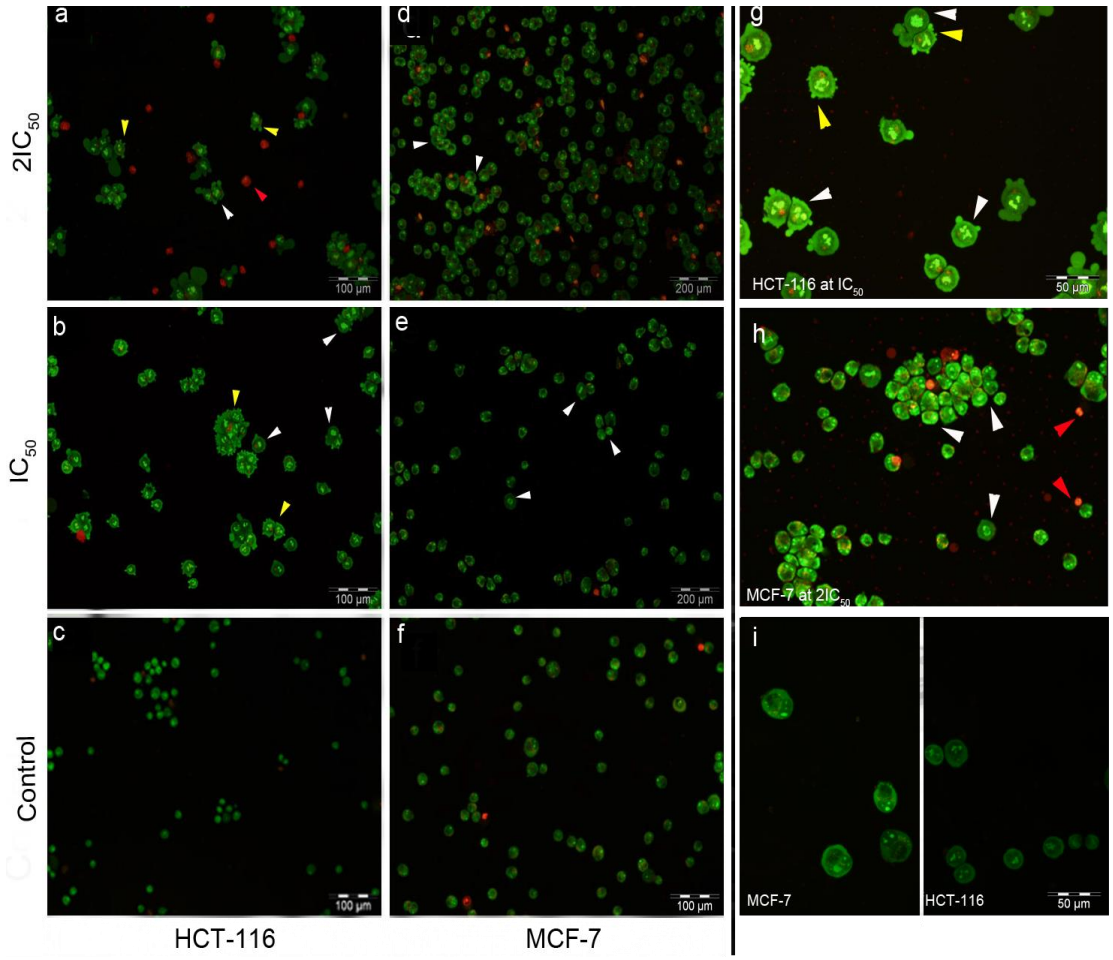

(a)-(f): Treated and control cells at 200x magnification; (g)-(h): Treated cells showing apoptotic features under 400x magnification. Cells showing condensed chromatin, membrane blebbing, apoptotic bodies and necrosis are indicated by white, yellow and red arrowheads, respectively. (i): Untreated/control cells as comparison under 400 x magnifications. Images are representative of one of three similar experiments.

Appendix 76: HCT-116 and MCF-7 cells observed with AO/EB double staining after 24 hours treatment with cudraflavone C **(13)** in comparison to untreated cells as control.

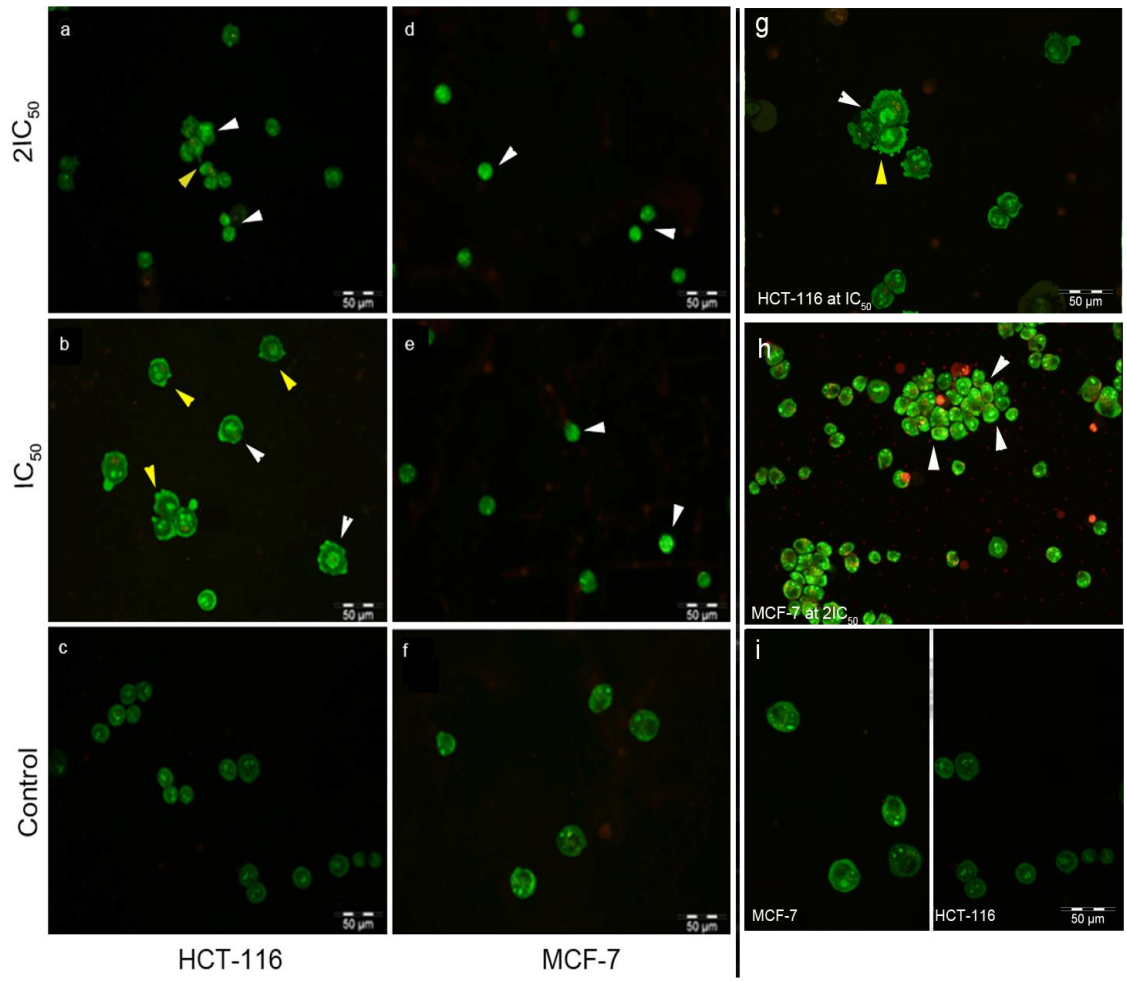

(a)-(f): Treated and control cells at 400x magnification; (g)-(h): Treated cells showing apoptotic features under 400x magnification. Cells showing condensed chromatin, membrane blebbing, apoptotic bodies and necrosis are indicated by white, yellow and red arrowheads, respectively; (i): Untreated/control cells as comparison under 400 x magnifications. Images are representative of one of three similar experiments.

Time	Sample	HCT-116											
		Pre-G1			G1			S			G2/M		
		Mean	SD	N	Mean	SD	N	Mean	SD	N	Mean	SD	N
24 hours	Control	3.01	1.86	8	39.23	4.18	8	23.15	2.67	8	34.75	2.29	8
	Fistulopsine A	3.55	0.60	4	51.63	2.15	4	19.08	1.57	4	26.13	1.49	4
	Fistulopsine B	4.63	2.01	4	50.15	0.95	4	17.98	1.04	4	27.48	2.53	4
48 hours	Control	2.64	1.20	8	41.54	2.49	8	25.06	2.50	8	30.85	1.68	8
	Fistulopsine A	2.81	0.74	4	44.30	1.68	4	18.40	2.18	4	25.59	2.65	4
	Fistulopsine B	2.68	0.64	4	56.53	1.23	4	16.88	0.53	4	23.98	0.83	4
72 hours	Control	3.95	2.79	6	55.53	3.54	6	12.05	1.73	6	28.72	7.37	6
	Fistulopsine A	4.55	1.50	4	58.38	3.39	4	11.90	1.15	4	25.28	5.98	4
	Fistulopsine B	6.48	1.27	4	61.80	1.56	4	11.60	1.47	4	20.40	2.66	4

Time	Sample	MCF-7											
		Pre-G1			G1			S			G2/M		
		Mean	SD	N	Mean	SD	N	Mean	SD	N	Mean	SD	N
24 hours	Control	0.31	0.12	8	39.69	3.59	8	23.48	1.87	8	36.74	4.26	8
	Fistulopsine A	0.33	0.19	4	56.55	8.10	4	17.65	0.73	4	25.70	7.85	4
	Fistulopsine B	0.25	0.17	4	61.03	10.39	4	15.90	0.85	4	23.00	10.00	4
48 hours	Control	0.49	0.54	8	39.69	4.47	8	25.99	2.26	8	33.88	2.79	8
	Fistulopsine A	0.43	0.15	4	56.85	2.99	4	13.30	2.68	4	29.38	5.43	4
	Fistulopsine B	0.43	0.10	4	54.58	1.24	4	16.40	3.04	4	28.75	4.15	4
72 hours	Control	1.01	0.59	8	46.75	2.86	8	20.46	1.63	8	32.15	1.73	8
	Fistulopsine A	1.88	1.36	4	67.28	4.95	4	8.98	1.49	4	22.00	7.19	4
	Fistulopsine B	3.13	2.65	4	66.33	5.54	4	11.05	4.38	4	19.60	2.19	4

Appendix 77: Percentage of events at each phases of the cell cycle after treatment with fistulopsine A **(4)** and fistulopsine B **(5)** at IC_{50} concentration.
(Data is expressed as mean value of more than more than three experiments (N).)

Appendix 78: Two-way ANOVA of cell cycle analysis of HCT-116 cells treated with fistulopsines A **(4)** and B **(5)** for 24, 48 and 72 hours.
(Generated using GraphPad Prism 6 software from mean values generated from more than three independent experiments).

Number of families	4
Number of comparisons per family	2
Alpha	0.05

Time	HCT-116				
	Dunnett's multiple comparisons test	Mean Diff.	95% CI of diff.	Significant ?	Summary
24 hours	Pre-G1				
	Control vs. Fistulopsine A	-0.54	-3.881 to 2.806	No	ns
	Control vs. Fistulopsine B	-1.61	-4.956 to 1.731	No	ns
	G1				
	Control vs. Fistulopsine A	-12.40	-15.74 to -9.056	Yes	****
	Control vs. Fistulopsine B	-10.93	-14.27 to -7.581	Yes	****
	S				
	Control vs. Fistulopsine A	4.08	0.7314 to 7.419	Yes	*
	Control vs. Fistulopsine B	5.18	1.831 to 8.519	Yes	**
	G2/M				
	Control vs. Fistulopsine A	8.63	5.281 to 11.97	Yes	****
	Control vs. Fistulopsine B	7.28	3.931 to 10.62	Yes	****
48 hours	Pre-G1				
	Control vs. Fistulopsine A	-0.17	-2.692 to 2.357	No	ns
	Control vs. Fistulopsine B	-0.04	-2.562 to 2.487	No	ns
	G1				
	Control vs. Fistulopsine A	-2.76	-5.286 to -0.2378	Yes	*
	Control vs. Fistulopsine B	-14.99	-17.51 to -12.46	Yes	****
	S				
	Control vs. Fistulopsine A	6.66	4.137 to 9.185	Yes	****
	Control vs. Fistulopsine B	8.19	5.663 to 10.71	Yes	****
	G2/M				
	Control vs. Fistulopsine A	5.26	2.732 to 7.781	Yes	****
	Control vs. Fistulopsine B	6.88	4.351 to 9.399	Yes	****
72 hours	Pre-G1				
	Control vs. Fistulopsine A	-0.60	-5.958 to 4.758	No	ns
	Control vs. Fistulopsine B	-2.53	-7.883 to 2.833	No	ns
	G1				
	Control vs. Fistulopsine A	-2.84	-8.199 to 2.516	No	ns
	Control vs. Fistulopsine B	-6.27	-11.62 to -0.9091	Yes	*
	S				
	Control vs. Fistulopsine A	0.15	-5.208 to 5.508	No	ns
	Control vs. Fistulopsine B	0.45	-4.908 to 5.808	No	ns
	G2/M				
	Control vs. Fistulopsine A	3.44	-1.916 to 8.799	No	ns
	Control vs. Fistulopsine B	8.32	2.959 to 13.67	Yes	**

Appendix 79: Two-way ANOVA of cell cycle analysis of MCF-7 cells treated with fistulopsines A **(4)** and B **(5)** for 24, 48 and 72 hours.
(Generated using GraphPad Prism 6 software from mean values generated from more than three independent experiments).

Number of families	4
Number of comparisons per family	2
Alpha	0.05

Time	MCF-7				
	Dunnett's multiple comparisons test	Mean Diff.	95% CI of diff.	Significant?	Summary
24 hours	Pre-G1				
	Control vs. Fistulopsine A	-0.01	-6.843 to 6.818	No	ns
	Control vs. Fistulopsine B	0.06	-6.768 to 6.893	No	ns
	G1				
	Control vs. Fistulopsine A	-16.86	-23.69 to -10.03	Yes	****
	Control vs. Fistulopsine B	-21.34	-28.17 to -14.51	Yes	****
	S				
	Control vs. Fistulopsine A	5.83	-1.005 to 12.66	No	ns
	Control vs. Fistulopsine B	7.58	0.7446 to 14.41	Yes	*
	G2/M				
	Control vs. Fistulopsine A	11.04	4.207 to 17.87	Yes	**
	Control vs. Fistulopsine B	13.74	6.907 to 20.57	Yes	****
48 hours	Pre-G1				
	Control vs. Fistulopsine A	0.06	-4.046 to 4.171	No	ns
	Control vs. Fistulopsine B	0.06	-4.046 to 4.171	No	ns
	G1				
	Control vs. Fistulopsine A	-17.16	-21.27 to -13.05	Yes	****
	Control vs. Fistulopsine B	-14.89	-19.00 to -10.78	Yes	****
	S				
	Control vs. Fistulopsine A	12.69	8.579 to 16.80	Yes	****
	Control vs. Fistulopsine B	9.59	5.479 to 13.70	Yes	****
	G2/M				
	Control vs. Fistulopsine A	4.50	0.3914 to 8.609	Yes	*
	Control vs. Fistulopsine B	5.13	1.016 to 9.234	Yes	*
72 hours	Pre-G1				
	Control vs. Fistulopsine A	-0.86	-5.290 to 3.565	No	ns
	Control vs. Fistulopsine B	-2.11	-6.540 to 2.315	No	ns
	G1				
	Control vs. Fistulopsine A	-20.53	-24.95 to -16.10	Yes	****
	Control vs. Fistulopsine B	-19.58	-24.00 to -15.15	Yes	****
	S				
	Control vs. Fistulopsine A	11.49	7.060 to 15.91	Yes	****
	Control vs. Fistulopsine B	9.41	4.985 to 13.84	Yes	****
	G2/M				
	Control vs. Fistulopsine A	10.15	5.723 to 14.58	Yes	****
	Control vs. Fistulopsine B	12.55	8.123 to 16.98	Yes	****